

Improving the Performance of Reinforced Concrete Decks in California

by

Pablo E. Hurtado

A dissertation submitted to the Graduate Faculty of
Auburn University
in partial fulfillment of the
requirements for the Degree of
Doctor of Philosophy

Auburn, Alabama
December 10, 2022

Keywords: Bridge Decks, Reinforced Concrete, Live Loads,
Shrinkage, Steel Reinforcement, Finite Element Analysis

Copyright 2022 by Pablo E. Hurtado

Approved by

Andrzej S. Nowak, Chair and Professor, Department of Civil and Environmental Engineering
Anton K. Schindler, Professor and Director, Department of Civil and Environmental Engineering
Robert W. Barnes, Associate Professor, Department of Civil and Environmental Engineering
James S. Davidson, Professor, Department of Civil and Environmental Engineering

ABSTRACT

The poor performance observed over the years starts at the very early age of the bridge, like in California. The literature review suggests that restraining effects on the deck may cause excessive early-age transverse cracking and affect the service performance. Cast-in-place reinforced concrete decks exhibit early numerous and wide transverse cracking in California bridges. Prestressed and reinforced concrete continuous box girder bridges are the most affected by transverse cracking in the decks. In this dissertation, the performance of cast-in-place reinforced concrete decks in California is evaluated considering the increasing traffic in the state, the current and past design provisions and the restraining effects provided by the webs of box girders.

Statistical analysis was performed in this study to select the types of structures with the worst performance in California. Box girder bridges with cast-in-place reinforced concrete decks were selected for further analysis. Inspection reports, a cracking database of California bridge decks, and weigh-in-motion (WIM) data of selected sites for live-load evaluation were available for the study. The availability of inspection reports and cracking database of selected box girder bridges allowed the analysis of deck designs, cracking data, and condition rating over time.

The different analyses performed in this research provided insights into the level of traffic in California and how it compares with the rest of the nation and AASHTO LRFD design live loads. The deck detailing was evaluated based on the inspection reports available for 94 cast-in-place box girder bridges. It was found that the main reinforcement spacing does not comply with AASHTO LRFD design requirements and that the truss bar detail is ineffective for the strength limit state. Shrinkage and temperature reinforcement spacing provided was found to be one of the largest in the nation, and the amount of steel reinforcement was very low compared to other states. It was recommended that the spacing should be reduced to a maximum of 9 in. and an increased

amount of reinforcement (greater than 0.32% of gross deck area) should be provided for shrinkage and temperature reinforcement to better control the transverse cracking widths in concrete bridge decks.

Early-age concrete behavior of two box girder bridges was simulated using the finite element method (FEM) with Abaqus software. Creep and shrinkage, using the Modified B3 Model, properties of concrete at early ages were incorporated into the FEM model to obtain the magnitude of strains in the decks in the first 14 days. Data from two bridge decks constructed in California in 2010 was used to develop restraining factors for the box girder bridges. It was found that restraining effects can be up to 88% in these bridges, verifying the high level of restraint provided by the box girders to the decks.

ACKNOWLEDGEMENTS

I would like to thank Dr. Andrzej S. Nowak for his trust in me during these four years doing my Ph.D. It has been a pleasure to work under his direction, with very challenging research projects, and for always believing in my abilities to perform a well-done job. I want to thank Dr. Anton K. Schindler, Robert W. Barnes, Dr. James S. Davidson, and Dr. Maria Auad for being part of my committee and for providing insightful comments on how to improve the presented work. My committee members were my professors, and today I can say that I really value what I learned from you.

This research would have been impossible without the support provided by the California Department of Transportation. I want to thank Keith Nakaoka for always being accessible and providing everything I asked to conduct this research. I want to thank some collaborators for their hard work during this research and for all the support they gave me: Dr. Sylwia S. Stawska, Dr. Jacek Chmielewski, Dr. Anjan R. Babu, Karina Popok, and Andrea Kouame.

Looking back to 2018, when Patricia and I decided to start our Ph.D. programs at Auburn, it was not an easy decision. The process was difficult these past four years, but with the support of family and dearest friends who believed in me made this dream journey become something that I could do. I would like to thank my friends Riffo, Mon, Pipe, Pazi, Oscar, Bea, Christian, Fran, Daniel, Cristobal, Juan, and Tami for always being present, for their encouragement and for supporting us in the distance, and for always receiving us with open arms when we came back to Chile, thank you.

I want to thank all the fantastic people that I met these past years here at Auburn. First, I want to thank Dr. Victor Aguilar for without him this journey would have never come true. Victor made my student life easier, teaching me how to be a doctoral student, and I will always be grateful to you. Life in Auburn was not easy at the beginning until we met Anjan, who helped us with living arrangements and getting groceries the first days, and for offering us his unique friendship, which will last forever. Anjan became one of my dearest friends in a couple of months, and I will always be grateful to you for all you have done for Patricia and me. Sylwia, my friend, I would like to thank you for all your support in work and in life, for always being there when I needed you.

To my fiancée Patricia, for giving me the opportunity to be here with her doing this. For always believing in what I can achieve and for helping me even when I thought I did not need it. You made this dream come true and helped me through it at difficult times. I could not have made it without you, my love.

Finally, I would like to thank my parents, Carla and Jovino, for always being there when I needed them and for their support, love, and encouragement. For believing in what I could do and for their trust in me despite my mistakes. My lovely sisters Carolina and Laura for always supporting me in the distance, for being there for my parents when I could not, and for always believing in me. My dear family, this achievement is for you, for all you have done, for all we have lived in the past. I love you all.

TABLE OF CONTENTS

ABSTRACT.....	ii
ACKNOWLEDGEMENTS.....	iv
TABLE OF CONTENTS.....	vi
LIST OF FIGURES	ix
LIST OF TABLES.....	xiv
CHAPTER 1. INTRODUCTION.....	1
1.1 Highway Bridges in the United States	1
1.1.1 Bridge Statistics in the United States	1
1.1.2 Bridge Condition in the United States.....	3
1.1.3 Cracking in Concrete Decks.....	10
1.1.4 Transportation and Infrastructure Spending in the U.S.....	12
1.2 Motivation and Goals	15
1.3 Research Objectives	17
1.4 Dissertation Organization.....	17
CHAPTER 2. LITERATURE REVIEW	19
2.1 Introduction	19
2.2 Bridge Deck Design	19
2.2.1 Deck Design Methods	20
2.2.2 Cracking Control Design Provisions and Recommendations	23
2.3 Concrete Bridge Deck Deterioration: Causes and Mitigation Techniques	26
2.3.1 Previous Studies	27
2.4 Concrete Behavior.....	31
2.4.1 Creep and Shrinkage	31
2.4.2 Thermal Stress Development	37
2.5 Degree of Restraint in Concrete Structural Elements	39
CHAPTER 3. SELECTION OF REPRESENTATIVE STRUCTURES	42
3.1 National Bridge Inventory Statistics	42
3.1.1 Bridge Condition Rating in California.....	48
3.1.2 Summary of NBI Statistics.....	53
3.2 Bridge Deck Cracking Database	54

3.2.1	Bridge Inspection	55
3.2.2	Cracking Distribution.....	57
3.3	Representative Structures.....	60
CHAPTER 4.	LIVE LOADS AND EFFECTS ON BRIDGES.....	62
4.1	WIM Stations in California.....	62
4.1.1	Data decryption (iAnalyze).....	63
4.1.2	Average Daily Truck Traffic.....	63
4.1.3	FHWA WIM Data.....	66
4.1.4	Quality Control Procedure	71
4.2	Probability Paper.....	75
4.3	Gross Vehicle Weight	77
4.4	Axle Loads	79
4.5	Load Effects	81
4.6	Finite Element Model of Box Girder Bridges for Live Load Evaluation	82
4.6.1	Influence Lines.....	82
4.6.2	Simplified Model Bridge #02 0036L	83
4.6.3	Material Properties: Concrete Damage Plasticity	84
4.6.4	Bridge Geometry.....	86
4.6.5	Finite Element Model.....	87
4.6.6	Transverse Flexural Stresses	89
CHAPTER 5.	CAST-IN-PLACE BRIDGE DECK REINFORCEMENT ANALYSES	91
5.1	Introduction.....	91
5.2	Bridge Deck Data.....	91
5.3	Strength Limit State	92
5.3.1	Main Steel Reinforcement.....	92
5.3.2	Summary and Comments	103
5.4	Serviceability.....	104
5.4.1	Main Steel Reinforcement.....	104
5.4.2	Longitudinal Steel Reinforcement	110
5.4.3	Restraint Effects on Concrete Stresses.....	115
5.4.4	Summary	120
CHAPTER 6.	EVALUATING DEGREE OF RESTRAINT IN BOX GIRDER BRIDGES.....	121
6.1	Introduction.....	121

6.2	Selected Bridges	121
6.2.1	Markham Ravine Bridge – Lincoln, California	122
6.2.2	Olive Lane Bridge – Santee, California	125
6.3	Finite Element Modeling.....	127
6.3.1	Boundary Conditions.....	127
6.3.2	Creep and Shrinkage Model Implementation.....	128
6.3.3	Bridge Model.....	132
6.4	Strain Results.....	133
6.5	Restraint Factor of Selected Bridges.....	134
CHAPTER 7.	CONCLUSIONS AND RECOMMENDATIONS.....	137
7.1	FUTURE RESEARCH	139
CHAPTER 8.	REFERENCES	140
APPENDIX A	INSPECTION REPORTS DATA	143
APPENDIX B	FHWA WIM DATA.....	145
B.1	ADTT	145
B.2	WIM records	147
B.3	Wim Quality Control.....	149
APPENDIX C	WIM DATA PLOTS	155
C.1	Gross Vehicle Weight Per Year	155
C.2	Gross Vehicle Weight By Class	158
C.3	Axle Loads	161

LIST OF FIGURES

Figure 1.1: Deck Type Distribution as of 2022 in the US (Adapted from NBI, 2022)	2
Figure 1.2: Deck protection type for Concrete CIP Bridge Decks (Adapted from NBI, 2022)	3
Figure 1.3: Bridge condition percentage (Adapted from NBI 2009-2022)	6
Figure 1.4: Bridge condition percentage (Adapted from NBI 2009-2022)	7
Figure 1.5: Plastic shrinkage cracking in freshly placed concrete (Mehta and Monteiro, 2014) .	11
Figure 1.6: Typical deck transverse cracking (Adapted from Russell, 2004)	11
Figure 1.7: Transportation and infrastructure spending (Adapted from USAFacts (2022)).....	14
Figure 2.1: Basic creep and creep relaxation over time (Adapted from Mehta and Monteiro (2014)).....	31
Figure 2.2: Influence of shrinkage and creep on concrete cracking. (Adapted from Mehta and Monteiro (2014)).....	32
Figure 2.3: Graphical representation of development of thermal stresses (Schindler and McCullough, 2002).....	38
Figure 2.4: Degree of tensile restraint at center section (ACI 207, 2007)	40
Figure 3.1 California bridge by structural types (number of bridges is indicated in parenthesis)	42
Figure 3.2: California bridges by material.....	43
Figure 3.3: Bridge deck material type.....	46
Figure 3.4: Number of California bridges by year built.	47
Figure 3.5: Bridge structural type for selected time periods.....	47
Figure 3.6: Bridge material for selected time periods.....	48
Figure 3.7: Bridge material types built in the last decade,.....	48
Figure 3.8: California deck condition rating percent by bridge structural type.....	49
Figure 3.9: Superstructure condition rating percent by bridge structural type.	50
Figure 3.10: Deck condition rating percent by bridge material type.	51
Figure 3.11: Deck condition of CIP reinforced concrete decks in Box girder bridges.....	52
Figure 3.12: Bridge general condition according to PBCPM rule (FHWA, 2017)	52
Figure 3.13: Distribution of Cracking Data Available by Structural Material Type (percent of total in orange dots)	54
Figure 3.14: Cracked Deck Area Ratio Distribution of Box Girder Decks in California.....	55
Figure 3.15: Crack frequency in Box Girder Bridges.....	57

Figure 3.16 Typical locations of cracking reported in Box Girder Bridges	58
Figure 3.17: Ratio of cracked decks treated with methacrylate in Box Girder Bridges	59
Figure 3.18: Cracking condition state in Box Girder Bridges	59
Figure 4.1: Location of selected WIM stations in California	64
Figure 4.2: iAnalyze Software Information	64
Figure 4.3: California WIM site locations based on FHWA data.....	67
Figure 4.4: Satellite pictures of FHWA WIM station location.....	67
Figure 4.5: Traffic trends for WIM station 129000 for 12 traffic lanes.	68
Figure 4.6: Traffic trends for WIM station 129000 for 12 traffic lanes, and vehicles class 5 and 9.	68
Figure 4.7: Traffic trends for WIM station 129000 for 12 traffic lanes, and vehicles class 6 and 11.....	69
Figure 4.8: Traffic trends for WIM station 49000for 8 traffic lanes.	69
Figure 4.9 Traffic trends for WIM station 129000 for 8 traffic lanes, and vehicles class 5 and 9.	70
Figure 4.10: Traffic trends for WIM station 49000 for 4 traffic lanes and vehicles class 6 and 11.	70
Figure 4.11: RAW vs. duplicated WIM records in California.....	72
Figure 4.12: S-shaped CDF for a normal random variable. Adapted from Nowak and Collins (2012).....	75
Figure 4.13: Interpretation of a straight-line plot on normal probability paper in terms of mean and standard deviation. Adapted from Nowak and Collins (2012)	76
Figure 4.14: CDF plot of GVW for selected WIM stations in California for 2014.....	77
Figure 4.15: CDF plots of GVW for the selected WIM stations in California for 2017.	78
Figure 4.16: CDF plots of GVW for various vehicle classes in California for 2017	79
Figure 4.17: CDF plot for the second axle load, WIM 072-Bowman, California, 2014-2018.....	80
Figure 4.18: CDF plot for the fifth axle load, WIM 072-Bowman, California, 2014-2018.	80
Figure 4.19: CDF plot of WIM truck/HL93 moment ratio in California for 2015.....	81
Figure 4.20: CDF plot for WIM truck/HL93 moment ratio in California for 2016.....	82
Figure 4.21: Influence lines for Moment, 3 Box Model	83
Figure 4.22: Typical section bridge 02 0036L, Inspection Report from Caltrans	84

Figure 4.23: Response of Concrete to uniaxial loading condition: (a) Compression, (b) Tension (Hafezolghorani et al., 2017)	85
Figure 4.24: Material input data in Abaqus,(Abaqus, 2020)	85
Figure 4.25: Simplified Cross Section of RC Bridge 02 0036L.....	86
Figure 4.26: 3D Model View of 02 0036L Bridge, Abaqus.....	86
Figure 4.27: Mesh of Cross Section of the Bridge Model	87
Figure 4.28: 3D Meshed Finite Element Model	88
Figure 4.29: Reinforcement Detail of FEM Model	88
Figure 4.30: 2 Truck Loads applied in 3D FEM model.....	89
Figure 4.31: Load cases for transverse stress.....	89
Figure 4.32: Stress in the transverse direction in the bridge model, Load Case 2.....	90
Figure 4.33: Summary of transverse stresses in top fiber of the deck from load cases.	90
Figure 5.1: Table 10-20.1(b) from MTD 10-20 Attachment 2(Caltrans, 2017b)	92
Figure 5.2: Deck Slab Reinforcement Details (Caltrans, 2017b)	93
Figure 5.3: As-built vs. MTD Drop-Off Distance for the truss bar. Bridges with some deck maintenance reported (left), bridges without deck maintenance reported (right).....	94
Figure 5.4: Cross section used in the FEM analysis, 4-cell box girder bridge example.....	95
Figure 5.5: 4 Box girder bridge moving load - Moment envelope	95
Figure 5.6: Flexural analysis of deck in conditions before and after truss bar drops.	97
Figure 5.7: R/C Continuous Box Girder Bridge 02 0036L analysis example.	98
Figure 5.8: 28C0228 P/C Continuous.....	98
Figure 5.9: 37 0368L P/C Simple.	99
Figure 5.10: 08 0163 P/C Continuous.	99
Figure 5.11: 28 0322K R/C Continuous.	100
Figure 5.12: 33 0212L P/C Continuous.....	100
Figure 5.13: 33 0585 P/C Continuous.	101
Figure 5.14: 37 0366L P/C Continuous.....	101
Figure 5.15: 56 0362 P/C Continuous.	102
Figure 5.16: As-built vs. Required Drop-Off distance.	103
Figure 5.17: Main Reinforcement Details	104
Figure 5.18: As-built vs MTD Steel Reinforcement in Box Girder Bridges	105

Figure 5.19: Cracking control required spacing vs. Tensile stress in steel reinforcement at Service Limit State.....	106
Figure 5.20: Tensile Stress in Reinforcement at Service Limit State vs. Box Girder Spacing ..	107
Figure 5.21: Transverse Deck Reinforcement Diagrams (Caltrans, 2015).....	107
Figure 5.22: Detail 5-10 Main Reinforcement Distribution	108
Figure 5.23: Detail 5-10 Before (top) and After (bottom), the bar drops down.	108
Figure 5.24: Main reinforcement spacing Required vs. As-built before and after truss bar drops.	109
Figure 5.25: Transverse crack width vs box girder bridge age.....	111
Figure 5.26: Transverse crack width vs top shrinkage and temperature reinforcement	112
Figure 5.27: Typical reinforced concrete deck cross section (Caltrans, 2015).....	113
Figure 5.28: S&T reinforcement distribution of box girder bridges sample.	113
Figure 5.29:S&T reinforcement spacing comparison by state.....	115
Figure 5.30: S&T steel reinforcement amount per state.	115
Figure 5.31: Restrained shrinkage in concrete (Adapted from ACI 224R-01 R08)	117
Figure 5.32: Steel reinforcement for S&T in concrete deck.....	118
Figure 5.33: S&T distribution if 50% of required amount is distributed in top and bottom layers.	119
Figure 5.34: S&T Reinforcement configuration proposed.	119
Figure 6.1: Typical Cross Section (Caltrans, 2021).....	122
Figure 6.2: Typical Instrument Cluster Diagram at Markham Ravine Bridge (WJE Associates, 2011)	123
Figure 6.3: Location of instrument clusters, 32 ft from CL support at Markham Ravine Bridge (WJE Associates, 2011)	123
Figure 6.4: Thermocouples data – Markham Ravine bridge	124
Figure 6.5: Concrete deck temperature selected	124
Figure 6.6: Typical Cross Section.....	125
Figure 6.7: Thermocouples data – Olive Lane Bridge.....	126
Figure 6.8: Concrete deck temperature selected	126
Figure 6.9: 3D and 2D View of FEM model – Markham Bridge.....	132
Figure 6.10: Simulated and measured deck strains.....	133

Figure 6.11: Simulated and measured deck strains.....	134
Figure 6.12: Degree of restraint in concrete (Frosch et al., 2006).....	135
Figure 6.13: Longitudinal restraint factors over time for Markham Bridge at location A.	136
Figure 6.14: Longitudinal restraint factors over time for Markham Bridge at location A.	136

LIST OF TABLES

Table 1-1: Percentage of deck structure type vs. superstructure type (Adapted from NBI, 2022).	2
Table 1-2: Deck Condition Coding Guide (FHWA, 1995).....	4
Table 1-3: Total number of bridges and structurally deficient percentages per state (Adapted from NBI, 2022)	5
Table 1-4: Percentage of CIP Concrete Deck and CIP Concrete Deck Area Ratio (Adapted from NBI, 2022)	8
Table 1-5: SNBI deck reinforcing protective system specification (FHWA, 2022).....	9
Table 3-1: Bridge Structural Type vs. Material Type.....	44
Table 3-2: Bridge Structural Type vs. Deck Structural Type	45
Table 3-3: Bridge type vs. bridge deck condition rating.	49
Table 3-4: Bridge type vs. superstructure condition rating.....	50
Table 3-5: Statistics of bridge material type vs. deck condition rating.	51
Table 3-6: Condition State to address cracking in decks (Caltrans, 2000).....	56
Table 3-7: Condition state per Caltrans bridge element inspection manual (Caltrans, 2017a)	56
Table 3-8: Selected Box Girder Bridge Database (R/C : Reinforced Concrete; P/C : Prestressed Concrete; Cont. : continuous span; Simple : simple span)	61
Table 4-1: Number of RAW and duplicated WIM records for selected sites in California	73
Table 4-2: Summary of WIM quality control analysis.	74
Table 5-1: Equivalent Strip Method for Live Load Moments	96
Table 5-2: Summary of Drop-Off distance analysis of Box Girder Bridges	102
Table 5-3: Main Reinforcement in other states with empirical design.....	105
Table 5-4: Comparison of deck design provisions for shrinkage and temperature for several states.	114
Table 6-1: Design Mixture Markham Bridge (WJE Associates, 2011).....	122
Table 6-2: Design Mixture Olive Lane Bridge (WJE Associates, 2011)	125
Table 6-3: Bridge Data for Design Thermal Movement.....	127
Table 6-4: Shear stiffness for bearing modeling.....	128
Table 6-5: Concrete Deck Material Properties and Creep Parameters	131
Table 6-6: Shrinkage Parameters	131

CHAPTER 1. INTRODUCTION

1.1 Highway Bridges in the United States

Bridges are an essential infrastructure of the national transportation network. In the year 2022, there were on inventory 620,669 bridges and culverts in the United States of America Highway Network reported by state agencies to the National Bridge Inventory (NBI), which is managed by the Federal Highway Administration (FHWA). The American Road & Transportation Builders Association (ARTBA) estimated in the 2022 bridge report that 36% of the U.S. bridges need repair and that approximately 78,800 bridges should be replaced. Premo (2022) reports that at the current pace of repair and rehabilitation of bridges, it would take almost 30 years to repair them.

1.1.1 Bridge Statistics in the United States

The public NBI data allows agencies and researchers to analyze the reported bridge information. In Table 1-1, the percentage of bridges according to the structural deck type and the superstructure type is shown. NBI data for 2022 shows that more than 53% of the U.S bridges are either of concrete or prestressed concrete superstructures. The bridge information reported by the different state agencies to the NBI also shows that only 25% of the bridge structures are built as continuous superstructures between concrete, prestressed concrete, and steel.

Approximately 76.7% of the reported number of bridges and culverts corresponds to bridge structures, approximately 475,000 bridges. The distribution of different types of deck, from the NBI data (NBI, 2022) is shown in Figure 1.1, and it shows that around 338,000 bridges (71%) in the U.S. have a Cast-in-Place (CIP) reinforced concrete deck and 65,000 bridges (14%) have concrete precast panels.

Table 1-1: Percentage of deck structure type vs. superstructure type (Adapted from NBI, 2022)

Structure Material	Deck Structural Type			Total
	Concrete CIP	Concrete Precast Panels	Wood/Timber	
Other	0%	0%	0%	0%
Concrete	12%	4%	0%	18%
Concrete Continuous	10%	0%	0%	10%
Steel	16%	0%	3%	22%
Steel Continuous	10%	0%	0%	11%
Prestressed Concrete	18%	9%	0%	29%
Prestressed Concrete Continuous	5%	0%	0%	6%
Wood or Timber	0%	0%	3%	3%
Masonry	0%	0%	0%	0%
Aluminum or Iron	0%	0%	0%	0%
Total	71%	14%	7%	100%

Note: The table does not show all superstructure or deck structure types, but percentages are related to all bridges. Cont.: continuous structures. NBI differentiates superstructure material as simply supported and continuous for Concrete, Prestressed Concrete (P/C) and Steel.

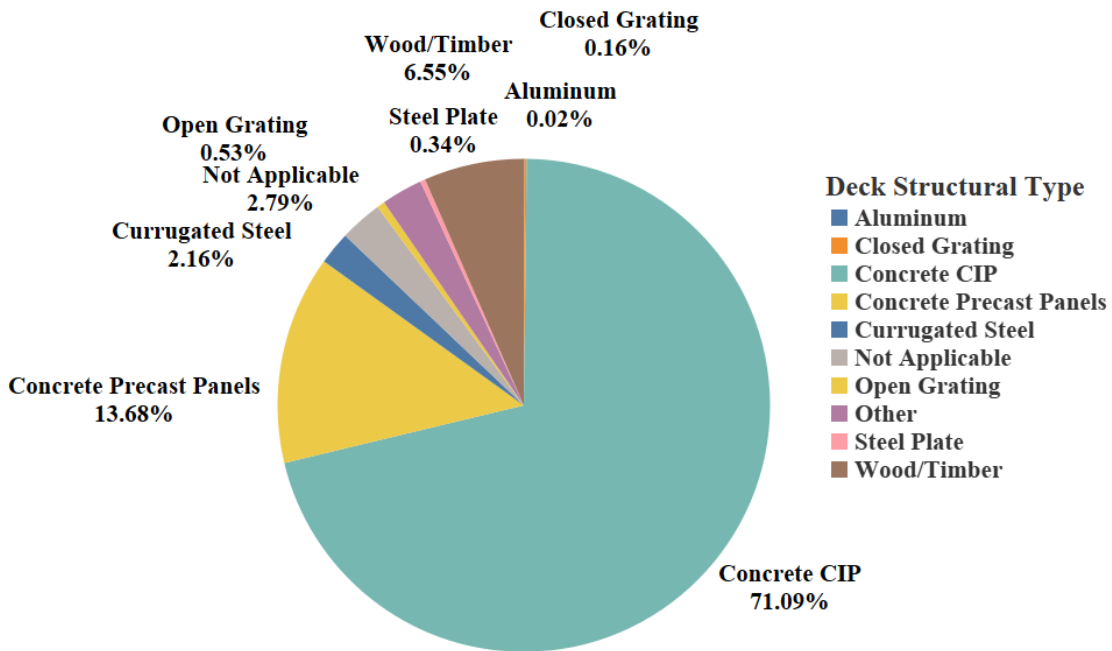


Figure 1.1: Deck Type Distribution as of 2022 in the US (Adapted from NBI, 2022)

The NBI data shows that the most common deck structure selected by bridge designers or owners is the reinforced concrete CIP. Figure 1.2 shows the distribution of the deck protection system defined by the NBI Coding Guide of 1995. Approximately 65% of the concrete CIP bridge decks do not report any protective system for the reinforcing steel, while almost 27% of these bridge decks report having epoxy-coated reinforcing steel as a protective system.

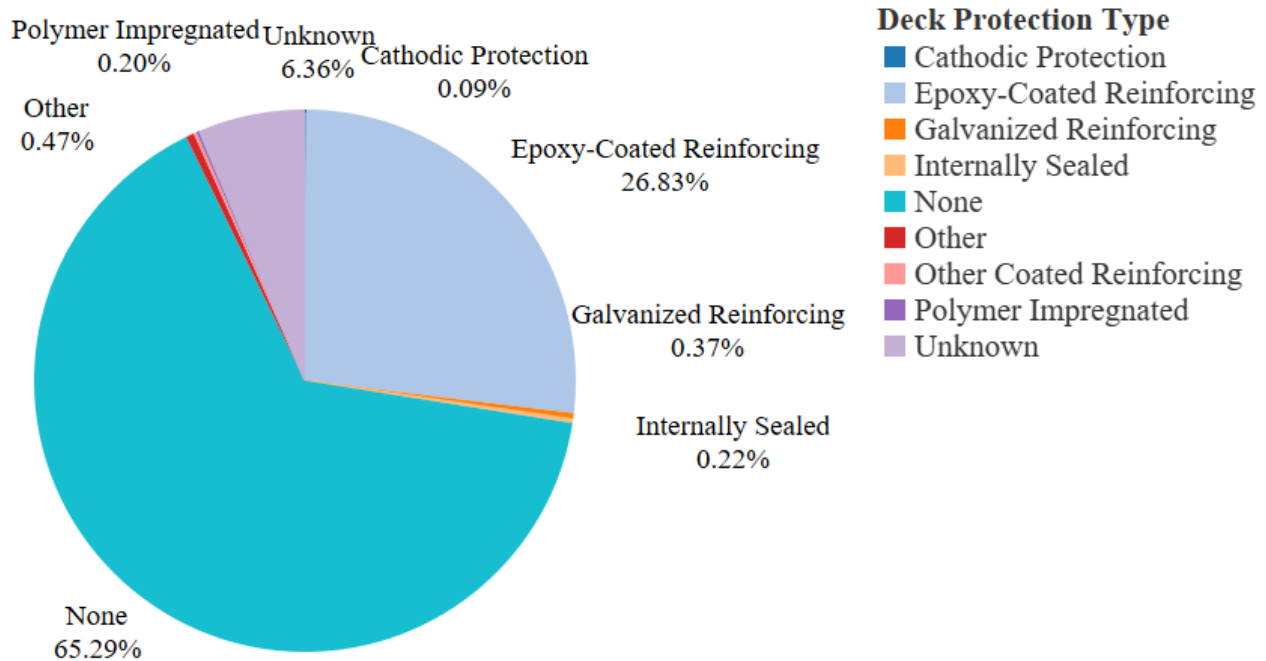


Figure 1.2: Deck protection type for Concrete CIP Bridge Decks (Adapted from NBI, 2022)

1.1.2 Bridge Condition in the United States

The National Bridge Inspection Standards (NBIS) program started in 1968 as a part of the Federal-Aid Highway Act. The objective of this program was to set a national standard for proper safety inspection and evaluation of all highway bridges. ASCE (2021) reports that almost 42% of all bridges are at least 50-years old and that 7.5% of the total bridges are considered structurally deficient. It has been estimated that between 160 and 180 million trips are taken across these structurally deficient bridges every day.

The NBI reports in the year 2022 that about 6.9% or 43,000 bridges and culverts are classified as Structurally Deficient (SD), meaning that bridge deck, superstructure, substructure, or culverts are in poor or below condition (see Table 1-2) according to the NBI Coding Guide (FHWA, 1995).

Table 1-2: Deck Condition Coding Guide (FHWA, 1995)

Code	Description	
N	NOT APPLICABLE	
9	EXCELLENT CONDITION	
8	VERY GOOD CONDITION	No problems noted.
7	GOOD CONDITION	Some minor problems.
6	SATISFACTORY CONDITION	Structural elements show some minor deterioration.
5	FAIR CONDITION	All primary structural elements are sound but may have minor section loss, cracking, spalling or scour.
4	POOR CONDITION	Advanced section loss, deterioration, spalling or scour.
3	SERIOUS CONDITION	loss of section, deterioration, spalling or scour have seriously affected primary structural components. Local failures are possible. Fatigue cracks in steel or shear cracks in concrete may be present.
2	CRITICAL CONDITION	Advanced deterioration of primary structural elements. Fatigue cracks in steel or shear cracks in concrete may be present or scour may have removed substructure support. Unless closely monitored it the bridge until corrective action is taken. may be necessary to close
1	"IMMINENT" FAILURE CONDITION	Major deterioration or section loss present in critical structural components or obvious vertical or horizontal movement affecting structure stability. Bridge is closed to traffic, but corrective action may put back in light service.
0	FAILED CONDITION	Out of service - beyond corrective action.

Table 1-3 shows the total amount of bridges and the percentage of structurally deficient bridges in each state. There is a wide range of percentages, from 1.5% in Delaware to almost 23% in Iowa. The highest percentages of structurally deficient bridges are in the Central North part of the U.S, specifically in Iowa, South Dakota, and North Dakota. In the East, a high percentage is reported in West Virginia, with almost 21%.

Table 1-3: Total number of bridges and structurally deficient percentages per state (Adapted from NBI, 2022)

State	Total Bridges	Structurally Deficient [%]	State	Total Bridges	Structurally Deficient [%]
Alabama	9,729	5.40	Nebraska	11,122	10.54
Alaska	1,521	8.22	Nevada	1,194	1.93
Arizona	3,763	2.55	New Hampshire	2,245	7.62
Arkansas	9,446	6.84	New Jersey	6,182	7.21
California	22,275	6.66	New Mexico	2,210	8.10
Colorado	6,884	5.98	New York	15,493	9.88
Connecticut	3,680	5.27	North Carolina	13,638	8.26
Delaware	669	1.49	North Dakota	3,087	13.93
District Of Columbia	247	1.62	Ohio	25,056	4.55
Florida	10,240	3.74	Oklahoma	15,665	12.11
Georgia	9,357	2.83	Oregon	7,810	5.03
Hawaii	987	6.89	Pennsylvania	20,217	14.84
Idaho	4,430	5.21	Rhode Island	742	17.12
Illinois	21,977	10.18	South Carolina	8,310	5.57
Indiana	17,062	5.60	South Dakota	4,334	21.44
Iowa	19,069	22.97	Tennessee	11,210	6.59
Kansas	16,437	6.82	Texas	34,912	1.95
Kentucky	11,441	8.06	Utah	2,418	2.52
Louisiana	10,169	14.88	Vermont	2,605	2.57
Maine	2,108	14.85	Virginia	10,831	4.03
Maryland	4,148	5.28	Washington	7,835	5.32
Massachusetts	4,928	8.83	West Virginia	6,767	20.85
Michigan	9,355	11.68	Wisconsin	12,202	6.78
Minnesota	7,425	6.56	Wyoming	2,626	7.50
Mississippi	12,845	8.37	Guam	43	18.60
Missouri	19,227	10.64	Puerto Rico	1,998	14.26
Montana	4936	7.21	Virgin Islands	13	30.77

The FHWA defines general bridge conditions as Good(G), Fair (F), and Poor(P) in accordance with Pavement and Bridge Condition Performance Measures (PBCPM) final rule (FHWA, 2017). The condition is determined by the lowest condition rating reported by state agencies for the deck, superstructure, substructure, and culvert. If the lowest condition rating is greater or equal to 7, the bridge is classified as Good; if any item is rated 4 or lower, the bridge structure is classified as Poor, and all other cases are classified as Fair. Historically, as shown in Figure 1.3, it can be seen that the percentage of bridges in Good condition has been decreasing in

the past 14 years from 47.5% to 44.5%, a 3-point difference which follows a slow tendency to keep decreasing over time. During the same period, the bridges in Fair condition have been increasing from 42% to more than 48%, and at a faster rate in the past 6 years. Figure 1.4 shows the percentage of bridges in poor condition in the past 14 years. Between years 2009 and 2015, the number of bridges in Poor condition decreased by almost 2 percentage points, while from 2016 to 2022, there has only been a reduction of 1 percentage point. Number of bridges is shown in labels for both Figure 1.3 and Figure 1.4 for selected years.

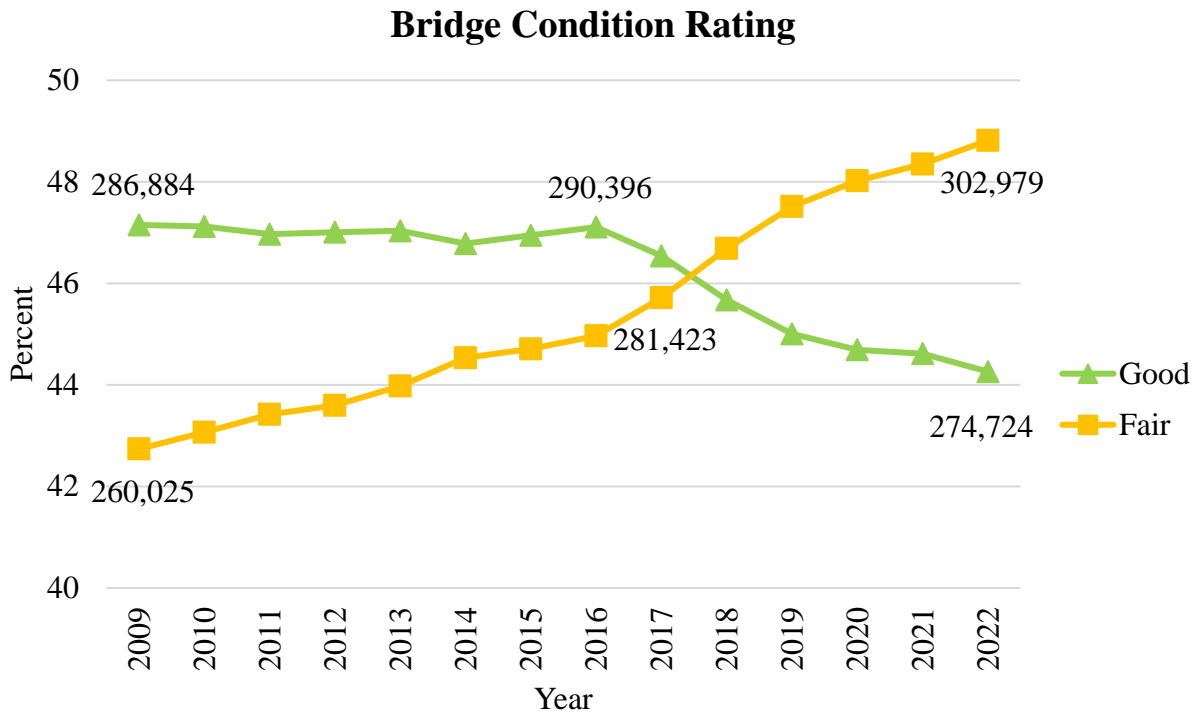


Figure 1.3: Bridge condition percentage (Adapted from NBI 2009-2022)

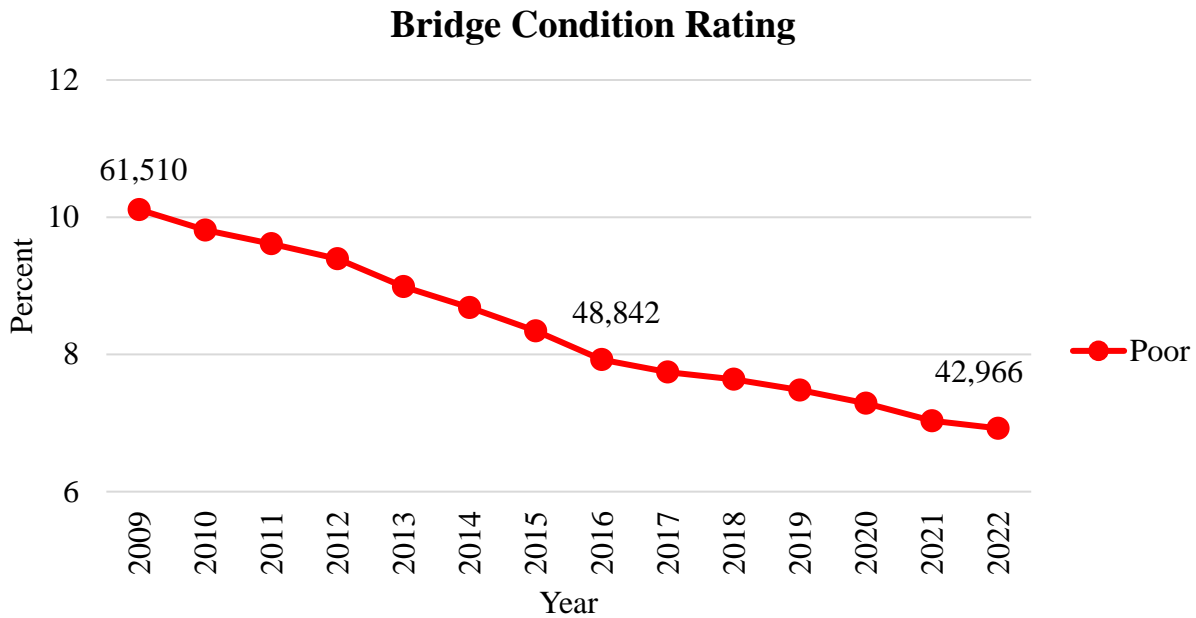


Figure 1.4: Bridge condition percentage (Adapted from NBI 2009-2022)

Table 1-4 shows the percentage of bridges with a CIP concrete deck and the percentage of deck area corresponding to CIP concrete in reference to the total amount of bridges and total bridge deck area, respectively, for each state. The data shows that even though a state could have a low percentage of CIP concrete bridge decks, the CIP concrete deck area ratio is quite large, like Alabama, Kentucky, or West Virginia. The highest CIP concrete deck area ratio percentages are found in California, the District of Columbia, Nevada, Oklahoma, and Wisconsin.

CIP reinforced concrete bridge decks are key structural elements that support live loads, providing the riding surface for traffic. It also suffers the most frequent distress due to its use and environmental exposure. Table 1-4 shows the percentage of bridges with CIP reinforced concrete decks and the CIP deck area ratio for each state. The NBI data presented in Figure 1.1 and Table 1-4 show that CIP reinforced concrete bridge decks are the most common deck solutions for bridges in the U.S., with some differences between states, but still the most wide used deck structure. Even with this information, the NBI data does not report detailed information on the

structural elements and their design, which makes it more challenging to evaluate the data properly.

Table 1-4: Percentage of CIP Concrete Deck and CIP Concrete Deck Area Ratio (Adapted from NBI, 2022)

State	CIP Deck [%]	CIP Deck Area Ratio [%]	State	CIP Deck [%]	CIP Deck Area Ratio [%]
Alabama	68	89	Nebraska	73	91
Alaska	19	37	Nevada	93	98
Arizona	92	95	New Hampshire	75	90
Arkansas	69	90	New Jersey	80	88
California	91	96	New Mexico	81	95
Colorado	61	74	New York	62	79
Connecticut	71	88	North Carolina	54	82
Delaware	83	97	North Dakota	53	83
District of Columbia	94	99	Ohio	80	94
Florida	74	89	Oklahoma	90	98
Georgia	82	94	Oregon	52	82
Hawaii	92	91	Pennsylvania	76	91
Idaho	62	87	Rhode Island	72	89
Illinois	46	79	South Carolina	50	85
Indiana	69	89	South Dakota	59	85
Iowa	74	93	Tennessee	67	72
Kansas	67	65	Texas	73	65
Kentucky	66	92	Utah	75	88
Louisiana	65	85	Vermont	80	91
Maine	82	88	Virginia	70	87
Maryland	80	90	Washington	63	89
Massachusetts	74	84	West Virginia	48	88
Michigan	75	92	Wisconsin	93	97
Minnesota	80	94	Wyoming	76	93
Mississippi	56	85	Guam	67	69
Missouri	87	92	Puerto Rico	97	94
Montana	47	83	Virgin Islands	92	82

As of 2022, the Federal Highway Administration (FHWA) is transitioning from Recording and Coding Guide for the Structure Inventory and Appraisal of the Nation’s Bridges (NBI Coding Guide) to the Specifications for the National Bridge Inventory (SNBI) (FHWA, 2022). The new specification was developed in coordination with the American Association of State Highway and

Transportation Officials (AASHTO) for the update of standards such as the Manual for Bridge Evaluation (MBE), AASHTO Manual for Bridge Element Inspection, and the FHWA Bridge Inspector Reference Manual (BIRM).

The new specifications are extensively more detailed than the previous Coding Guide of 1995. Specifically, State Departments of Transportation (DOTs) are required to report deck interaction, material and type, wearing surface, protective system, reinforcing protective system, and stay-in-place forms (FHWA, 2022). The deck reinforcing protective system was not reported in previous editions of the NBI. State agencies are required to report the type of deck reinforcing protective system as shown in Table 1-5, which now are 17 different classifications (9 in the previous Coding Guide), including several types of fiber-reinforced polymers. The additional details required by the SNBI will expand the knowledge of built bridges and might improve the evaluation of bridge decks.

Table 1-5: SNBI deck reinforcing protective system specification (FHWA, 2022)

Code	Description
0	None
C01	Coating – Epoxy Coated
C02	Coating – Galvanized
C03	Coating – Metalized
CX	Coating – Other
R01	Reinforcing – Stainless, Clad
R02	Reinforcing – Stainless, Solid
R03	Reinforcing – High Chromium
R04	Reinforcing – FRP, Aramid Fiber
R05	Reinforcing – FRP, Carbon Fiber
R06	Reinforcing – FRP, Glass fiber
R07	Reinforcing – FRP, Other
RX	Reinforcing – Other
S01	Sacrificial – Cathodic, Passive
S02	Sacrificial – Cathodic, Active
SX	Sacrificial – Other
X	Other

1.1.3 Cracking in Concrete Decks

Cracking in concrete has been historically studied based on the tensile stresses due to loads that the concrete members can support. Tensile strength depends on the concrete constituent materials and curing environment, and it increases with age. Tensile stresses primarily cause most cracks due to internal or external restraint produced by temperature or shrinkage differentials (Leonhardt, 1977).

Cracks in concrete decks caused by external loads are generally flexural, or shear cracks that occur after the concrete deck has hardened. Types of cracks that are not dependent on external loading include plastic shrinkage, plastic settlement, autogenous shrinkage, drying shrinkage, thermal, and map or pattern (Russell, 2017). The most common cracks can be described by their orientation, such as longitudinal, transverse, diagonal, or random.

Plastic shrinkage cracking, Figure 1.5, occurs near the surface of the fresh concrete when the moisture is lost by evaporation at a faster rate than when it is replaced by bleed water (Mehta and Monteiro, 2014). Mindess et al. (2002) states that when water is removed from the paste from evaporation, capillary pressures arise within the paste until they reach a critical pressure, at which point the maximum rate of plastic shrinkage can be expected. Plastic shrinkage cracking is a problem for large flat structures, such as bridge decks and pavements, in which the exposed surface area is high relative to the volume of the placed concrete (TRB, 2006).

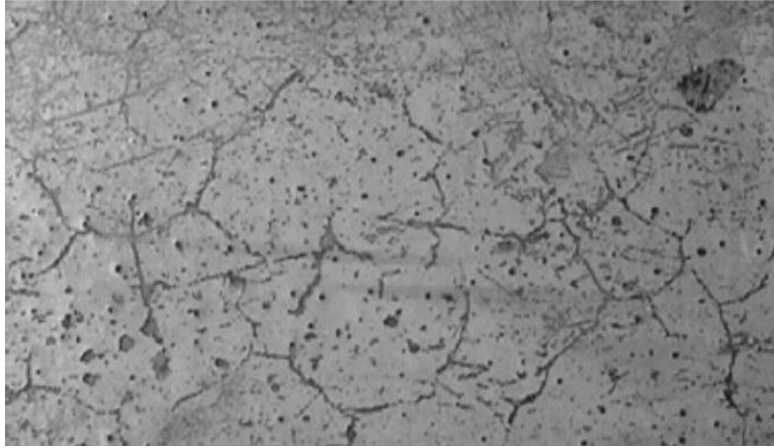


Figure 1.5: Plastic shrinkage cracking in freshly placed concrete (Mehta and Monteiro, 2014)

In 1961, a study on concrete deck durability performed by the Portland Cement Association (PCA) in association with 10 state highway departments found after surveying more than 1,000 bridges that transverse cracking, Figure 1.6, was the most common type of crack, and it is mentioned that shrinkage and thermal volume changes in concrete might be the primary factors producing transverse cracking (Freyermuth et al., 1970).



Figure 1.6: Typical deck transverse cracking (Adapted from Russell, 2004)

It has been recognized that cracks perpendicular to reinforcement are subjected to a faster rate of corrosion by facilitating the ingress of moisture, oxygen, and chloride ions to the reinforcement. Corrosion of the reinforcing steel is one of the major factors in concrete deterioration, reducing the serviceability of the structure in regard to safety, stability, and aesthetics (Alexander and Beushausen, 2019).

Russell (2017) sent a survey to state agencies to evaluate the frequency and type of cracking experienced in the past 5 years in CIP concrete bridge decks. More than 50% of the agencies reported that cracks occurred frequently. The survey observed that most agencies specify minimum compressive strength, the minimum and maximum temperature at placement, maximum w/cm ratio, maximum slump, and minimum curing period. Some agencies also reported that high early-age concrete strength, high-strength concrete, silica fume, larger cement content, fly ash, and evaporation retardant contributed to increased deck cracking. The NCHRP Synthesis #500, developed by Russell (2017), shows the different effects observed by agencies and researchers due to concrete constituent materials, construction practices, and reinforcement type on cracking. Restrained concrete shrinkage is mentioned as one of the major factors in early-age transverse cracking.

The condition rating assigned by the NBI to decks, superstructure, substructure, and culverts is fair (Code 5) when the structural element is showing cracks. With this criteria, approximately 52,000 or 16% of CIP concrete bridge decks in the U.S. show cracking issues (NBI, 2022). In California, one of the states with the highest CIP concrete deck area ratio (96%) and the one with the most CIP concrete bridge decks (20,314), the number of bridges in Fair or Poor condition is about 30%.

1.1.4 Transportation and Infrastructure Spending in the U.S.

In 2015, the Fixing America's Surface Transportation Act or FAST Act was the first Federal law providing long-term funding for surface transportation. This Act authorized \$305B over 5 fiscal years, 2016-2020. \$35B were apportioned to the National Highway Performance Program (NHPP) and the Surface Transportation Block Grant (STBG), both programs that aid

flexible funding to be used by state agencies to preserve, repair and improve bridge and tunnels on any public road.

In 2021, the Bipartisan Infrastructure Law was signed with the objective to improve the condition of the transportation infrastructure of the country. More than \$27.5B destined to state and tribal transportation agencies to repair or rehabilitate 15,000 bridges nationwide over five years. It also provides with the creation a of new Bridge Investment Program (BIP) with \$12.5B, which is a program focused on reduced the overall number of bridges in poor condition, or in fair condition at risk of falling into poor condition.

Figure 1.7 shows the transportation and infrastructure spending since 2009 by state, local, and federal agencies. State and local agencies have increased their spending continuously since 2011, reaching \$191B in 2019. Federal direct spending increased in almost \$40B from 2019 to 2020. This information shows that even though federal, state, and local agencies have increased the funding for transportation and infrastructure, the condition of bridges has not improve as expected. The bridges in fair condition keep increasing over time, and the bridges in poor condition decrease at a very slow rate over the years, with risk of having more in the future as the fair condition bridges keep increasing.

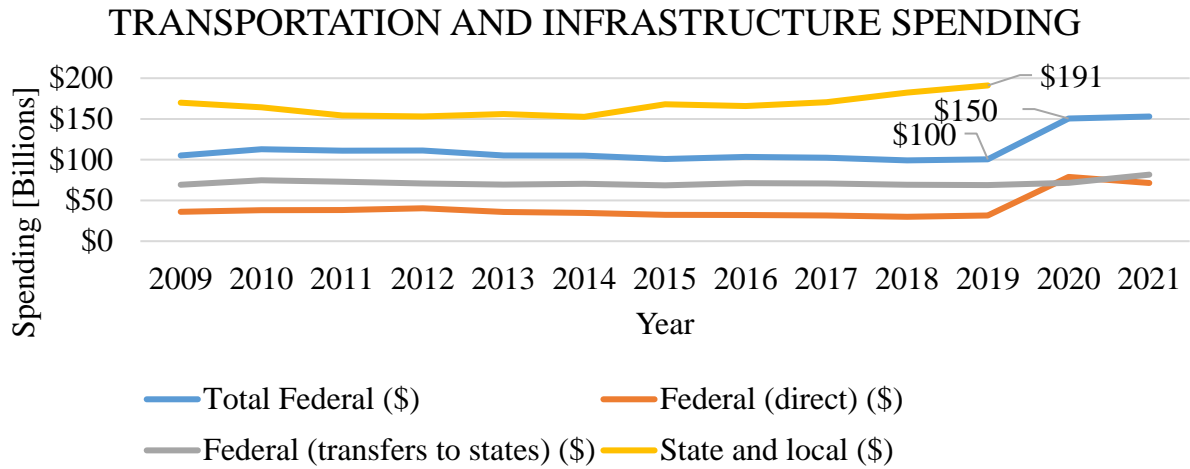


Figure 1.7: Transportation and infrastructure spending (Adapted from USAFacts (2022))

1.2 Motivation and Goals

In 1970, it was published the NCHRP Synthesis of Highway Practice #4: Concrete Bridge Deck Durability (Copas, 1970). This report was the first document that synthesized the current practice throughout the different Highway State Agencies. At this time, deck deterioration was already a major maintenance problem, but the magnitude of it was not fully understood. Copas (1970) reported that the most common conditions in bridge decks were cracking, scaling, and spalling.

In the following decades, three more synthesis reports were developed with regard to concrete durability, deck performance, and cracking control in bridge decks (Copas and Pennock, 1979; Russell, 2017, 2004). State agencies responded to these research efforts with excellent and valuable information to draw conclusions and recommendations on how to improve the condition of newly designed bridges based on their respective performance evaluation. Based on the collected data, the number of structurally deficient bridges has decreased slowly in the last decade, but the number of bridges in fair condition has rapidly increased in the past 14 years, while bridges in good condition have continuously decreased since 2009. ASCE (2021) estimates that the nation's backlog of bridge repair needs is \$125B and that only for rehabilitation, there is a need for increased spending from \$14.4B to \$22.7 annually. Then in 2022, the Bipartisan Law became effective and additional funding was allocated for repair and rehabilitation, but the problem of early-age poor performance is still there. Consequently, there is a need to evaluate more variables influencing the performance of bridges, such as traffic, reinforcing detailing, and restraining effects.

Bridges are subjected to heavy traffic, which includes traffic volume, high weight of permit or overloaded vehicles, and different axle configurations. Weigh-in-motion (WIM) data collected

by state and local agencies can be used to assess the traffic in a particular location. In California, concrete box girder bridges represent almost 41% (8,269) of the total CIP concrete deck bridges, and from these 8,269 bridges, 4,286 or 52% are in Fair or Poor conditions, according to the NBI 2022 data. It is unclear if live loads in bridge decks significantly affect the poor performance observed in California. Still, the availability of the WIM database has made possible the analytical evaluation of concrete bridges.

Public access to design guidelines and standards has made possible the assessment of current concrete deck design practices from the different state agencies. The bridge inspection reports, which are the basis of the information reported to the National Bridge Inventory, serve as a starting point for the analysis and evaluation of bridge decks. The information that can be gathered through the revision of inspection reports and design guidelines has made it possible for this study to identify, compare, and recommend changes to the current practice of bridge deck design. The main goal of this research is to first use the WIM database of California to assess the level of traffic for the analytical evaluation, secondly, review old and new design guidelines and standard codes that are used for bridge deck design to find the possible causes affecting the performance of bridge decks for service and strength limit states, and thirdly, evaluate the level of restraint provided by box girders to the CIP concrete decks using finite element model to assess the early-age behavior of CIP concrete, the development of tensile stresses due to temperature changes and develop restraining factors for box girder bridges.

1.3 Research Objectives

The primary research objectives for this dissertation are outlined below:

- Determine structural bridge types with the most cracking issues in California using the NBI database and FHWA criteria to identify the poor-performance bridges.
- Develop an analytical procedure to evaluate the effect of live loads in California box girder bridges using WIM data and finite element methods
- Examine deck design provisions to assess possible causes of poor performance of bridge CIP concrete decks.
- Assess the level of deterioration of CIP concrete decks by evaluating cracking data and reinforcement detailing provisions.
- Model restraining effects of post-tensioned box girders in CIP concrete decks with finite element methods, including the development of material properties at early ages of concrete.

1.4 Dissertation Organization

This dissertation is divided into seven chapters as follows:

- Chapter 1 – Introduction: This chapter provides general background on the current condition of bridges in the U.S. and shows the importance of bridge deck cracking and maintenance costs in the U.S. The motivation for this research and its objectives are provided. The organization of content within this dissertation is also outlined.
- Chapter 2 – Literature Review: This chapter describes the current practice of bridge deck design and construction in the U.S., the live load effects on decks, and describes several studies performed in the past to evaluate the deterioration of concrete bridge

- decks. It also presents the basics behind the degree of restraint in concrete elements and the development of concrete material properties.
- Chapter 3 – Bridge Statistics and Selection of Representative Structures: This chapter details the statistical analysis performed with the NBI data of California to find the most critical structures that have poor performance at early and later ages.
 - Chapter 4 – Live Load and Effects on Bridges: This chapter details the available WIM database used to assess the traffic volume and configuration of several sites in California. Live loads and configurations established from the WIM database are used in 3D and 2D finite element models. Influence lines for bridge decks are developed in order to assess the most critical scenarios and evaluate the loading effects in the bridges.
 - Chapter 5 – Cast-in-Place Bridge Deck Reinforcement Analysis: This chapter details the analysis performed on bridge decks using cracking data from inspection reports of box girder bridges. Finite element models were used to assess the level of flexural demand on bridge decks to evaluate the effectiveness of as-built bridge deck reinforcing details for service and strength limit states.
 - Chapter 6 – Development of Restraining Factors: This chapter shows the procedure developed to model the early-age behavior of CIP concrete decks. Field data from 2 box girder bridge decks were used to evaluate the level of restraint that box girders provide to the concrete deck.
 - Chapter 7 –Conclusions and Recommendations: This chapter summarizes the research conclusions covered in this dissertation. In addition, the relevance of research findings to practicing engineers and potential opportunities for future research are discussed.

CHAPTER 2. LITERATURE REVIEW

2.1 Introduction

Relevant research and design standard provisions are summarized in this literature review. The review includes the standard design provisions used for CIP concrete bridge decks, live load effects in concrete decks, research performed in the past regarding concrete deck cracking and deterioration, and the factors affecting the development of concrete material properties and degree of restraint.

2.2 Bridge Deck Design

Bridges in the United States are designed in accordance with the standard specifications published by the American Association of State Highway and Transportation Officials (AASHTO). AASHTO (2020) published the AASHTO LRFD Bridge Design Specifications, 9th Edition (hereafter AASHTO LRFD). These specifications provide the minimum standards for highway bridge design according to the Code of Federal Regulations (23 CFR § 625.4). The FHWA, through a policy, requested that all bridges designed after 2007 shall be designed on the Load and Resistance Factor (LRFD) method. Since each Department of Transportation has developed design guidelines using as a basis what is published in the AASHTO LRFD and peer-reviewed research, the Code of Federal Regulations does not have a conflict with them.

The AASHTO LRFD includes in Chapter 9 the specifications for all deck and deck systems, specifically section 9.7 for concrete deck slabs, where the requirements of the different design methods are specified. Other sections of the specifications related to concrete structures and reinforcing minimum steel requirements are available.

2.2.1 Deck Design Methods

In general, state Departments of Transportation (DOTs) define their deck design philosophy according to the Traditional Design Method (TDM) or the Empirical Design Method (EDM), both from the AASHTO LRFD , articles 9.7.3 and 9.7.2, respectively (AASHTO, 2020). According to the available Design Manuals or Design Guidelines from state DOTs, only 14 states may use the Empirical Design Method.

2.2.1.1 Empirical Design Method

The EDM is based on extensive research where it was discovered that the primary structural action by which the slabs resist concentrated wheel loads is not flexure but a complex internal membrane stress state referred to as internal arching (AASHTO, 2020).

In AASHTO LRFD Article 9.7.2.4, design conditions are established for the purpose of using this design method. The conditions that are required to be satisfied to use the method are:

- Use of cross-frames or diaphragms throughout the cross-section at support lines;
- Use of Intermediate diaphragms between boxes, spaced not to exceed 25 ft.;
- Supporting components made of steel and/or concrete;
- Deck fully cast-in-place and water cured;
- Uniform depth deck, except for haunches;
- Effective length to design depth ratio between 6.0 and 18.0;
- Minimum depth of 7 in., excluding sacrificial wearing surface;
- Minimum core depth of 4 in.;
- Maximum effective length, per Article 9.7.2.3, of 13.5 ft.;
- Composite action of deck and supporting structural components;
- The specified 28-day concrete strength of the deck is not less than 4.0 ksi; and
- Overhang beyond centerline of the outside girder at least 5 times the depth of slab.

The EDM requires four layers of isotropic reinforcement. Reinforcement shall be provided in each face of the slab, with the outermost layers placed in the direction of the effective length. The minimum amount of reinforcement is 0.27 in.²/ft of steel for each bottom layer and 0.18 in.²/ft for each top layer. Spacing must be less than 18 in., and the use of Grade 60 steel is required (AASHTO, 2020)

The amount of reinforcement required by the EDM is substantially less than what is required by the TDM. Fang et al. (1986) conducted an experimental and analytical investigation for decks designed in accordance with the EDM and concluded that bridge decks having about 60% of the reinforcement required by the TDM perform satisfactorily under LRFD design live load levels.

Csagoly and Lybas (1989) confirmed that the load-carrying mechanism in concrete bridge decks is internal arching and not elastic plate bending. They also concluded that 0.3% isotropic reinforcement provides adequate serviceability, fatigue, and ultimate capacity.

Some DOTs require the use of EDM without additional requirements of minimum amount or spacing of steel reinforcement (DEDOT, 2021; MoDOT, 2022; PADOT, 2019; WVDOT, 2016). Other states that specify the EDM have some requirements regarding the size and spacing of reinforcement, and generally, the same steel reinforcement distribution for transverse and longitudinal directions (NEDOT, 2016; NYDOT, 2021; TXDOT, 2022; UDOT, 2017).

2.2.1.2 Traditional Design Method

The TDM, also known as the Equivalent Strip Method, is based on the assumption that the concrete deck works as a flexural component in the transverse direction. Design loads for the deck consist of dead loads of structural and non-structural components and vehicular live loads. The deck spans typically in the transverse direction, and flexural positive and negative moments are

analyzed using continuous elastic supports. The live load use in the analysis should be either the HL-93 design truck or design tandem loads. The live load effects may be determined using approximate methods of analysis, LRFD Article 4.6.2.1, in which the deck is subdivided into strips perpendicular to the supporting components. The strip width is dependent on the deck material and, for cast-in-place decks, is defined in Table 4.6.2.1.3-1 of LRFD as:

$$\begin{aligned} +M &: 26.0 + 6.6S \\ -M &: 48.0 + 3.0S \end{aligned} \qquad \text{Eq. 2.1}$$

where S is the spacing between the supporting components, and for overhangs, a different equivalent width is used.

The main reinforcement (transverse) is designed using conventional principles of reinforced concrete design, like a one-way slab. The design location for the positive moment region is usually taken at the midbay of the deck, while the negative design moment is usually located at one-half of the flange width from the centerline of the concrete girder.

Unfactored design live load moments are provided in Table A4-1 of the AASHTO LRFD. In this table, design moments are provided as a function of the spacing between girders for the positive moment and the distance of the centerline of the girder to the design section for the negative moment.

Article 9.7.3.2 of the AASHTO LRFD requires that distribution reinforcement shall be provided in the secondary direction as a percentage of the primary reinforcement as:

$$\begin{aligned} 100/\sqrt{S} \leq 50 \text{ percent} & \quad \text{for primary reinforcement parallel to traffic} \\ 220/\sqrt{S} \leq 67 \text{ percent} & \quad \text{for primary reinforcement perpendicular to traffic} \end{aligned} \qquad \text{Eq. 2.2}$$

where S is the effective span length as specified in Article 9.7.2.3, in feet.

2.2.2 Cracking Control Design Provisions and Recommendations

2.2.2.1 AASHTO

The AASHTO LRFD, in its article 5.6.7, defines the cracking control provisions for the service limit state by the distribution of steel reinforcement. Based on extensive laboratory work, the cracking width was found to be proportional to the steel stress and the most significant variables were the concrete cover thickness and the reinforcement spacing (AASHTO, 2020).

The provisions specified in this article shall apply to those sections where the concrete's tensile stresses exceed 80% of the concrete modulus of rupture defined in Article 5.4.2.6 (AASHTO, 2020). In Article 5.6.7 (AASHTO, 2020), the spacing s of nonprestressed reinforcement in the layer closest to the tension face is specified in:Eq. 2.3

$$s \leq \frac{700\gamma_e}{\beta_s f_{ss}} - 2d_c \quad \text{Eq. 2.3}$$

in which:

$$\beta_s = 1 + \frac{d_c}{0.7(h - d_c)} \quad \text{Eq. 2.4}$$

where:

γ_e = Exposure factor: 1.00 for Class 1, 0.75 for Class 2

β_s = Ratio of flexural strain at the extreme tension face to the strain at the centroid of the layer closest to the tension face.

f_{ss} = Tensile stress in nonprestressed reinforcement at service limit state, less than $0.60 f_y$ (ksi).

d_c = Thickness of concrete cover measured from extreme tension fiber to center of the flexural reinforcement.

h = Overall thickness or depth of the component.

Equation 2.3 is based on a physical crack model developed by Frosch (2001) and is expected to provide control of flexural cracking. The commentary C5.6.7 of AASHTO LRFD mentions that cracking could occur in reinforced concrete members due to any load condition, including effects or restraint of deformation, but it is also stated that the provisions presented in Article 5.6.7 are used for the distribution of tension reinforcement to control only flexural cracking (AASHTO, 2020).

Previous research indicates that there appears to be little or no correlation in the long term between crack width and corrosion (Beeby, 1983). However, the different classes of exposure conditions have been so defined to provide flexibility in the application of these provisions to meet the needs of the owner (AASHTO, 2020).

Article 5.10.6 of AASHTO LRFD provides the specifications for shrinkage and temperature reinforcement. It states that reinforcement shall be provided near surfaces of concrete exposed to daily temperature changes.

For bars or welded wire reinforcement, the area of reinforcement per foot on each face and in each direction shall satisfy the following:

$$A_s \geq \frac{1.30bh}{2(b+h)f_y}$$

Eq. 2.5

except that:

$$0.11 \leq A_s \leq 0.60$$

where:

A_s = area of reinforcement in each direction and each face ($in.^2 / ft$)

b = least width of component section ($in.$)

h = least thickness of component section ($in.$)

f_y = specified minimum yield strength of reinforcement $\leq 75ksi$

The spacing of shrinkage and temperature reinforcement shall not exceed three times the thickness and no more than 18 in.

2.2.2.2 American Concrete Institute – ACI

ACI 318-19: Building Code Requirements for Structural Concrete and Commentary (ACI 318, 2019a) refers the designer to section 4.4.5, which simply states that structural systems shall be designed to accommodate anticipated volume change and differential settlement. The commentary of section 4.4.5 gives some additional information regarding how to accommodate these effects:

“Minimum shrinkage and temperature reinforcement control cracking to an acceptable level in many concrete structures of ordinary proportions and exposures.”

Article 7.7.6.2.1 states that spacing of deformed shrinkage and temperature reinforcement shall not exceed the lesser of $5h$ or 18 in. Section 24.4 refers to shrinkage and temperature reinforcement to minimize cracking in concrete. It is also mentioned that the $0.0018A_g$ area of shrinkage and temperature reinforcement has been satisfactory where shrinkage and temperature movements are permitted to occur. The commentary in section R24.4.2 mentions that when significant restraint is provided, tensile stresses are developed due to restrained volume changes, and for these cases, it may be necessary to increase the amount of reinforcement in both principal directions (ACI 318, 2019b).

Article 24.3.2 establish the maximum limits of spacing for bonded reinforcement in one-way slabs. The spacing of reinforcement is limited to control cracking. The spacing of deformed bars or wires shall be:

$$s_{\max} = \text{Lesser} \left\{ \begin{array}{l} 15 \left(\frac{40,000}{f_s} \right) - 2.5c_c \\ 12 \left(\frac{40,000}{f_s} \right) \end{array} \right. \quad \text{Eq. 2.6}$$

where, f_s is the tensile stress (psi) in reinforcement at service loads, and c_c is the clear cover of reinforcement (in.).

ACI 224R-01 Control of Cracking in Concrete Structures - Reapproved 2008 (ACI 224, 2001) in its section 3.5 mentions that the control of cracking consists of reducing the cracking tendency to a minimum, using adequate and properly positioned reinforcement, and using contraction joints. It is also stated that the minimum amount of reinforcement 0.18%, given in ACI 318, does not normally control cracks to within generally acceptable design limits, and to control cracks to an acceptable level, the percentage needs to exceed about 0.60% (ACI 224, 2001).

2.3 Concrete Bridge Deck Deterioration: Causes and Mitigation Techniques

When concrete is adequately designed for the environment to which it will be exposed during its service life, and with good quality control procedures, it can be maintenance-free for decades without needing protective coatings (Mindess et al., 2002). Concrete bridge decks may deteriorate as a result of concrete distress from several sources, such as corrosion of reinforcement, excessive cracking, alkali-aggregate reactivity, freeze-thaw cycles, and abrasion damage (Russell, 2004). There is no doubt that even with high-technology advances in the concrete industry (fibers, corrosion-resistant reinforcement, admixtures, and supplemental cementitious materials), cracking is still one of the biggest challenges that many bridge owners are concerned about (Russell, 2017).

Several studies have been conducted on evaluating bridge deck performance in the past 50 years, usually supported by federal agencies and state Departments of Transportation (DOT). These studies are mainly focused on current performance, control of cracking in concrete, construction practices, and materials (Frosch et al., 2006, 2003; Krauss and Rogalla, 1996; Russell, 2004).

2.3.1 Previous Studies

Krauss and Rogalla (1996) conducted a survey to 52 state agencies from the United States and Canada, and the agencies estimated that over 100,000 bridge decks developed early-age transverse cracking. Their project identified and ranked the factors that contribute to transverse concrete cracking of newly constructed bridges. It was found that the major design factors were span type, concrete strength, and girder type. The team concluded that the major design factors affecting cracking were related to restraint, specifically bridge type and girder type and size, and concrete volume changes from shrinkage and thermal effects.

Aktan et al. (2003) investigated the causes of early-age deck cracking on Michigan bridge decks. The team found that early-age cracking is the most prevalent deck distress reported by all State Highway Agencies. Restraint in concrete decks with thermal and shrinkage effects and poor construction practices are the main variables influencing early-age deck cracking.

Qiao et al. (2010) studied different mitigation strategies to reduce early-age shrinkage cracking in Washington bridge decks. The study focused its efforts on the evaluation of concrete mix designs (aggregate size and source, shrinkage-reducing admixtures (SRA), and supplemental cementitious materials) and found that the use of SRA significantly reduces the free shrinkage of all concrete mixes with aggregates from the state of Washington. Based on the experimental evaluation, they recommended reducing the partial replacement of cement with fly ash due to the

reduction of early-age strength of concrete and that the use of larger aggregates would improve the free shrinkage and cracking tendency of concrete.

Nadelman et al. (2017) performed an investigation on bridge deck cracking for Montana Department of Transportation. The research team performed evaluation of 12 young bridges (less than 10 years old), between newly constructed decks and overlays. They recommended changing placement times to late afternoon or evening allowing peak concrete temperatures to coincide with cooling evening ambient temperatures and increasing concrete strength prior to the cooling period. Under design considerations, they recommended the use of 8 in. minimum deck thickness, staggered top and bottom mats of main reinforcement, limit cementitious material content to 600 lb/yd³, and specify w/cm ratio between 0.42 and 0.45.

In 2005 the Minnesota Department of Transportation started collecting bridge deck placement data using the “Bridge Deck Placement Data Forms”, which gathers information related to design, structural type, concrete mixture design, placement, curing methods, weather, and preliminary crack survey. Rettner (2014) used this database to statistically identify the most significant variables that affect the bridge decks in terms of cracking deterioration. The research team made recommendations for skewed structures, deck preparation prior to overlay placement, and some limitations related to concrete mixture design, specifically on paste volume, w/cm ratio, and type of cement. Nelson (2014) studied NBI data for Minnesota Department of Transportation to evaluate deck condition states and the variables that could influence the rate of deterioration of concrete decks. The research found that type of reinforcement and geographic location within the state are the main factors influencing the deck condition over time. Data showed that bridges built with epoxy-coated reinforcement and increased cover, built between 1975 and 1989, deteriorated slower than bridges with uncoated reinforcement.

Frosch et al. (2006) studied several factors that affect the extent of cracking in concrete bridge decks, and how these factors are in control of the designer. The objective was the evaluation of different design parameters on bridge deck performance with respect to cracking. They found based on a parametric study that the amount and spacing of reinforcement in the deck directly influenced the extent of the cracking developed. They also attribute early-age transverse cracking in bridge decks to girder volumetric changes resulting from thermal and shrinkage effects. Based on their analytical model and parametric study, the maximum crack width in a bridge deck was proposed, Eq. 2.7:

$$w = \frac{135}{E_r} \gamma \sqrt{\frac{f_c}{\rho_g}} \sqrt{d_c^2 + \left(\frac{s}{2}\right)^2} \quad \text{Eq. 2.8}$$

where,

w = crack width, in.

E_r = reinforcement modulus of elasticity, psi

γ = reinforcement bond factor: 1.0 for steel bars, 1.5 for FRP

f_c = concrete compressive strength, psi

ρ_g = reinforcement ratio of the gross section

d_c = clear cover, in.

s = reinforcement spacing, in.

Frosch et al. (2006) proposed design recommendations to prevent excessive crack growth.

A minimum amount of steel reinforcement and spacing were recommended, as shown in Eq. 2.9:

$$\rho_g = \frac{6\sqrt{f_c}}{f_y} \quad \text{Eq. 2.9}$$

$$s = 9\alpha_r\beta_e \left[2.5 - \frac{d_c}{2\alpha_s} \right] \leq 9\alpha_r\beta_e$$

where,

ρ_g = reinforcement ratio of the gross section

f'_c = specified 28-day concrete compressive strength, psi

f_y = reinforcement yield stress, ksi

f_{fu} = ultimate tensile strength for FRP reinforcement, ksi

α_r = stress factor: $60/f_y$ for steel reinforcement; $90/f_{fu}$ for FRP reinforcement

β_e = modular factor: 1.0 for steel; $E_r/7000$ for FRP

There is no doubt that many institutions and researchers have been devoting efforts to try to solve the problem of cracking and early deterioration of concrete decks in the past decades. The published information is reaching to the same conclusion regarding what are the possible causes of early-age cracking: drying shrinkage, temperature differences, and the effect of girder restraint on concrete decks.

2.4 Concrete Behavior

2.4.1 Creep and Shrinkage

ACI 209 (2002) defines shrinkage as the decrease in time of concrete volume, due to changes in moisture content and physico-chemical changes, which occur without stress from external actions. There are different types of shrinkage, such as drying shrinkage due to moisture loss, autogenous shrinkage caused by hydration of the cement paste, and carbonation shrinkage caused by carbonated products of the cement hydration in the presence of CO_2 .

Creep is defined as a time-dependent increase in strain of hardened concrete when subjected to sustained stress (ACI 209, 2002). The phenomenon of gradual decrease in stress with time under a given level of sustained strain is called stress relaxation. Creep and relaxation, are typical behavior of viscoelastic materials (Mehta and Monteiro, 2014).

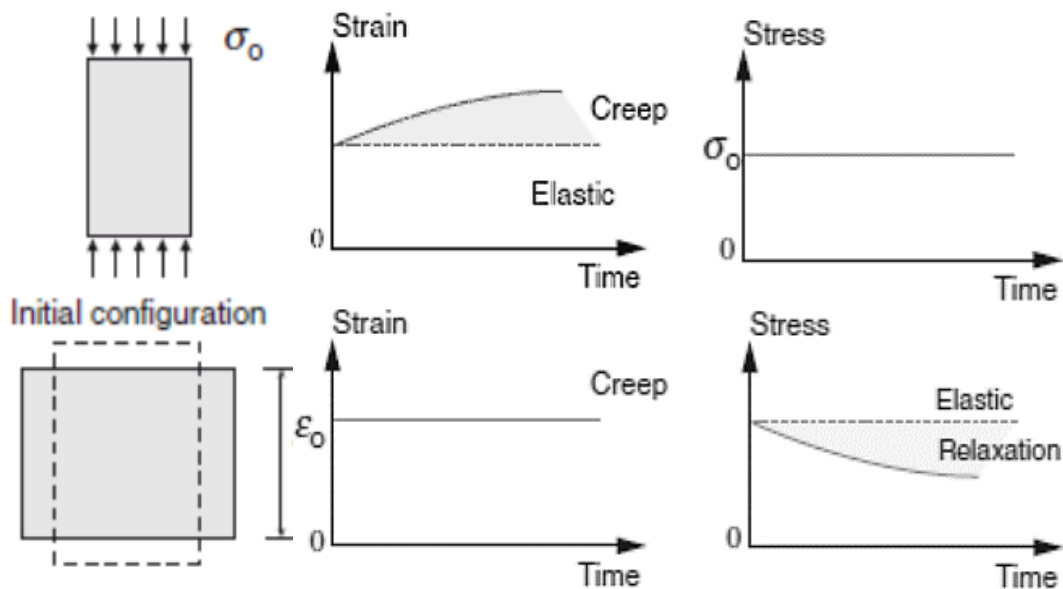


Figure 2.1: Basic creep and creep relaxation over time (Adapted from Mehta and Monteiro (2014))

Under restraining conditions, concrete develops elastic tensile stresses induced by shrinkage strains and stress relief due to the viscoelastic behavior, Figure 2.2. This behavior is the main cause of deformations and cracking in most concrete structures (Mehta and Monteiro, 2014).

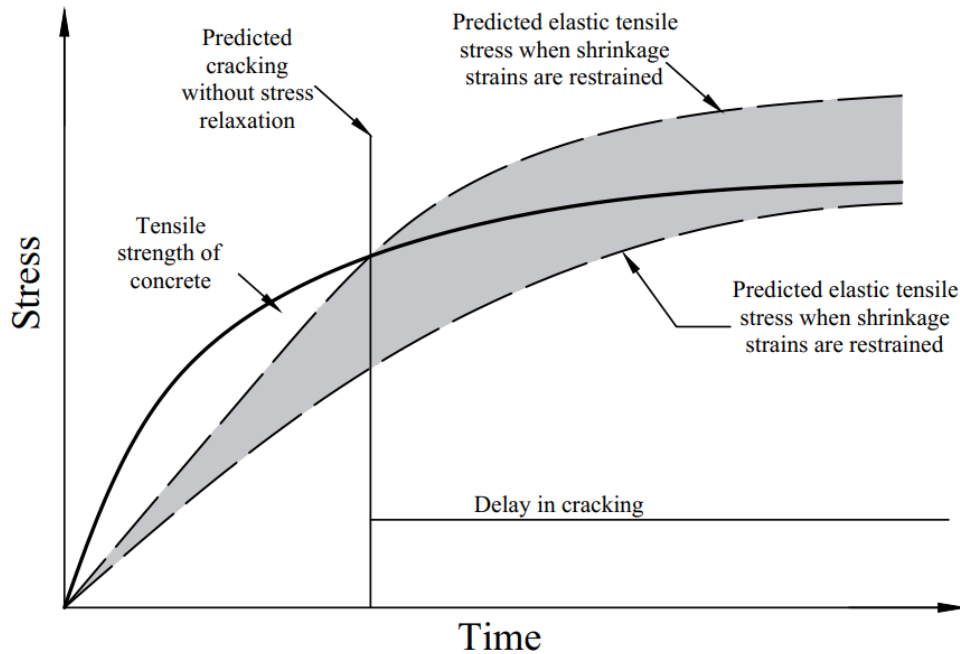


Figure 2.2: Influence of shrinkage and creep on concrete cracking. (Adapted from Mehta and Monteiro, 2014)

When concrete is exposed to the environment, the drying process starts. This is usually a long-term drying process and causes additional creep and shrinkage.(Bažant and Baweja, 2000)

2.4.1.1 B3 Creep Model

Bažant and Prasannan, (1989a)proposed a new general constitutive law for creep in which the hydration of the cement (concrete aging) is considered. The constitutive law is based on solidification theory and the creep strains are obtained as a summation of aging and nonaging viscoelastic strains.

B3 Creep Model (Bažant and Baweja, 2000) is restricted to portland cement concrete with the following parameter ranges:

$$\begin{aligned}
 0.35 &\leq w/c \leq 0.85 \\
 2.5 &\leq a/c \leq 13.5 \\
 2,500 \text{ psi} &\leq \bar{f}_c \leq 10,000 \text{ psi} \\
 10 \text{ pcf} &\leq c \leq 45 \text{ pcf}
 \end{aligned}$$

where,

w/c = water to cementitious material ratio, by weight

a/c = aggregate-cement ratio, by weight

\bar{f}_c = mean 28-day standard cylinder compressive strength in psi

c = cement content of concrete in lb/ft^3

The model is restricted to service level of stress of about $0.45 \bar{f}_c$. The strains developed in concrete at a constant level of stress are defined as:

$$\varepsilon(t) = J(t, t')\sigma + \varepsilon_{sh}(t) + \alpha\Delta T(t) \quad \text{Eq. 2.10}$$

where,

$J(t, t')$ = compliance function or strain (creep and elastic) at age t caused by a unit uniaxial constant stress applied at age t' , $10^{-6}/\text{psi}$

σ = uniaxial stress

$\varepsilon_{sh}(t)$ = shrinkage strain at age t , 10^{-6}

α : coefficient of thermal expansion

$\Delta T(t)$: temperature variation at age t

The compliance function can be decomposed as shown in Eq. 2.11 as:

$$J(t, t') = q_1 + C_0(t, t') + C_d(t, t', t_0) \quad \text{Eq. 2.11}$$

where,

q_1 = instantaneous strain due to unit stress

$C_0(t, t')$ = compliance function for basic creep (constant moisture content and no moisture movement through the material)

$C_d(t, t', t_0)$ = compliance function for additional creep due to drying

t = time representing concrete age, in days

t' = time representing concrete age at loading, in days

t_0 = time representing beginning of concrete drying, in days

Using the compliance function, the material creep is incorporated into structural analysis with the creep coefficient, $\phi(t, t')$, defined as:

$$\phi(t, t') = E(t')J(t, t') - 1 \quad \text{Eq. 2.12}$$

where $E(t')$ is the static modulus of elasticity at the loading age t' . The basic creep compliance is defined in Eq. 2.13 and the additional creep due to drying is defined in Eq. 2.14:

$$C_0(t, t') = q_2 Q(t, t') + q_3 \ln[1 + (t - t')^n] + q_4 \ln\left(\frac{t}{t'}\right) \quad \text{Eq. 2.13}$$

$$C_d(t, t', t_0) = q_5 \left[e^{-8H(t)} - e^{-8H(t_0)} \right] \quad \text{with } t_0' = \max(t', t_0) \quad \text{Eq. 2.14}$$

$$H(t) = 1 - (1 - h)S(t) \quad \text{Eq. 2.15}$$

where q_1, q_2, q_3, q_4 , and q_5 (Eq. 2.16) are empirical material constitutive parameters based on concrete strength and composition, and $H(t)$ is the spatial average of pore relative humidity within the cross section.

$$\begin{aligned}
 q_1 &= 0.6 \cdot 10^6 / E_{28} \\
 q_2 &= 451.1 c^{0.5} \bar{f}_c^{-0.9} \\
 q_3 &= 0.29 (w/c)^4 \cdot q_2 \\
 q_4 &= 0.14 (a/c)^{-0.7} \\
 q_5 &= 7.57 \cdot 10^5 \bar{f}_c^{-1} |\varepsilon_{sh\infty}|^{-0.6}
 \end{aligned}
 \tag{Eq. 2.16}$$

$Q(t, t')$ is obtained from the approximate formula (Bažant and Prasannan, 1989a) as defined in Eq. 2.17 and Eq. 2.18:

$$Q(t, t') = Q_f(t') \left[1 + \left(\frac{Q_f(t')}{Z(t, t')} \right)^{r(t')} \right]^{-1/r(t')}
 \tag{Eq. 2.17}$$

with

$$\begin{aligned}
 r(t') &= 1.7(t')^{0.12} + 8 \\
 Z(t, t') &= (t')^{-m} \ln \left[1 + (t - t')^n \right] \\
 Q_f(t') &= \left[0.086(t')^{2/9} + 1.21(t')^{4/9} \right]^{-1}
 \end{aligned}
 \tag{Eq. 2.18}$$

The average shrinkage at a drying state of concrete is evaluated as:

$$\varepsilon_{sh}(t, t_0) = -\varepsilon_{sh\infty} k_h S(t)
 \tag{Eq. 2.19}$$

where,

$\varepsilon_{sh}(t, t_0)$ = average shrinkage in cross section at concrete age t based on curing time t_0

$\varepsilon_{sh\infty}$ = ultimate drying shrinkage

$S(t)$ = time/size dependence factor
 k_h = humidity correction factor for final shrinkage

The following equations define the required parameters to calculate the average shrinkage in the cross section:

$$k_h = \begin{cases} 1-h^3 & \text{for } h \leq 0.95 \\ -0.2 & \text{for } h = 1 \text{ (swelling in water)} \\ \text{linear interpolation} & \text{for } 0.98 \leq h \leq 1 \end{cases} \quad \text{Eq. 2.20}$$

$$S(t) = \tanh \sqrt{\frac{t-t_0}{\tau_{sh}}} \quad \text{Eq. 2.21}$$

$$\tau_{sh} = k_t (k_s D)^2 \quad (\text{days})$$

$$D = 2V / S \quad (\text{in.})$$

$$k_s = \begin{cases} 1.00 & \text{infinite slab} \\ 1.15 & \text{infinite cylinder} \\ 1.25 & \text{infinite square prism} \\ 1.30 & \text{sphere} \\ 1.55 & \text{cube} \end{cases} \quad \text{Eq. 2.22}$$

$$k_t = 190.8 t_0^{-0.08} \bar{f}_c^{-1/4} \quad (\text{days} / \text{in.}^2)$$

where,

h = relative humidity of environment, $0 \leq h \leq 1$

τ_{sh} = size dependence factor

V / S = volume to surface ratio in inches

k_s = cross section shape factor

k_t = parameter used in calculation of τ_{sh}

The time dependence of the ultimate shrinkage is evaluated in terms of concrete elasticity, concrete strength, type of cement, water content, and type of curing (Bazant and Baweja, 2000), as shown in Eq. 2.23 through Eq. 2.27:

$$\varepsilon_{sh\infty} = \varepsilon_{s\infty} \frac{E(607)}{E(t_0 + \tau_{sh})} \quad \text{Eq. 2.23}$$

$$E(t) = E(28) \left(\frac{t}{4 + 0.85t} \right)^{1/2} \quad \text{Eq. 2.24}$$

$$\varepsilon_{s\infty} = -\alpha_1 \alpha_2 \left[26w^{2.1} \bar{f}_c^{-0.28} + 270 \right] \left(10^{-6} \right) \quad \text{Eq. 2.25}$$

$$\alpha_1 = \begin{cases} 1.00 & \text{for type I cement} \\ 0.85 & \text{for type II cement} \\ 1.10 & \text{for type III cement} \end{cases} \quad \text{Eq. 2.26}$$

$$\alpha_2 = \begin{cases} 0.75 & \text{for steam-curing} \\ 1.20 & \text{for sealed or normal curing in air with initial protection against drying} \\ 1.00 & \text{for curing in water or at 100\% relative humidity} \end{cases} \quad \text{Eq. 2.27}$$

2.4.2 Thermal Stress Development

Thermal stresses of early-age concrete are influence by changes of its temperature, coefficient of thermal expansion, the modulus of elasticity, creep or relaxation, and the degree of restraint. The development of thermal stress can be calculated with Eq. 2.28 (Schindler and McCullough, 2002).

$$\sigma = K_r \cdot CTE \cdot \Delta T \cdot E_c \quad \text{Eq. 2.28}$$

where,

- σ = thermal stress [psi]
- K_r = internal/external restraint factor
- CTE = coefficient of thermal expansion [in/in/°F]
- ΔT = temperature change [°F]
- E_c = creep-adjusted modulus of elasticity of the concrete [psi]

Figure 2.3 shows a graphical representation of a fully restrained concrete subjected to temperature change and mechanical properties development over time. At the time of the final set, concrete starts developing tensile strength while is experiencing compressive stress due to the increase in temperature by heat of hydration. Strength and stiffness start developing rapidly as concrete is aging. When concrete reaches its maximum temperature and starts decreasing, the concrete starts its contraction until it reaches a point of zero-stress (point C). After the zero-stress temperature is reached, the concrete develops tensile stresses, which eventually with temperature changes, will be higher than the tensile strength (point D), and cracking occurs.

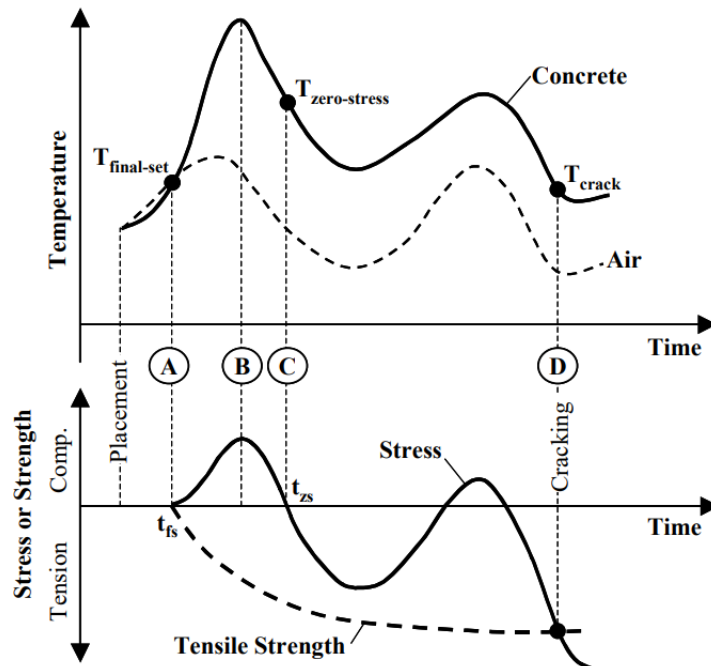


Figure 2.3: Graphical representation of development of thermal stresses (Schindler and McCullough, 2002)

2.5 Degree of Restraint in Concrete Structural Elements

Changes in temperature induce length or volume changes in concrete elements. If a concrete element is free to move freely under temperature changes, no stress is developed in the element. If restrained, tensile stress or strain will developed due to potential contractions between contiguous structural elements. ACI 207 (2007) defines the degree of restraint, K_R , as the ratio of actual stress resulting from volume change to the stress that would result if completely restrained. In concrete structures, almost all elements are subjected to some level of restraint by the supporting or adjacent members of the structure. Restrained volume change can induce tensile, compressive, or even flexural stresses in concrete elements, depending on the type of restraint that the element is subjected to.

The degree of restraint depends primarily on the relative dimensions, strength, and modulus of elasticity of the concrete and the restraining material. ACI 207 (2007) defines 2 restraint factors: structural shape restraint factor, K_R , and foundation restraint factor, K_f . The structural shape restraint factor is shown in graphical form in Figure 2.4. The foundation restraint factor is defined in Eq. 2.29:

$$K_f = \frac{1}{1 + \frac{A_g E_c}{A_F E_F}} \quad \text{Eq. 2.29}$$

where,

A_g = gross area of concrete cross section

A_F = area of foundation or other element restraining shortening of element

E_c = modulus of elasticity of concrete

E_F = modulus of elasticity of foundation or restraining element

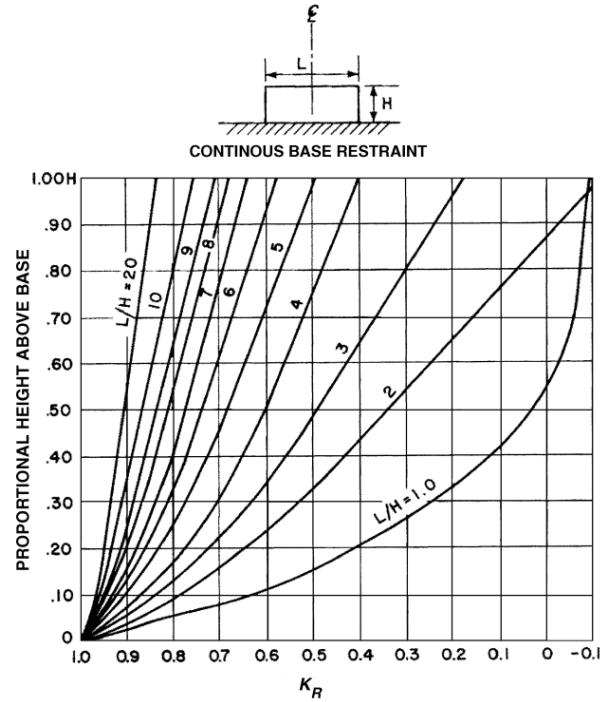


Figure 2.4: Degree of tensile restraint at center section (ACI 207, 2007)

Restraint experienced by the concrete deck varies depending on the girder type used (concrete or steel) and the end conditions of the bridge supports (Frosch et al., 2006). They measured strains at a reinforced concrete deck over the girders and at the midbay between the girders, and they also prepared a slab specimen to match field conditions to compare the level of shrinkage between the deck and the sample. The degree of restraint on reinforced concrete decks from concrete and steel girders was quantified by Frosch et al. (2006) with a proposed equation, Eq. 2.30, for decks partially restrained to compute the degree of restraint:

$$k = \frac{1}{2} \left[1 - \frac{\varepsilon_m}{\varepsilon_f} \right] \quad \text{Eq. 2.30}$$

where,

k = degree of restraint

ε_m = measured strain

ε_f = unrestrained (free) shrinkage strain

Frosch et al. (2006) estimated degrees of restraint of 41% at midbay and 75% over the girder for a steel bridge, using measured data of 80 days of age.

Restraint of bridge decks is primarily provided by the composite action of girders and some internal restraint due to reinforcing steel or concrete components. The restraint provided by the girders will develop tensile stress in the bridge deck and eventually these stresses will exceed the tensile strength developed by the concrete, specially at early ages, and transverse cracking will occur.

CHAPTER 3. SELECTION OF REPRESENTATIVE STRUCTURES

3.1 National Bridge Inventory Statistics

The NBI data of 2022 was used to develop statistics of California bridges. All the information presented in the following graphs has been adapted from NBI (2022). There are 25,810 available records in the California NBI ASCII Files (NBI, 2022), where 22,275 are bridges, and 3,535 are culverts. The number of bridges by structural type is shown in Figure 3.1. Most of the bridges are box beam bridges or box girder bridges, 8,329 (37% of all bridges). The second most common type in terms of the number are slab bridges, 5,926 (27%), followed by multi-beam 3,916 (18%), and T-beam bridges, 2,806 (13%). Other bridges include arches, truss, suspension, etc., with less than 5% of the California bridge population overall.

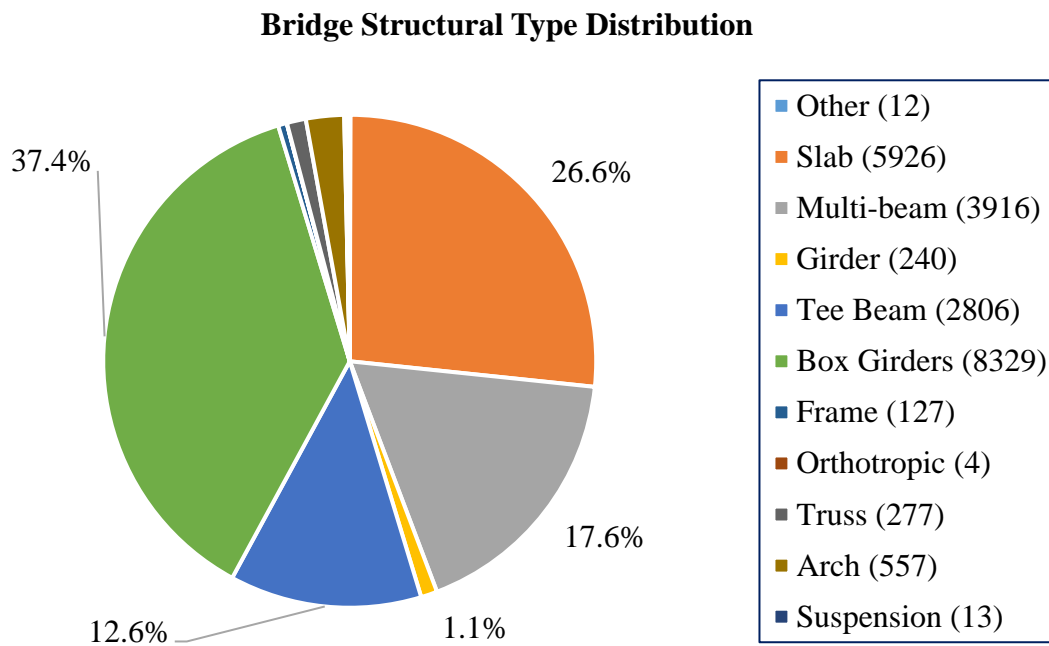


Figure 3.1 California bridge by structural types (number of bridges is indicated in parenthesis)

In terms of materials, reinforced concrete (simple and continuous structures) is the most common, see Figure 3.2, representing around 56%, with 12,478 bridges. Prestressed concrete (P/C) bridges represent over 29% of the total bridges, with 6,531 records as of 2022.

Bridge Structural Material Distribution

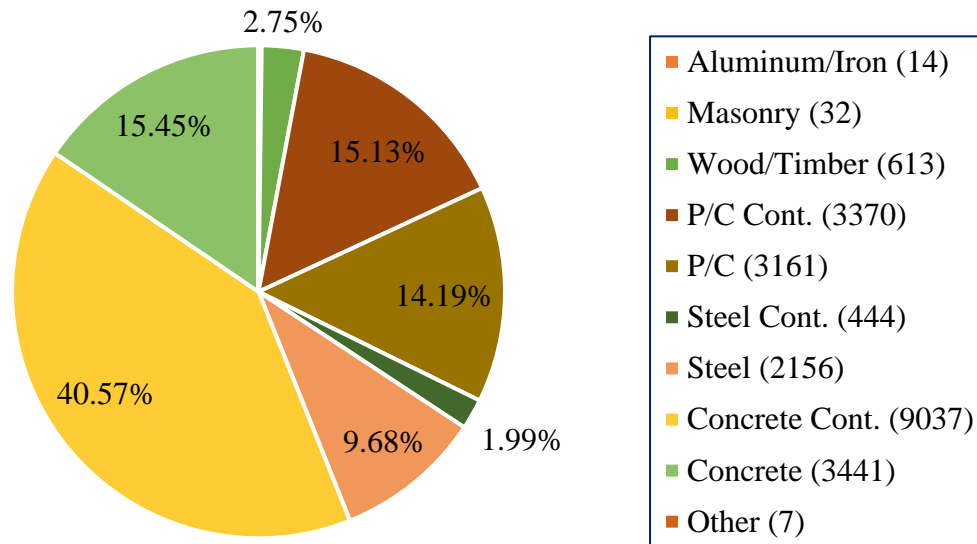


Figure 3.2: California bridges by material

Table 3.1 summarizes structural bridge types vs. material used for construction in California bridges, according to NBI 2022. From the table, reinforced concrete and prestressed concrete boxes are the most common. In Table 3-1, the most significant amount is shown for box-type bridges with cast-in-place reinforced concrete decks.

Table 3-1: Bridge Structural Type vs. Material Type

Structure Type	Structure Material Type										Total
	Concrete Cont.	P/C Cont.	P/C	Concrete	Steel	Steel Cont.	Wood or Timber	Aluminum or Iron	Masonry	Other	
Arch - Deck	21		3	334	143	1		12	30	1	545
Arch - Thru	4			3	3				2		12
Box Girder - Multiple	3,005	2,777	1,623	624	11	10	1				8,051
Box Girder - Single	57	98	64	51	7	1					278
Channel Beam		1	1	16	1						19
Frame	21		1	104	1						127
Girder	46	1	17	55	91	20	10				240
Mixed				1							1
Movable - Bascule					16	1					17
Movable - Lift					4						4
Movable - Swing					12	3					15
Orthotropic					4						4
Other	1	1		3	6					1	12
Segmental Box		8	3								11
Slab	4,102	91	488	1,220	2	1	20			2	5,926
Stayed Girder					1						1
Stringer	41	371	803	144	1,592	393	570			2	3,916
Suspension					11	2					13
Tee Beam	1,739	22	158	886	1						2,806
Truss - Deck					39	7					46
Truss - Thru					211	5	12	2		1	231
Total	9,037	3,370	3,161	3,441	2,156	444	613	14	32	7	22,275

Table 3-2: Bridge Structural Type vs. Deck Structural Type

Structure Type	Deck Structural Type										
	Aluminum	Closed Grating	Concrete CIP	Concrete Precast Panels	Corrugated Steel	Not Applicable	Open Grating	Other	Steel Plate	Wood/Timber	Total
Arch - Deck			141	2	1	398				3	545
Arch - Thru			9			3					12
Box Girder - Multiple		1	7,995	28	3	7		10	5	2	8,051
Box Girder - Single			267	2	2	1		3	3		278
Channel Beam			9	10							19
Frame			86	2		37	1	1			127
Girder		16	170		8	1	16		4	25	240
Mixed			1								1
Movable - Bascule			3				14				17
Movable - Lift			2				2				4
Movable - Swing		1	12		1					1	15
Orthotropic									4		4
Other			8						3	1	12
Segmental Box			11								11
Slab			5,659	174		59		17		17	5,926
Stayed Girder				1							1
Stringer		7	3,034	53	258	5	13	4	49	493	3,916
Suspension			4		1				3	5	13
Tee Beam			2,788	9	1	4		4			2,806
Truss - Deck			32	1	1		3		1	8	46
Truss - Thru		2	84		46		12		10	77	231
Total	2	25	20,315	282	322	515	61	39	82	632	22,275

In terms of concrete deck material, CIP-reinforced concrete decks are the most common, with more than 91% of all California bridges, as shown in Figure 3.3. California bridges have CIP concrete decks in most of the bridges, much more than the national average of 71%.

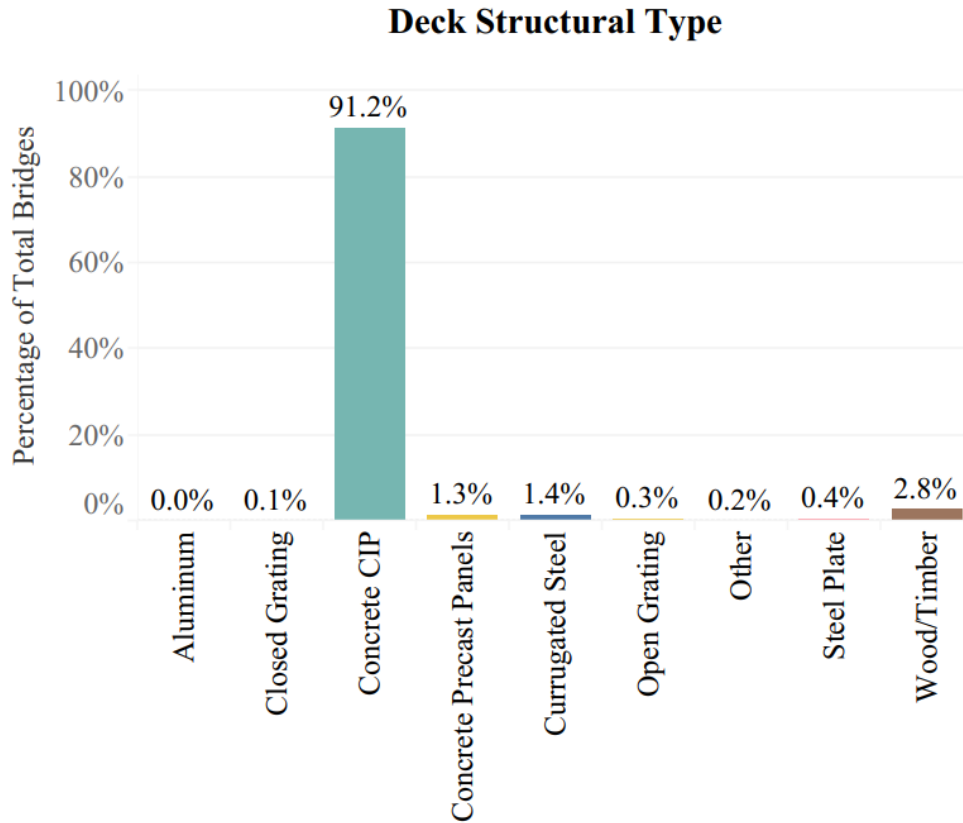


Figure 3.3: Bridge deck material type

For further review, California bridges were divided into three groups by year built. The first group considers all bridges built prior to 1943, the second group are bridges built from 1944 to 1983, and the last group bridges built since 1984 – see Figure 3.4. In 40 years, between 1944 and 1983, over 61% of all bridges in California were built, while since 1984, only 26% of them have been built.

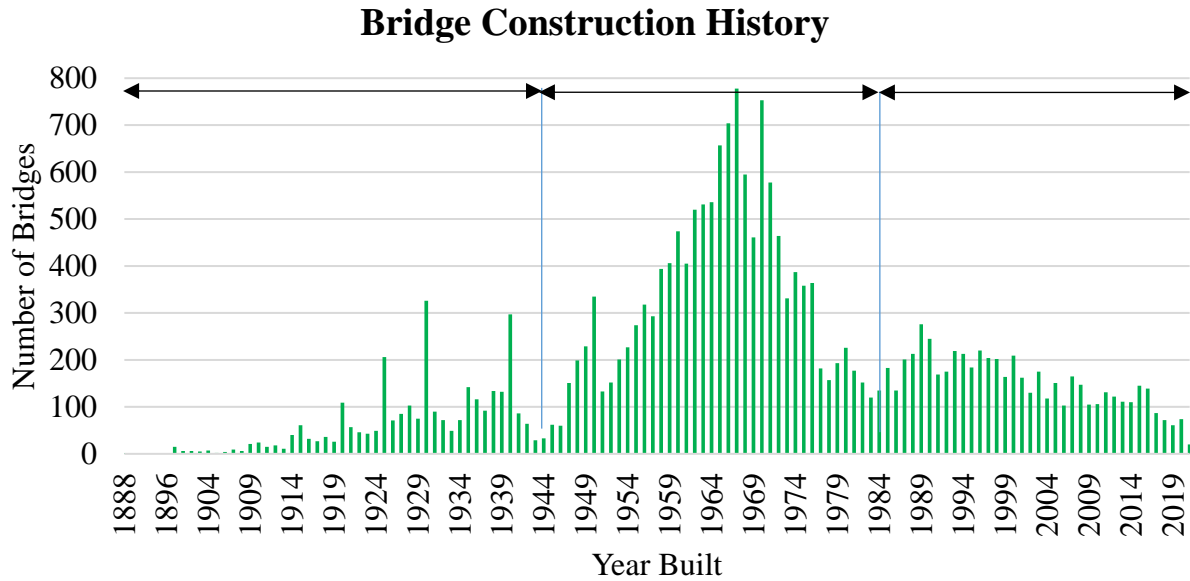


Figure 3.4: Number of California bridges by year built.

Figure 3.5 shows the most common structural types bridges. 58% of all bridges built after 1983 were box bridges, which makes box beam bridges the most common structural type in California. Reinforced concrete bridge structures were the most popular between 1944 and 1983, and after 1983 prestressed concrete material became the most common practice (see Figure 3.5).

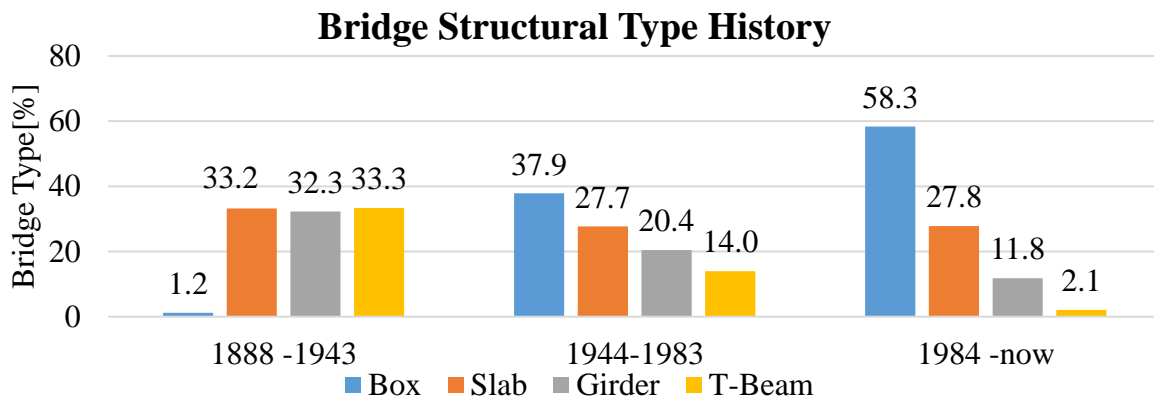


Figure 3.5: Bridge structural type for selected time periods.

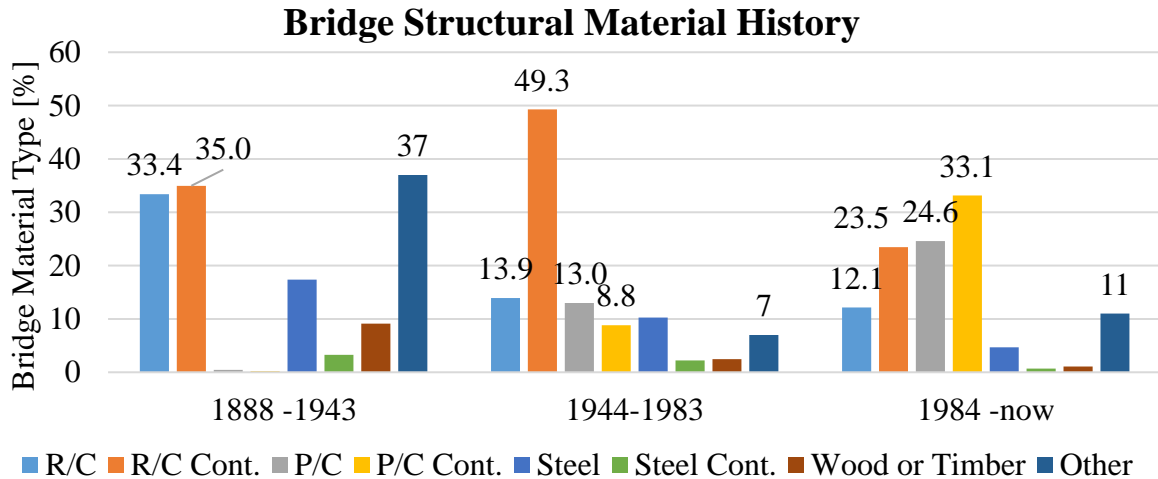


Figure 3.6: Bridge material for selected time periods.

In the last decade, Figure 3.7 , over a 65% of new bridge construction is with prestressed concrete, and 29% with reinforced concrete. Steel is used for a small percentage of new bridge construction, only 5%.

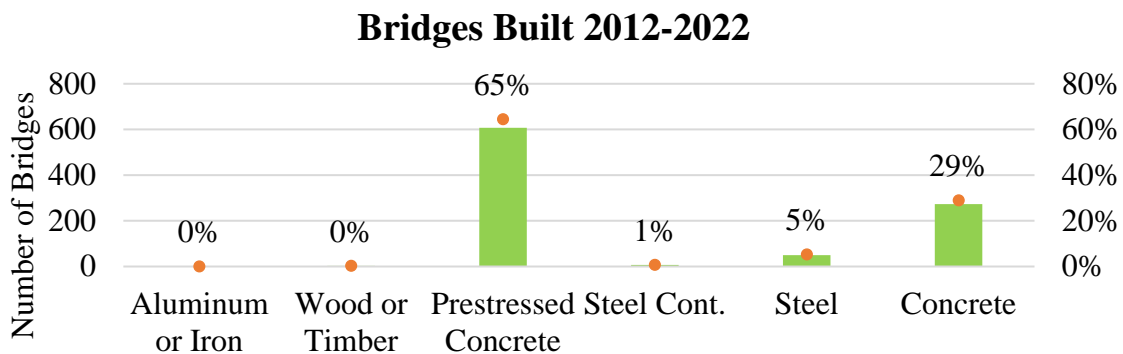


Figure 3.7: Bridge material types built in the last decade,

3.1.1 Bridge Condition Rating in California

Bridge condition rating is annually reported in the NBI and LTBP InfoBridge databases. Conditions rating can be defined as 9 to 0 from excellent to field condition. Figure 3.8 and Figure 3.9 show the percentage of bridges in each deck and superstructure condition rating category. Table 3-3 and Table 3-4 show the detailed number of bridges by deck and superstructure condition ratings.

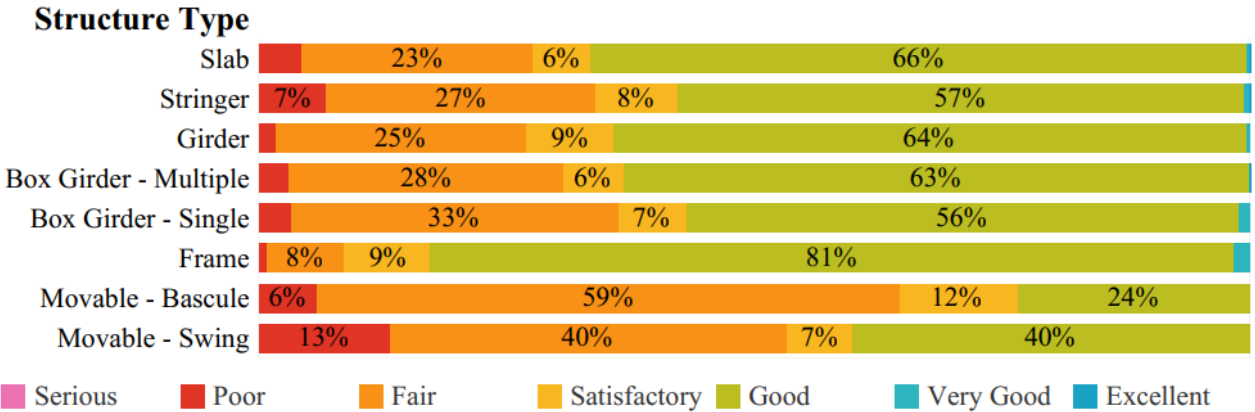


Figure 3.8: California deck condition rating percent by bridge structural type.

Table 3-3: Bridge type vs. bridge deck condition rating.

Structure type	Deck Condition								
	Excellent	Very good c	Good	Satisfactory	Fair	Poor	Serious	Critical	Imminent failure
Arch	0	1	120	10	10	0	0	0	0
Box	1	114	5,531	294	2,149	221	1	0	0
Channel Beam	0	0	1	0	0	0	0	0	0
Frame	0	2	33	5	2	0	0	0	0
Girder	0	2	152	20	53	4	1	0	0
Mixed Types	0	0	1	0	0	0	0	0	0
Movable	0	0	19	1	14	2	0	0	0
Orthotropic	0	0	1	0	0	0	0	0	0
Segmental Box	0	0	9	0	1	0	0	0	0
Slab	5	127	4,020	303	1,303	222	2	0	0
Multi-Beam	2	48	2,340	249	1,041	269	7	1	0
Suspension	0	0	7	2	4	0	0	0	0
Tee Beam	0	24	1,723	138	758	194	2	0	0
Truss	1	4	132	18	95	25	1	1	0
Total	9	322	14,089	1,040	5,430	937	14	2	0

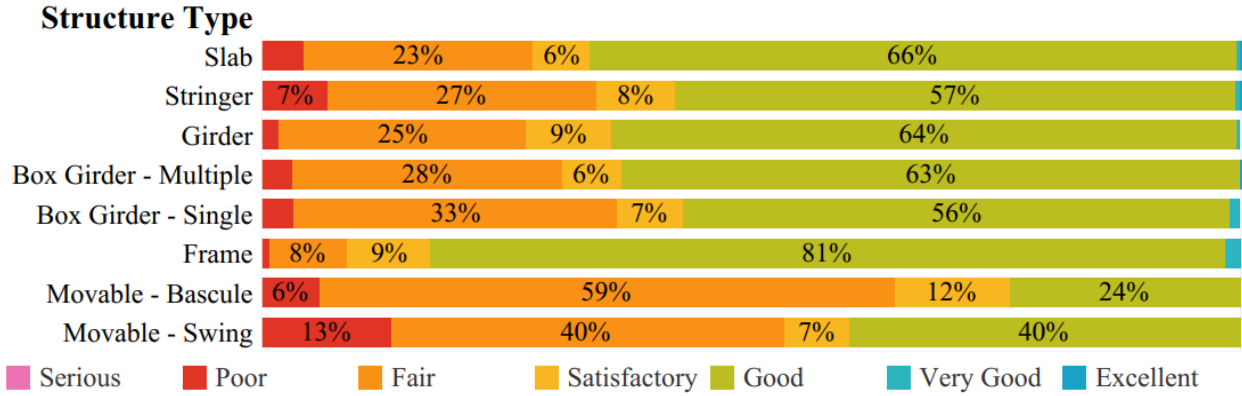


Figure 3.9: Superstructure condition rating percent by bridge structural type.

Table 3-4: Bridge type vs. superstructure condition rating.

Structure type	Superstructure Condition								
	Excellent	Very Good	Good	Satisfactory	Fair	Poor	Serious	Critical	Imminent Failure
Arch	0	18	410	13	88	14	3	3	0
Box	0	118	7,287	97	788	19	2	0	0
Channel Beam	0	1	0	0	0	0	0	0	0
Frame	0	2	31	5	4	0	0	0	0
Girder	0	4	138	19	56	13	2	0	0
Mixed Types	0	1	0	0	0	0	0	0	0
Movable	0	0	14	0	21	0	1	0	0
Orthotropic	0	0	0	0	1	0	0	0	0
Segmental Box	0	0	10	0	0	0	0	0	0
Slab	7	215	4,463	142	1,070	74	2	9	0
Girder	0	86	2,570	137	1,000	142	9	12	1
Suspension	0	0	7	0	6	0	0	0	0
Tee Beam	0	48	2,083	68	580	50	2	8	0
Truss	0	4	161	18	84	6	2	2	0
Total	7	497	17,174	499	3,698	318	23	34	1

Additionally, the deck condition rating was evaluated by bridge material type. Figure 3.10 shows the percentages of bridges in each deck condition rating category. Table 3-5 shows the number of bridges by material in each deck condition rating.

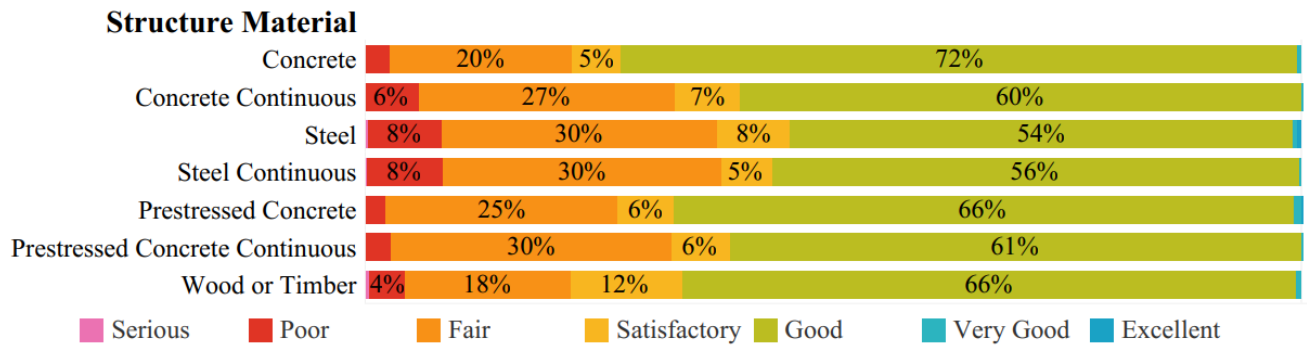


Figure 3.10: Deck condition rating percent by bridge material type.

Table 3-5: Statistics of bridge material type vs. deck condition rating.

Material type	Deck Condition								
	Excellent	Very Good	Good	Satisfactory	Fair	Poor	Serious	Critical	Imminent failure
Aluminum or Iron	0	0	2	0	0	0	0	0	0
Concrete	0	55	2,374	200	624	79	3	0	0
Concrete Cont.	0	152	5,823	395	2,250	472	2	0	0
Masonry	0	0	7	0	0	0	0	0	0
Other	0	0	4	1	0	2	0	0	0
P/C	6	65	2,097	152	799	75	0	0	0
P/C Cont.	0	17	1,965	88	936	95	0	0	0
Steel	3	26	1,132	125	609	151	6	2	0
Steel Cont.	0	1	258	19	125	40	1	0	0
Wood or Timber	0	6	432	61	115	25	3	0	0
Total	9	322	14,094	1,041	5,458	939	15	2	0

CIP Concrete Deck Condition Box Girder Bridges

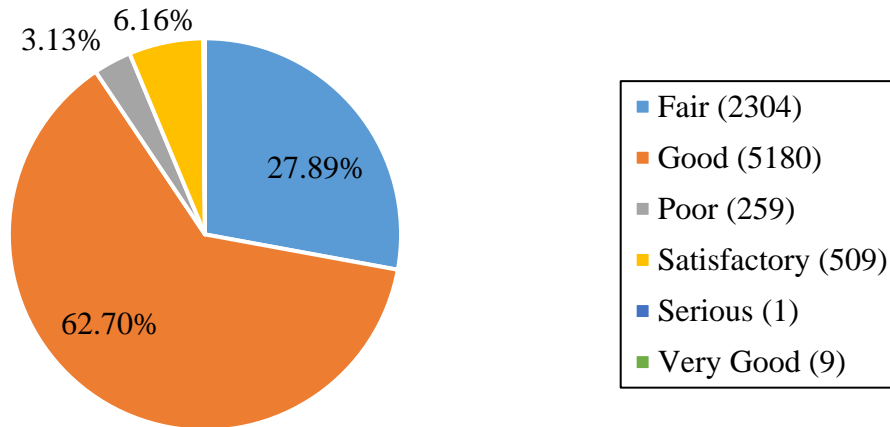


Figure 3.11: Deck condition of CIP reinforced concrete decks in Box girder bridges

Figure 3.11 summarizes the deck condition rating of CIP decks in box girder bridges reported in the NBI 2022 data. Almost 28% is in Fair condition, and almost 63% is in Good condition. In Figure 3.12, the percentage of bridges in each condition category is presented, where more than half of total box girder bridges are in Fair or below condition as of 2022.

Bridge General Condition - Box Girder Bridges

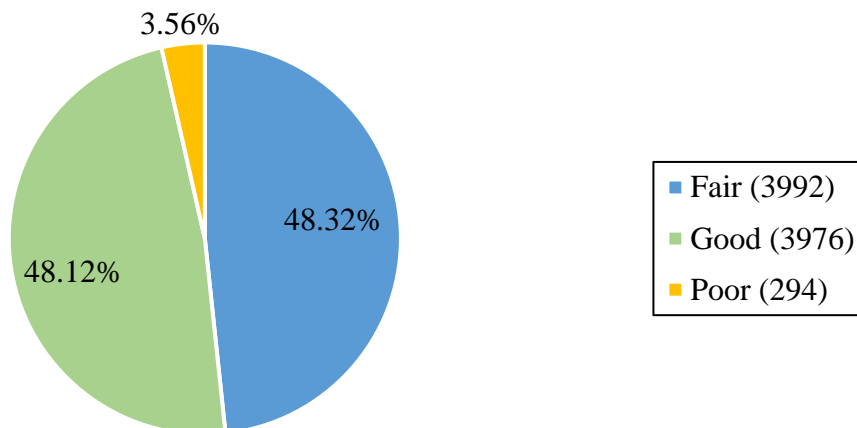


Figure 3.12: Bridge general condition according to PBCPM rule (FHWA, 2017)

3.1.2 Summary of NBI Statistics

NBI 2022 database was used to review bridge information statistics in California. The NBI data showed that there are about 25,810 records, of which 22,275 are bridges, and 3,535 are culverts. In summary, bridges in California show:

- Only 26% (5,781) of bridges have been built since 1984.
- In the last decade, prestressed concrete and reinforced concrete bridges represent 65% and 29% of bridges built, respectively.
- Box girder bridges represent 37.4% of the total amount of bridges in California.
- Bridges are built with CIP Reinforced Concrete decks in more than 91% of the cases.
- Prestressed Concrete and Reinforced Concrete are the materials used for more than 85% of bridges built historically. In the last decade, this number increased to 94%.
- More than 57% of bridges are designed as continuous structures.
- Bridge condition indicates that more than 51% of bridges are in Fair or Poor condition.
- Deck condition rating indicates that more than 31% of CIP decks are in fair or poor condition.

Box girder bridges are the most common bridge type used in the state of California. In these bridges, CIP reinforced concrete deck is the structural system selected in more than 91% of the cases. Condition ratings of these decks indicate issues that are pertinent to assess and improve.

3.2 Bridge Deck Cracking Database

California Department of Transportation (Caltrans) provided a database of field-observed cracking data on their bridge decks. In this database of about 8,650 bridge decks, 4,357 matched with structural types of reinforced concrete and prestressed concrete box girder bridges, representing a 52% of the total amount of box girder bridges in the state of California. The data were filtered by:

- Owner: State Highway Agency
- Structural Design Material: Reinforced Concrete and Prestressed Concrete, Continuous and Simply Supported bridge types
- Structural Type: Box Girder - Single and Multiple

Figure 3.13 shows that approximately 34% corresponds to continuous reinforced concrete (R/C Cont.) bridges and 40% to continuous prestressed concrete bridges (P/C Cont.). The collected database shows only a 5% of cracking data for simply supported reinforced concrete (R/C Simple) bridges. The database shows that most cracking information is regarding prestressed concrete structures.

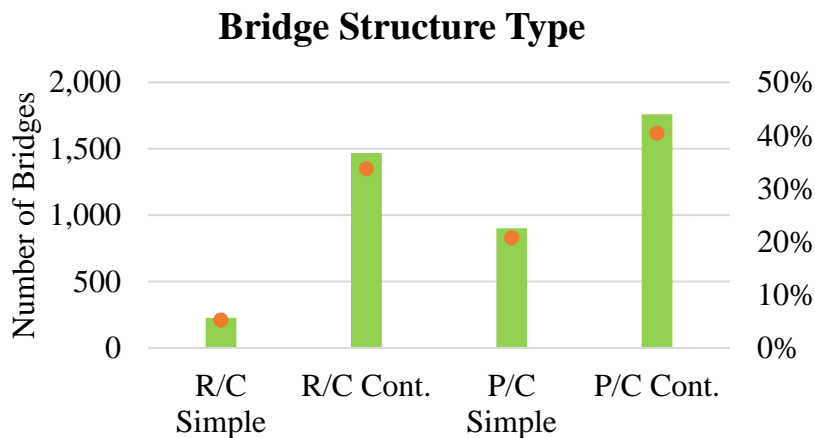


Figure 3.13: Distribution of Cracking Data Available by Structural Material Type (percent of total in orange dots)

The 4,357 bridge Identification Numbers (ID) were then located in the current NBI database to obtain more information, such as the total deck area. The cracking database also provided the amount of cracked area for each bridge deck. Figure 3.14 shows the distribution of cracked area ratio for each type of structure. From the figure, it can be noted that prestressed concrete structures reach up to 20% of cracked area, but for a few bridges, while reinforced concrete structures the maximum ratios are found to be between 11% and 13%. On average (50% probability in the figure), simple structures show lower percentages of cracked deck area, when compared to continuous structures, for both reinforced concrete and prestressed concrete, but the extreme cases are found to be on prestressed concrete box girder bridges.

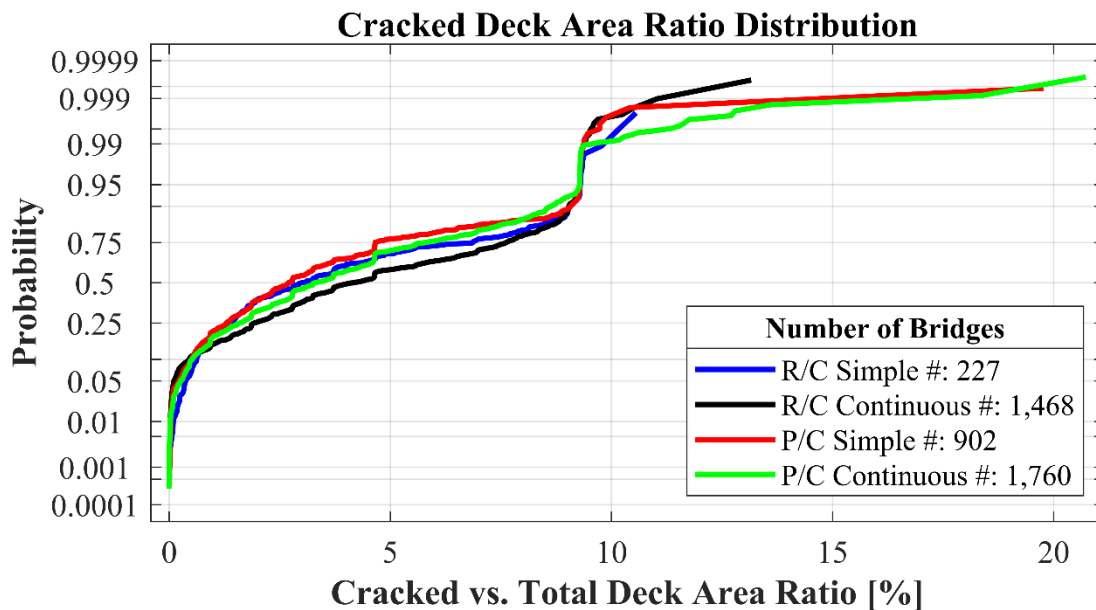


Figure 3.14: Cracked Deck Area Ratio Distribution of Box Girder Decks in California

3.2.1 Bridge Inspection

Inspection reports of bridges are based on different methods, historically. As of 2000, there was a manual for element inspections in which deck cracking was indicated as element 358 (Caltrans, 2000). Table 3-6 shows the description of different condition states for the type of cracking and the inclusion of density and size in the inspection report.

Table 3-6: Condition State to address cracking in decks (Caltrans, 2000)

Condition	Description	
1	The surface of the deck is cracked, but the cracks are either filled/sealed or insignificant in size and density to warrant repair activities.	
2	Unsealed cracks exist, which are of moderate size or density.	
3	Unsealed cracks exist, which are of moderate size and density.	
4	Unsealed cracks exist which are of severe size and/or density.	
	Moderate	Severe
Density	Cracks at a spacing of 1 foot or larger.	Cracks at a spacing of fewer than 1 foot.
Size	Cracks of 0.02 to 0.08 inch wide	Cracks more than 0.08 inch wide.

In 2017, a new version of the inspection manual was published and in here the deck element ID and the defects and condition states were revised, as shown in Table 3-7.

Table 3-7: Condition state per Caltrans bridge element inspection manual (Caltrans, 2017a)

Defect	Condition States			
	1	2	3	4
	GOOD	FAIR	POOR	SEVERE
Cracking (RC and Other) (1130)	Insignificant cracks or moderate width (0.012 to 0.05 inches) cracks that have been sealed.	Unsealed moderate width (0.012 to 0.05 inches) cracks or unsealed moderate pattern (map) cracking.	Wide cracks (greater than 0.05 inches) or heavy pattern (map) cracking.	The condition warrants a structural review to determine the effect on strength or serviceability of the element or bridge. OR A structural review has been completed and the defects impact strength or serviceability of the element or bridge.

Caltrans (2017a) states that when cracks have been treated with methacrylate, the quantity can be moved from Fair to Good condition, but if the treated cracks are in Poor condition, they remain in Poor condition. Cracking is only considered fully repaired when they have been injected with epoxy.

3.2.2 Cracking Distribution

The cracking database was used to evaluate the frequency and location of different types of cracks in the concrete decks of box girder bridges. In the database, box girder bridges report different types of cracks, such as longitudinal, transverse, diagonal, or pattern. Cracking is also reported over bents, piers, and near abutments for these four types of bridges, and there is also information provided when these bridge deck cracks have been treated with methacrylate.

Figure 3.15 shows the ratio of bridges reporting different types of cracks, relative to the total number of bridges from Figure 3.13 for each structural type. Longitudinal cracks are more frequent in prestressed concrete structures in almost 70% of the cases, while reinforced concrete bridges show longitudinal cracks in 21% and 33% for simply supported and continuous bridges, respectively. Transverse cracking is more frequent in continuous bridges, 72% of the cases for reinforced concrete bridges and 56% for prestressed concrete bridges, while the lowest frequency is found on simply supported bridges of prestressed concrete. Diagonal and pattern cracks are present in all four types of structures in lower frequency, but a 46 % of the cases show diagonal cracks in simply supported prestressed concrete bridges.

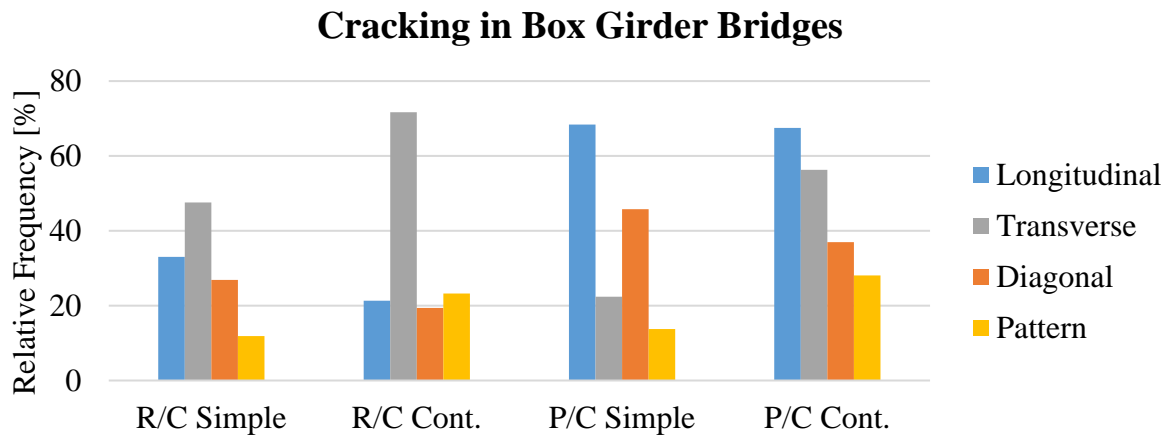


Figure 3.15: Crack frequency in Box Girder Bridges

Figure 3.16 shows the most common locations for cracking reported in box girder bridges. In prestressed concrete continuous structures almost 50% of the cases exhibit cracking over bents, and very lower percentage (2%) in simply supported structures. Cracking near the abutments is exhibited by all four types of bridges, with greater frequency in prestressed concrete bridges. Cracking throughout the deck area is reported on average in same proportions for all four types of bridges, 37% on average, meaning that the cracking is spread in the whole deck area for more of one-third of the total number box girder bridges.

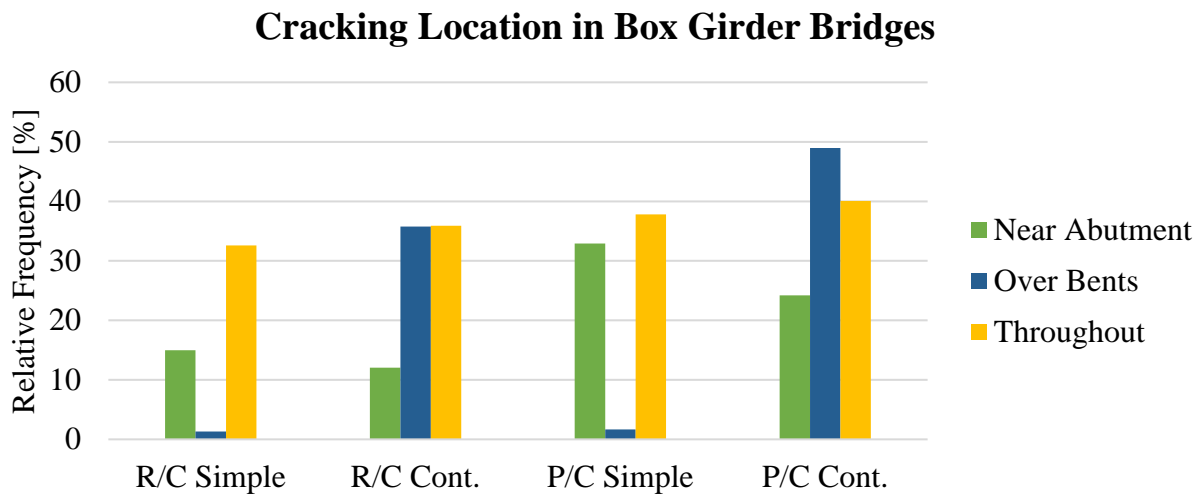


Figure 3.16 Typical locations of cracking reported in Box Girder Bridges

Figure 3.17 shows the frequency of cracking treatment with methacrylate in box girder bridges. From the database, continuous reinforced concrete bridges exhibit the greatest percentage among all four types of box girder bridges with 33% of the cases, while the other structures are close to 20% on average.

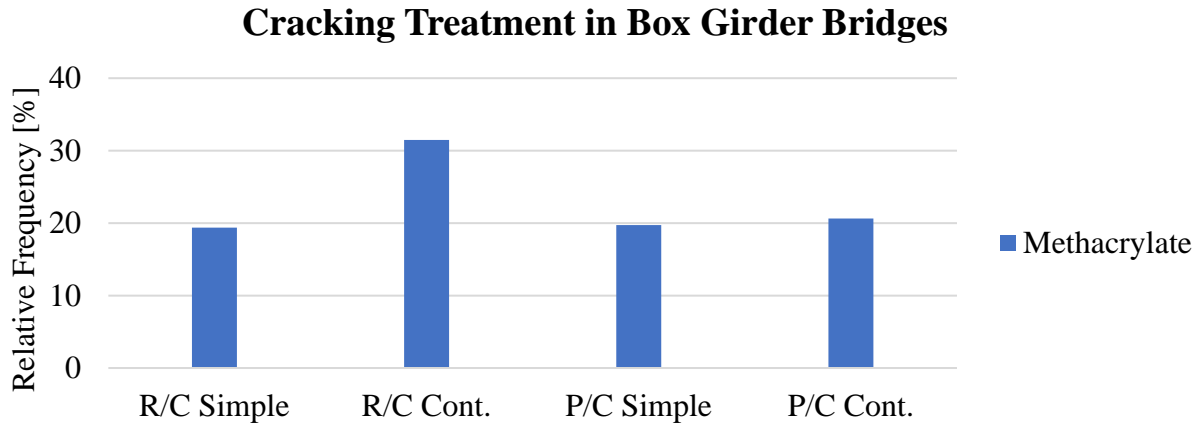


Figure 3.17: Ratio of cracked decks treated with methacrylate in Box Girder Bridges

Figure 3.18 shows the cracking condition state per Table 3-7. Reinforced concrete bridges report cracking in Good condition (sealed cracks below 0.05 in. wide) in greater percentage when compared to prestressed concrete bridges. Prestressed concrete bridges report between 40% and 50% of cracking in Fair condition (unsealed cracks below 0.05 in. wide), while reinforced concrete bridges show up to 30% of Fair condition state. Poor condition cracking, wider than 0.05 in. wide, is more frequent in continuous structures of reinforced concrete up to 20% of the cracked area. There are no cracks reported in severe condition state.

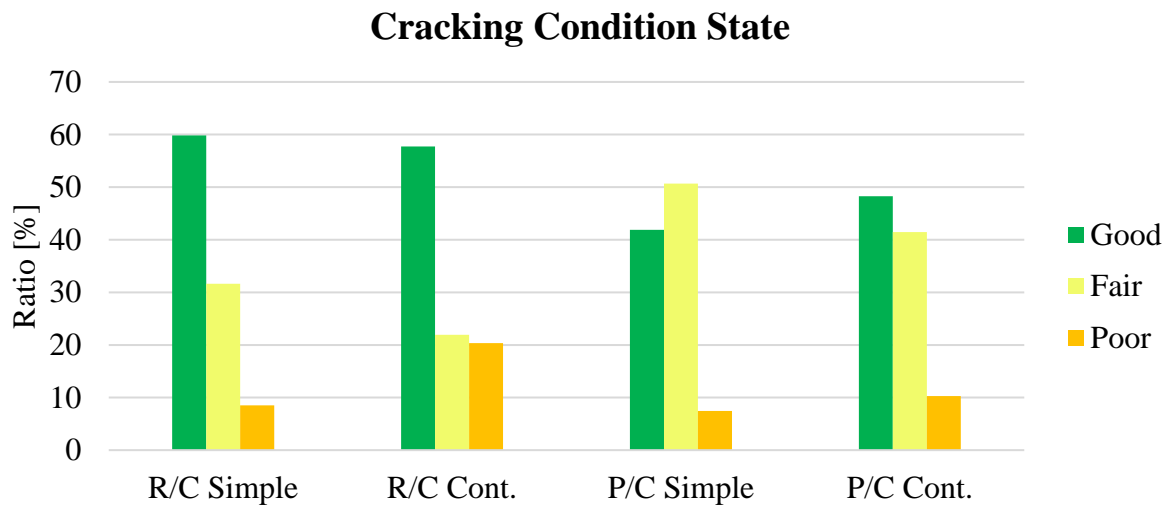


Figure 3.18: Cracking condition state in Box Girder Bridges

3.3 Representative Structures

A total of 94 inspection reports of Box Girder Bridges were available for this study provided by the California Department of Transportation (Caltrans). The bridges selected for this study were based on a statistical assessment. Since the NBI data has been available since 1992, and the inspection of bridges vary from 2 to 3 years after construction, the following criteria were used:

- Box girder bridges
- Reinforced Concrete and Prestressed Concrete
- Built after 1989
- Major maintenance reported

From the inspection reports, the following information was be obtained:

- Geometric properties of the bridge: cross-section, number of lanes, span, number of girders, girder spacing, number of boxes, type of supports, and deck width.
- Design information: deck thickness, reinforcing details, shrinkage reinforcement, rebar spacing, reinforcing size.
- Bridge defects: cracking, delamination, and spalling.
- Works did to the bridge: repairs and work recommendations.
- Graphical information: blueprints, pictures of the bridge elements, cracking of structural elements.

From the inspection reports, information about different types of cracks on the bridge decks that, include longitudinal, transverse, diagonal, and map pattern cracks, was obtained. Using the photographs available in the inspection reports, the location of the cracks was estimated on the bridge cross-section drawings. Detailed information about the 94 box girder bridges is attached in **Appendix A.**

Table 3-8: Selected Box Girder Bridge Database (**R/C**: Reinforced Concrete; **P/C**: Prestressed Concrete; **Cont.**: continuous span; **Simple**: simple span)

Bridge ID	Year Built	Material	Structure Type	Bridge ID	Year Built	Material	Structure Type
02 0036L	1964	R/C	Cont.	17 0030	1991	P/C	Simple
19 0178	2001	P/C	Cont.	23 0020	1993	P/C	Cont.
20 0284L	2007	P/C	Cont.	23 0205L	1992	P/C	Cont.
27 0115	2006	P/C	Cont.	23 0205R	1992	P/C	Cont.
28 0183L	1997	P/C	Cont.	28 0104	1998	P/C	Cont.
28C0228	1996	P/C	Simple	28 0161	1994	P/C	Cont.
33 0212L	1994	P/C	Cont.	28 0322K	1997	R/C	Cont.
33 0585	1993	P/C	Cont.	29 0306L	1992	P/C	Simple
37 0366L	1991	P/C	Cont.	29 0306R	1992	P/C	Simple
37 0368L	1990	P/C	Simple	33 0580S	1991	R/C	Cont.
37 0414F	1991	P/C	Cont.	33 0581S	1991	R/C	Cont.
37 0420L	1990	P/C	Cont.	33 0582S	1991	R/C	Cont.
37 0421L	1990	P/C	Cont.	33 0616L	1998	P/C	Cont.
37 0421R	1990	P/C	Cont.	33 0616R	1998	P/C	Cont.
37 0434L	1990	P/C	Simple	37 0037S	2005	P/C	Cont.
37 0467L	1991	P/C	Cont.	37 0431L	1991	R/C	Cont.
37 0547L	1994	P/C	Cont.	37 0431R	1991	R/C	Cont.
37 0547R	1994	P/C	Cont.	37 0470L	1994	P/C	Cont.
53 2790L	1994	P/C	Cont.	37 0470R	1994	P/C	Cont.
53 2790R	1994	P/C	Cont.	37 0470S	1994	P/C	Cont.
53 2795F	1994	P/C	Cont.	37 0553	1997	P/C	Cont.
53 2795G	1994	P/C	Cont.	37 0636	2001	P/C	Cont.
54 1114R	1996	P/C	Cont.	37 0660R	2008	P/C	Cont.
54C0617	1991	P/C	Cont.	39 0015L	1997	P/C	Cont.
55 0655	1992	P/C	Simple	39 0015R	1999	P/C	Cont.
55 0670	1990	P/C	Cont.	39 0028R	1997	P/C	Cont.
55 0678	1995	P/C	Cont.	39 0224R	1997	P/C	Simple
55 0700L	1995	P/C	Cont.	39 0225L	1997	P/C	Simple
55 0701L	1995	P/C	Simple	41 0001	1995	R/C	Cont.
55 0701R	1995	P/C	Simple	49 0060R	1991	P/C	Cont.
55 0709L	1993	P/C	Simple	49 0165R	1992	P/C	Cont.
55 0709R	1993	P/C	Simple	51 0162K	1997	R/C	Cont.
55 0759R	1996	P/C	Cont.	51 0162L	1997	R/C	Cont.
55 0862R	1996	P/C	Simple	55 0730L	1996	P/C	Cont.
55C0557	1991	R/C	Cont.	55 0730R	1996	P/C	Cont.
55C0628	1997	P/C	Cont.	55 0850R	1995	P/C	Cont.
55C0629	1997	R/C	Cont.	57 1019L	1999	P/C	Simple
55C0637	2000	P/C	Cont.	57 1019R	1999	P/C	Cont.
56 0362	1992	P/C	Cont.	04 0311R	2012	R/C	Cont.
04 0311L	2011	P/C	Simple	28 0389L	2008	P/C	Cont.
08 0163	2007	P/C	Cont.	28 0389R	2008	P/C	Cont.
08 0164	2002	P/C	Simple	39 0225R	1997	P/C	Cont.
12 0196	1998	P/C	Cont.	49 0060L	1991	P/C	Cont.
12 0198	2008	P/C	Cont.	49 0165L	1992	P/C	Cont.
14 0014	2003	R/C	Cont.	55 0850L	2014	P/C	Cont.
14 0058	1991	P/C	Simple	57 1017L	1999	P/C	Cont.
15 0086	2009	P/C	Cont.	57 1017R	1999	P/C	Cont.

CHAPTER 4. LIVE LOADS AND EFFECTS ON BRIDGES

4.1 WIM Stations in California

Weigh-in-Motion (WIM) measurements enable continuous recording of trucks passing sensors. The WIM systems can collect traffic volume, vehicle configurations (axle or wheel load and spacing), and load spectra. It is a powerful tool for collecting a massive traffic database. Data is recorded for every vehicle, including a detailed description of vehicle configuration, vehicle class, measurement date and time, occupied lane, trip direction, moving speed, and truck axle weights and spacings.

To accurately assess traffic-induced load effects, it is required to verify the data quality. There are uncertainties in the measurement process that must be considered while dealing with big data. Assessment of the live load effect plays a key role in designing and evaluating roads and bridges to maintain the infrastructure's safety. Hence, it is important to assess the load effects adequately and not underestimate or overestimate them. Underestimation of live load effects can cause premature damage to bridges and roads, and overestimation can cause a significant increase in cost.

According to FHWA data, there are over 90 WIM stations in California. Data from selected 24 WIM stations were available for this study. All available data was collected and implemented in the GIS system, where main roads and WIM stations are presented. The map of 24 selected WIM sites is shown in Figure 4.1. These WIM sites are located near California's biggest cities: Los Angeles and San Francisco, along the interstate road I-5. Collected WIM data is available for the years 2014 to 2019.

4.1.1 Data decryption (iAnalyze)

Vehicle attributes measured by WIM equipment are stored in binary files. Without human intervention, this data consists of a direct recording of the system vehicle's attributes. Therefore, this data is called RAW data. It is necessary to convert binary data to a user-friendly format, where CSV text format is sufficient. This format is a commonly used ASCII one (American Standard Code for Information Interchange). Every data record is stored in one line, and every single data is delimited by a definite sign (comma or semicolon). It is required to use dedicated software for such data decryption. The iAnalyze software provided by IRD Traffic Data DLL, version 7.9, was used (Figure 4.2). Massive RAW WIM data was processed to transform traffic data into a user-friendly format. Approximately 420 million vehicle records were decrypted.

4.1.2 Average Daily Truck Traffic

The first analysis was prepared to check trends in truck traffic and validate the number of vehicles captured by every WIM station. The analysis was prepared based on Average Daily Truck Traffic (ADTT). Decrypted WIM records and CSV text files were transferred to SQL Database, what enabled efficient data validation. Moreover, it enabled statistical analyses for every WIM station and every year of data. Table 4.1 show the summarized results of this analysis for every WIM station and six years of data: 2014-2019. It clearly shows that traffic data is consistent, and the increment in truck traffic over the years is observed in most stations.

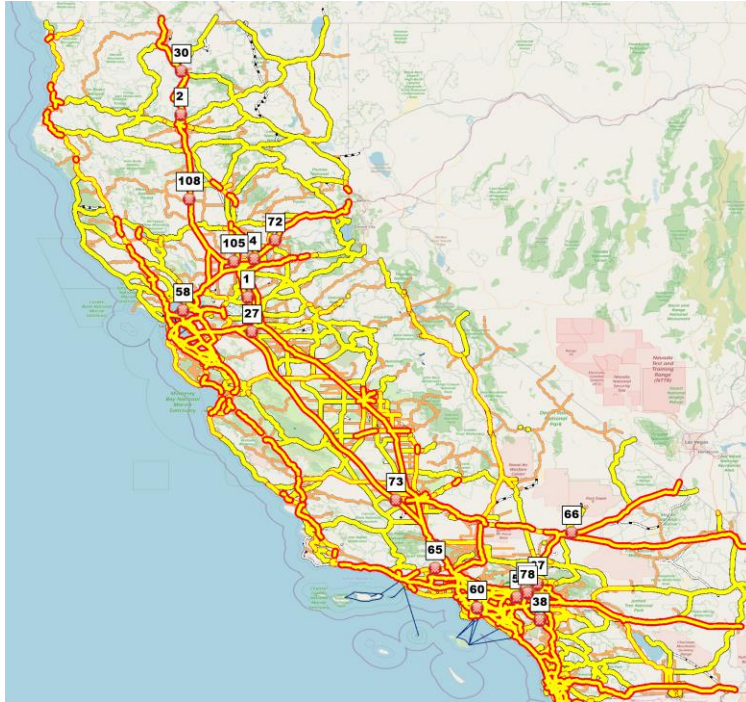




Figure 4.1: Location of selected WIM stations in California



International Road Dynamics
INTERNATIONAL ROAD DYNAMICS



**CUSTOMER
DRIVEN**

iANALYZE

Data Analysis/Reporting Software

IRD P/N 152146 Release 7.9, 64-bit

No update available.

Build: 7.9.7095.22773

IRD Traffic Data DLL: 2.1.0.0

Language File: Language.resources

Copyright(c) 2003-2019

Warning: This product is protected by copyright and international treaties.

Figure 4.2: iAnalyze Software Information

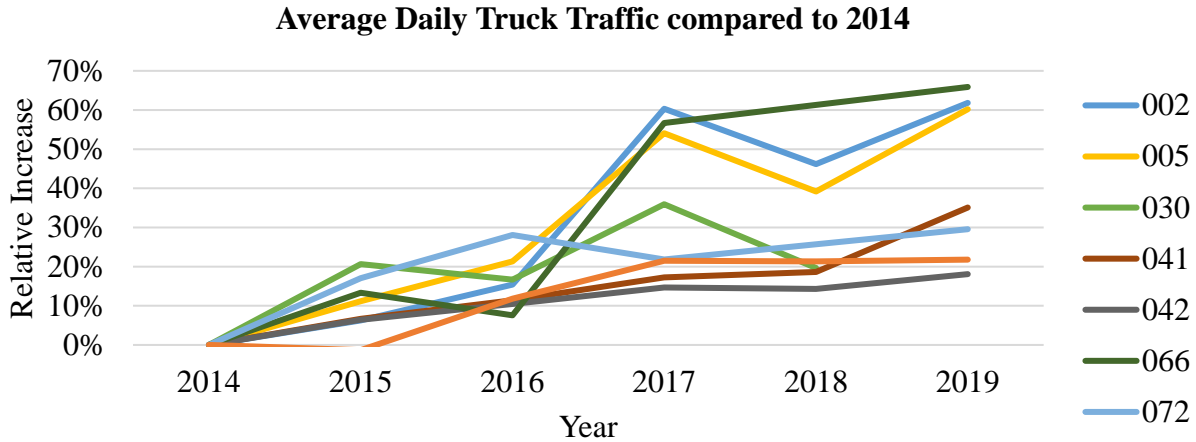


Figure 4.3 Percentage of change in ADTT versus 2014 for the selected WIM sites

Table 4.1 California ADTT by years in WIM Stations

WIM Station ID									
Year	001	002	003	004	005	027	030	037	038
2014	10,696	6,202	4,669	4,502	8,452	7,679	5,494	5,196	6,790
2015	9,278	6,590	4,980	5,011	9,396	8,459	6,629	5,548	6,902
2016	11,198	7,159	8,269	9,715	10,257	11,052	6,411	5,747	7,169
2017	7,977	9,942	17,375	8,552	13,022	13,645	7,468	11,126	7,024
2018	22,122	9,067	16,680	7,679	11,763	10,146	6,575	11,488	7,321
2019	25,490	10,036	14,919	7,619	13,540	12,618		9,226	4,309
	041	042	057	058	059	060	065	066	067
2014	5,200	5,028	6,605	6,066	14,689	15,120		7,724	15,610
2015	5,546	5,351	5,991	6,225	14,290	15,336		8,755	14,783
2016	5,793	5,555	5,382	6,626	15,043	15,377		8,307	13,145
2017	6,096	5,765	18,210	14,034	15,827	15,689	4,976	12,102	9,872
2018	6,170	5,748	19,451	11,911	15,863				7,548
2019	7,025	5,937	18,161	15,261	16,529	16,251		12,813	9,914
	069	070	072	073	077	078	105	108	
2014	9,749	6,909	5,857	9,260	9,181	8,580		7,651	
2015	9,929	7,314	6,855	9,562	9,059	8,254		8,266	
2016	11,817	7,309	7,502	9,802	10,267	10,963		8,690	
2017	11,943	8,041	7,136	11,009	11,155	23,088		9,700	
2018	10,841	7,882		10,522	11,141	22,540		8,758	
2019			7,588	10,731	11,181	22,827	19,007	9,040	

4.1.3 FHWA WIM Data

California's overall truck traffic analysis can be done using FHWA WIM data. For this analysis, available FHWA data was used. Data for 85 WIM stations was provided by FHWA, and the map of FHWA WIM sites is presented in Figure 4.3. Figure 4.4 shows the precise location of WIM sites based on the satellite Google Maps.

Appendix B lists all active FHWA WIM stations, ADT, ADTT, a share of heavy vehicles in overall traffic flow, and the number of traffic lanes. FHWA traffic data was shared in text WGT-coded format files, and it includes counts from 2014 to 2019. Separate files were obtained for traffic volume and vehicle weights. A special procedure was developed in MATLAB software to decrypt these massive files and convert all WGT-coded files into MATLAB matrices. The number of recorded vehicles per WIM station and year is presented in Appendix B.

Over 7.6 billion records were processed and transferred to the SQL Server database. It enabled efficient data analyses with such a massive number of records. Traffic trends are one of such analysis, where a huge sample of data was used. WIM traffic trends are presented for two selected locations: WIM 129000, located in Los Angeles, I-5 (six traffic lanes per direction), and WIM 49000, located in Dublin, CA, I-680 (four traffic lanes per each direction). Observed truck traffic can be called very heavy, where the average ADTT = 12,300 trucks/day and ADTT = 8,600 trucks/day, respectively, and the busiest lane: 2,600 trucks/day (21% of ADTT) and 1,950 trucks/day (23% of ADTT), meaning a truck passing a cross section as an average every 45 seconds. While trends in ADT show a slight increase in traffic (mainly because of the high saturation level index), in both cases, a significant increase in ADTT is observed – on average 2.3% and 6.5% per year. The increasing trend in vehicle class 5 (single units 2 axles trucks) volume is noticeable. In both cases, vehicle class 11 volume (multi-trailer, 5 or fewer axle trucks) increased

in 2014 and 2015; a significant decrease has been noticed. Moreover, the volume of the most common vehicles class 9 (single trailer 5 axle trucks) between 2015 and 2019 did not change significantly (see Figure 4.5 and Figure 4.9).

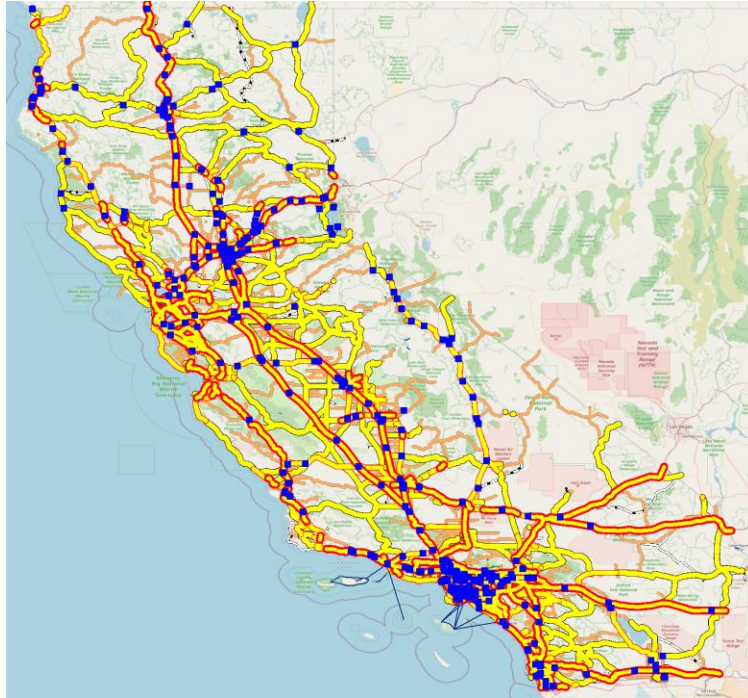
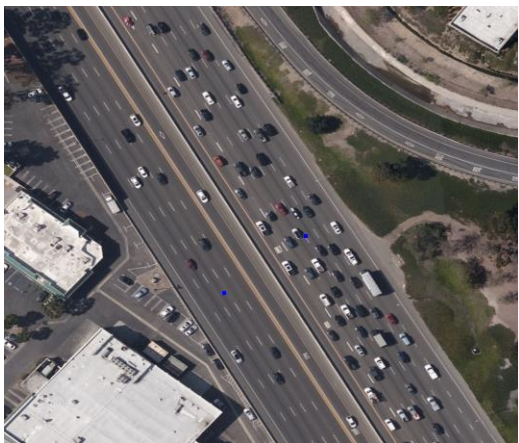


Figure 4.3: California WIM site locations based on FHWA data.



(a) 129000 – I-5 (Los Angeles, CA)



(b) I-680 (Dublin, CA)

Figure 4.4: Satellite pictures of FHWA WIM station location

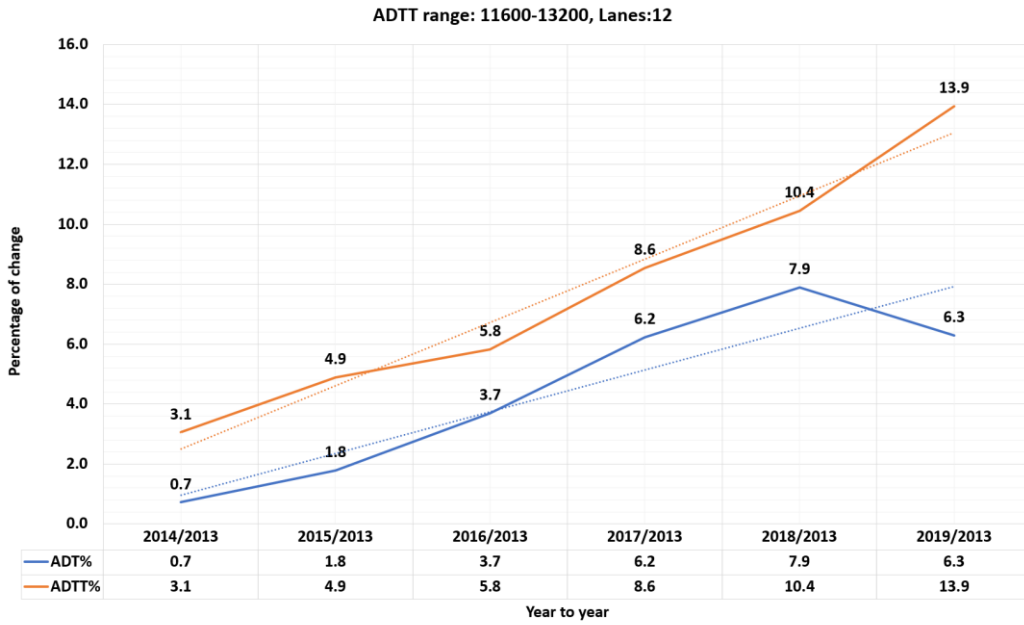


Figure 4.5: Traffic trends for WIM station 129000 for 12 traffic lanes.

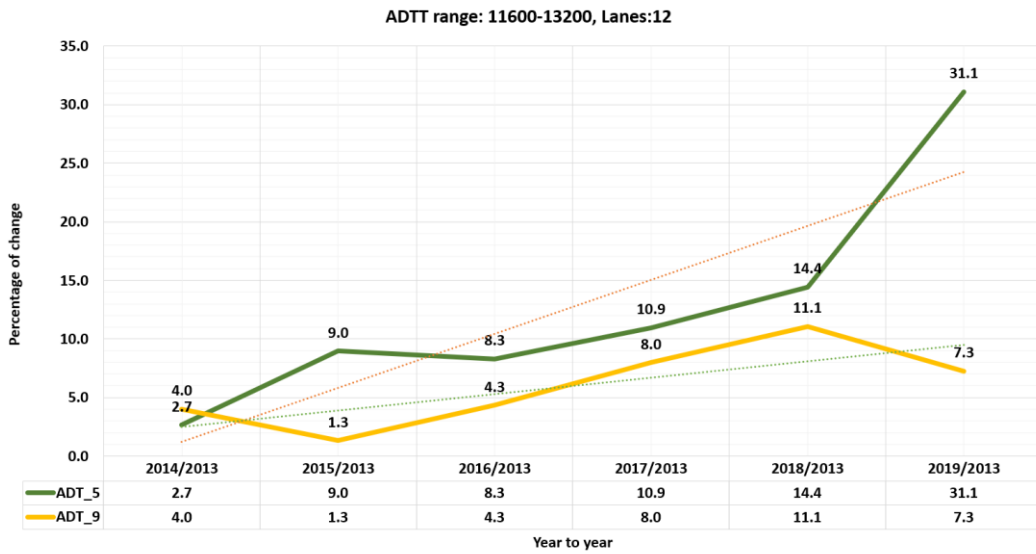


Figure 4.6: Traffic trends for WIM station 129000 for 12 traffic lanes, and vehicles class 5 and 9.

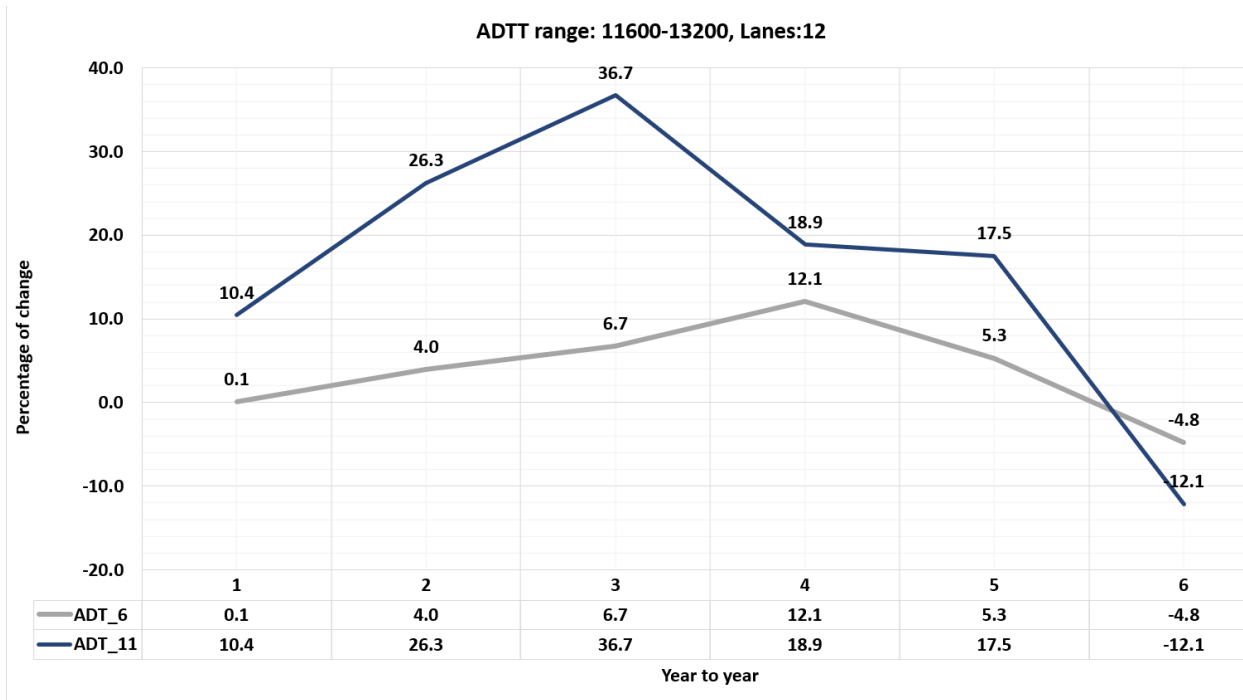


Figure 4.7: Traffic trends for WIM station 129000 for 12 traffic lanes, and vehicles class 6 and 11.

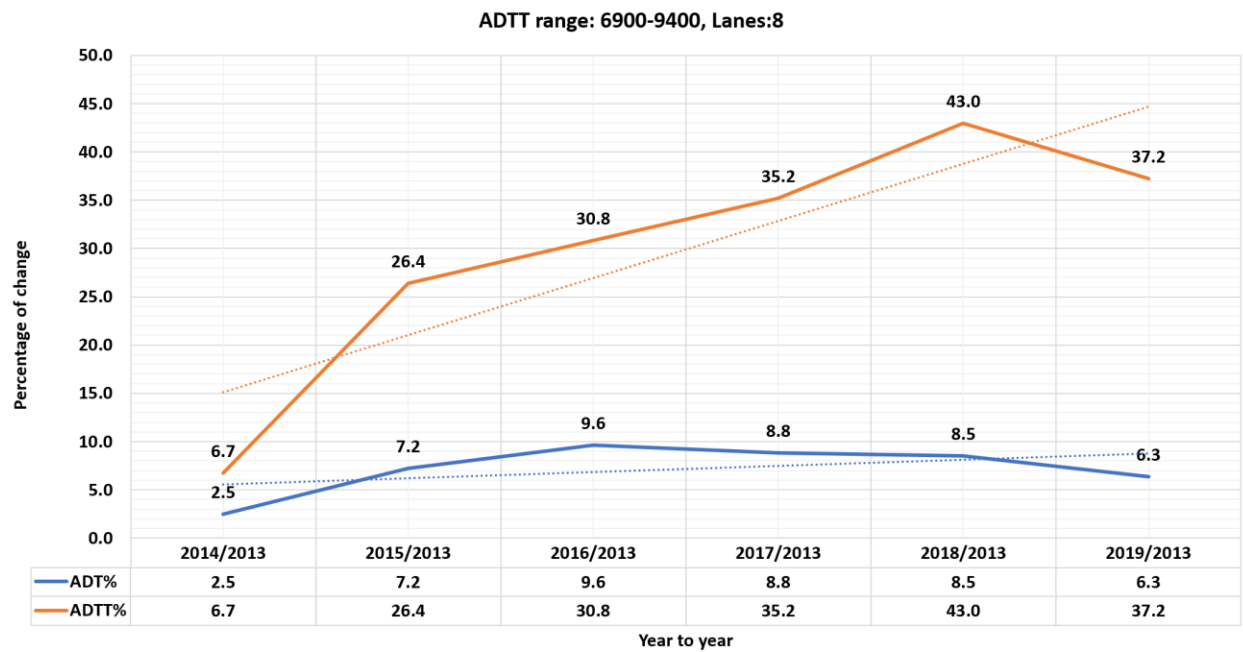


Figure 4.8: Traffic trends for WIM station 49000 for 8 traffic lanes.

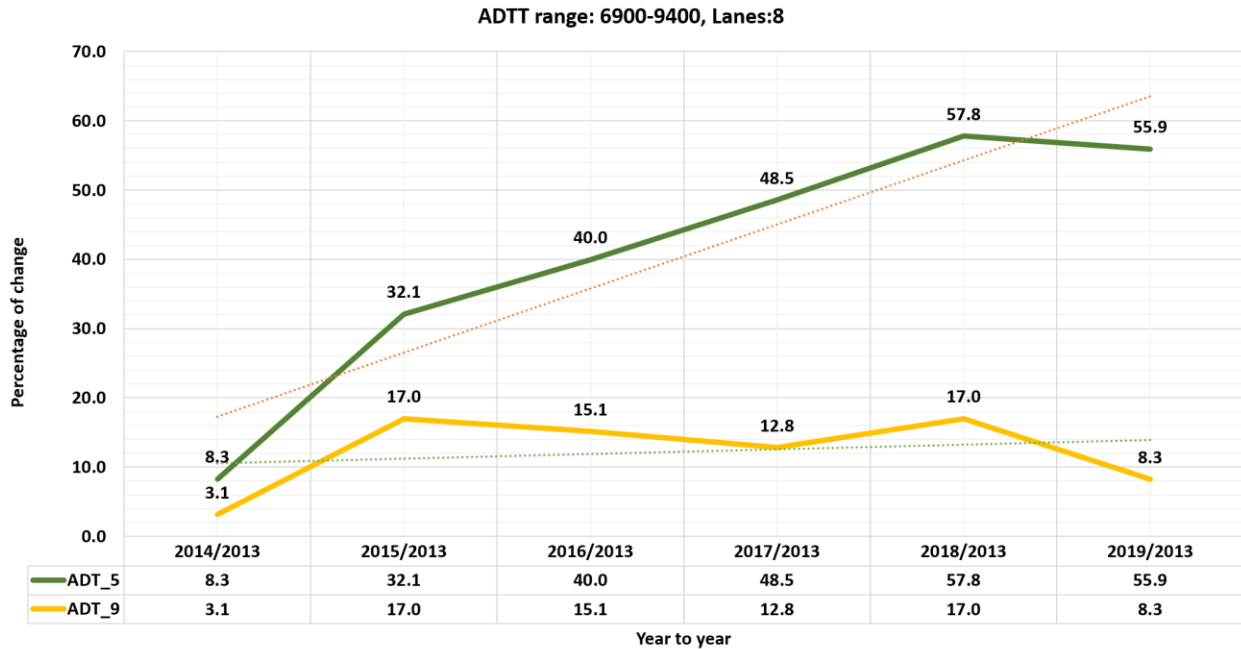


Figure 4.9 Traffic trends for WIM station 129000 for 8 traffic lanes, and vehicles class 5 and 9.

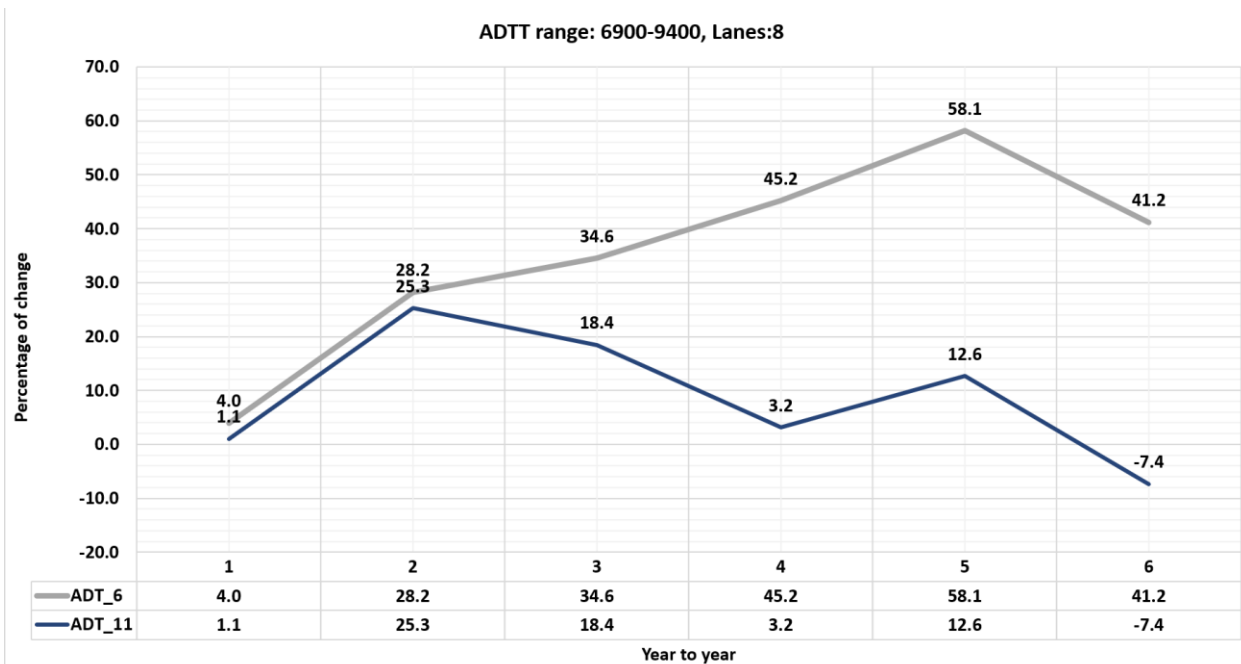


Figure 4.10: Traffic trends for WIM station 49000 for 4 traffic lanes and vehicles class 6 and 11.

If trends in traffic growth presented in Figures 4.6-4.10 continues, a domination of vehicles class 5 and 9 will be much more significant in a few years.

4.1.4 Quality Control Procedure

FHWA WIM data was preliminarily cleaned by the FHWA criteria, and all outliers were discarded. Moreover, all records for truck with GVW over 150 kips were eliminated. Caltrans WIM data was sent in RAW format and required additional procedures to eliminate possible errors. Therefore, quality control (QC) procedure was introduced to remove questionable records. The QC procedure was based on the literature review and experience with WIM data analysis. This procedure requires several filters to be applied to verify all data. The following criteria were used to filter WIM records in the Caltrans WIM database:

1) Data description:

- duplicated records,
- with all or more consecutive axles with the same weight,
- with wrong station identification,
- missed or wrong date and/or time,
- wrong lane of travel,
- vehicle speed below 10 mph or over 90 mph

2) Vehicle configuration:

- vehicles class below 1 or over 13,
- GVW equal 0,
- number of axles below two or not the equivalent number of loaded axles,
- steering axle weight below 40 kips,
- single axle weight below 60 kips,
- tandem weight below 80 kips,
- tridem weight below 120 kips,
- axle spacing over 3.3 ft,
- the left and right wheel weights of any axle have a difference of 40%, or either of the wheel weights of such axle exceeds 2.0 kip.

Duplicated records are a common problem, which may be caused by device malfunction. The number of records and percentage of duplicated records per WIM station is presented in Figure 4.11 and Table 4.1. The data shows that duplicated records for the state of California are on average 2.4%, with most of the stations showing no duplicated records and some of them up to 10.8% of the recorded data.

Quality control tests included 66 different checks. The results of the quality control analysis are presented in Appendix B.3 and summarized in Table 4-2. The most critical check was the difference between a left and right axle weight. As it is assumed, it should not differ more than 40%. It must be emphasized that 85% of all WIM records passed all quality control tests. California WIM data includes a large percentage of good quality data.

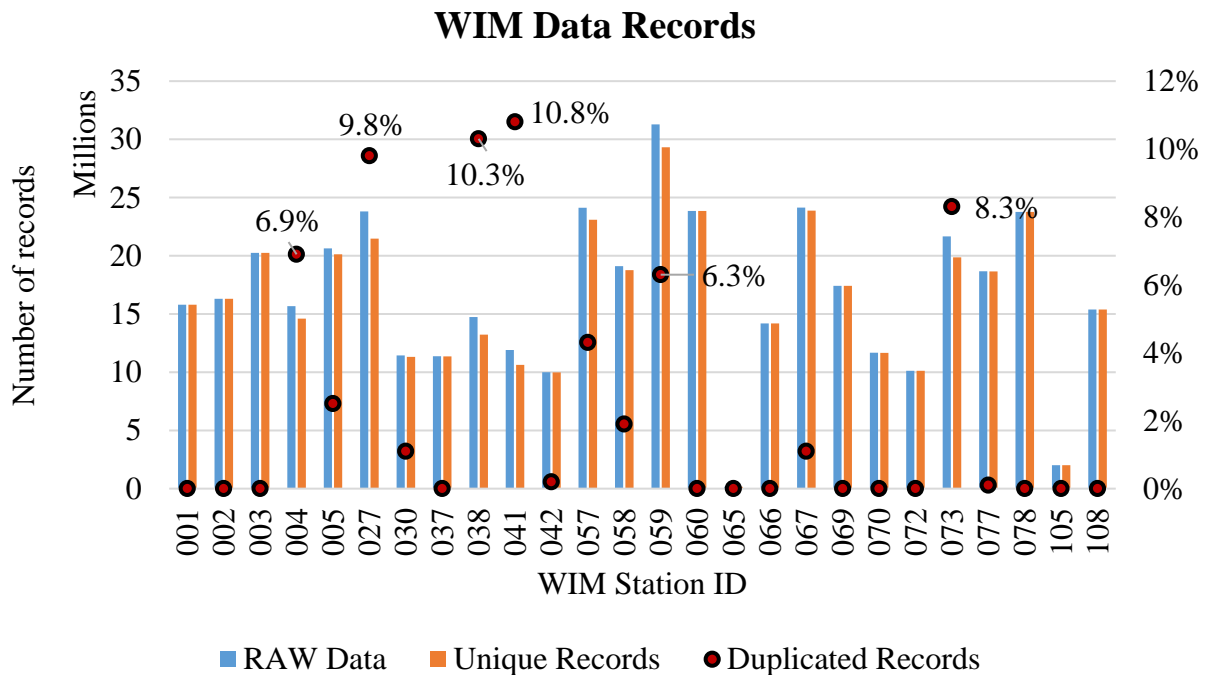


Figure 4.11: RAW vs. duplicated WIM records in California

Table 4-1: Number of RAW and duplicated WIM records for selected sites in California

WIM ID	RAW data	Unique Records	Duplicated Records
001-Lodi	15,800,340	15,797,723	0.0%
002-Redding	16,302,682	16,302,647	0.0%
003-Antelope EB	20,246,892	20,246,813	0.0%
004-Antelope WB	15,676,845	14,597,851	6.9%
005-Indio	20,637,273	20,129,791	2.5%
027-Tracy	23,809,733	21,466,505	9.8%
030-Mt Shasta	11,444,742	11,316,327	1.1%
037-Elsinore SB	11,367,389	11,362,159	0.0%
038-Elsinore NB	14,744,712	13,225,239	10.3%
041-Vacaville EB	11,913,044	10,629,066	10.8%
042-Vacaville WB	10,002,909	9,985,859	0.2%
057-Pinole EB	24,125,716	23,092,796	4.3%
058-Pinole WB	19,113,866	18,759,184	1.9%
059-La710 SB	31,279,870	29,319,042	6.3%
060-La710 NB	23,851,541	23,851,510	0.0%
065-Piru	160,108	160,107	0.0%
066-Calico	14,182,520	14,182,498	0.0%
067-Devore	24,142,148	23,874,630	1.1%
069-Fontana SB	17,419,707	17,419,464	0.0%
070-Fontana NB	11,667,228	11,663,237	0.0%
072-Bowman	10,127,943	10,127,943	0.0%
073-Stockdale	21,667,396	19,863,320	8.3%
077-Colton EB	18,662,739	18,653,003	0.1%
078-Colton WB	23,765,634	23,765,393	0.0%
105-Elkhorn	2,018,119	2,018,095	0.0%
108-Willows	15,389,442	15,389,427	0.0%

Table 4-2: Summary of WIM quality control analysis.

Station ID	RAW Data	Filtered Data	% of tests passed
001-LODI	15,800,340	11,807,641	74.7
002-REDDING	16,302,682	13,200,852	81.0
003-ANTELOPE_EB	20,246,892	18,021,030	89.0
004-ANTELOPE_WB	15,676,845	14,394,432	91.8
005-INDIO	20,637,273	16,939,466	82.1
027-TRACY	23,809,733	19,813,507	83.2
030-MT_SHASTA	11,444,742	9,178,557	80.2
037-ELSINORE_SB	11,367,389	9,446,925	83.1
038-ELSINORE_NB	14,744,712	11,317,127	76.8
041-VACAVILLE_EB	11,913,044	9,749,468	81.8
042-VACAVILLE_WB	10,002,909	8,846,183	88.4
057-PINOLE_EB	24,125,716	19,112,465	79.2
058-PINOLE_WB	19,113,866	17,117,862	89.6
059-LA710_SB	31,279,870	25,653,122	82.0
060-LA710_NB	23,851,541	21,356,980	89.5
065-PIRU	160,108	126,909	79.3
066-CALICO	14,182,520	12,463,996	87.9
067-DEVORE	24,142,148	19,811,892	82.1
069-FONTANA_SB	17,419,707	15,576,319	89.4
070-FONTANA_NB	11,667,228	10,604,519	90.9
072-BOWMAN	10,127,943	8,804,069	86.9
073-STOCKDALE	21,667,396	18,226,614	84.1
077-COLTON_EB	18,662,739	16,095,829	86.2
078-COLTON_WB	23,765,634	21,589,819	90.8
105-ELKHORN 108-WILLOWS	2,018,119	1,871,600	92.7
108-WILLOWS	15,389,442	13,861,240	90.1
Total	429,520,538	364,988,420	85.0

Overall, almost 365 million records for 24 WIM stations and 7.6 billion records shared by FHWA were considered for the analysis. FHWA WIM data was preliminarily cleaned, and all records with GVW over 150 kips were discarded. Therefore, only Caltrans data was used for deck live load analysis after Quality Control procedure was applied, and 85% of all WIM records shared by Caltrans was filtered as good and used. This amount of data is considered representative of the state.

4.2 Probability Paper

Probability Paper is a special scale for the statistical interpretation of data. It can be used to determine if a set of data follows a particular probability distribution (Nowak and Collins, 2012). The most common is the probability paper for the normal distribution. The cumulative density function (CDF) for the normal distribution has an “S-shape,” as shown in Figure 4.12. The idea of the probability paper is to redefine the vertical scale so that the normal CDF will be a straight line. The horizontal axis remains on a regular scale.

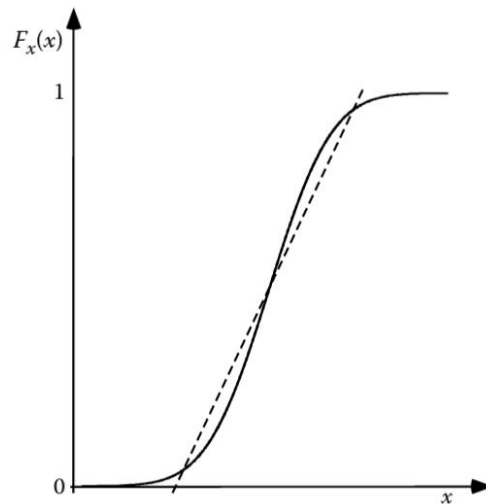


Figure 4.12: S-shaped CDF for a normal random variable. Adapted from Nowak and Collins (2012)

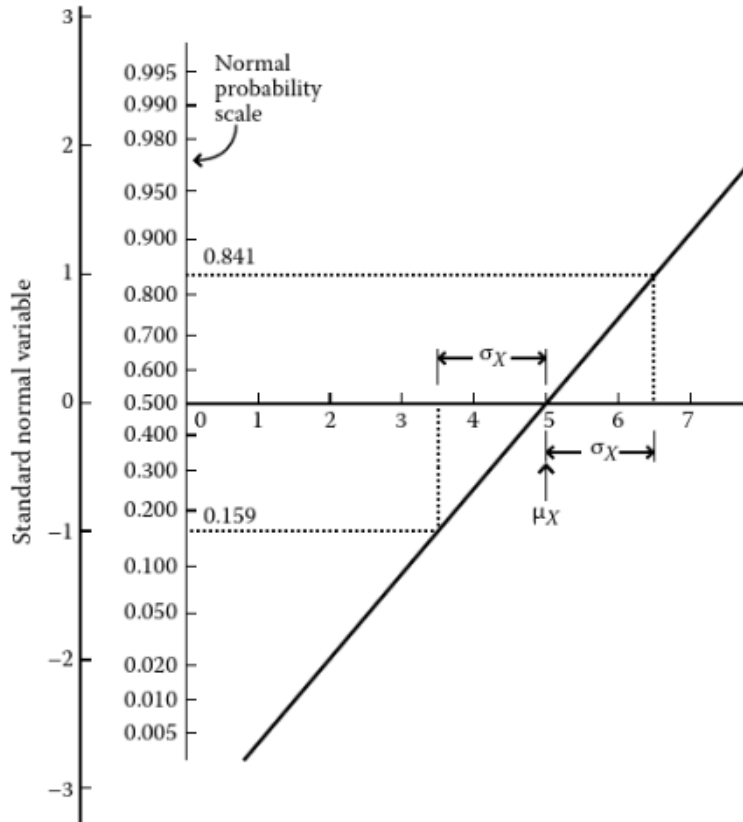


Figure 4.13: Interpretation of a straight-line plot on normal probability paper in terms of mean and standard deviation. Adapted from Nowak and Collins (2012)

In Figure 4.13 it can be seen that a straight line can server as a basis to understand what the standard deviation and mean value of a set of data are. An 84.1% of probability means that there is one standard deviation above the mean value, or 15.9% a standard deviation below the mean value. The mean value is at 50% of probability and is where the horizontal axis is placed.

All the data that has been analyzed from the WIM database will be presented in the following sections in normal probability scale (vertical).

4.3 Gross Vehicle Weight

Gross Vehicle Weight (GVW) is calculated as a sum of all axle loads recorded by WIM sensors. Cumulative distribution functions (CDF) plots were prepared for all WIM stations and for particular years. Data consistency check was the primary goal of this task. Figure 4.14 and Figure 4.15 show GVW plots for selected WIM stations for the years 2014 and 2017. All WIM data plots are attached in Appendix C.

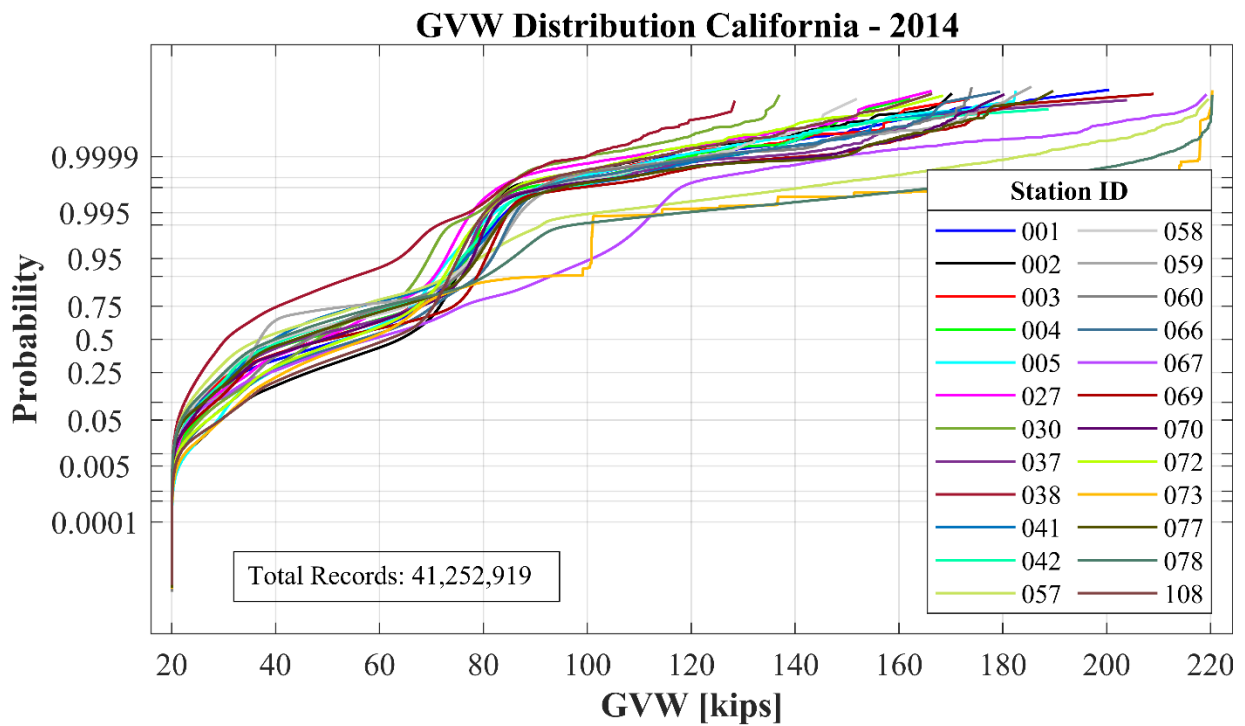


Figure 4.14: CDF plot of GVW for selected WIM stations in California for 2014.

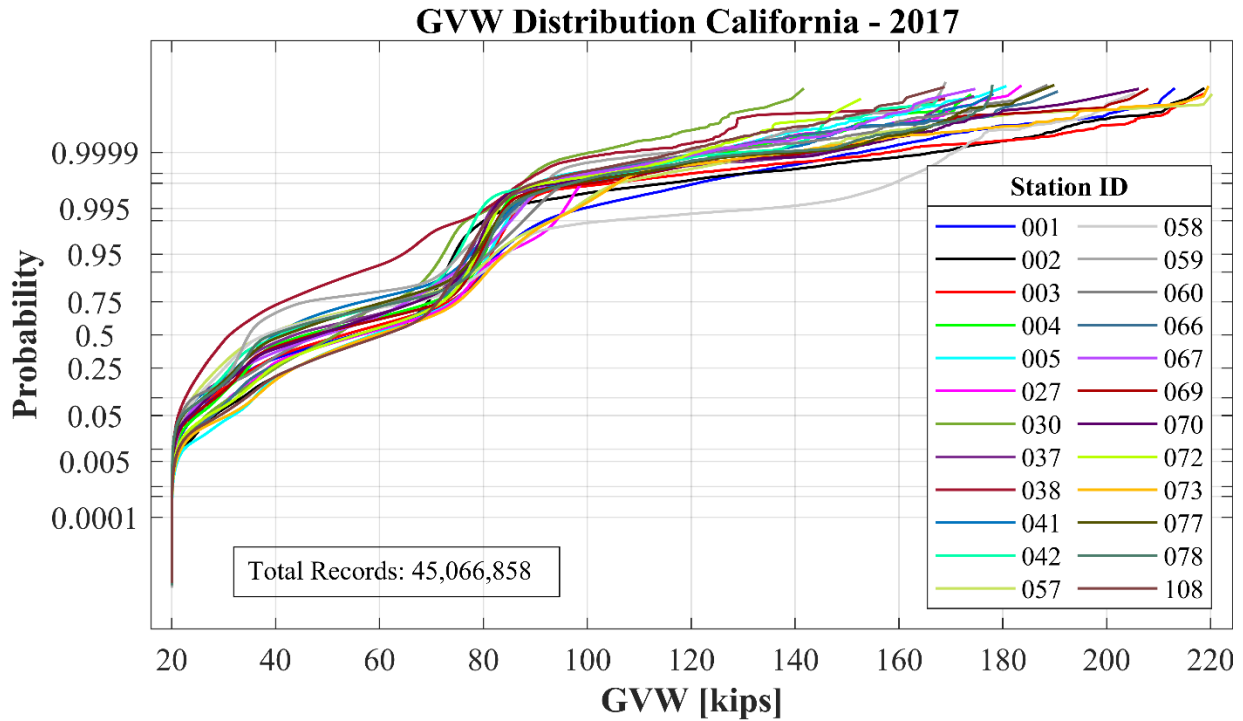


Figure 4.15: CDF plots of GVW for the selected WIM stations in California for 2017.

Gross Vehicle Weight plots show that the change in weight distribution from site to site is insignificant. It can be observed the probability plots for different stations are very similar, which concludes that selected WIM stations are representative of the state. Moreover, GVW weight was analyzed for vehicle classes, where CDF was plotted for vehicle classes 1 to 13 – see Figure 4.16 as an example for the year 2017. Vehicles classes 13 are the heaviest ones, where over 50% of the vehicle exceed 80 kips of GVW limitation.

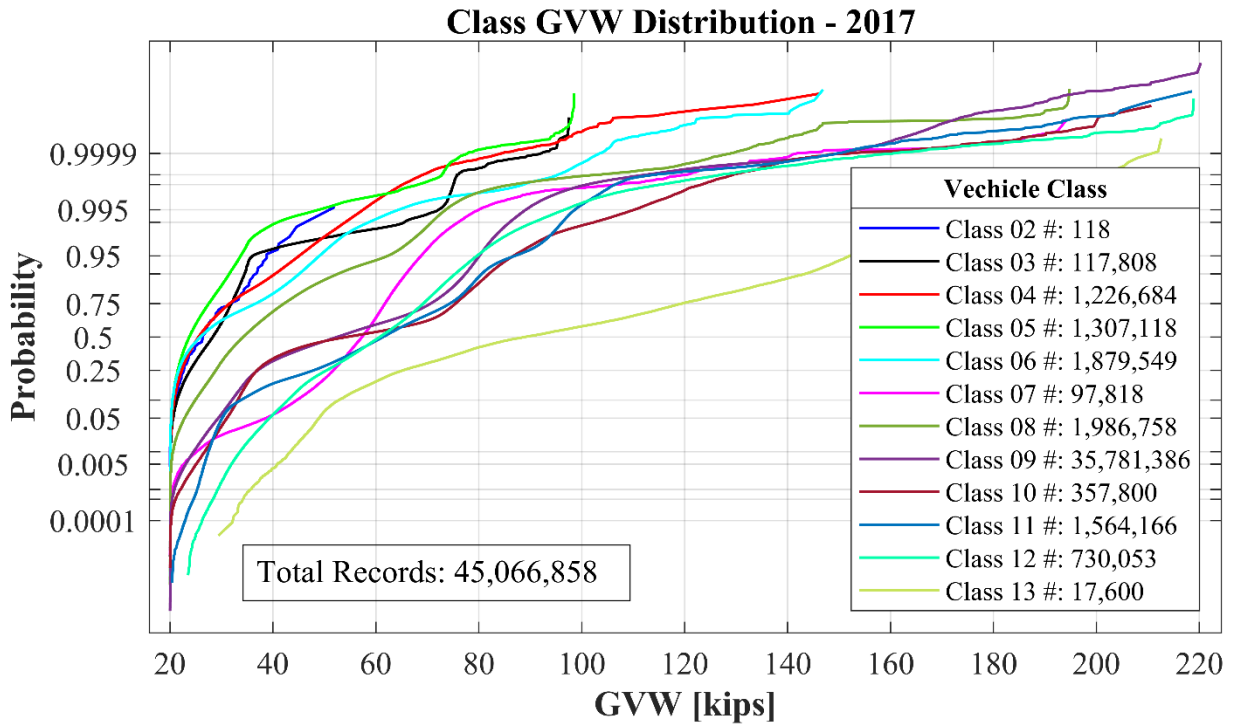


Figure 4.16: CDF plots of GVW for various vehicle classes in California for 2017

4.4 Axle Loads

CDF plots for axle load were prepared for each WIM station to check data consistency and trends. Figure 4.17 and Figure 4.18 show the CDF plots of the second and the fifth axle load, respectively, of truck class 9 vehicles for selected WIM stations 072 – Bowman and years 2014-2018. The axle load distribution is consistent from year to year. All axle loads were plotted and verified for all WIM sites.

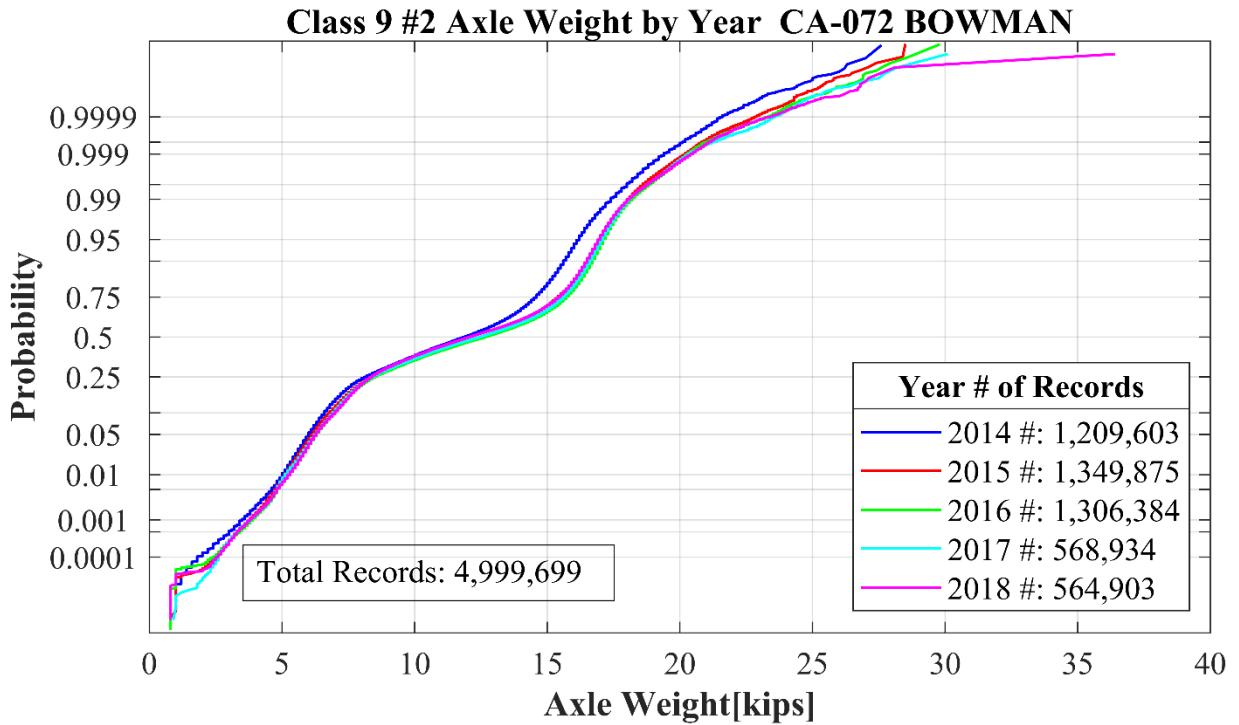


Figure 4.17: CDF plot for the second axle load, WIM 072-Bowman, California, 2014-2018.

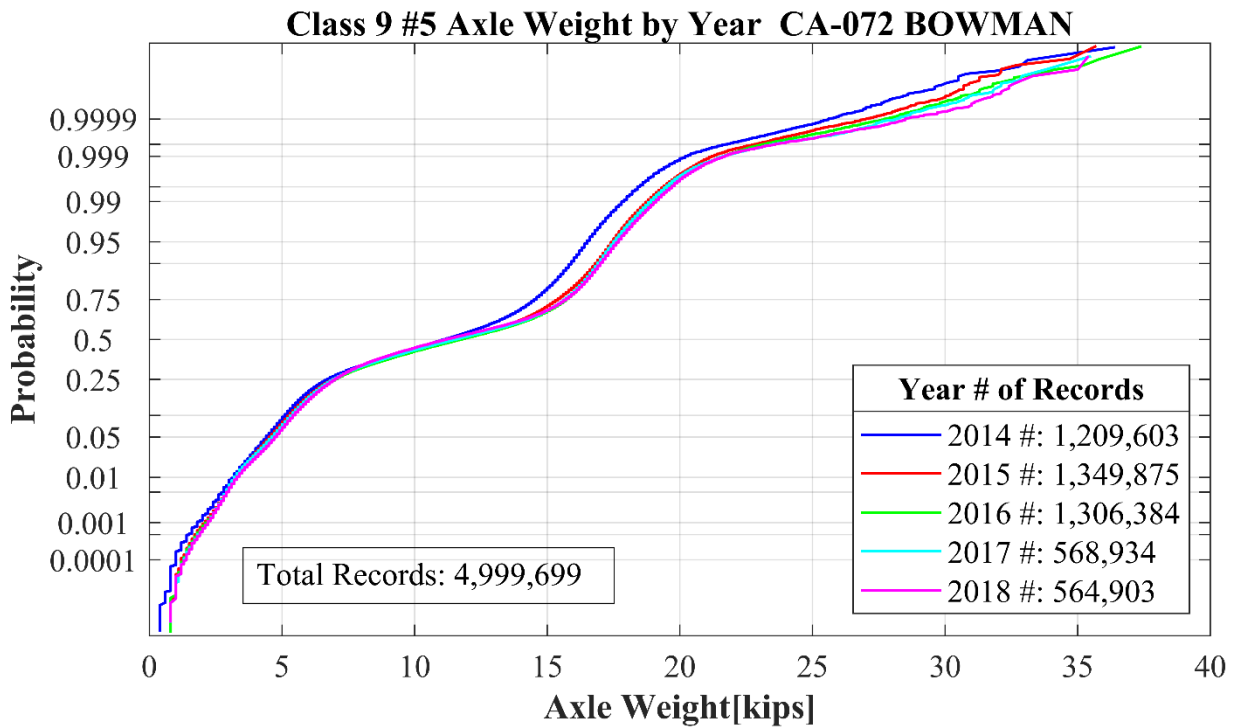


Figure 4.18: CDF plot for the fifth axle load, WIM 072-Bowman, California, 2014-2018.

4.5 Load Effects

The load effects were calculated in terms of the moment on simply supported bridges. For each of the WIM-recorded vehicles, the moment was calculated using influence line analysis and then compared to the moment caused by the HL93 design truck. The concrete bridge with a maximum span length of 120 ft was selected. The results of the calculation are presented in Figure 4.19 and Figure 4.20. It was noticed that only five WIM stations have a ratio greater than 1.0, while in 2016, such observation was done for ten WIM stations. The percentage of vehicles exceeding a ratio of one is very low, less than 0.05%. Therefore, it can be stated that California traffic is no different than the national AASHTO live load model.

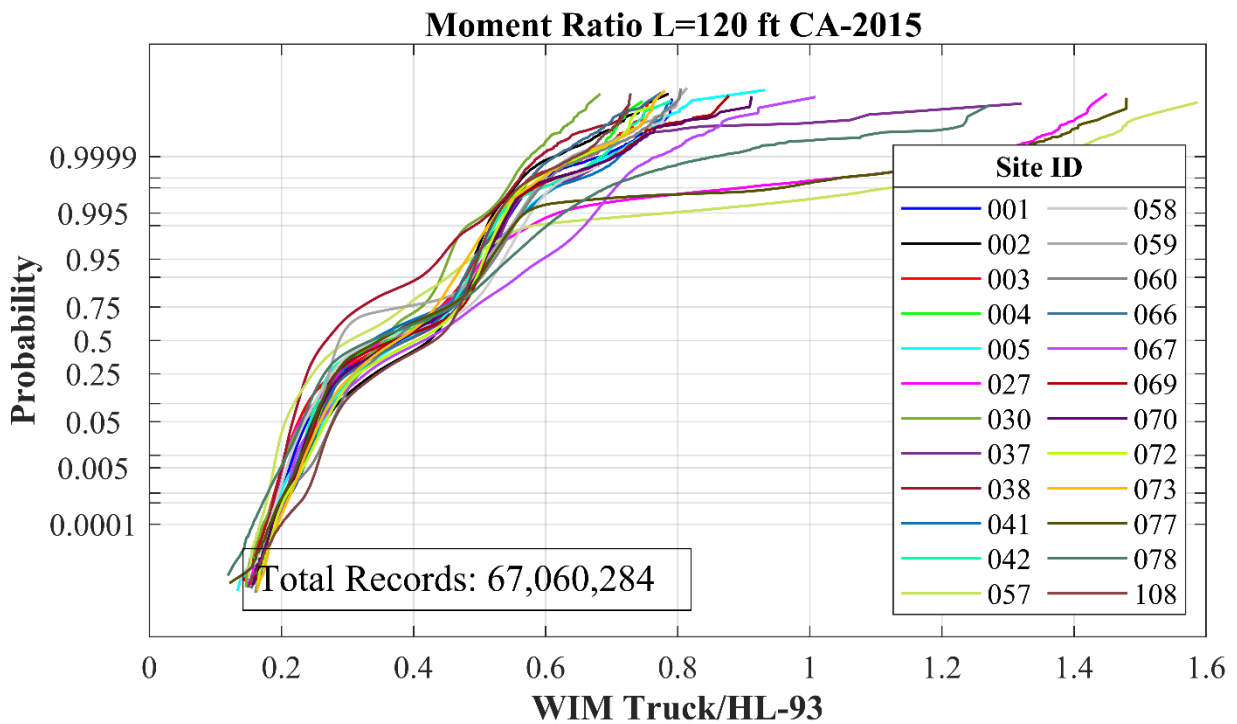


Figure 4.19: CDF plot of WIM truck/HL93 moment ratio in California for 2015

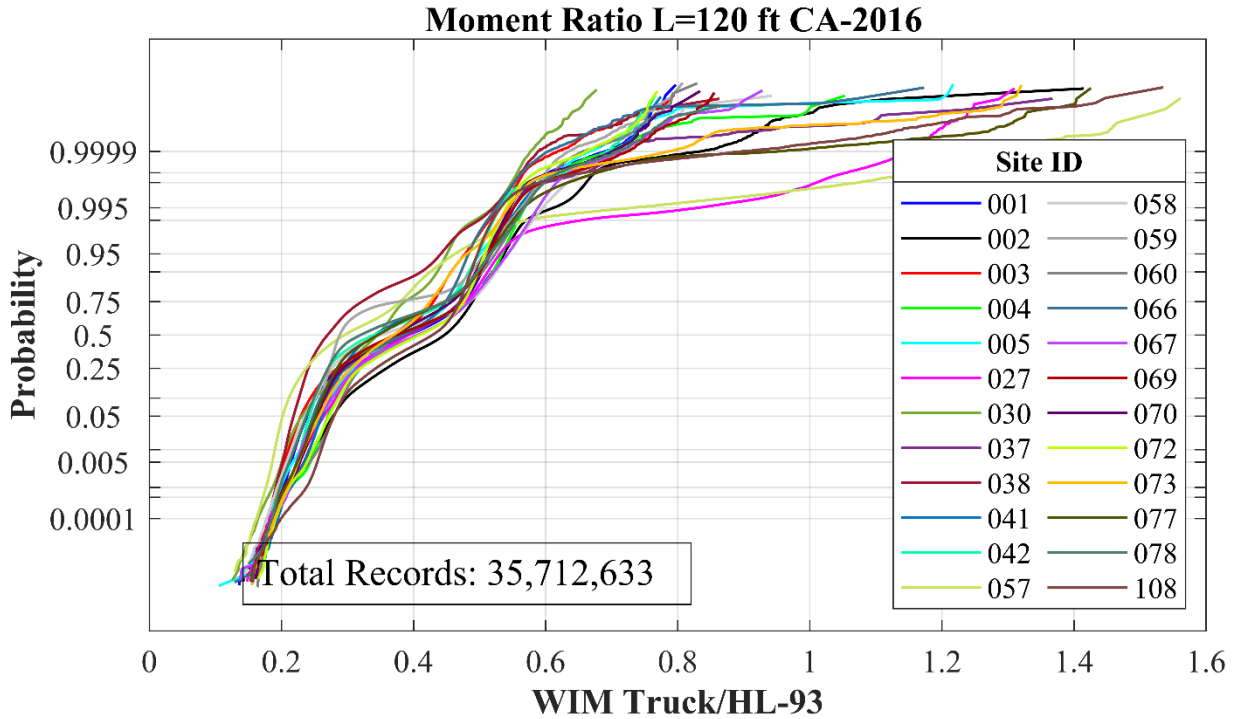


Figure 4.20: CDF plot for WIM truck/HL93 moment ratio in California for 2016.

4.6 Finite Element Model of Box Girder Bridges for Live Load Evaluation

4.6.1 Influence Lines

The use of influence lines for statically indeterminate structures is the same as those for statically determinate structures. They enable the designer to locate the critical positions for placing the live loads and to compute forces for various positions of the loads.

For our purpose, Müller-Breslau's principle was used. In summary, the interior supports are removed with the conjugate-beam method to obtain the deflection, and subsequently, the influence line for each reaction can be obtained, as well as ordinates for other functions (moment, shear, and so on) can be computed with simple statics (McCormac, 2006).

Influence lines were calculated for the moment in the 3 Boxes Model of Bridge #02 0036L, as can be seen in Figure 4.21. Each curve represents an influence line for the moment in that location of the beam due to moving the load throughout the beam.

Influence Lines - Moment in Deck Transverse Section - Midspan

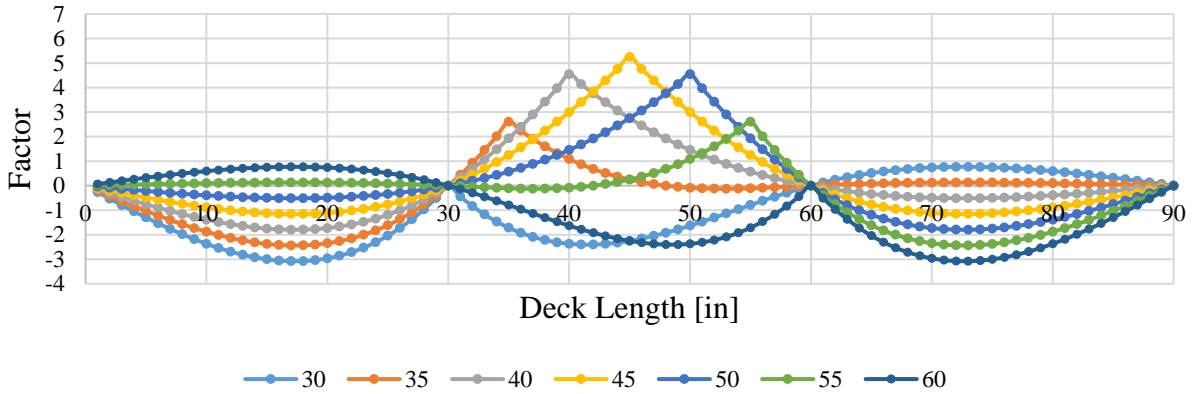
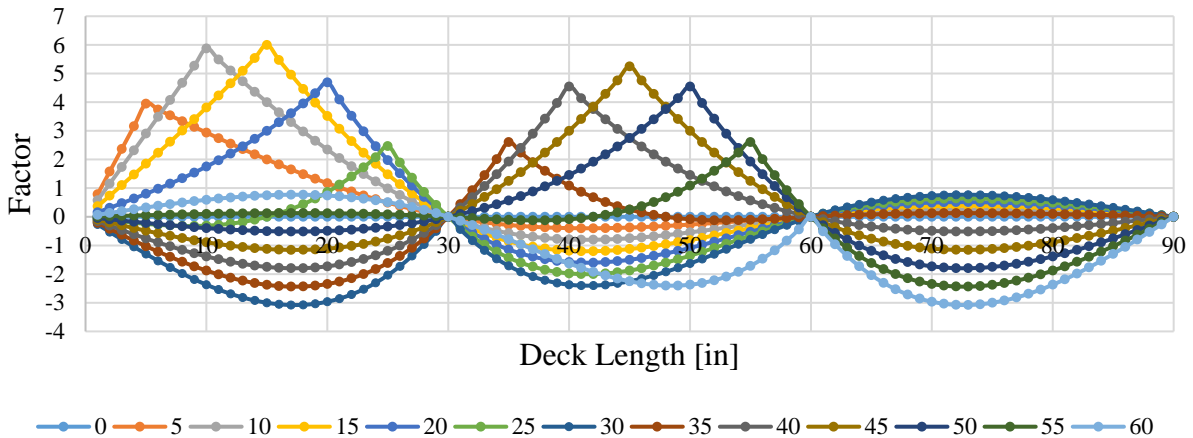


Figure 4.21: Influence lines for Moment, 3 Box Model

Influence Lines - Moment in Deck Transverse Section - 1st and 2nd spans



4.6.2 Simplified Model Bridge #02 0036L

The simplified model of bridge #02 0036L consists of the modeling of the three interior boxes, considering several boundary conditions to study their effect on the stresses developed after the load is applied. A concrete-damaged plasticity model was used to study concrete behavior.

Solid elements to model the boxes of the bridges and common beam elements to model the reinforcing steel. Figure 4.22 presents the cross section of the bridge selected for the first model.

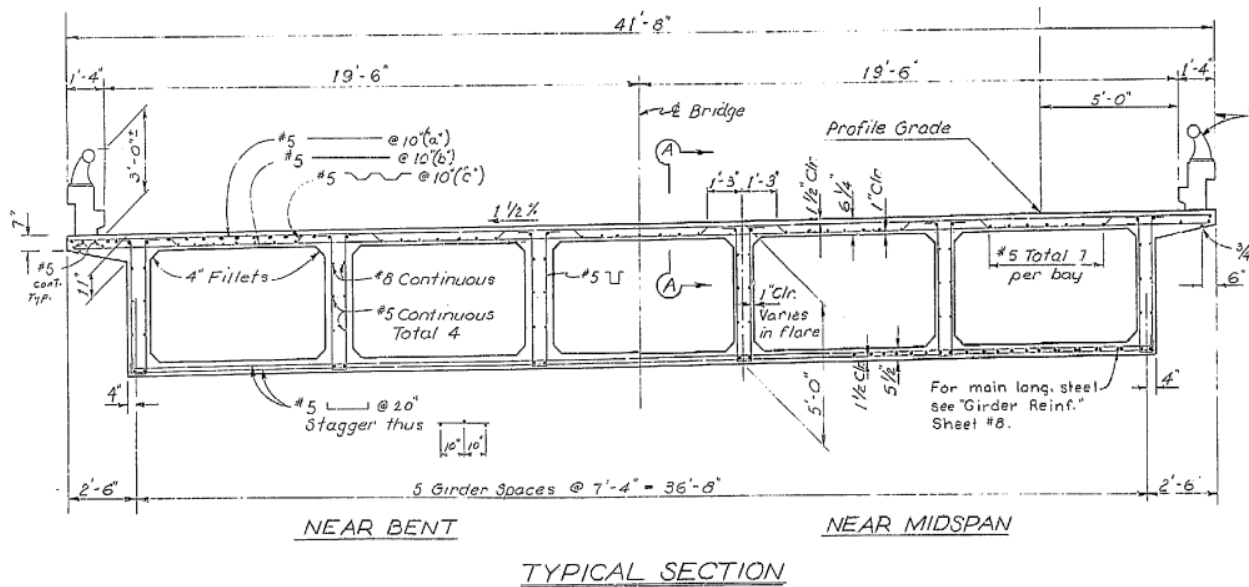


Figure 4.22: Typical section bridge 02 0036L, Inspection Report from Caltrans

4.6.3 Material Properties: Concrete Damage Plasticity

This model provides a general capability for modeling concrete and other quasi-brittle materials in all types of structures (beams, trusses, shells, and solids). The model uses concepts of isotropic damaged elasticity in combination with isotropic tensile and compressive plasticity to represent the inelastic behavior of concrete (SIMULIA, 2019).

The concrete damaged plasticity model is designed for applications in which concrete is subjected to monotonic, cyclic, and dynamic loading. It allows the user to control stiffness recovery effects during cyclic load reversals and enables the failure of elements.

The model assumes that the concrete's uniaxial tensile and compressive response is characterized by damaged plasticity, as shown in Figure 4.23.

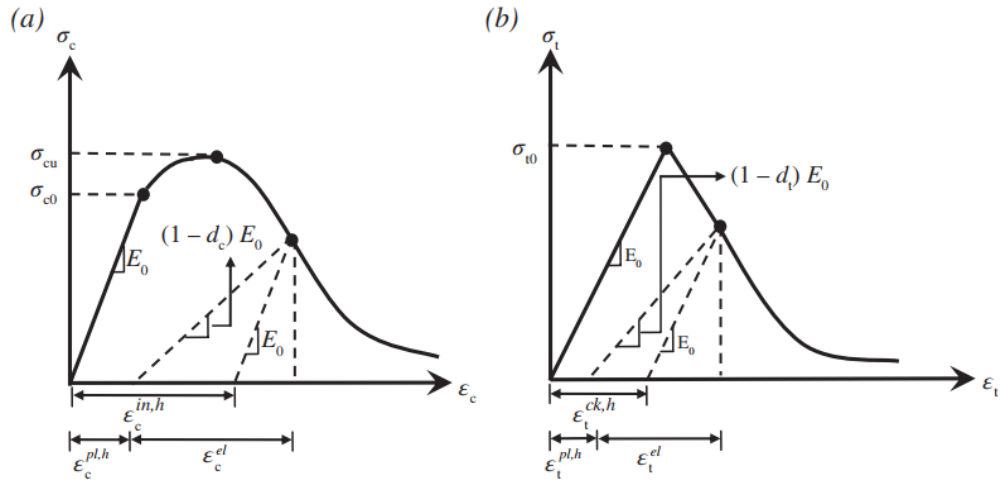


Figure 4.23: Response of Concrete to uniaxial loading condition: (a) Compression, (b) Tension (Hafezolghorani et al., 2017)

In ABAQUS, the concrete damaged plasticity is defined in the module “Edit Material” as shown in Figure 4.24. All input data, including dilatation angle, eccentricity, equibiaxial compressive yield stress ratio, are defined as second stress invariant, etc. In addition, the compressive and tensile behavior parameters need to be entered, as well as the concrete's density and elastic material properties. Parameters that were unavailable for the modeled bridges were assumed from Hafezolghorani et al. (2017).

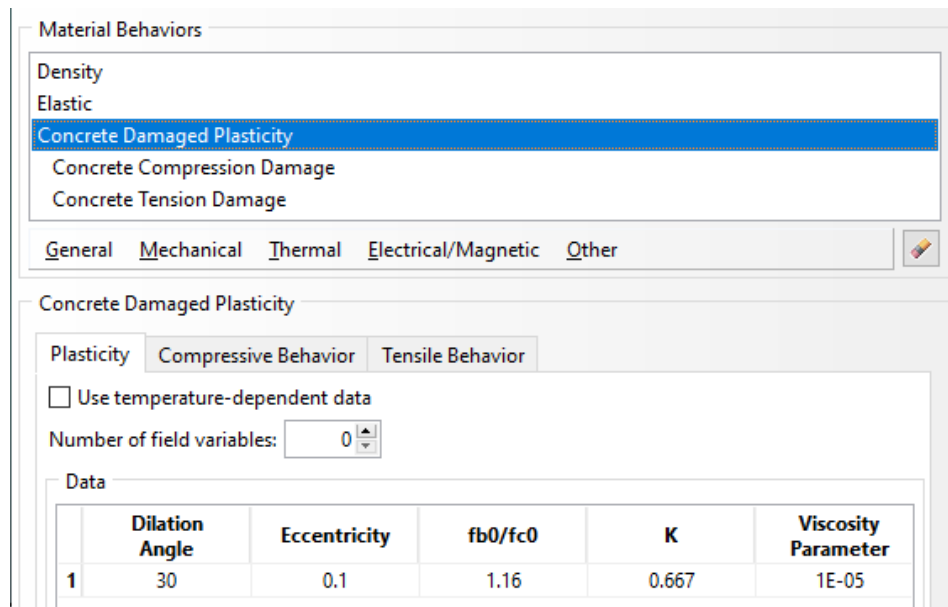


Figure 4.24: Material input data in Abaqus, (Abaqus, 2020)

4.6.4 Bridge Geometry

To construct the finite element model (FEM Model), the geometry of the bridge was obtained from the plans in the inspection reports. The geometry considered for the modeling includes the deck slab reinforcement and the girder reinforcement (flexural and shear reinforcement), see Figure 4.25. Since the focus of the analysis is the behavior of the decks, the bottom slab reinforcement was not considered for the models. In Figure 4.26, the bridge cross section and isometric view are presented.

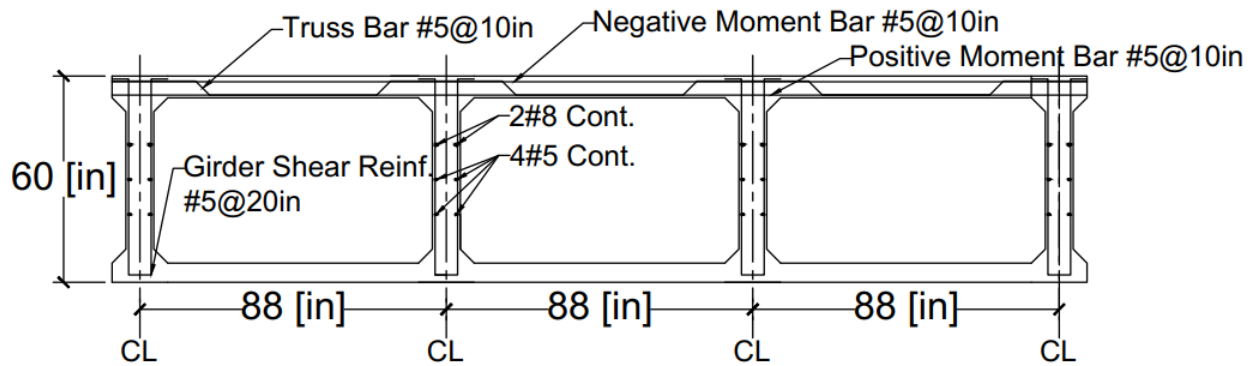


Figure 4.25: Simplified Cross Section of RC Bridge 02 0036L

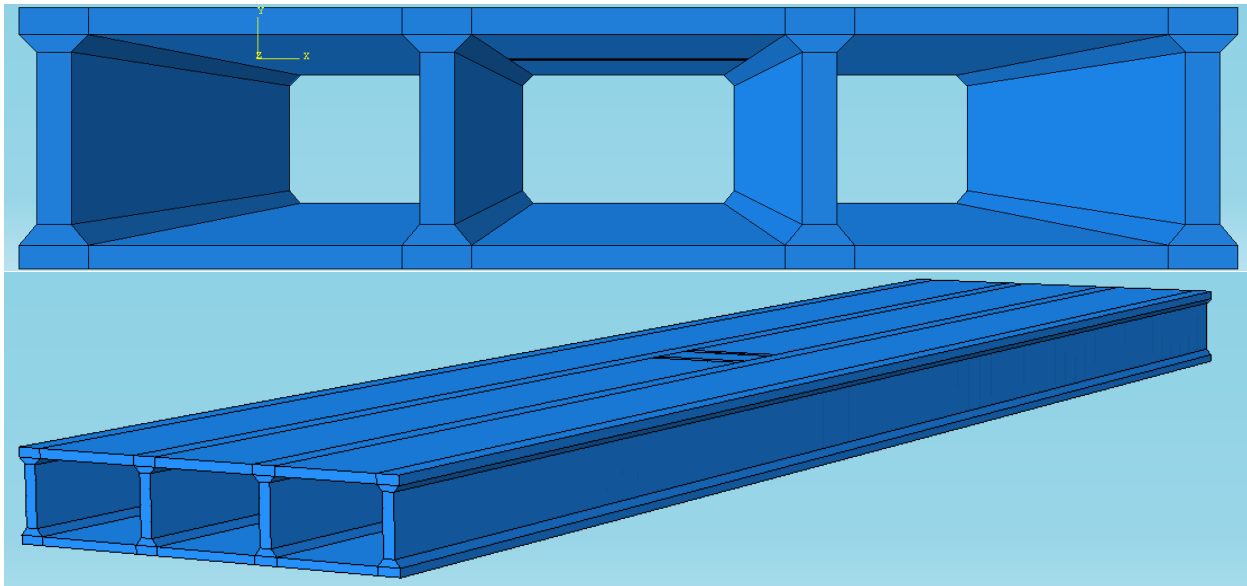


Figure 4.26: 3D Model View of 02 0036L Bridge, Abaqus

4.6.5 Finite Element Model

The finite element model includes solid elements for the concrete and beam truss elements for the reinforcing steel. The solid elements include 8-node hexahedral (C3D8R) with reduced integration, while the embedded reinforcement was modeled using linear elements (T3D2) embedded into the solid elements with the constraint type “Embedded Region”. The mesh selected for the bridge models was of approximate size of 2 in. for all solid elements and linear elements, see Figure 4.27 and Figure 4.28 showing both the cross section and 3D view of the fine mesh used for the FEM. In Figure 4.29 the location of the reinforcement embedded in the bridge is presented. Each model consisted of approximately 2.5 million or more elements and was run in a high parallel computer, lasting between 15 min – 8 hours to obtain the calculation outputs.

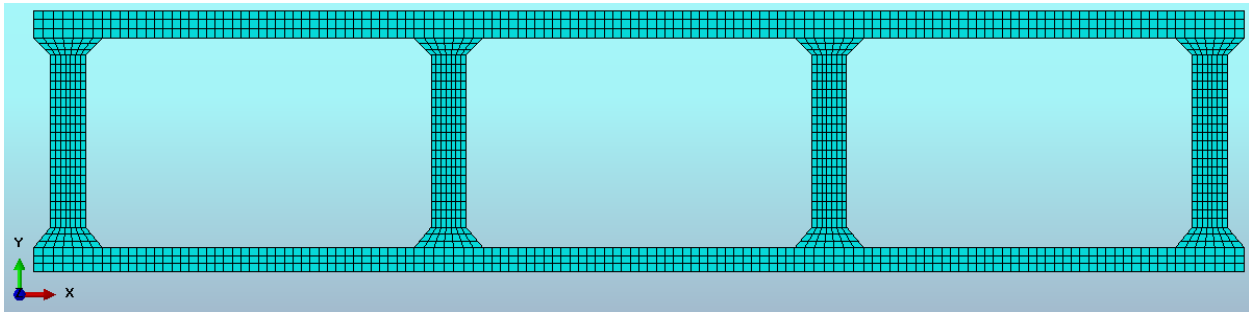


Figure 4.27: Mesh of Cross Section of the Bridge Model

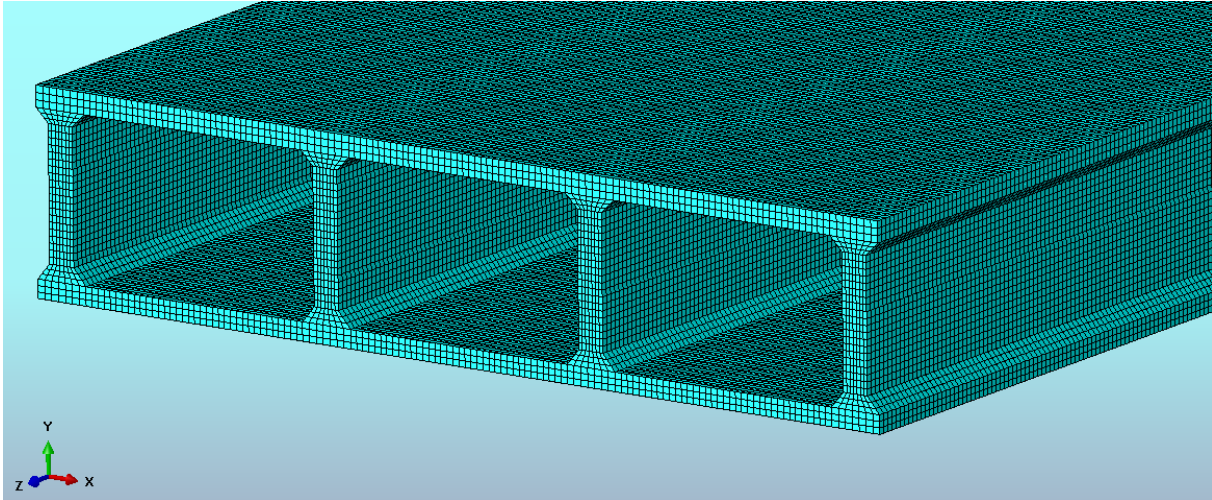


Figure 4.28: 3D Meshed Finite Element Model

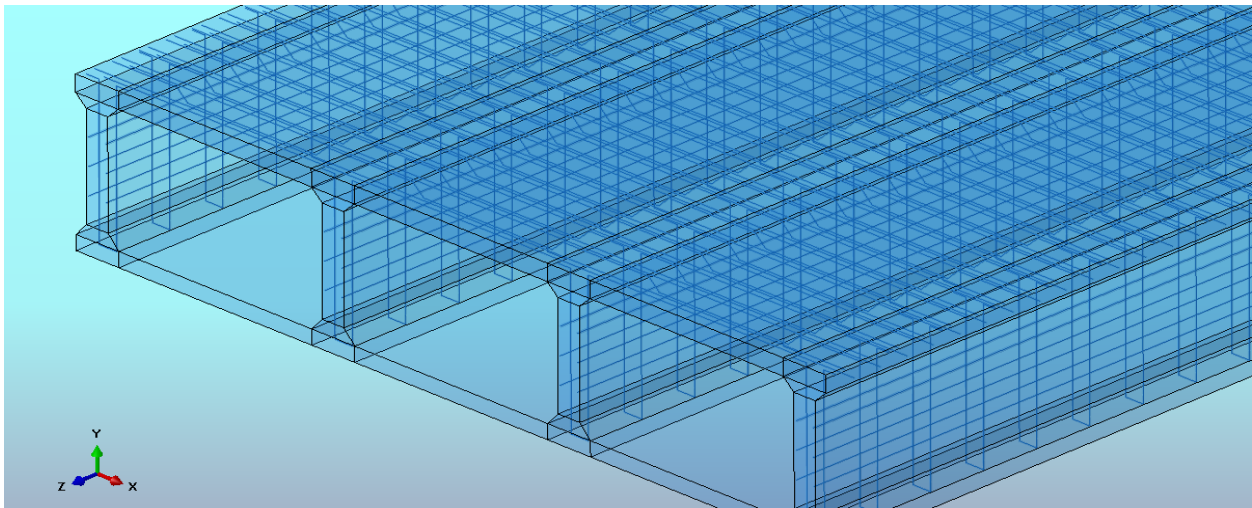


Figure 4.29: Reinforcement Detail of FEM Model

In section 4.6.1, influence lines were determined for the transverse direction. Using this information and the location of the truck loads into the bridge deck were selected, as can be seen in Figure 4.30.

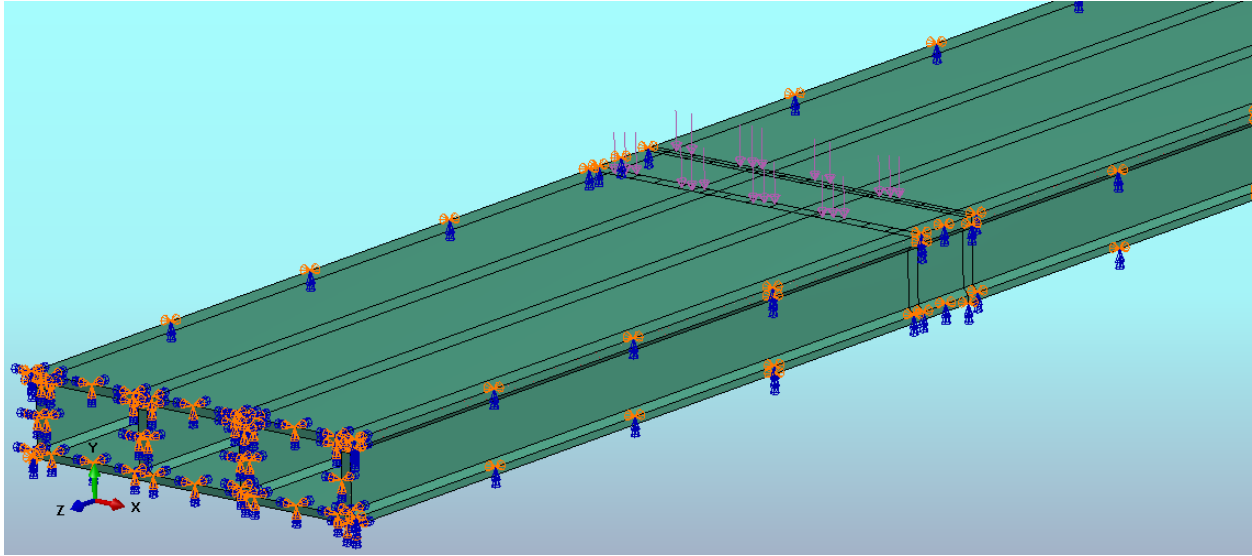


Figure 4.30: 2 Truck Loads applied in 3D FEM model

4.6.6 Transverse Flexural Stresses

Axle loads obtained from the WIM data showed that a very small percentage, less than 0.004%, exceeded 25 kips for interior axles of Class 9 trucks. All load cases considered 2 trucks side by side with 25 kips per axle. In Figure 4.31, each load case is presented with a color to differentiate trucks side by side. Each truck axle load is at a distance of 6 ft and the distance between two trucks is 4 ft, following the design recommendations of AASHTO LRFD.

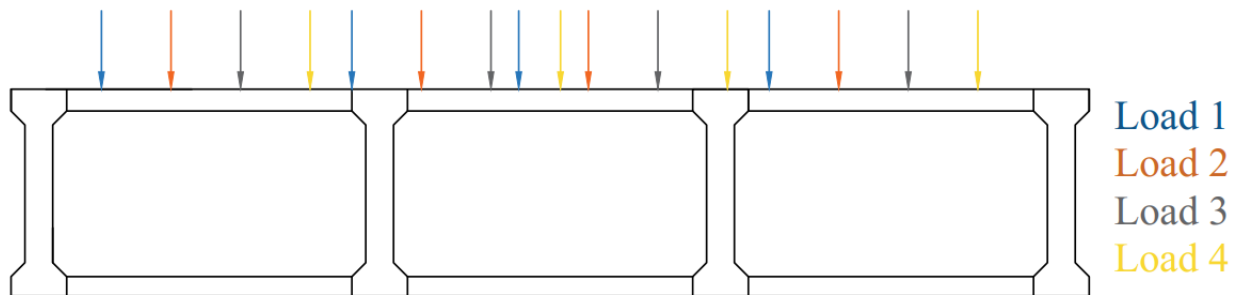


Figure 4.31: Load cases for transverse stress

In Figure 4.32 from the Abaqus model output, the stresses can be observed due to design tandem loads. From Abaqus output, positive values correspond to tensile stresses and negative values correspond to compressive stresses.

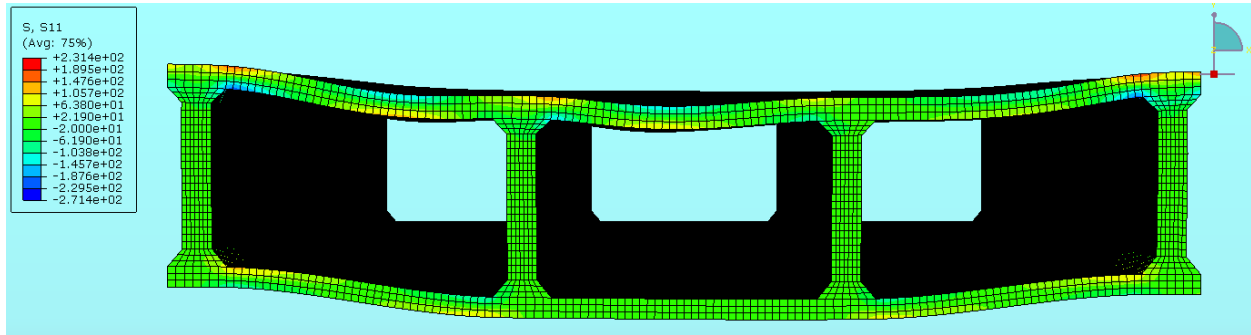


Figure 4.32: Stress in the transverse direction in the bridge model, Load Case 2

Figure 4.33 is a summary of the load cases presented in Figure 4.31 from the FEM models. In this figure, signs were inverted, showing compressive stresses as positive and tensile stresses as negative values for the top fiber of the deck. From the graph, it can be observed that moving the load from one extreme to the other creates an envelope of tensile stresses of around 220 psi and 280 psi compressive stress at the midbay of the deck at the far right box girder.

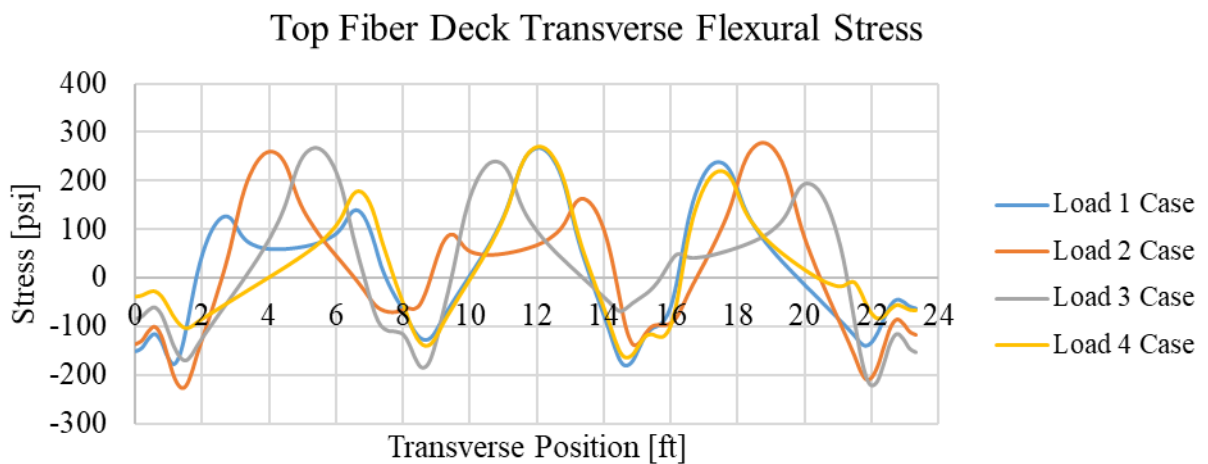


Figure 4.33: Summary of transverse stresses in top fiber of the deck from load cases.

CHAPTER 5. CAST-IN-PLACE BRIDGE DECK REINFORCEMENT ANALYSES

5.1 Introduction

The following sections describe the different analyses performed using the inspection reports data and other relevant information gathered from already published research reports. Finite element analysis was used for the purpose of evaluating the stress development of concrete decks and detailing analysis.

5.2 Bridge Deck Data

The following sections show the results of the longitudinal and transverse analysis performed on 98 bridges for which inspection reports were available. Some of the inspection reports do not show the bridge plans, so only 94 of these bridges were used, see Table 3-8.

As mentioned in CHAPTER 3, the selection criteria for these bridges were based on:

- Cast-in-place Box Girder Bridge Decks
- Reinforced concrete or prestressed concrete girders
- Built after 1989
- Reconstructed or maintenance completed

The information gathered from the inspection reports was used to evaluate bridge deck conditions with two approaches for serviceability and strength limit states.

5.3 Strength Limit State

5.3.1 Main Steel Reinforcement

5.3.1.1 Detail 5-10: Truss Bar Drop-Off Distance

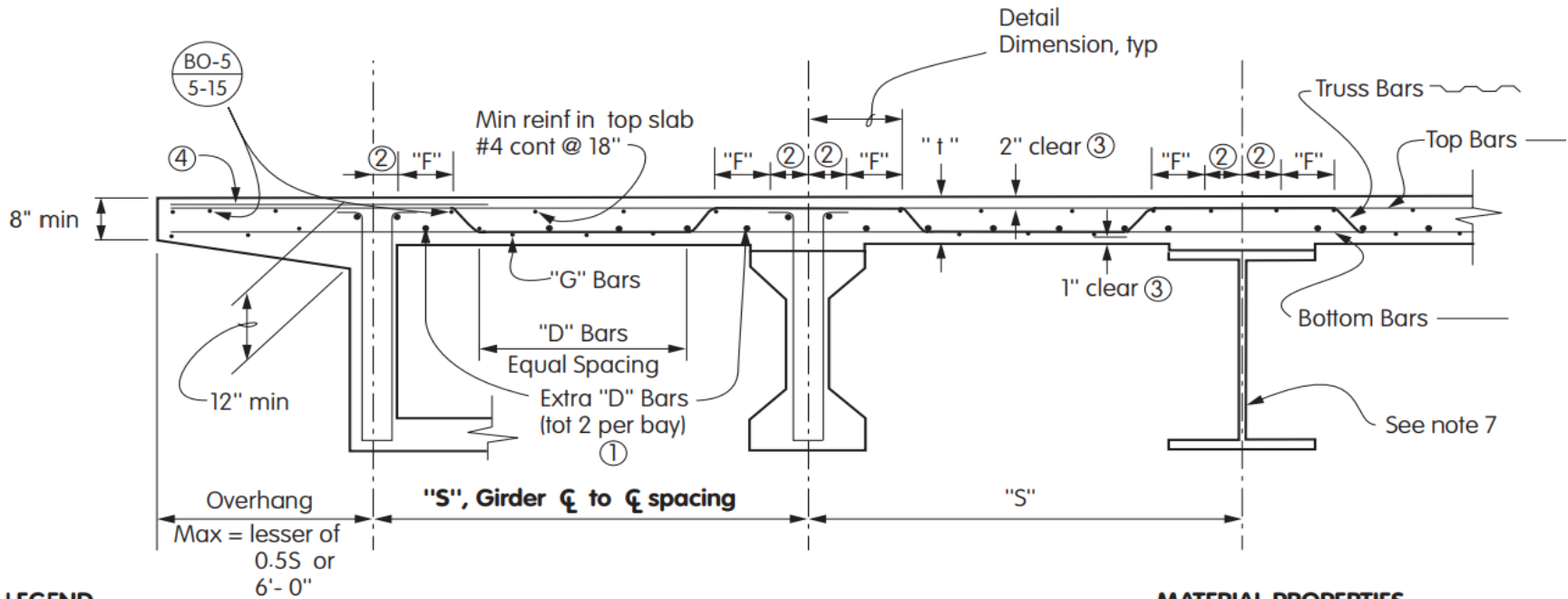
In MTD10-20 (Caltrans, 2017b) deck slab reinforcement details, for a box girder bridge, the distance where the truss bar drops down to become positive moment steel reinforcement is

$\frac{1}{2}S + F$ (Figure 5.2), where:

- Distance $\frac{1}{2}S$ is one-half of the girder web width for box girder bridges.
- Distance “F” is tabulated in MTD 10-20 Tables 10-20.1(a) and 10-20.1(b), and the value is dependent on the girder spacing and the thickness of the slab, see Figure 5.1.

CIP PRESTRESSED BOX, PRECAST-I, & STEEL GIRDERS w/ flange width ≥ 24"						
"S"	"t"	Dimension	Transverse Bars		"D" Bars	"G" Bars
Girder CL to CL Spacing	Top Slab Thickness	"F"	Size	Spacing ¹	#5 Bars	#4 Bars
4'- 0"	7"	5"	#5	12"	3	2
4'- 3"	7"	5"	#5	12"	3	2
4'- 6"	7"	6"	#5	12"	3	2
4'- 9"	7"	6"	#5	12"	3	2
5'- 0"	7"	6"	#5	12"	3	2
5'- 3"	7"	7"	#5	12"	3	2
5'- 6"	7"	7"	#5	12"	4	2
5'- 9"	7"	7"	#5	12"	4	3
6'- 0"	7"	8"	#5	12"	4	3
6'- 3"	7"	8"	#5	12"	4	3

Figure 5.1: Table 10-20.1(b) from MTD 10-20 Attachment 2(Caltrans, 2017b)



LEGEND

- ① Extra "D" bars are to be added when span "S" \geq 11'-6"
- ② Distance from ζ girder to design section for negative moment (Art.4.6.2.1.6)
 - Concrete box girders: 1/2 the girder web width
 - Precast concrete I-shaped and T-shaped beams: 1/3 the flange width (15" max)
 - Steel girders: 1/4 the flange width
- ③ Increase cover over bars and adjust slab thickness if required for environmental conditions. See Table 5.12.3-1 and MTD 8-2.
- ④ Provide additional top transverse deck reinforcement in the overhangs when "S" \leq 11'-6". See note 10

MATERIAL PROPERTIES

$f'_c = 3.6$ ksi - Normal Weight Concrete
 $f_y = 60$ ksi

Figure 5.2: Deck Slab Reinforcement Details (Caltrans, 2017b)

The Drop-Off As-Built distance vs. the MTD required distance for the 94 bridges selected in the study is shown in Figure 5.3. The graphs show that for those bridges on the left, almost 25% do not meet the design distance according to the MTD 10-20, but it should be considered that the MTD 10-20 guide used for this study is dated in May 2008 and some of these bridges were built before that date. The 9 bridges on the right meet design.

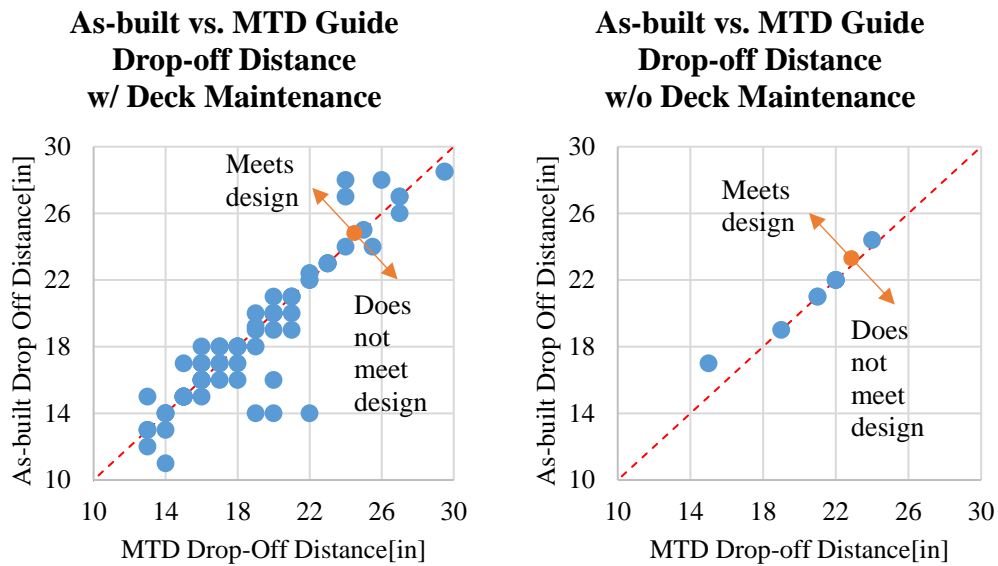


Figure 5.3: As-built vs. MTD Drop-Off Distance for the truss bar. Bridges with some deck maintenance reported (left), bridges without deck maintenance reported (right).

5.3.1.2 Finite Element Analysis

Finite element analysis was used to determine the loading effects of the HL-93 truck in the transverse direction. The FEM model considered different configurations of Box Girder Bridges with different numbers of cells, as Figure 5.4 shows an example of a 4-cell Box Girder Bridge.

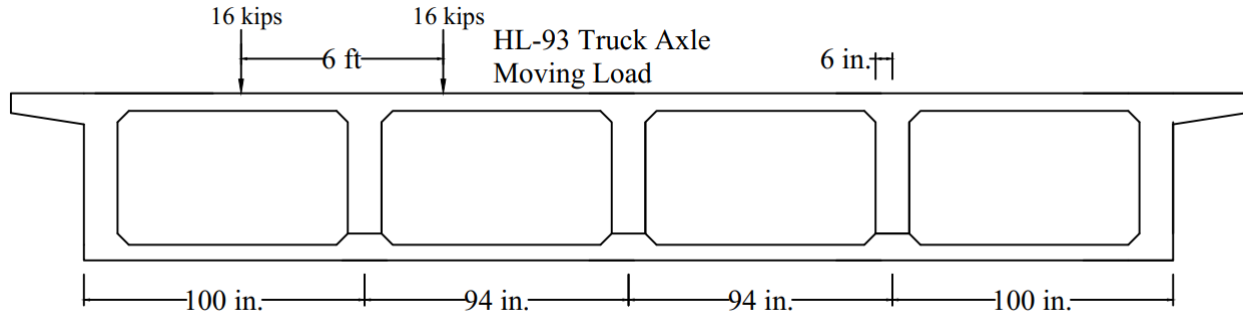


Figure 5.4: Cross section used in the FEM analysis, 4-cell box girder bridge example

The FEM model considered the following:

- One truck load: HL-93 Axle Moving Load
- Equivalent Strip Method (ESM) for Live Load Moment
- Dead Load: Deck Slab plus 3 in. of Asphalt wearing surface (as Caltrans BDP10 example)

Live Load Moment Envelopes

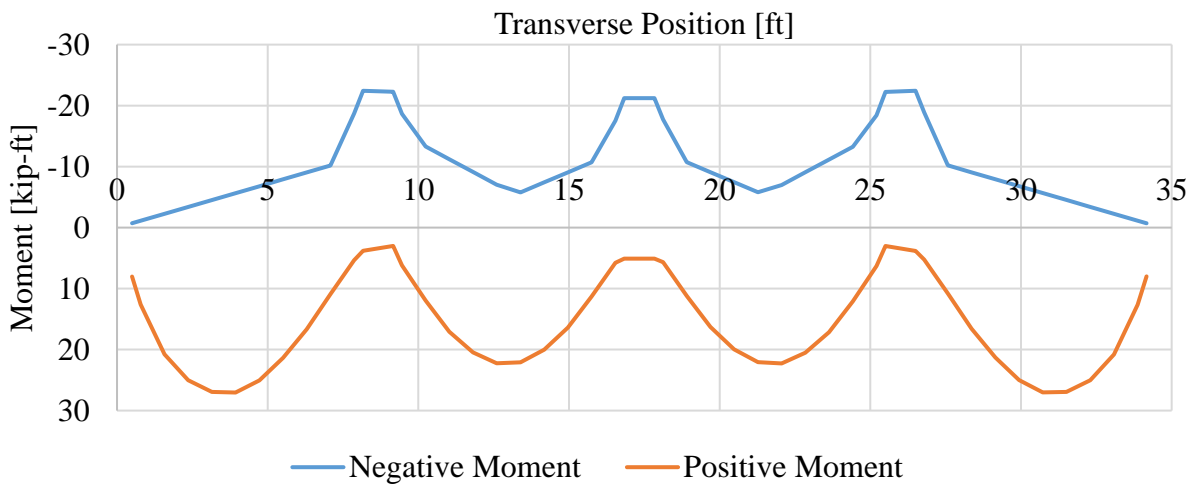


Figure 5.5: 4 Box girder bridge moving load - Moment envelope

Figure 5.5 shows the moment envelope due to the live load applied to the deck as a moving load. Using the Equivalent Strip Method for positive and negative moments and applying the multiple presence factor and dynamic allowance of 33%, the load were calculated as follows:

$$M_{DC} = -0.378 \text{ kip} \cdot \text{ft} / \text{ft}$$

$$M_{DW} = -0.130 \text{ kip} \cdot \text{ft} / \text{ft}$$

$$M_{LL} = -21.223 \text{ kip} \cdot \text{ft} \rightarrow \frac{M_{LL}}{S^-} = \frac{-21.223 \text{ kip} \cdot \text{ft}}{6.17 \text{ ft}} = -3.442 \text{ kip} \cdot \text{ft} / \text{ft}$$

$$M_u = \eta [\gamma_{DC} M_{DC} + \gamma_{DW} M_{DW} + (m)(1 + IM) \gamma_{LL} M_{LL}]$$

$$M_u = 1.0 [1.25 M_{DC} + 1.5 M_{DW} + (1.2)(1 + 33\%) 1.75 M_{LL}] \leftarrow 1 \text{ Lane Loaded}$$

$$M_u = 1.0 [1.25 \cdot -0.378 + 1.5 \cdot -0.130 + (1.2)(1 + 33\%) 1.75 \cdot -3.442]$$

$$M_u = -10.28 \text{ kip} \cdot \text{ft} / \text{ft}$$

Table 5-1 shows the values obtained for the example shown in Figure 5.5, for the live load moments in comparison with AASHTO LRFD deck design table A4, which includes multiple presence factor and dynamic allowance.

$$M_{LL} = -3.442 \text{ kip} \cdot \text{ft} / \text{ft} \cdot 1.2 \cdot (1 + 33\%) = 5.76 \text{ kip} \cdot \text{ft} / \text{ft}$$

Table 5-1: Equivalent Strip Method for Live Load Moments

	AASHTO A4	FEM
M_{LL+} [kip-ft/ft]	6.29	5.12
M_{LL-} [kip-ft/ft]	5.13	5.76

The flexural resistance of the concrete decks was computed for comparison with load effects and to verify if the drop-off distances were enough to comply with AASHTO LRFD provisions for bridge design. In Figure 5.23, Detail 5-10 is shown before and after the truss-bar drops down, and with these configurations, two cases for resistance were computed, moment resistance with one bar and two bars, as shown in Figure 5.6. For this analysis, 9 of the 94 bridges were modeled with FEM for the live load effects, and flexural resistance was computed for each one of them.

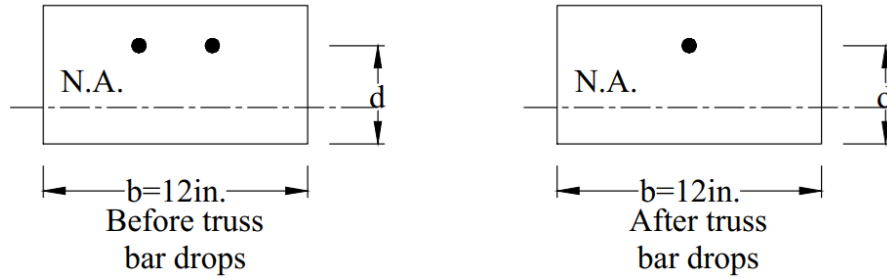


Figure 5.6: Flexural analysis of deck in conditions before and after truss bar drops.

$$a = \frac{A_s f_y}{0.85 f'_c b} \rightarrow M_n = A_s f_y \left(d - \frac{a}{2} \right)$$

Strain Check

$$\varepsilon = \frac{\varepsilon_{cu} (d - c)}{c} \geq 0.005 \rightarrow \phi = 0.9$$

$$\phi M_n = \phi A_s f_y \left(d - \frac{a}{2} \right)$$

AASHTO LRFD Article 5.10.8.1.2a states that the flexural termination point shall extend at least $15d_b$ (for shear influence on bar stress). The required drop-off distance was calculated for each bridge in the analysis considering the extension of AASHTO requirements. A flexural termination point was selected where the ultimate moment matches the resistance with 1 bar, red dot, as shown in Figure 5.7. The green circles in Figure 5.7 are the required extension of $15d_b$ per AASHTO LRFD Article 5.10.8.1.2.

Figure 5.7 to Figure 5.15 show the analysis result for the 9 bridges mentioned above. The values shown in the following figures represent interior support (girder) for the deck. M_{u+} and M_{u-} are the ultimate positive and negative moment, respectively; ϕM_n is the resistant moment for positive and negative regions calculated for 1 and 2 reinforcing bars; $ExtL$ and $ExtR$ are the extensions per Article 5.10.8.1.2a; and $DropDist$ is the distance where flexural resistance is no longer needed or flexural termination point.

Bending Moments - Ultimate and Resistance

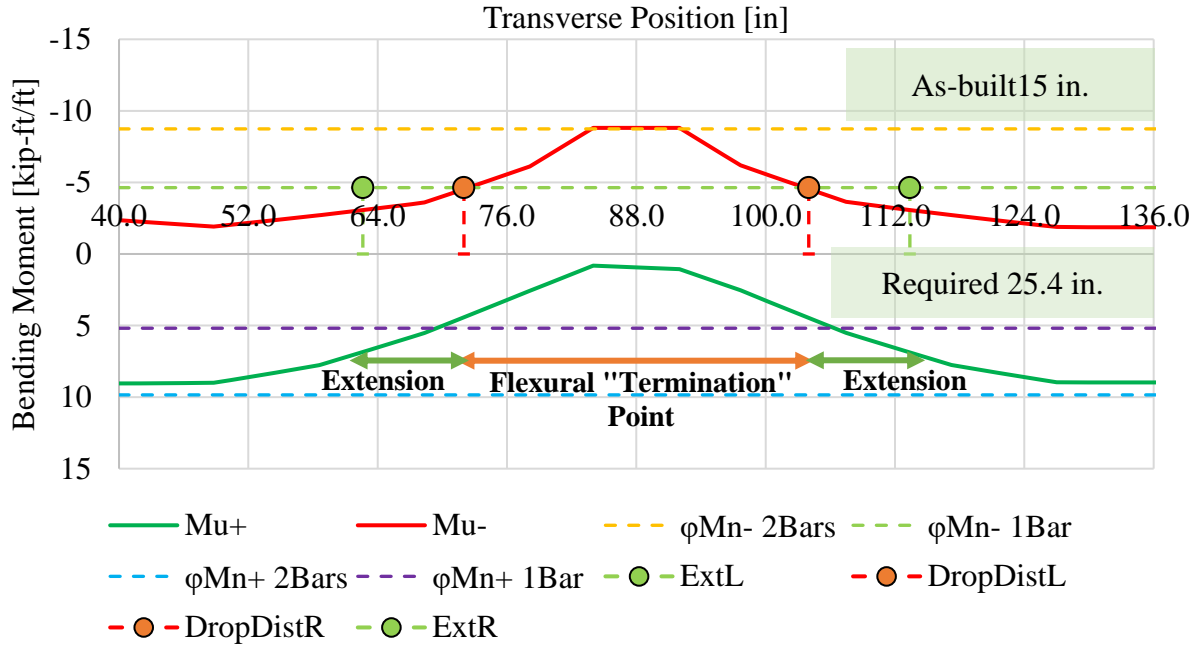


Figure 5.7: R/C Continuous Box Girder Bridge 02 0036L analysis example.

Bending Moments - Ultimate and Resistance

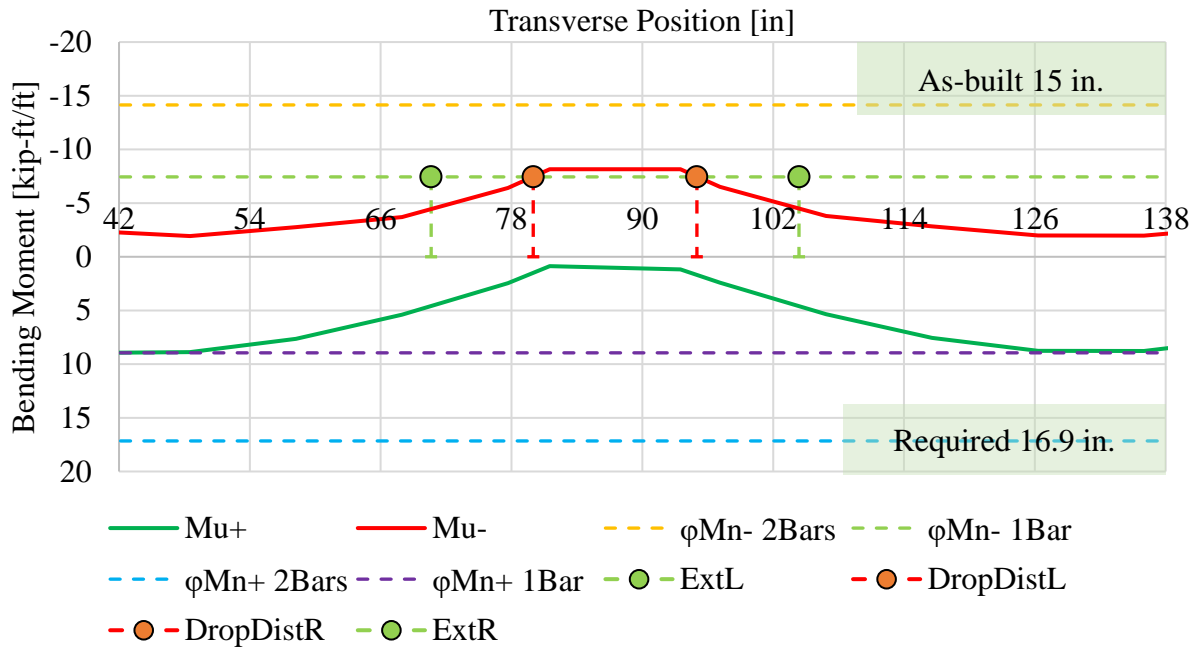


Figure 5.8: 28C0228 P/C Continuous.

Bending Moments - Ultimate and Resistance

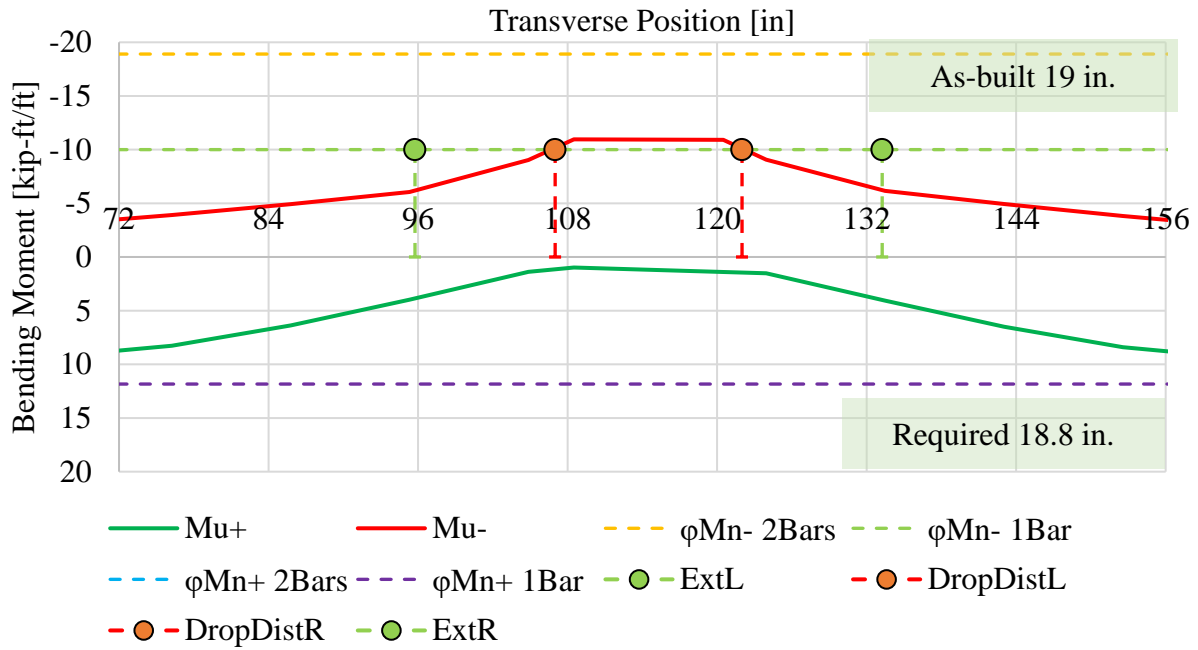


Figure 5.9: 37 0368L P/C Simple.

Bending Moments - Ultimate and Resistance

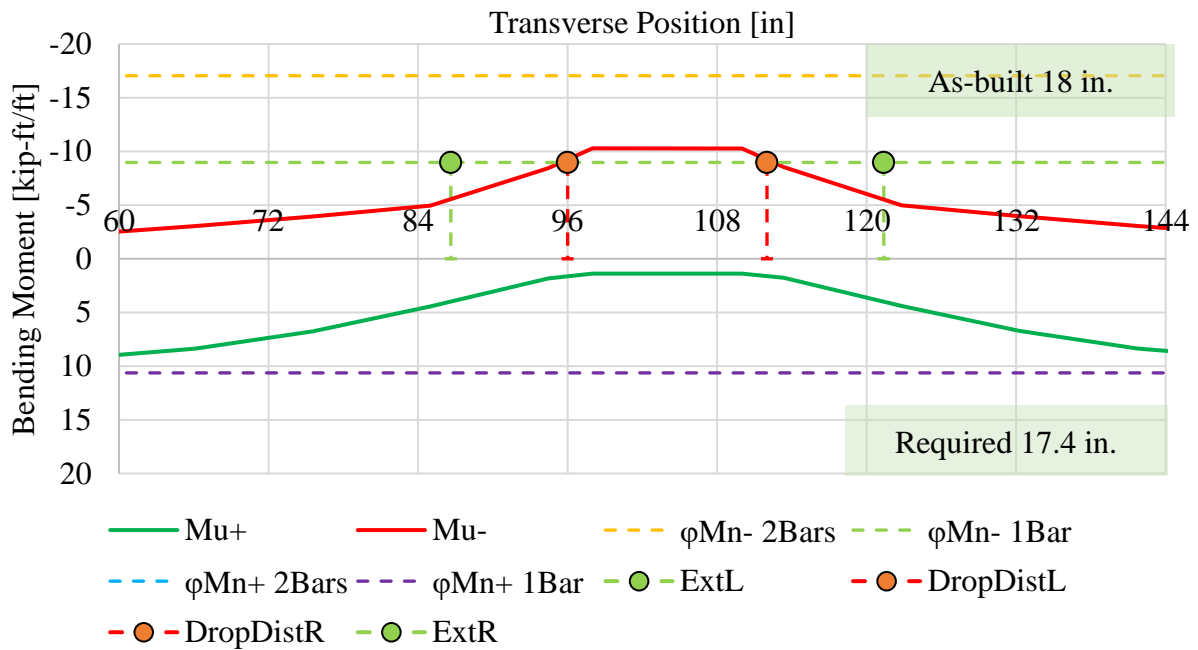


Figure 5.10: 08 0163 P/C Continuous.

Bending Moments - Ultimate and Resistance

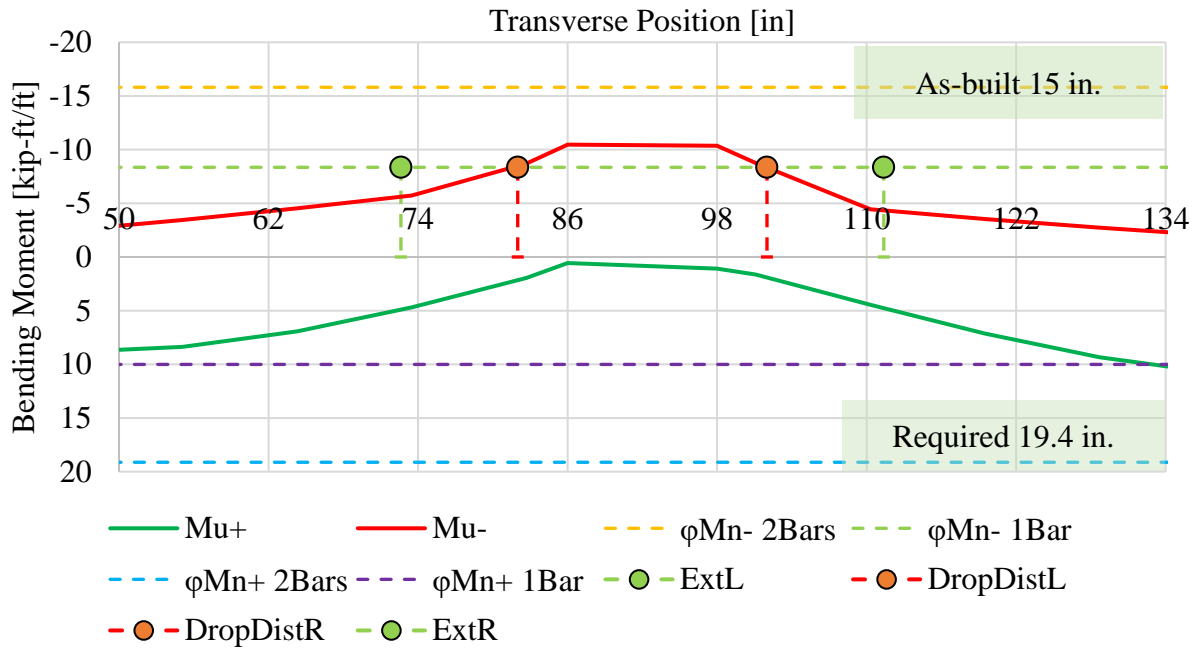


Figure 5.11: 28 0322K R/C Continuous.

Bending Moments - Ultimate and Resistance

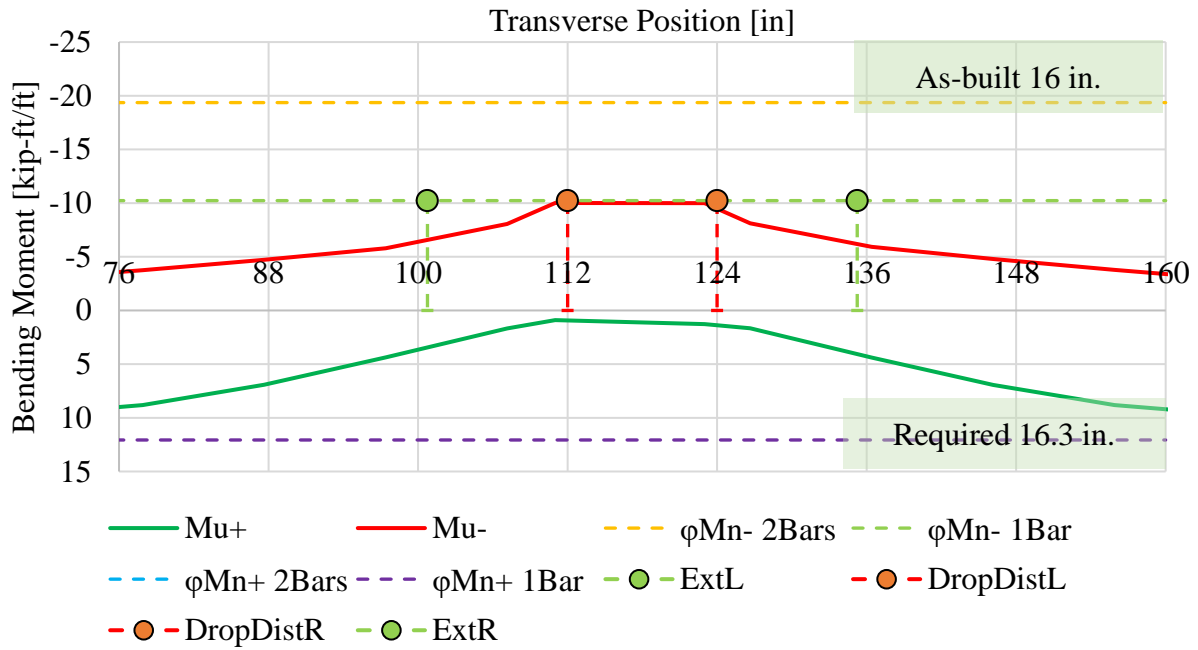


Figure 5.12: 33 0212L P/C Continuous.

Bending Moments - Ultimate and Resistance

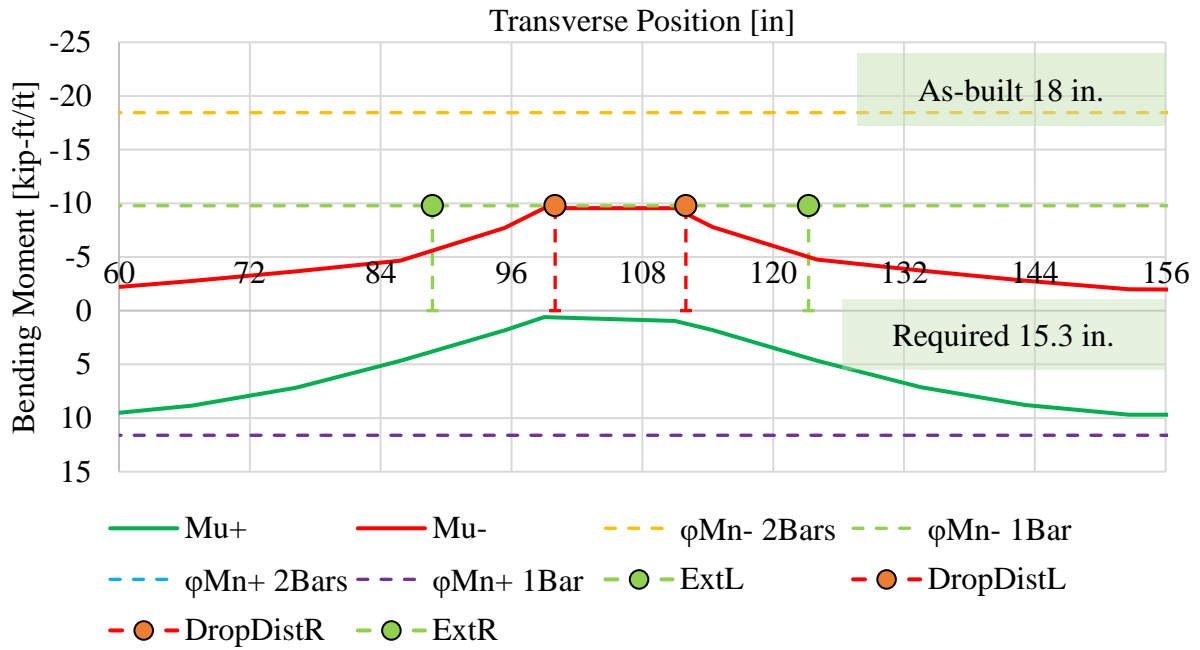


Figure 5.13: 33 0585 P/C Continuous.

Bending Moments - Ultimate and Resistance

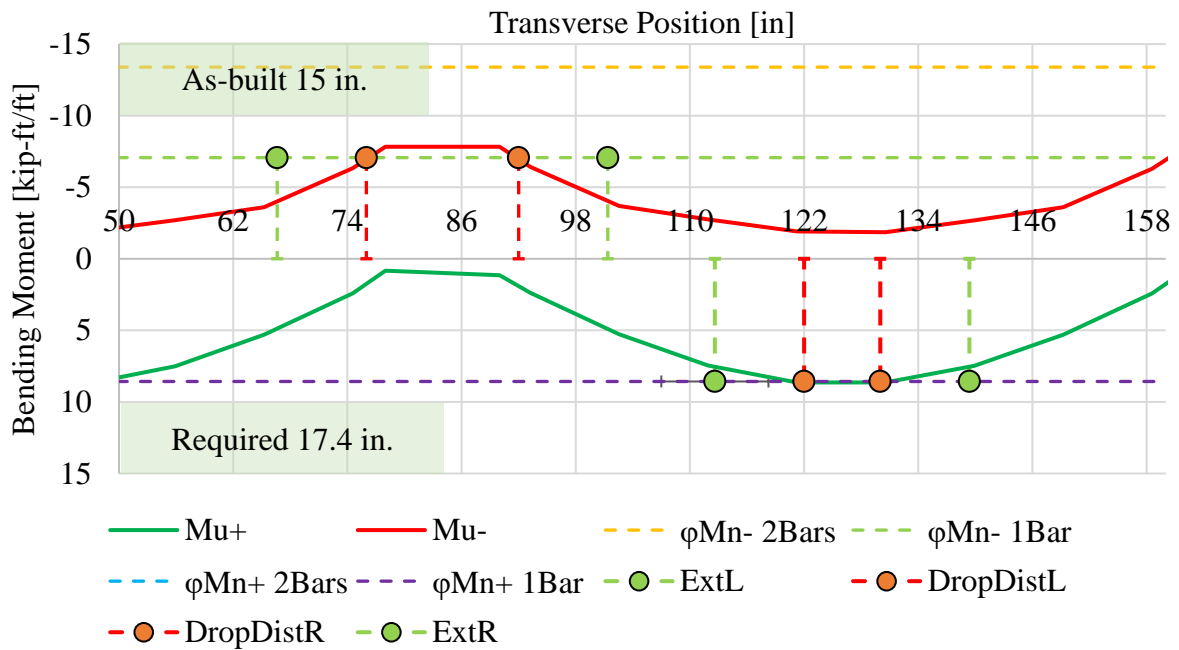


Figure 5.14: 37 0366L P/C Continuous.

Bending Moments - Ultimate and Resistance

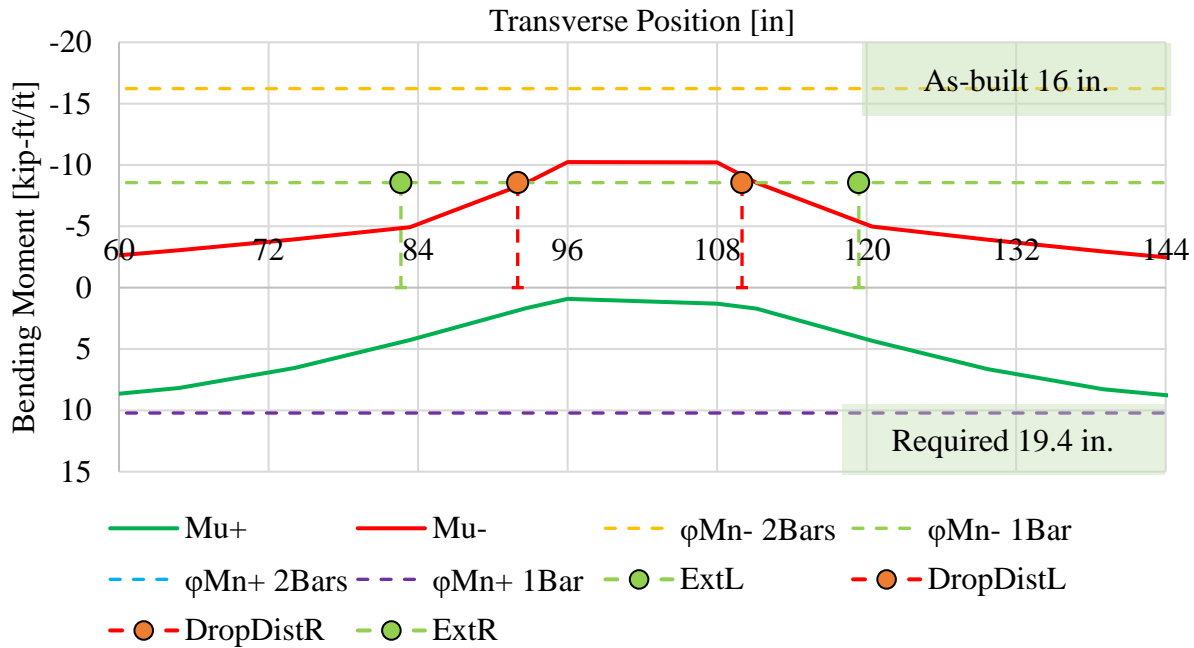


Figure 5.15: 56 0362 P/C Continuous.

Table 5-2 shows a summary of the results for these bridges and is incorporated the live load effects for each bridge using the AASHTO A4-1 table for comparison purposes. The last column of the table shows “N.G.” (Not Good) when the required distance is more than the As-built distance.

Table 5-2: Summary of Drop-Off distance analysis of Box Girder Bridges

Type	Bridge ID	Live Load Negative		Live Load Positive		Drop-Off Distance[in]		
		Moment[kip-ft/ft]		Moment[kip-ft/ft]		As-built	Required	Check
		AASHTO A4	FEM	AASHTO A4	FEM			
R/C	28 0322K	5.4	4.7	5.7	5.0	15.0	19.4	N.G.
R/C	02 0036L	4.8	4.7	5.7	4.4	15.0	17.4	N.G.
P/C	08 0163	5.1	5.5	6.3	5.1	18.0	17.4	OK
P/C	28C0228	4.8	4.4	5.7	4.9	15.0	16.9	N.G.
P/C	33 0212L	6.1	5.2	6.9	5.5	16.0	16.3	N.G.
P/C	33 0585	5.1	5.0	6.3	5.3	18.0	15.3	OK
P/C	37 0366L	4.4	4.2	5.2	4.9	15.0	17.4	N.G.
P/C	37 0368L	6.1	5.7	6.9	5.3	19.0	18.8	OK
P/C	56 0362	5.1	5.4	6.3	5.1	16.0	19.4	N.G.

This analysis showed that 67% of analyzed bridges have a shorter drop-off distance than needed according to the AASHTO provisions. This deficit is greater in reinforced concrete box girder bridges. Figure 5.16 shows the as-built vs needed drop of distance, where the bridges below the red line are not meeting design provisions.

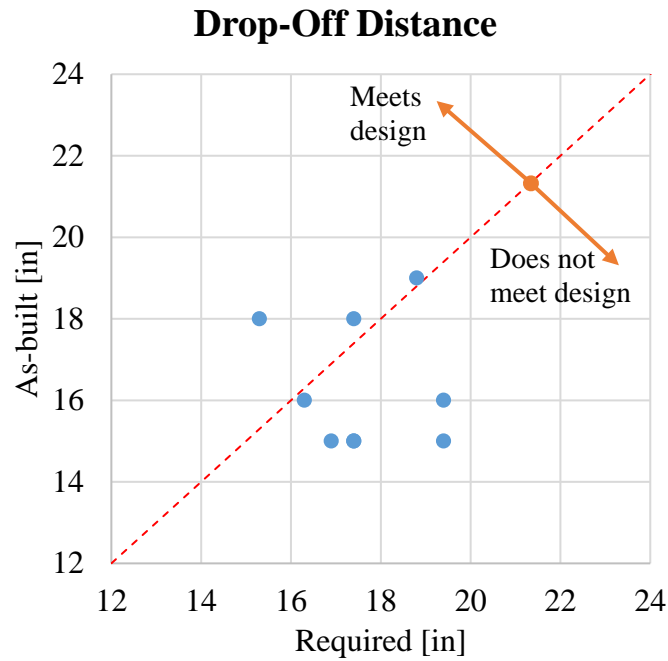


Figure 5.16: As-built vs. Required Drop-Off distance.

5.3.2 Summary and Comments

- In some cases, the drop-off distance used for Detail 5-10 is too short.
- Truss bars have to be reconsidered due to spacing issues.
- Detail 5-11 meets all AASHTO spacing and amount of reinforcement requirements; therefore, it is recommended to use Detail 5-11.
- It is recommended to discontinue the use of Detail 5-10.

5.4 Serviceability

5.4.1 Main Steel Reinforcement

According to Caltrans Bridge Design Practice (Caltrans, 2015), the main steel reinforcement in the transverse direction shall be detailed as one of the two diagrams shown in Figure 5.17.

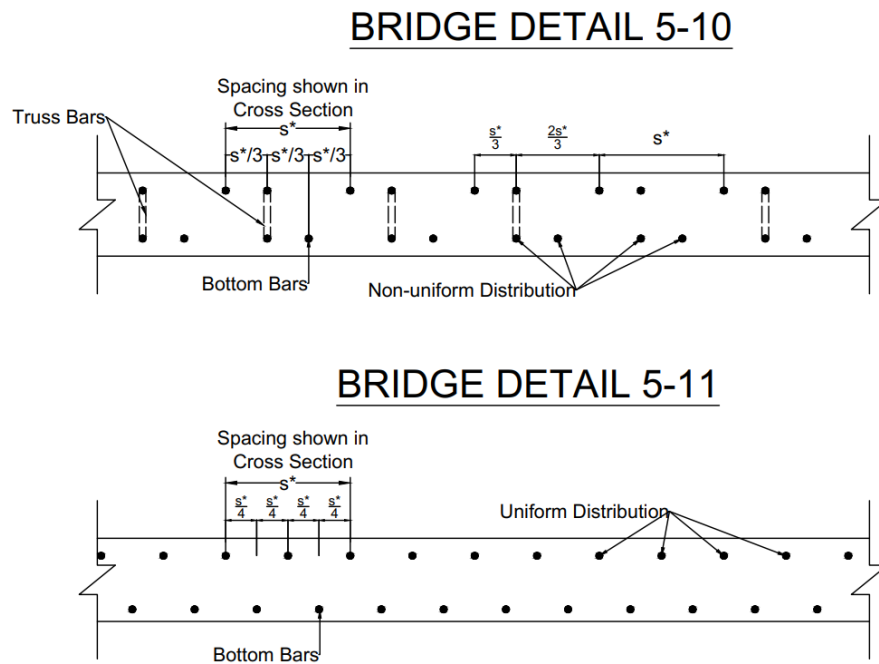


Figure 5.17: Main Reinforcement Details

Of the 94 bridges selected for the analysis, 93% of these show Detail 5-10 in the typical cross-sections from the inspection reports.

Two problems were detected with Detail 5-10:

- Spacing of the reinforcement is twice the required by AASHTO LRFD Article 5.6.7 for cracking control after the truss bar becomes positive moment reinforcement.
- The drop-off distance of the truss bar is too short. This was discussed in Strength Limit State Section.

Also, when comparing the As-built vs. Memo To Designer (MTD) guide for the steel reinforcement, 14% of the selected bridges showed less reinforcing steel area than what is required by the MTD 10-20.1, as shown in Figure 5.18.

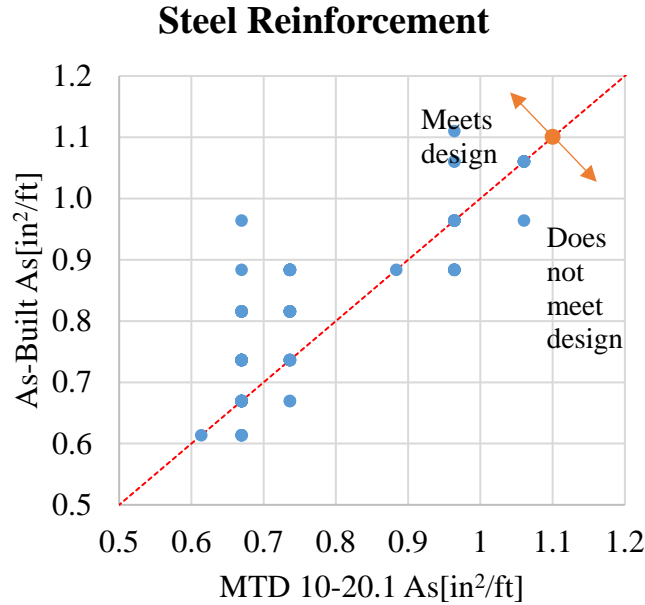


Figure 5.18: As-built vs MTD Steel Reinforcement in Box Girder Bridges

The distribution of main reinforcement in other states that use Empirical Design is provided in Table 5-3 for comparison purposes.

Table 5-3: Main Reinforcement in other states with empirical design

State	Manual Year	Design Method	Main Reinf #	Spacing [in]	in²/ft
Delaware	2019	Empirical Method	4	6	0.39
Florida	2018	Empirical/Strip	5	12	0.31
Michigan	2021	Empirical Method	5	10	0.37
Nebraska	2014	Empirical Method	5	12	0.31
New Mexico	2018	1979 Bridge Manual	5	6	0.61
New York	2019	Empirical	4	8	0.29
Texas	2020	Empirical/Strip	4	9	0.26
Utah	2017	Empirical/Strip	4	6	0.39

5.4.1.1 Cracking Control Reinforcement Spacing

AASHTO Article 5.6.7 (AASHTO, 2020) specifies control of cracking by distribution of reinforcement for all concrete components, except for deck slabs designed with the empirical method. The provisions presented in Article 5.6.7 are used to control flexural cracking through the spacing of the main reinforcement in tension. The spacing is defined, Eq. 2.3, in terms of exposure factor, tensile stress at service limit state, cover thickness and overall thickness of the component. The spacing shall comply with the provisions of article 5.10.3.1 and 5.10.3.2 of AASHTO LRFD for minimum and maximum spacing.

Using the provisions presented above from Article 5.6.7 of the AASHTO Specifications, the required spacing of the selected bridges against the tensile stress at service limit state, is presented in Figure 5.19.

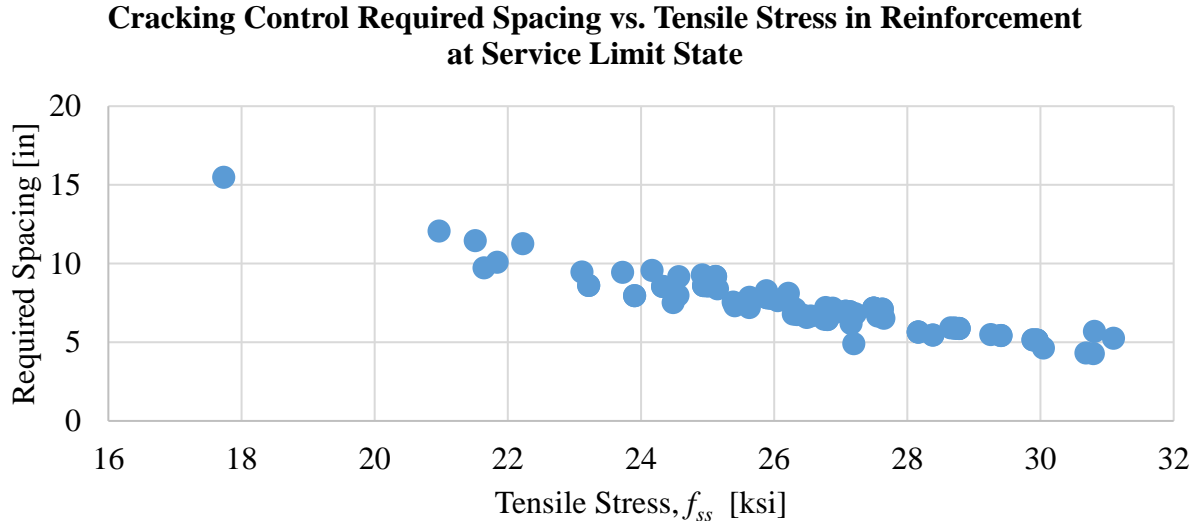


Figure 5.19: Cracking control required spacing vs. Tensile stress in steel reinforcement at Service Limit State

In Figure 5.20 the tensile stress vs. the box girder spacing is shown. The data shows that the tensile stress at service limit state are higher (approx.30 ksi) for girder spacings less than 8 ft and values close to 25 ksi can be seen for girder spacing close to 14 ft.

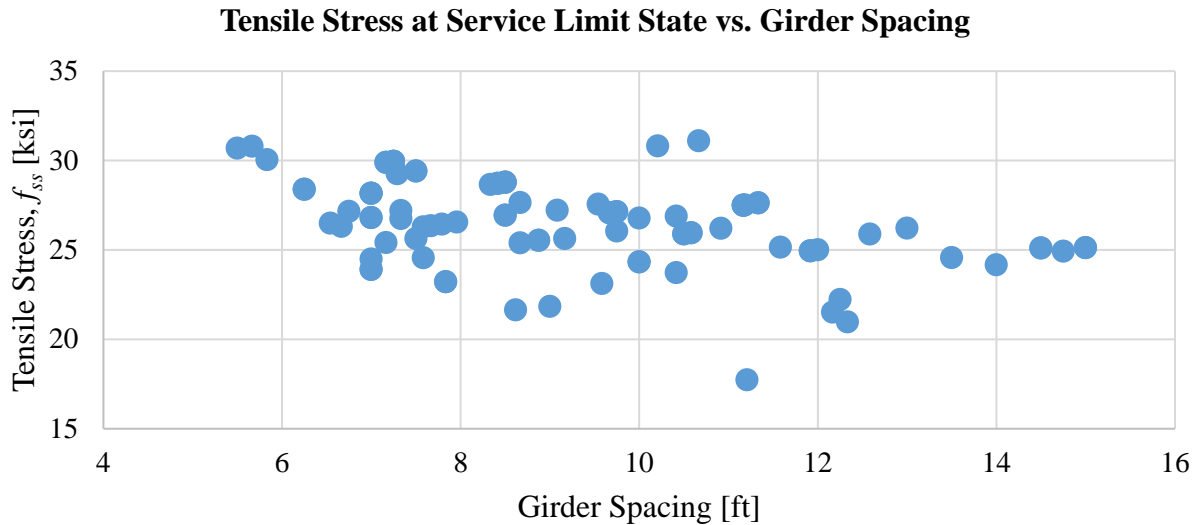


Figure 5.20: Tensile Stress in Reinforcement at Service Limit State vs. Box Girder Spacing

Following the directions of the BDP 10.6.9.2, the required spacing from Eq. 2.3 is multiplied by 2 when specifying Detail 5-10 or Detail 5-11, see Figure 5.21. The required spacing is symbolized by S^* ; see Figure 5.22. Comparing both details, it is observed that the distribution of the reinforcement is staggered and uniform for Detail 5-11, while for Detail 5-10 the distribution of reinforcement is not uniform.

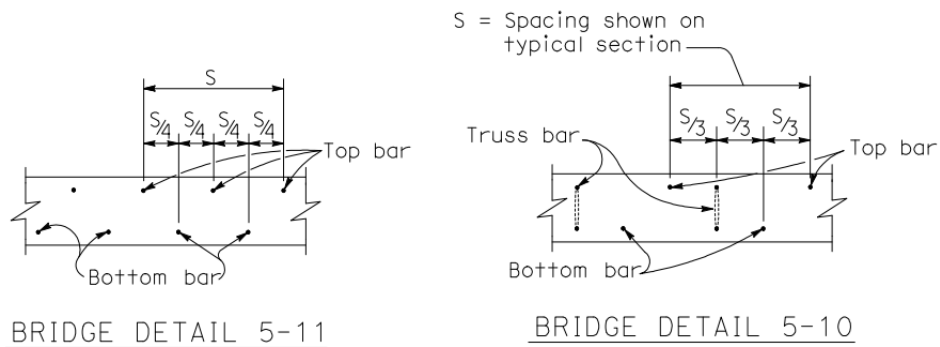


Figure 5.21: Transverse Deck Reinforcement Diagrams (Caltrans, 2015)

BRIDGE DETAIL 5-10

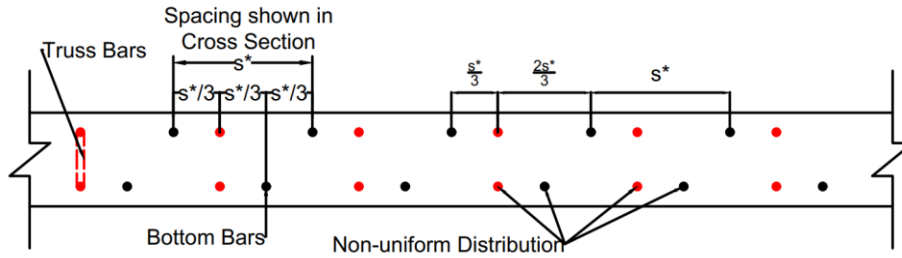


Figure 5.22: Detail 5-10 Main Reinforcement Distribution

As mentioned in the previous section, the spacing problem occurs when the truss bar of Detail 5-10 is in the top layer, and the spacing S^* of the steel reinforcement in the bottom layer is twice the spacing required for cracking control. The same happens when the truss bar drops down to become positive moment steel reinforcement; the spacing in the top layer becomes double the required spacing for cracking control. In Figure 5.23, the scheme of Detail 5-10 is shown in their respective distributions before and after the truss bar drops down.

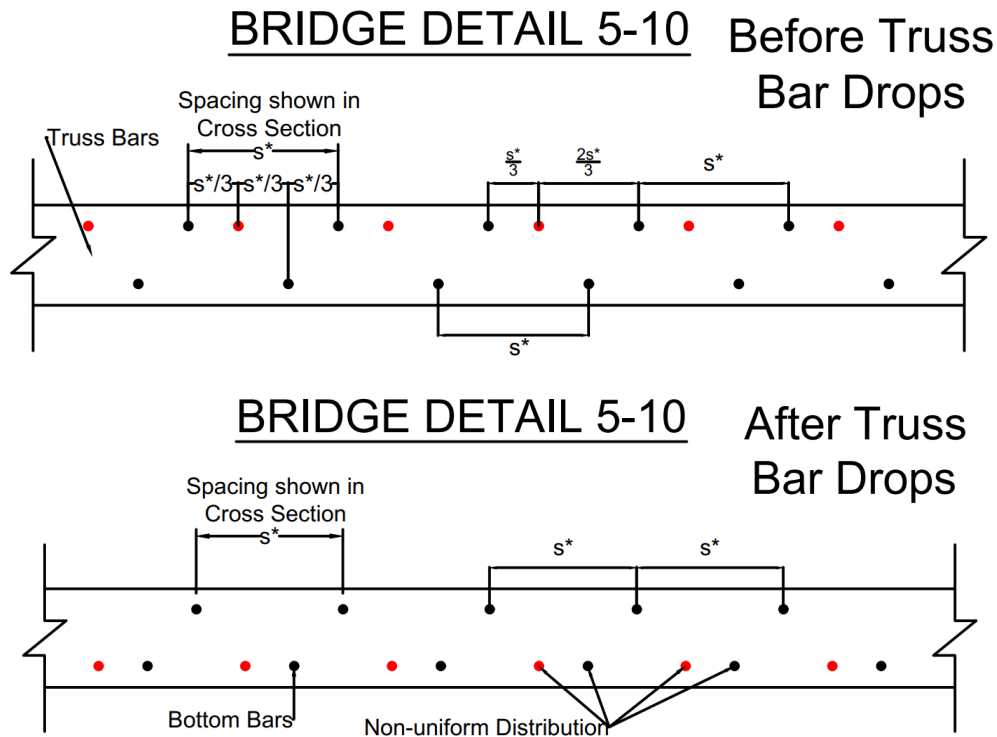


Figure 5.23: Detail 5-10 Before (top) and After (bottom), the bar drops down.

In Figure 5.24, the required spacing vs. As-built spacing is shown before and after the truss bar drops down for the 94 box girder bridges analyzed. After the bar bends down, 88% of the cases do not meet design requirements of spacing.

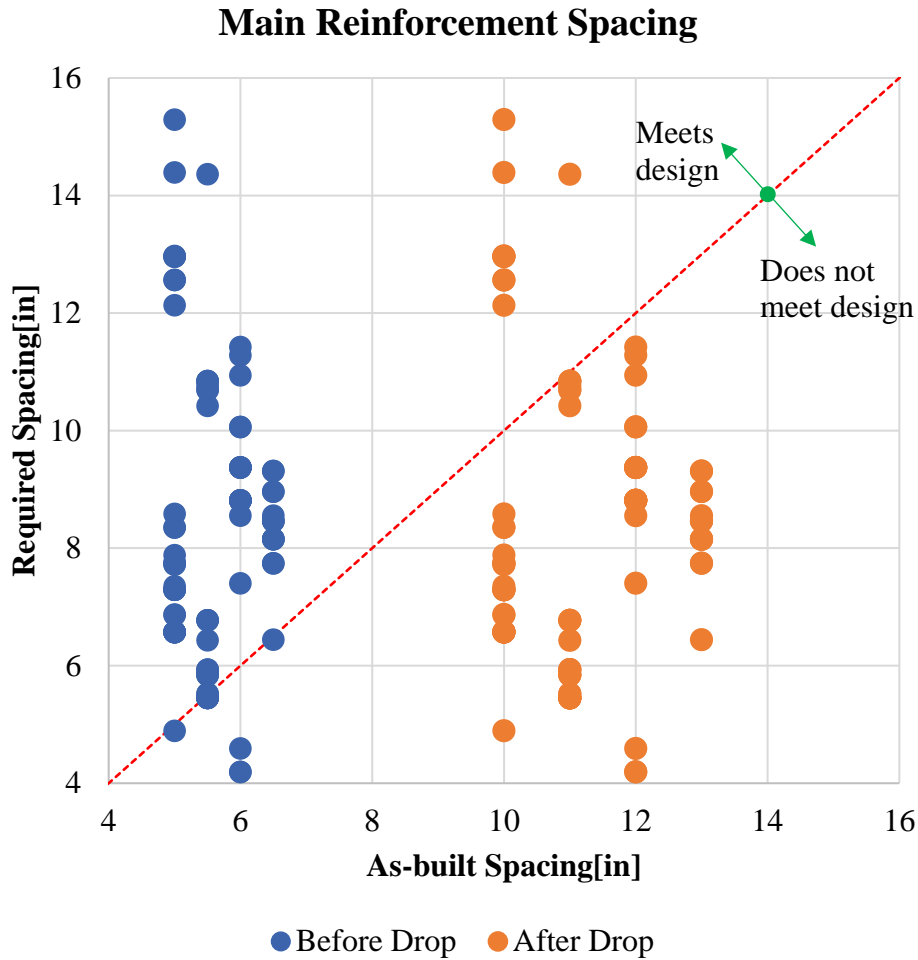


Figure 5.24: Main reinforcement spacing Required vs. As-built before and after truss bar drops.

The possible effects of wide spacing between steel reinforcement could lead to wide and numerous longitudinal cracks. Prestressed concrete box girder bridge cracking data showed a 68% of presence of longitudinal cracks, see Section 3.2.12

5.4.2 Longitudinal Steel Reinforcement

In BDP 10, minimum reinforcement is required to distribute loads across the slab for shrinkage and temperature changes. AASHTO specifications (Article 5.10.6) provide the area of reinforcement for shrinkage and temperature stresses per foot as:

$$A_s \geq \frac{1.30bh}{2(b+h)f_y}$$

except that:

$$0.11 \leq A_s \leq 0.60 \text{ in}^2 / \text{ft}$$

Where A_s , b , h and f_y are the area of reinforcement in each direction and each face, width, thickness, and yield strength of reinforcement, respectively. In this same article, maximum spacing is provided (18 in.), but not minimum.

To study the possible effect in transverse cracking of the amount of longitudinal reinforcement, the 94 box girder bridges database was used. Transverse crack widths were obtained from the inspection reports. 69 out of 94 bridges report transverse cracks in the inspection reports. Figure 5.25 shows the age of the box girder bridge when the first transverse crack was reported. From selected bridges, 70 % show transverse crack widths up to 0.08 in. in the first 10 years of service. Most of these bridges correspond to continuous structures of prestressed and reinforced concrete. According to the Element Inspection Manual (Caltrans, 2000), crack widths over 0.02 in. wide are considered moderate to severe cracks.

Bridge Age vs. First Transverse Crack Width (Reported)

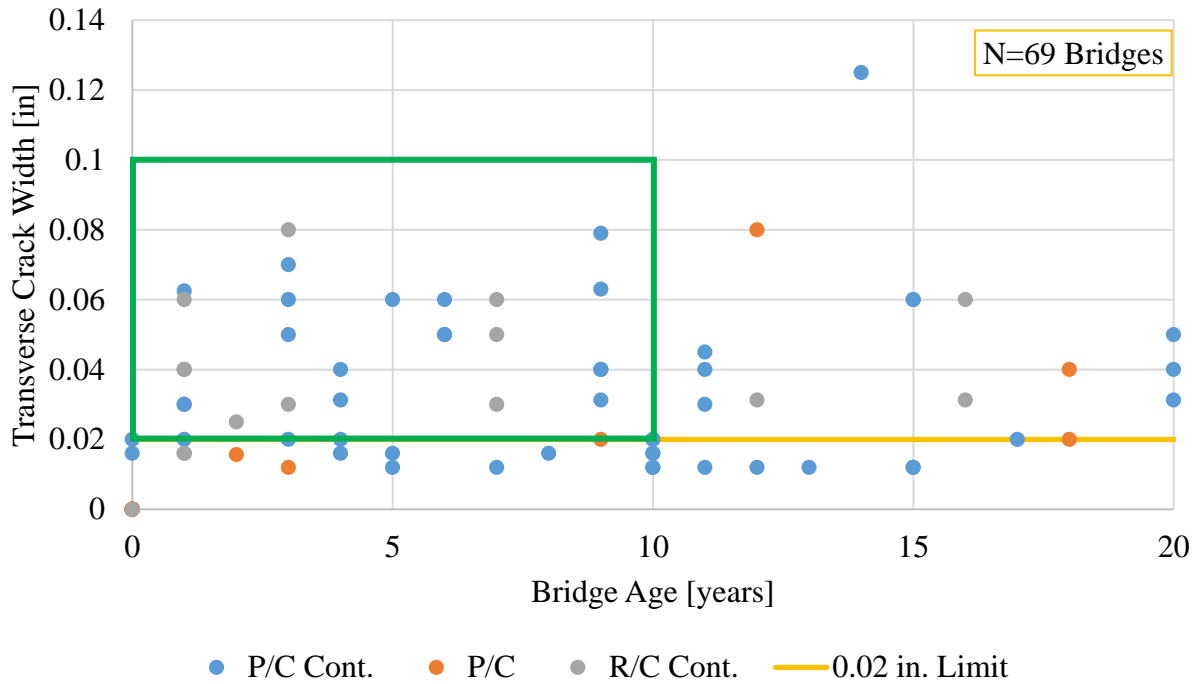


Figure 5.25: Transverse crack width vs box girder bridge age.

5.4.2.1 Shrinkage and Temperature Reinforcement

The same dataset of transverse crack widths was compared against the amount of shrinkage and temperature reinforcement (S&T). Figure 5.26 shows the 69 bridges that represent 70% of box girder bridges in the dataset that reported the presence of transverse cracks. The amount of S&T reinforcement most common (75% of cases) for these bridges is 0.13 in²/ft, corresponding to #4 bars spaced at 18 in. It is also noticeable that the most severe crack widths are present in bridges with #4@18 reinforcement configuration for the top layer. Crack widths reach up to 0.125 in.

Top S&T Reinforcement vs. First Transverse Crack Width (Reported)

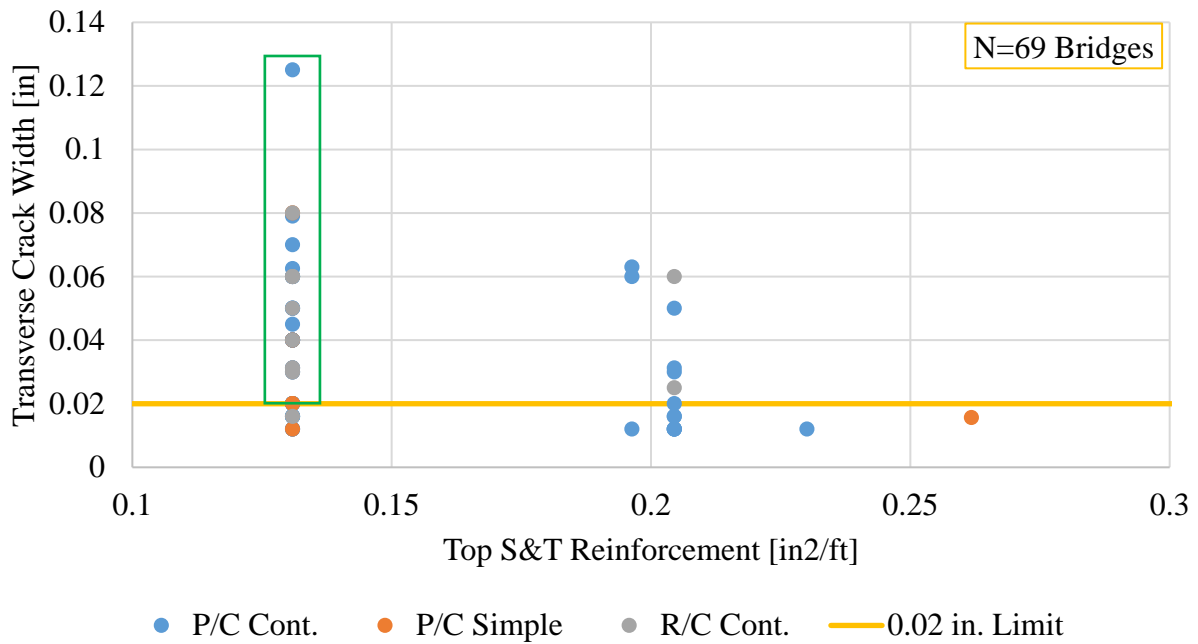


Figure 5.26: Transverse crack width vs top shrinkage and temperature reinforcement

Shrinkage and temperature reinforcement are provided using continuous bars #4 at 18 in. as typical configuration according to BDP. Figure 5.27 is from an example provided in the BDP10 where S&T reinforcement is calculated using the provisions of Article 5.10.6 from the AASHTO LRFD. AASHTO minimum requirements are fulfilled with this reinforcement configuration but very close to the lower boundary.

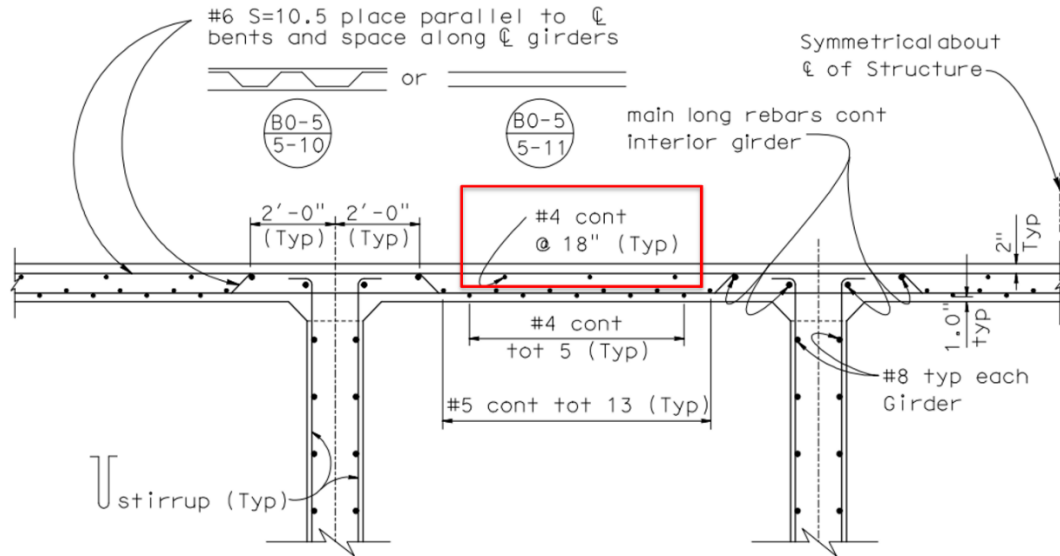


Figure 5.27: Typical reinforced concrete deck cross section (Caltrans, 2015)

The distribution of the S&T reinforcement for the 94 bridges in the dataset is presented in Figure 5.28, where the #4@18 configuration is the most common with over 70% of the cases.

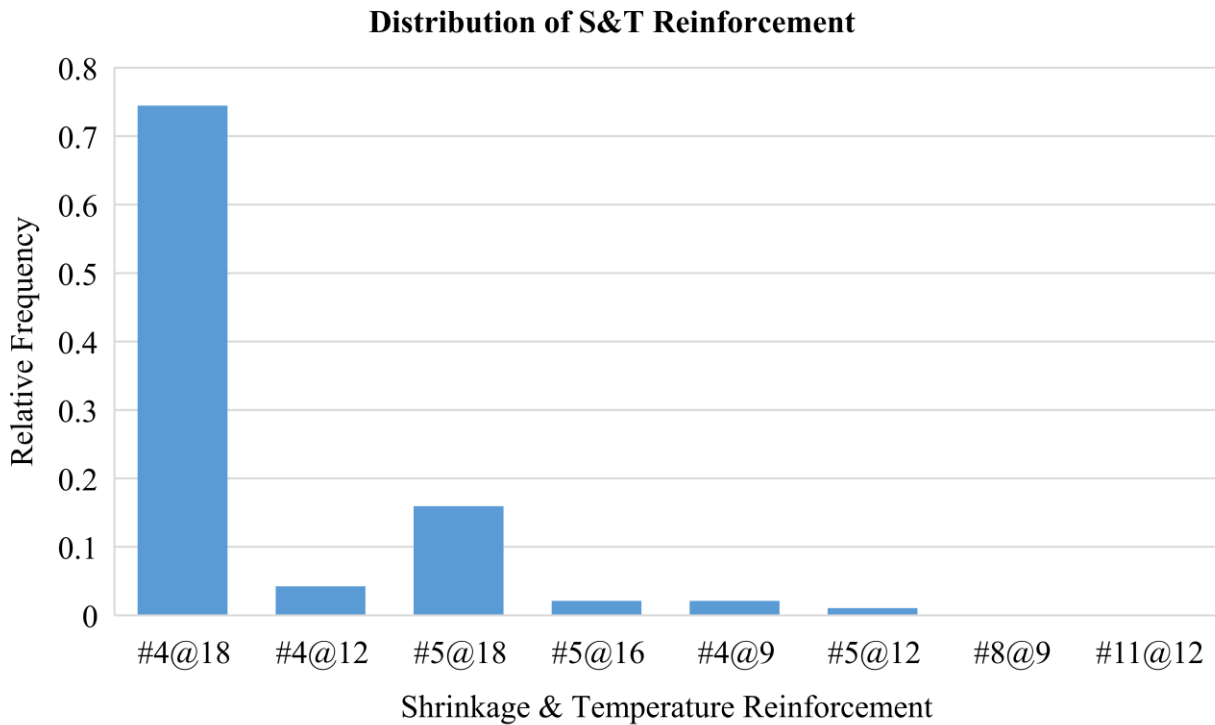


Figure 5.28: S&T reinforcement distribution of box girder bridges sample.

A comparison table is shown in Table 5-4. These states were selected based on the amount of box girder bridges that they have in inventory. Some of the differences can be seen regarding deck thickness, S&T reinforcement provisions, and spacing of it.

Table 5-4: Comparison of deck design provisions for shrinkage and temperature for several states.

State	Design	Limit States	Min. Deck Thick. [in]	S&T Reinf.	Top S&T Reinf. [in ² /ft]	Min. Top S&T Reinf. Specified	Supp. Long. Reinf.
California	Traditional	Strength I/ Service	7.0	A5.10.6	0.13	#4@18in	Yes
Florida	Empirical	-	8.5	#5@10	0.37	#5@10in	Yes
Illinois	Traditional	Strength I/ Service	8.0	A5.10.6	0.31	#5@12in	Yes
Texas	Empirical/ Traditional	Strength I/ Service	8.5	A5.10.6	0.20	#4@12in	No
Iowa	Traditional	Strength I	8.0	min A5.6.7, 5.10.6, 9.7.3.2	0.37	#5@10in	No
Ohio	Traditional	Strength I/ Service	8.5	A5.10.6	0.19	#4@12.5in	No
Arizona	Traditional	Service	8.0	A5.10.6	0.31	#5@12in	No

Florida, Illinois, Iowa, and Arizona typically provide bars #5 to their S&T reinforcement in concrete decks. It is also comparable to the spacing of this reinforcement, which varies between 10 and 12.5 in.

Shrinkage and Temperature Reinforcement Spacing

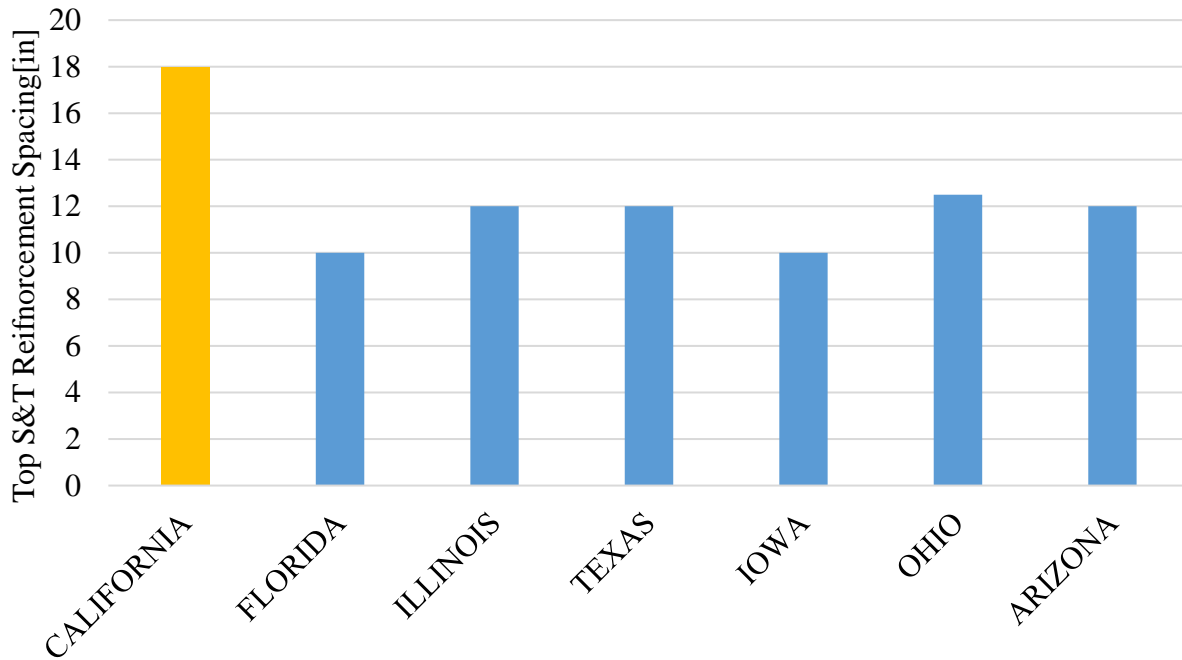


Figure 5.29: S&T reinforcement spacing comparison by state.

Shrinkage and Temperature Reinforcement Amount

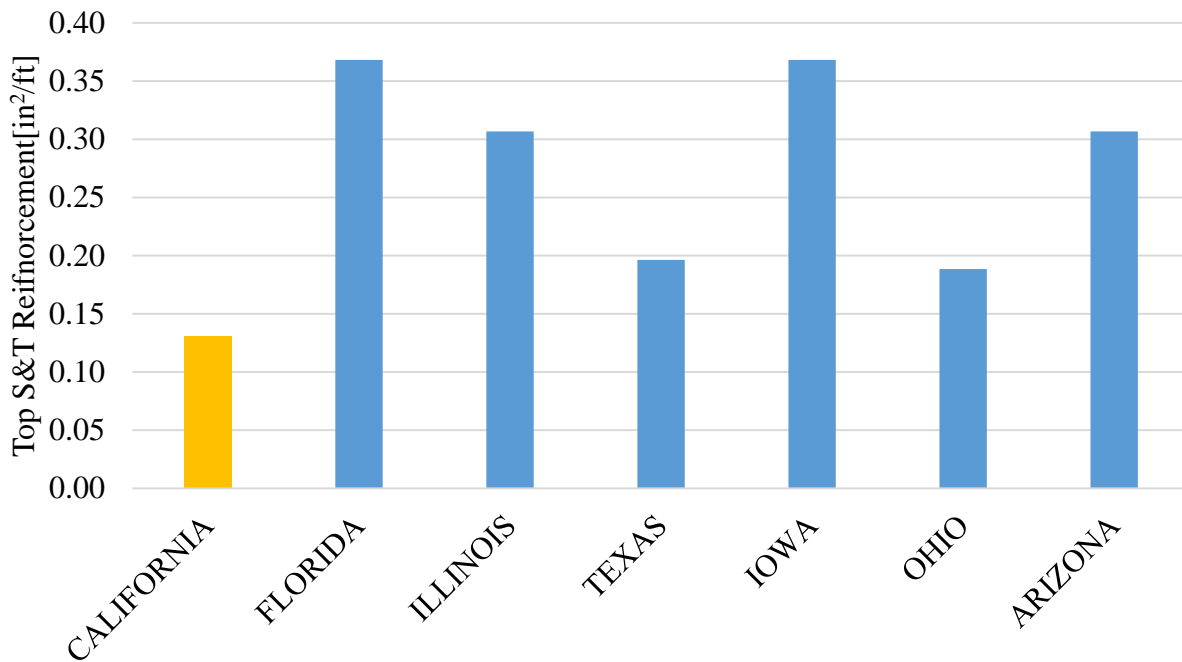


Figure 5.30: S&T steel reinforcement amount per state.

5.4.3 Restraint Effects on Concrete Stresses

Concrete develops stresses, Figure 5.31, when subjected to restraint effects. There are several factors affecting the magnitude of the stresses developed, such as:

- Concrete materials and proportions – Mixture Design
- Construction practices – Concreting Sequence, Curing Methods
- Weather conditions – Cold and hot temperatures
- Restraint conditions – Superstructure types

The magnitude of stresses in concrete decks is a function of the degree of restraint, the more restraint, the more stress is developed, and the risk of cracking is increased. In general, restraint effects are more likely to develop in previously cast webs of box girder bridges when compared to deck cast in concrete or steel girders.

From a design point of view, the crack widths caused by these stresses can be controlled through the amount of steel reinforcement and the spacing between them. Sufficient amount of steel reinforcement controls the level of stresses in the reinforcement, the crack widths in the concrete, and the level of tensile strains, while closer spacing reduces the magnitude of crack widths (Frosch et al., 2006).

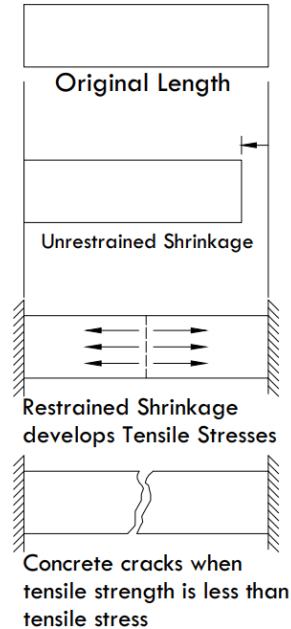


Figure 5.31: Restrained shrinkage in concrete (Adapted from ACI 224R-01 R08)

The minimum amount of shrinkage and temperature reinforcement is provided in the AASHTO LRFD Article 5.10.6 as:

$$A_s \geq \frac{1.30bh}{2(b+h)f_y}$$

except that:

$$0.11 \leq A_s \leq 0.60 \text{ in}^2 / \text{ft}$$

The requirements in Article 5.10.6 are based on ACI 318-14 and ACI 207.2R specifications for shrinkage and temperature changes. ACI 318 (2011) mentions in the commentary of section 7.12.1.2 that the area of S&T reinforcement required by the code has been satisfactory where S&T movements are permitted to occur. It also states that for the cases where significant restraint to S&T movements is provided, it may be necessary to increase the amount of reinforcement required. In box girder bridges, enough longitudinal restraint is provided by the webs of the box girders to the concrete deck, and such cases should consider additional S&T reinforcement.

Frosch et al. (2006) developed a new formula for computing the required amount of steel reinforcement and spacing based on controlling the restraint effect of shrinkage and temperature in bridge decks. The formula for the amount of steel includes the strength of concrete, steel strength, and the gross section of the concrete element:

$$A_s = \frac{6\sqrt{f'_c}}{f_y} A_g$$

The maximum spacing developed in this study is based on the concrete cover, and for mild steel is reduced to (Frosch et al., 2006):

$$s_{\max} = 9 \left[2.5 - \frac{d_c}{2} \right] \leq 9in.$$

For the classical and most common type of concrete and steel used in California, the required amount of steel in term of the gross section is:

$$A_s = \frac{6\sqrt{4,000^{psi}}}{60,000^{psi}} A_g = 0.63\% A_g$$

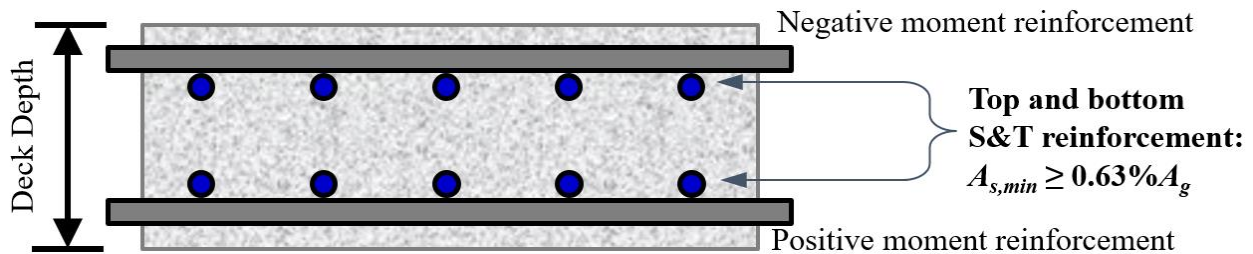


Figure 5.32: Steel reinforcement for S&T in concrete deck

The typical amount of reinforcement provided in box girder bridges in the top layer for S&T is between 0.11% A_g and 0.15% A_g according to the MTD10-20 (Caltrans, 2017b) for both reinforced concrete and prestressed concrete box girder bridges. Shrinkage and temperature effects are more focused in the top surface of concrete decks, therefore more S&T should be provided in

the top layer. If the steel reinforcement required using the equations developed by Frosch et al. (2006) is distributed in equal amounts of top and bottom layers, the required steel reinforcement provided would be $0.32\%A_g$ in each layer, as shown in Figure 5.33.

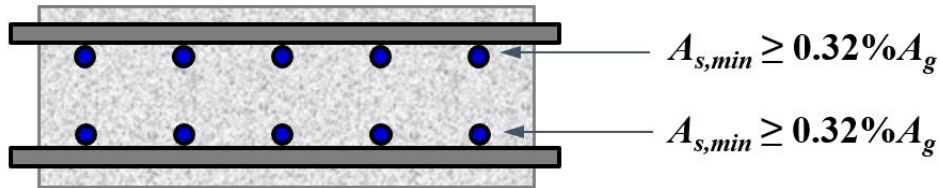


Figure 5.33: S&T distribution if 50% of required amount is distributed in top and bottom layers.

Assuming #5 reinforcement, the maximum spacing using the proposed formula is:

$$f_y = 60,000 \text{ psi} \quad d_c = 2 \text{ in.} \quad s_{\max} = 9.0 \text{ in.}$$

In summary, using the formulas proposed by Frosch et al. (2006), several configurations for S&T reinforcement distribution can be used, as seen in Figure 5.34.

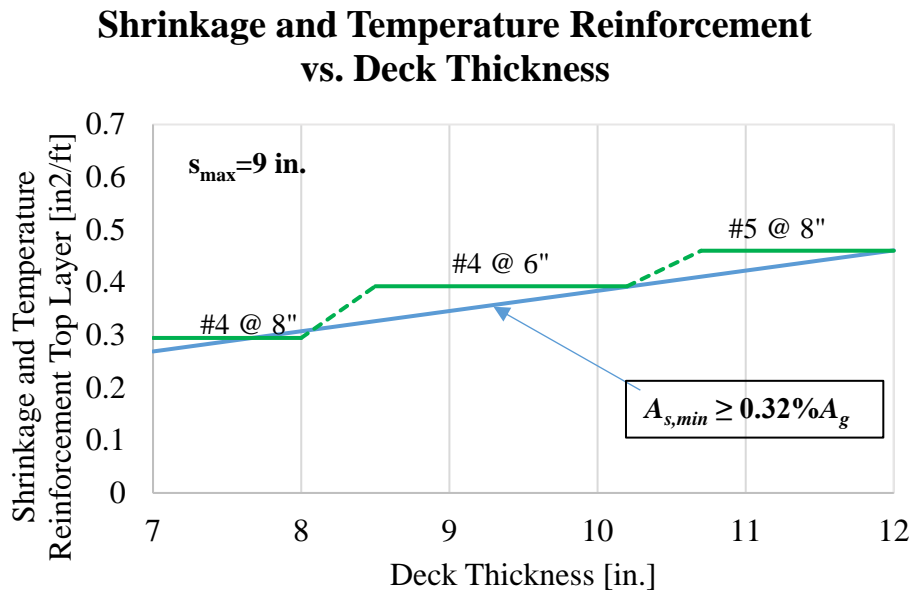


Figure 5.34: S&T Reinforcement configuration proposed.

5.4.4 Summary

- More than 70% of analyzed bridges reported transverse cracking.
- 35% of bridges reported moderate to severe transverse crack width (≥ 0.02 in.) in the first 10 years
- Caltrans S&T reinforcement practices
 - Are based on minimum requirements from AASHTO LRFD,
 - Use the least amount of S&T reinforcement in comparison with other states, and
 - Use the largest S&T reinforcement spacing (18 in.) in comparison with other states.
- For shrinkage and temperature reinforcement
 - Supply a larger amount of S&T reinforcement, at least 0.32% A_g for top and bottom layers
 - Space the S&T reinforcement closer, 9 in. or closer

As discussed before, restraint of concrete decks might lead to excessive tensile stresses. Continuous structures usually provide sufficient restraint to concrete decks, transversally and longitudinally. Transverse cracking over bents and piers is very common in continuous structures, not only due to global flexure but also due to excessive volume restraint, which can be noticed as early age cracking of these structures.

CHAPTER 6. EVALUATING DEGREE OF RESTRAINT IN BOX GIRDER BRIDGES

6.1 Introduction

Internal and external restraining conditions are provided to the deck by the reinforcing bars as well as can be provided by abutments, piers, diaphragms, girders or existing webs. Differences in elasticity of concrete may lead to a high degree of restraint at the interface of these structural elements. In this chapter, a procedure has been developed to estimate the restraint factor using bridge deck data measurements collected from two bridges in California. Temperature data and drying shrinkage were used to estimate longitudinal and transverse strains in the deck to evaluate the degree of restraint provided by concrete box girders. A finite element method (FEM) model was developed, including the effects of early age creep and shrinkage, using the Modified B3 Creep Model (Byard and Schindler, 2015).

6.2 Selected Bridges

The selected bridges consist of two cast-in-place box girder bridges that were constructed in California during the year 2010. Wiss, Janney, Elstner Associates, Inc (WJE) developed an investigation on early-age bridge deck cracking for the California Department of Transportation, in which they took field measurements of these two bridge decks during its construction stage. The first one, Markham Ravine Bridge, located in Lincoln City, part of the Sacramento Metropolitan Area, was instrumented, and data were collected for 17 days. The second one is Olive Lane Undercrossing Bridge, located in Santee City of San Diego County, in which data was collected for 23 days.

6.2.1 Markham Ravine Bridge – Lincoln, California

The first bridge is a 4-cell box girder bridge of two 118 ft continuous spans with girders spaced approximately at 9 ft. The deck thickness is 8 in. The bridge deck pictures (WJE Associates, 2011) indicate that Detail 5-10 were used for the detailing of the main reinforcing steel and #4 bars spaced at 18 in. for the shrinkage and temperature reinforcement. Table 6-1 indicates the design mixture used in this bridge.

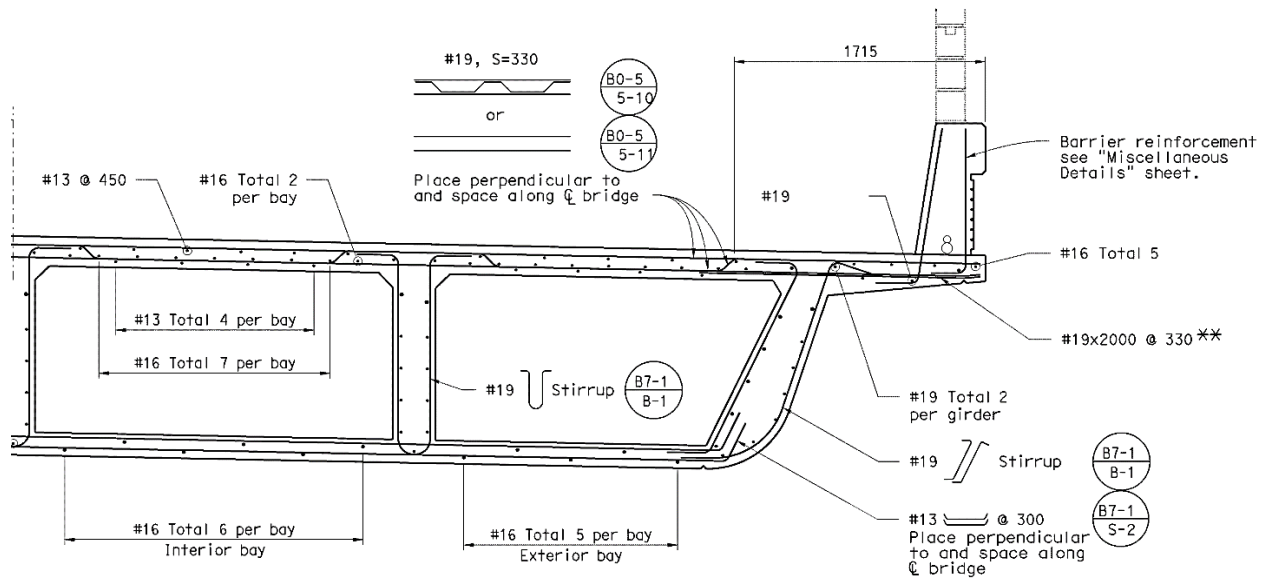


Figure 6.1: Typical Cross Section (Caltrans, 2021)

Table 6-1: Design Mixture Markham Bridge (WJE Associates, 2011)

Design Mixture	Unit	Quantity
Water Content	lb/yd ³	284
Cement Content	lb/yd ³	506
Class C Fly Ash	lb/yd ³	169
Cementitious Material Content	lb/yd ³	675
SSD Normalweight Coarse Agg.	lb/yd ³	1,858
SSD Normalweight Fine Agg.	lb/yd ³	1,243
Water-Reducing Admixture	oz/yd ³	27
Target Total Air Content	%	1.5
Water-to-Cementitious Materials Ratio		0.42

The instrument cluster is presented in Figure 6.2, and the location is shown in Figure 6.3.

The instrumentation consisted in 3 concrete embedment strain gages (EGP -5-120) and 3

thermocouples at 1 in., 4 in., and 7 in. depths. It was also measured the relative humidity at 1 in. and 7 in. depths. Longitudinal strains were measured by the strain gages.

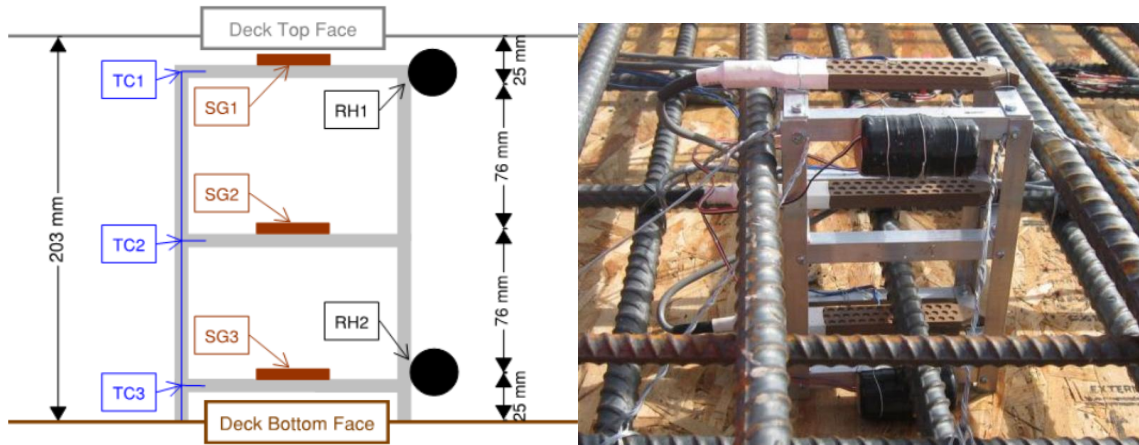


Figure 6.2: Typical Instrument Cluster Diagram at Markham Ravine Bridge (WJE Associates, 2011)

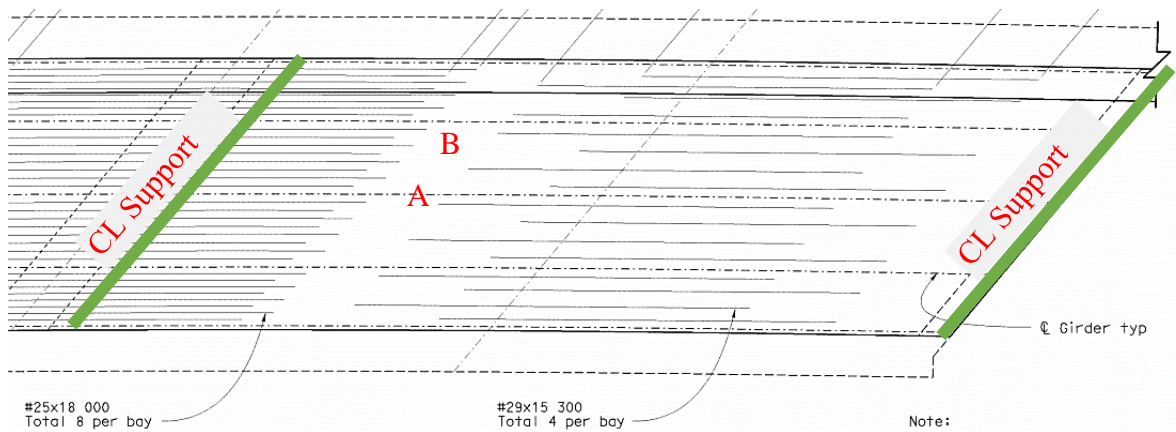


Figure 6.3: Location of instrument clusters, 32 ft from CL support at Markham Ravine Bridge (WJE Associates, 2011)

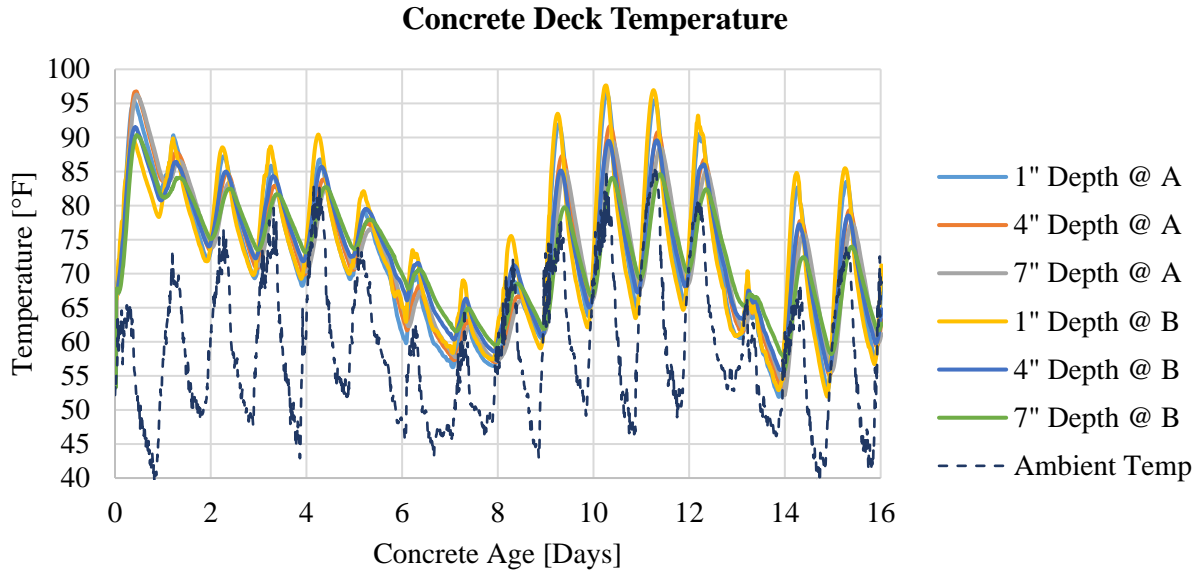


Figure 6.4: Thermocouples data – Markham Ravine bridge

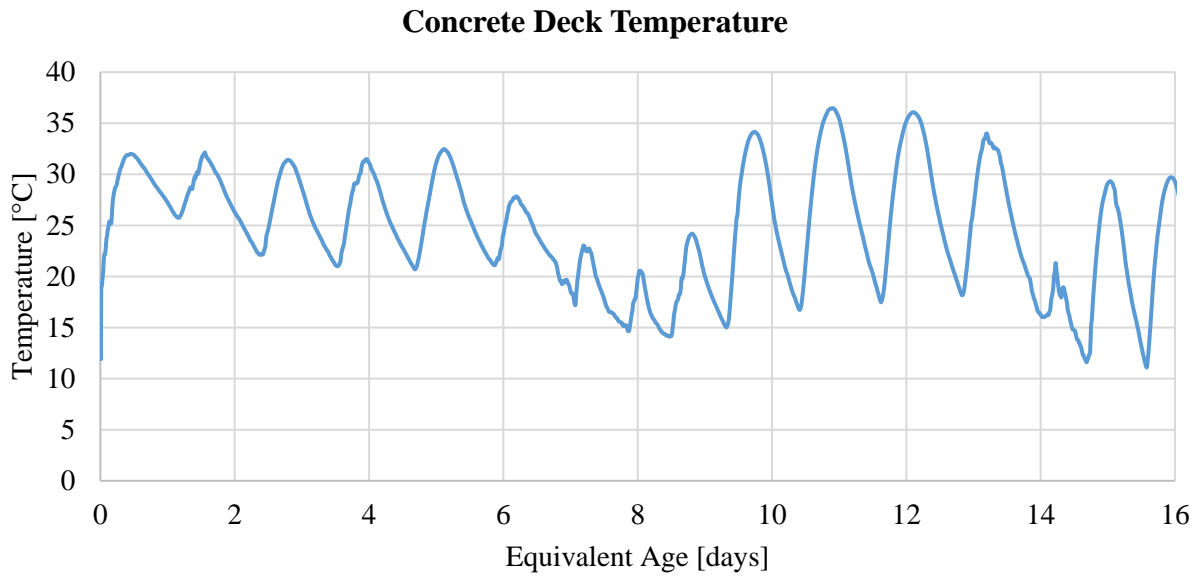


Figure 6.5: Concrete deck temperature selected

6.2.2 Olive Lane Bridge – Santee, California

This bridge is a 10-cell box girder bridge of approximately 157 ft span length, simply supported, with girders spaced approximately 10 ft. The deck thickness is 9 in. The bridge deck pictures (WJE Associates, 2011) indicate that Detail 5-11 were used for the detailing of the main reinforcing steel and #4 bars spaced at 18in. for the S&T reinforcement. Table 6-2 indicates the design mixture used in this bridge.

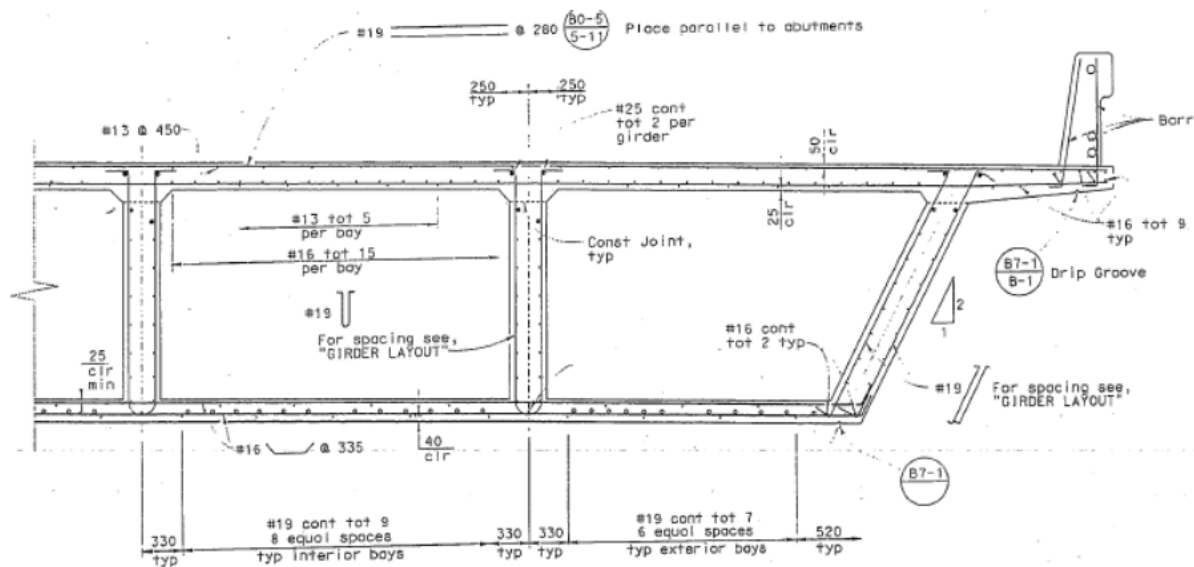


Figure 6.6: Typical Cross Section

Table 6-2: Design Mixture Olive Lane Bridge (WJE Associates, 2011)

Design Mixture	Unit	Quantity
Water Content	lb/yd ³	330
Cement Content	lb/yd ³	564
Class C Fly Ash	lb/yd ³	188
Cementitious Material Content	lb/yd ³	752
SSD Normalweight Coarse Agg.	lb/yd ³	1571
SSD Normalweight Fine Agg.	lb/yd ³	1155
Water-Reducing Admixture	oz/yd ³	30.1
Target Total Air Content	%	3
Water-to-Cementitious Materials Ratio		0.44

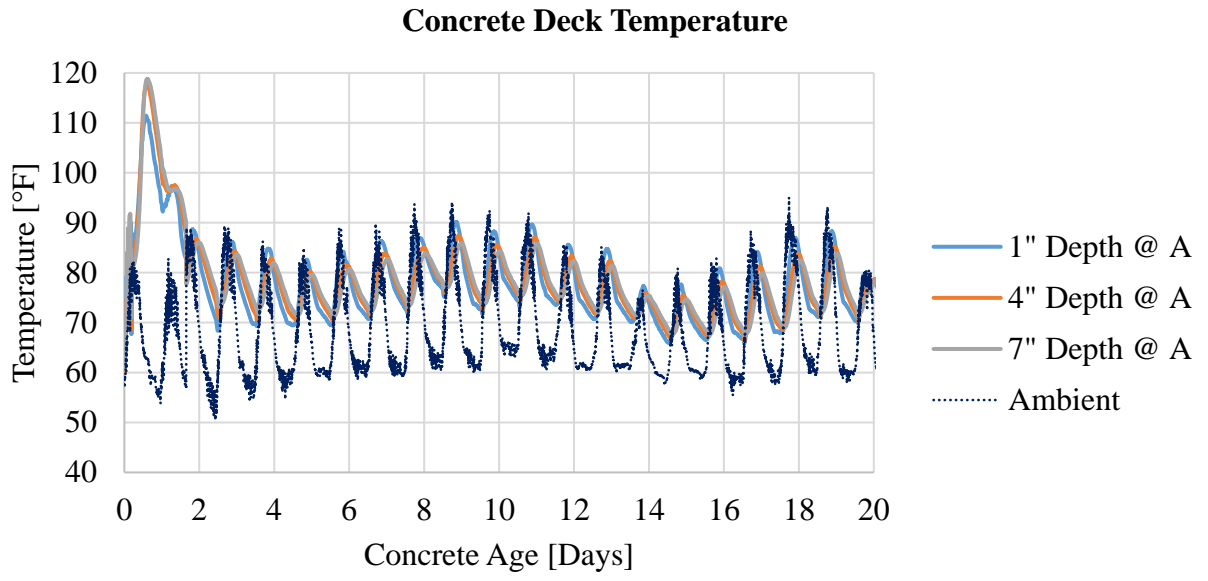


Figure 6.7: Thermocouples data – Olive Lane Bridge

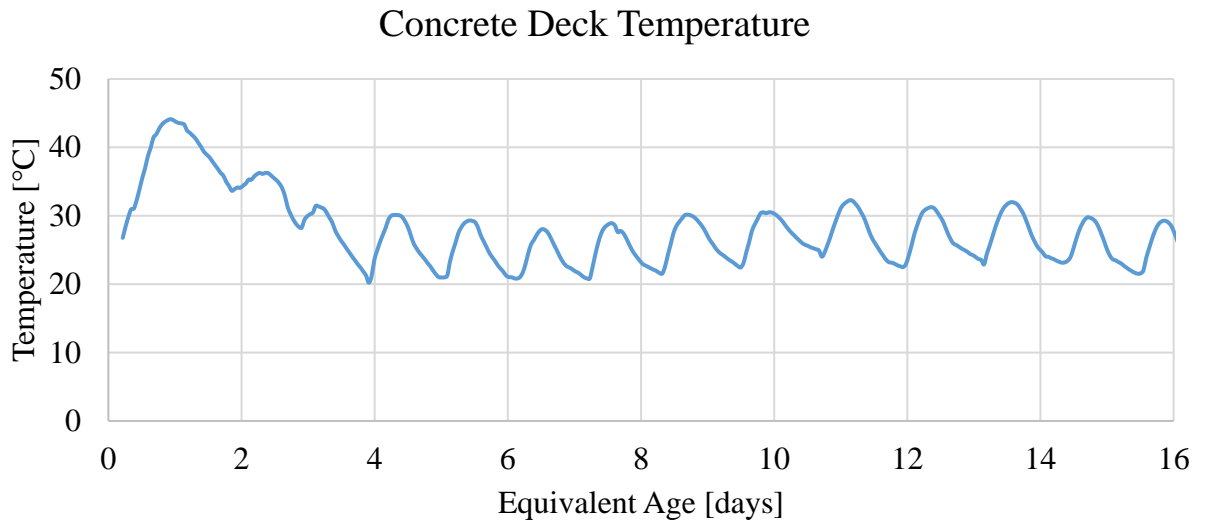


Figure 6.8: Concrete deck temperature selected

6.3 Finite Element Modeling

6.3.1 Boundary Conditions

To properly define the boundary conditions of the bridge, the design thermal movement range, Eq. 2.31 from Article 3.12.2.3 of the AASHTO LRFD was used to determine the longitudinal design movement of the bridge box girders. The thermal design movement is defined as:

$$\Delta_T = \alpha L (T_{MaxDesign} - T_{MinDesign}) \quad \text{Eq. 2.31}$$

where, α is the coefficient of thermal expansion, L is the span length, $T_{MaxDesign}$ is the maximum design temperature, and $T_{MinDesign}$ is the minimum design temperature. Using Procedure B (Article 3.12.2.2 (AASHTO, 2020)), the temperature range was defined for both bridges, and the thermal design movements are summarized in Table 6-3.

Table 6-3: Bridge Data for Design Thermal Movement

Bridge	α [$\mu\epsilon/^\circ\text{F}$] ($\mu\epsilon/^\circ\text{C}$)	L [in.]	TMaxDesign [$^\circ\text{F}$]	TMinDesign [$^\circ\text{F}$]	Δ_T [in.]
Markham	5.5(9.9)	1416	115	30	0.662
Olive	5.5(9.9)	1920	115	50	0.686

Both bridges were designed with reinforced elastomeric bearing pads in the end abutments. At Markham bridge, these pads are 18x18x2.5 in., while for Olive Lane bridge, they are 20x20x3 in. The shear modulus is approximately 100 psi (Caltrans, 1994), but for design is taken as 169 psi. In Table 6-4, shear stiffness values are presented for the modeling of the bearing pads. Linear spring elements were used with stiffness constants based on (AS, 2017), as shown in Table 6-4.

Table 6-4: Shear stiffness for bearing modeling

	Markham	Olive Lane
b [in]	18	20
h [in]	18	20
t [in]	2.5	3
G [psi]	169	170
K_s [psi/in]	21902	22667

For the Markham bridge, only one span is modeled, assuming a fixed connection at the middle at the bent. For the Olive Lane bridge, elastomeric pads were modeled for both ends as it is a simply supported bridge. Vertical displacement of the degrees of freedom at the elastomeric pad is restrained.

6.3.2 Creep and Shrinkage Model Implementation

Using ABAQUS software the material models can be incorporated into the input data of the model using subroutines. UMAT is the subroutine that allows the user to define any constitutive model for the mechanical behavior of the material in the ABAQUS/Standard module.

Liu (2018) used an already developed UMAT code based on the original B3 Creep Model (Bažant and Baweja, 2000) and modified it to account for the equivalent age. The modifications made to the B3 Creep Model and used simple models to verify the accuracy of the subroutine. A rate-type creep law based on a Kelvin chain model according to the solidification theory (Bažant and Prasannan, 1989b, 1989a) was used to incorporate the creep compliance function. More details of the algorithm and numerical implementation of the creep model can be found in Liu (2018).

Liu (2018) estimated that the Modified B3 Model (Byard and Schindler, 2015) provides the best prediction of early-age concrete stresses through a residual analysis compared with other 3 creep models. For this analysis, the early age behavior of concrete is of interest, and therefore

the Modified B3 Creep Model was selected to implement concrete creep and shrinkage on the bridge deck models.

The subroutines obtained from (Liu, 2018) use the equivalent age of concrete based on the maturity method (Carino, 2004) with the Arrhenius equation Eq. 2.32:

$$t_e = \sum e^{\frac{-E}{R}} \left[\frac{1}{273+T_c} - \frac{1}{273+T_r} \right] \Delta t \quad \text{Eq. 2.32}$$

where,

- t_e : equivalent age at the reference curing temperature
- T_c : average temperature of concrete during time interval Δt , °C
- T_r : reference temperature, °C
- E : activation energy, J/mol
- R : universal gas constant, 8.3144 J/(mol °K)

The activation energy of the concrete decks is calculated based on Eq. 2.33 developed by (Schindler, 2004):

$$E = 22,100 \cdot p_{C_3A}^{0.30} \cdot p_{C_4AF}^{0.25} \cdot Blaine^{0.35} \quad \text{Eq. 2.33}$$

where,

- p_{C_3A} : weight ratio of C_3A in terms of total cement content
- p_{C_4AF} : weight ratio of C_4AF in terms of total cement content
- $Blaine$: Blaine value specific surface area of cement [m²/kg]

6.3.2.1 Modified B3 Model

(Byard and Schindler, 2015) made modifications to the B3 Model to account for the early-age viscoelastic and elastic behavior of concrete. These modifications are limited to improving the early-age response without affecting the later-age compliance.

In the B3 Model, the compliance function is defined as Eq. 2.34:

$$J(t, t') = q_1 + C_0(t, t') + C_a(t, t', t_0) \quad \text{Eq. 2.34}$$

where the second term is the compliance function for basic creep:

$$C_0(t, t') = q_2 Q(t, t') + q_3 \ln[1 + (t - t')^n] + q_4 \ln\left(\frac{t}{t'}\right)$$

and the aging viscoelastic term:

$$q_2 Q(t, t') \quad \text{Eq. 2.35}$$

The modified aging viscoelastic term is defined as:

$$q_2' = q_2 \left(\frac{t'}{t' - q_5} \right) \quad \text{Eq. 2.36}$$

where the term q_5 is the structural setting time. A second modification to the early-age elastic compliance is also included:

$$q_1' = q_1 \left[\frac{t'}{t' - q_6} \right] \quad \text{Eq. 2.37}$$

Including both modifications, the Modified B3 Model can be expressed as:

$$J(t, t') = q_1' \left[\frac{t'}{t' - q_6} \right] + q_2' \left[\frac{t'}{t' - q_5} \right] Q(t, t') + q_3 \ln[1 + (t - t')^n] + q_4 \ln\left(\frac{t}{t'}\right) \quad \text{Eq. 2.38}$$

Since the information provided did not include setting times for the concrete in the deck, these values were assumed to be 5 hours. Table 6-5 show the input data for the creep

Table 6-5: Concrete Deck Material Properties and Creep Parameters

Mechanical Properties			
		Markham	Olive Lane
Elasticity at 28 days	ksi	4102	4146
Concrete Strength at 28 days	psi	5180	5290
Aggregate to cementitious Materials Ratio	a/c	4.6	3.6
Creep Parameters			
	Elastic q_1	0.146	0.145
	Aging Viscoelastic q_2	1.024	1.061
	Non-Aging Viscoelastic q_3	0.009	0.011
	Flow q_4	0.048	0.057
	Factor for Aging Viscoelastic Modification q_5	0.215	0.215
	Factor for Elastic Modification q_6	0.215	0.215

The shrinkage subroutine is called UEXPAN in Fortran language and it follows the same procedure described in Section 2.4.1. The parameters used

Table 6-6: Shrinkage Parameters

Shrinkage Parameters			
Water Content [lb/ft ³]	w	10.52	12.22
Relative Humidity	h	0.60	0.58
Humidity Dependence	k_h	0.79	0.80
Volume to Surface Ratio	V/S	3.85	4.39
Shape Factor	k_s	1	1
Cement Type Factor	α_1	0.85	0.85
Curing Factor	α_2	1.2	1.2

Table 6-5 and Table 6-6 show the input data for the creep and shrinkage subroutines used in the modeling of the bridges.

6.3.3 Bridge Model

The two bridges were modeled using Abaqus software. Solid elements 8-node hexahedral (C3D8) were used for modeling the concrete deck, and C3D8R – reduced integration were used for the soffit and the girders. Linear elements (T3D2) for the reinforcing steel and prestressing steel were used. Creep and shrinkage were incorporated using the two subroutines UMAT and UEXPAN (Liu, 2018). A concrete casting sequence was included to incorporate the age of the web and bottom flanges girders vs. the concrete deck age. Meshing and time steps are based on (Liu, 2018). Input data has been described in previous sections. Figure 6.9 shows a schematic picture of the bridge model with the typical application of boundary conditions, the incorporation of the temperature data in the deck and the elastomeric pads in the far end.

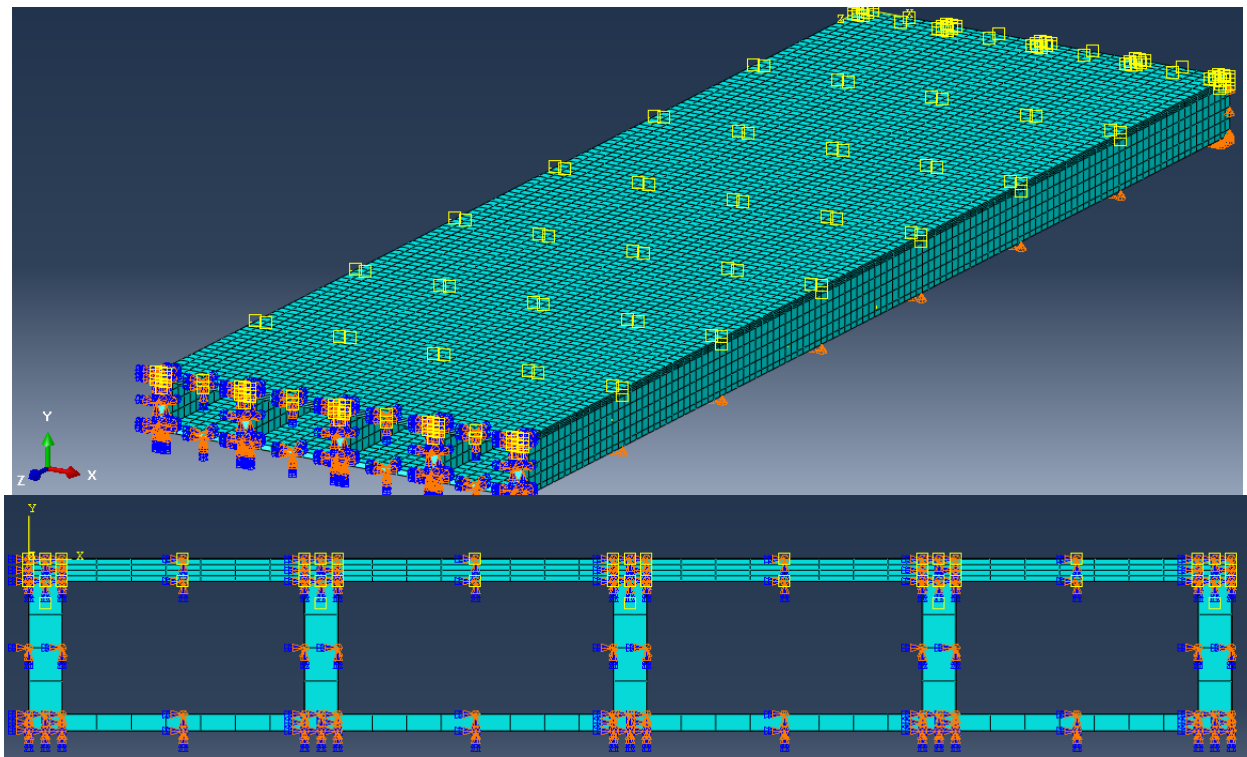


Figure 6.9: 3D and 2D View of FEM model – Markham Bridge

6.4 Strain Results

Simulated longitudinal strains of the Markham Bridge are presented in Figure 6.10 with the strain measurements on the field up until the time of the prestress applied. Strain amplitudes are in reasonable agreement between simulated and measured values. From Figure 6.5, there is a cooling period in the concrete deck between day 2 and 9, which should reflect in the development of tensile strains as can be seen in Figure 6.10 from the simulated model. Tensile strains reach up to $100 \mu\epsilon$.

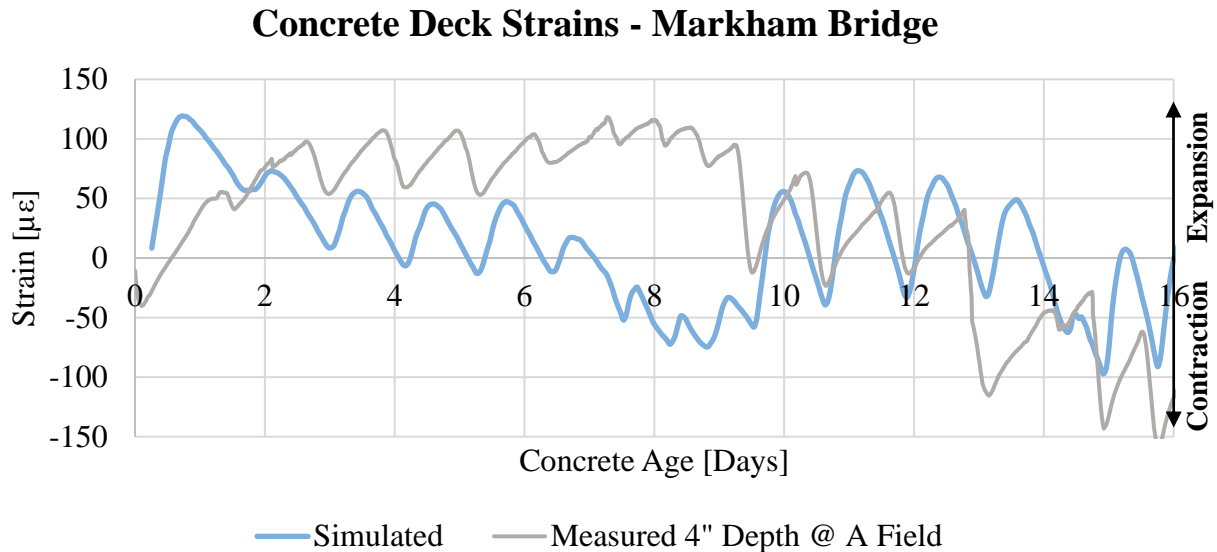


Figure 6.10: Simulated and measured deck strains.

The simulation of the Olive Lane bridge strains is presented in Figure 6.11. For this bridge the simulation agrees better than Markham Bridge. The amplitudes again are very similar to the field measurements. It is worth to mention that temperature histories for the two bridges is quite dissimilar. In both cases it can be seen that temperature history plays a main role in the development of strains.

Concrete Deck Strains - Olive Lane Bridge

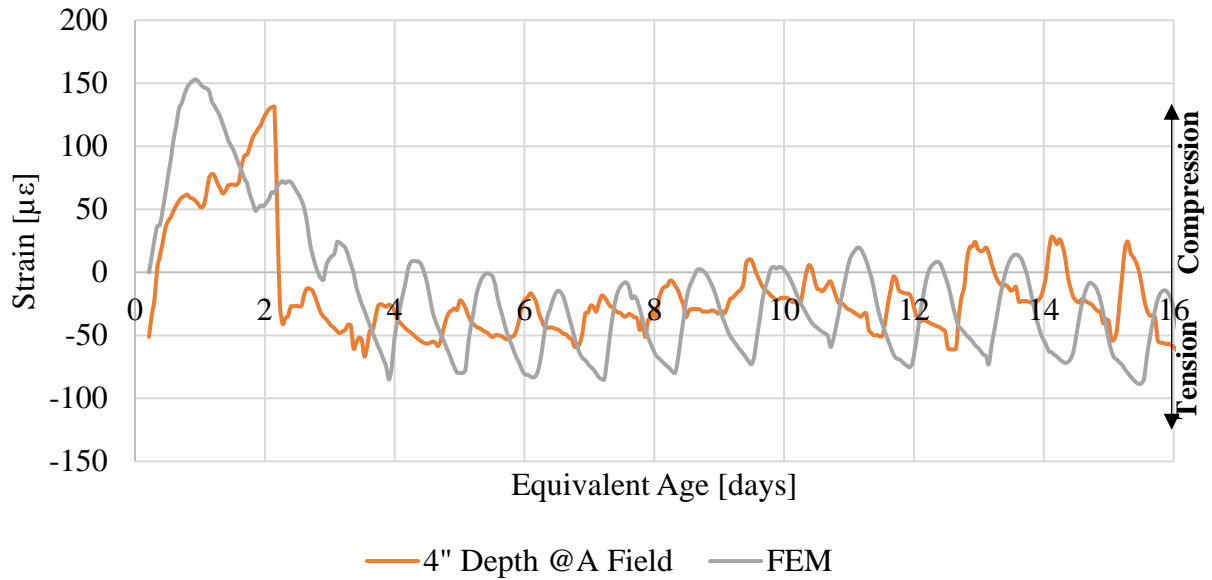


Figure 6.11: Simulated and measured deck strains.

6.5 Restraint Factor of Selected Bridges

The restraining factors are computed using the method provided by (Frosch et al., 2006), Figure 6.12. If the deck is partially restrained, then the restraint factor is computed using Eq. 2.39

:

$$k = \frac{1}{2} \left[1 - \frac{\varepsilon_m}{\varepsilon_f} \right] \quad \text{Eq. 2.39}$$

where,

ε_m = simulated strain

ε_f = free shrinkage strain

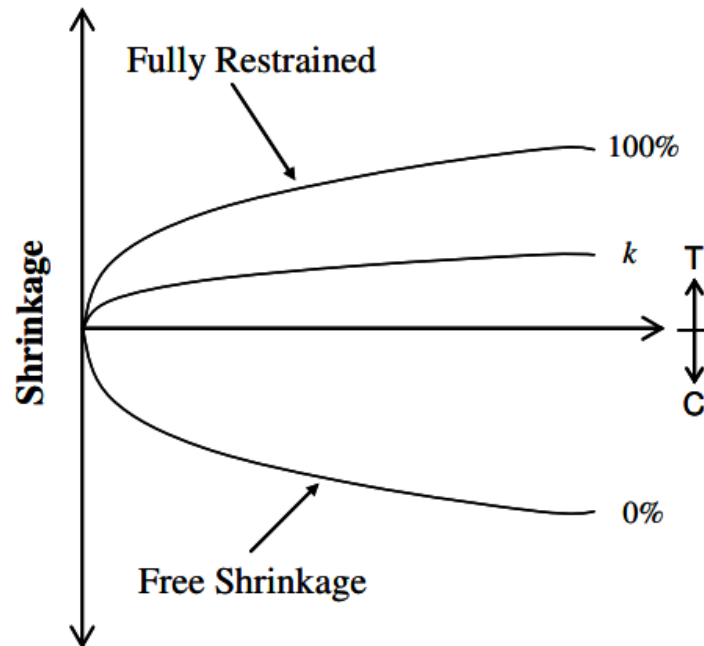


Figure 6.12: Degree of restraint in concrete (Frosch et al., 2006)

In Figure 6.13 and Figure 6.14 the restraint factors are shown for the longitudinal direction for both bridges at location A (1/3 of middle support for Markham bridge and midspan for Olive Lane bridge). Values were computed using free shrinkage strain taken from the FEM model (a free shrinkage model of the deck), and computed using the field free shrinkage measurements. Markham bridge shows ranges between 33 and 67% for the restraining factor in the longitudinal direction, whereas Olive Lane bridge shows higher values up to 88%. The difference in those values might be reflected by the temperature history, bridge geometry, and different concrete properties for the creep and shrinkage simulation. Frosch et al. (2006) estimated longitudinal restraint factors of 75% and 41% over the girder and at midbay, respectively, using a free shrinkage measurement from a lab specimen and of 70 days of age.

Restraining Factors - Markham Bridge

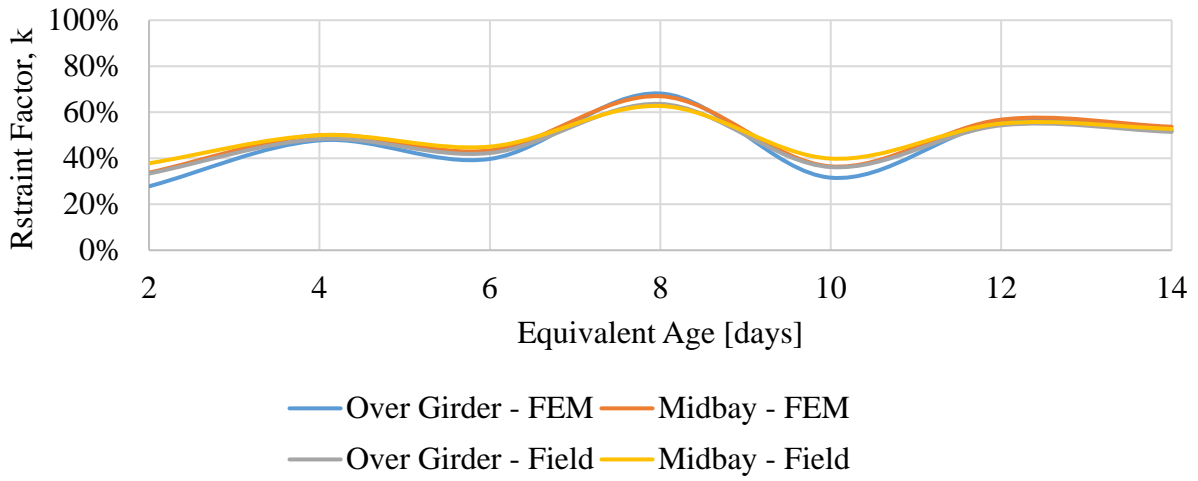


Figure 6.13: Longitudinal restraint factors over time for Markham Bridge at location A.

Restraining Factors - Olive Lane Bridge

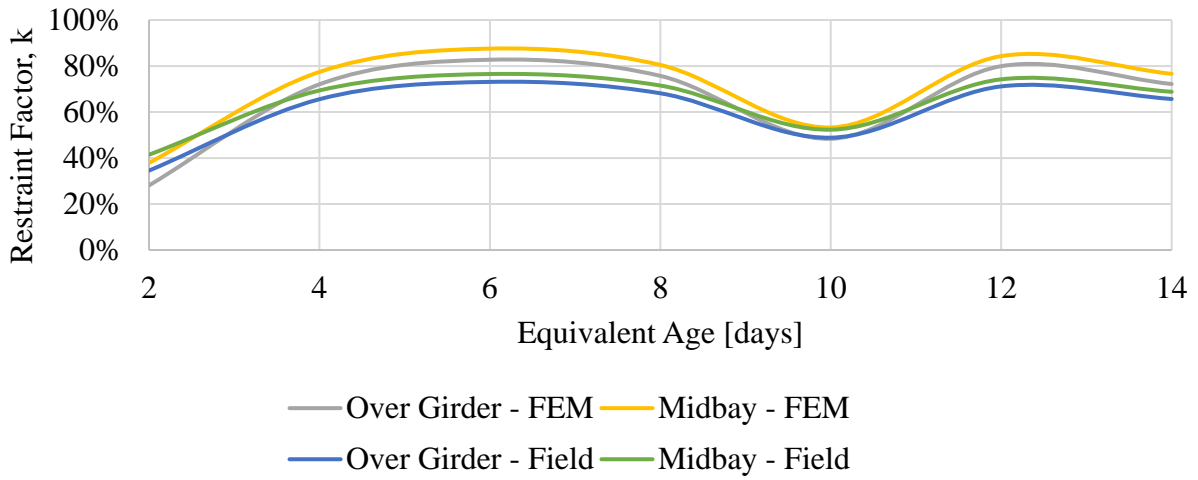


Figure 6.14: Longitudinal restraint factors over time for Markham Bridge at location A.

CHAPTER 7. CONCLUSIONS AND RECOMMENDATIONS

A statistical review of the current conditions and issues in bridges was performed. It was noticed that the most common type of deck solution is the cast-in-place reinforced concrete decks. Due to the availability of data, the state of California was selected to perform the study. Bridges were identified by means of statistical review identifying typical structural types, materials and other parameters with concrete deck issues. Box girder bridges were the greater number of structures with issues, and a set of 94 bridges provided by California was used to analyze bridge decks.

The data (inspection reports) plus the NBI information provided the basis to detect that most transverse cracking is observed in continuous structures of prestressed concrete and reinforced concrete. Seventy percent of these box girder bridges show transverse cracking up to 0.08 in. in the first 10 years of service, predominantly in prestressed concrete structures.

Traffic data from various WIM stations in California showed consistency. Furthermore, live load effect due to WIM trucks is lower than design loads (HL-93) for most sites, and only a small percentage of vehicles exceed it. Three-dimensional finite element analysis was performed to determine the effect of traffic in concrete decks. It was found that calculated WIM load effects for California are similar to HL-93 design load,.

Cracking control provisions of the AASHTO LRFD are modified by Caltrans provisions allowing for Detail 5-10 to use double the required spacing between truss bars when they become positive/negative moment reinforcement. A finite element analysis was performed with a selected number of box girder bridges to evaluate the drop-off distance of Detail 5-10. It was found that in almost 70% of the cases, the distance required was not achieved.

Shrinkage and temperature reinforcement is a key element in the deck design to prevent excessive crack widths in both transverse and longitudinal cracks. Data of shrinkage and temperature reinforcement showed that California allows larger spacing (18 in.) than most states, providing 0.13 in²/ft, which is very close to the lower limit specified by the AASHTO LRFD. This was the case for 70% of the bridges studied.

Restraining effects of concrete box girders was simulated incorporating the effects of early-age creep and shrinkage using finite element analysis. The results indicated that girders provide a very high restraining effect in the first 14 days after concrete placement. Restraining factors between 30 and 88% were found for two bridges constructed in California in 2010.

Based on the study performed, the following conclusions are made:

- The statistical analysis shows that cast-in-place box girder bridges are the bridge type with more susceptibility to poor performance, especially when continuous.
- WIM data showed that traffic is consistent with the AASHTO LRFD design load HL-93 when comparing moment ratios in the longitudinal direction. WIM axle loads are very consistent year to year and in great proportion lower than the 25 kips tandem design load of the AASHTO LRFD. Based on WIM data analysis and analytical procedure performed, traffic is not a cause for the poor performance of California bridge decks.
- Evaluation of deck design provisions showed that the main reinforcement detailing does not comply with AASHTO LRFD in terms of spacing. Detail 5-10 does not provide enough flexural termination length at the strength limit state for post-cracking shear influence. Therefore, it is recommended to discontinue its use for future designs.
- Shrinkage and temperature provisions used by Caltrans were among the least restrictive among several states, with the larger spacing and the least amount of steel reinforcement. Based on the cracking data, it was concluded that more closely

spaced bars might help control the widths of the cracks documented in Caltrans bridges.

- The level of deterioration observed in box girder bridges at early ages shows a design problem. The elevated restraint effect provided by webs of box girder to the deck needs evaluation and consideration at the time of design.
- Longitudinal restraint factors were developed for two box girder bridges constructed in California in 2010. Results showed that over a period of 14 days, the level of restraint could be up to more than 88%.

7.1 FUTURE RESEARCH

Restraint factors determined in this research showed that cast-in-place box girder bridges provide a large amount of movement restraint to the concrete deck. It is suggested to continue the development of a model for restraint factors that could be a function of the concrete design mixture and for typical geometrical configurations.

Further develop a field database from locations across the country and for different structural types to expand the understanding of restraint effects in concrete decks.

This study has provided a procedure to evaluate the degree of restraint that webs of box girders provide to the concrete deck. It could serve as a basis for developing restraining factors for other types of bridges, such as precast girders or steel girders. An extensive set of restraint factor data representative of the nation could serve as a basis to improve design specifications for concrete decks.

CHAPTER 8. REFERENCES

- AASHTO, 2020. AASHTO LRFD Bridge Design Specifications, 9th Edition. ed. American Association of State Highway Officials, Washington, D.C.
- Abaqus, 2020. Abaqus CAE - SIMULA™ by Dassault Systèmes® [WWW Document]. URL <https://www.3ds.com/products-services/simulia/products/abaqus/abaquscae/> (accessed 11.10.20).
- ACI 207, 2007. ACI PRC-207.2-07 Report on Thermal and Volume Change Effects on Cracking of Mass Concrete. American Concrete Institute.
- ACI 209, 2002. ACI PRC-209-92: Prediction of Creep, Shrinkage, and Temperature Effects in Concrete Structures (Reapproved 2008). American Concrete Institute.
- ACI 224, 2001. ACI PRC-224-01: Control of Cracking in Concrete Structures (Reapproved 2008). American Concrete Institute, Farmington Hills, MI.
- ACI 318, 2019a. ACI CODE-318-19: Building Code Requirements for Structural Concrete and Commentary. American Concrete Institute, Farmington Hills, MI.
- ACI 318, 2019b. ACI 318R-19: Commentary on Building Code Requirements for Structural Concrete. American Concrete Institute, Farmington Hills, MI.
- ACI 318, 2011. ACI CODE-318-11: Building Code Requirements for Structural Concrete and Commentary. American Concrete Institute, Farmington Hills, MI.
- Aktan, H.M., Fu, G., Dekelbab, W., Attanayaka, U., 2003. Investigate Causes & Develop Methods to Minimize Early-Age Deck Cracking on Michigan Bridge Decks.
- Alexander, M., Beushausen, H., 2019. Durability, service life prediction, and modelling for reinforced concrete structures review and critique. *Cem. Concr. Res.* 122, 17–29. <https://doi.org/10.1016/j.cemconres.2019.04.018>
- AS, 2017. Bridge Design Part 4: Bearings and deck joints AS 5100.4:2017 | Standards Australia, 5100.4:2017.
- ASCE, 2021. Infrastructure Report Card. American Society of Civil Engineers.
- Bažant, Z.P., Baweja, S., 2000. Creep and Shrinkage Prediction Model for Analysis and Design of Concrete Structures: Model B3. *ACI Spec. Publ.* 194, 1–84.
- Bazant, Z.P., Baweja, S., 2000. Creep and shrinkage prediction model for analysis and design of concrete structures: Model B3. *ACI Spec. Publ.* 194, 1–84.
- Bažant, Z.P., Prasannan, S., 1989a. Solidification Theory for Concrete Creep. I: Formulation. *J. Eng. Mech.* 115, 1691–1703. [https://doi.org/10.1061/\(ASCE\)0733-9399\(1989\)115:8\(1691\)](https://doi.org/10.1061/(ASCE)0733-9399(1989)115:8(1691))
- Bažant, Z.P., Prasannan, S., 1989b. Solidification Theory for Concrete Creep. II: Verification and Application. *J. Eng. Mech.* 115, 1704–1725. [https://doi.org/10.1061/\(ASCE\)0733-9399\(1989\)115:8\(1704\)](https://doi.org/10.1061/(ASCE)0733-9399(1989)115:8(1704))
- Beeby, A.W., 1983. Cracking, Cover, and Corrosion of Reinforcement. *Concr. Int.* 5, 35–40.

- Byard, B.E., Schindler, A.K., 2015. Modeling early-age stress development of restrained concrete. *Mater. Struct.* 48, 435–450. <https://doi.org/10.1617/s11527-013-0194-2>
- Caltrans, 2021. Bridge Inspection Report 19 0192R. Structure Maintenance & Investigation.
- Caltrans, 2017a. Caltrans Bridge Element Inspection Manual. California Department of Transportation.
- Caltrans, 2017b. Memo To Designers 10-20 : Deck Slab Reinforcement Details. California Department of Transportation.
- Caltrans, 2015. Bridge Design Practice - Chapter 10 Concrete Decks. California Department of Transportation.
- Caltrans, 2000. Element Level Inspection Manual. California Department of Transportation.
- Caltrans, 1994. Memo To Designers 7-1 Bridge Bearings. California Department of Transportation.
- Carino, N.J., 2004. *The Maturity Method*, 2nd Edition. ed. CRC Press.
- Copas, T.L., 1970. Concrete Bridge Deck Durability, NCHRP: Synthesis of Highway Practice. Highway Research Board, National Research Council, Washington.
- Copas, T.L., Pennock, H.A., 1979. Durability of Concrete Bridge Decks, NCHRP: Synthesis of Highway Practice. Transportation Research Board, National Research Council, Washington, D.C.
- Csagoly, P.F., Lybas, J.M., 1989. Advanced Design Method for Concrete Bridge Deck Slabs. *Concr. Int.* 11, 53–63.
- DEDOT, 2021. Bridge Design Manual.
- Fang, I.K., Worley, J.A., Burns, N.H., Klingner, R.E., 1986. Behavior of Ontario-Type Bridge Decks on Steel Girders 210.
- FHWA, 2022. Specifications for the National Bridge Inventory.
- FHWA, 2017. National Performance Management Measures; Assessing Pavement Condition for the National Highway Performance Program and Bridge Condition for the National Highway Performance Program.
- FHWA, 1995. Recording and coding guide for the structure inventory and appraisal of the nation's bridges.
- Freyermuth, C.L., Klieger, P., Stark, D.C., Wenke, H.N., 1970. Durability of concrete bridge decks—A review of cooperative studies 11.
- Frosch, R., Bice, J., Erickson, J., 2006. Design Methods for the Control of Restrained Shrinkage Cracking. JTRP Tech. Rep. <https://doi.org/10.5703/1288284313363>
- Frosch, R., Blackman, D., Radabaugh, R., 2003. Investigation of Bridge Deck Cracking in Various Bridge Superstructure Systems. JTRP Tech. Rep. <https://doi.org/10.5703/1288284313257>
- Frosch, R.J., 2001. Flexural Crack Control in Reinforced Concrete. *Spec. Publ.* 204, 135–154. <https://doi.org/10.14359/10817>

- Hafezolghorani, M., Hejazi, F., Vaghei, R., Jaafar, M.S.B., Karimzade, K., 2017. Simplified Damage Plasticity Model for Concrete. *Struct. Eng. Int.* 27, 68–78. <https://doi.org/10.2749/101686616X1081>
- Krauss, P.D., Rogalla, E.A., 1996. TRANSVERSE CRACKING IN NEWLY CONSTRUCTED BRIDGE DECKS. NCHRP Rep. 380.
- Leonhardt, F., 1977. Crack control in concrete structures. IABSE. <https://doi.org/10.5169/SEALS-43581>
- Liu, Y., 2018. Finite-Element Modeling of Early-Age Concrete Behavior.
- McCormac, J.C., 2006. *Structural Analysis: Using Classical and Matrix Methods*. John Wiley & Sons.
- Mehta, P.K., Monteiro, P.J.M., 2014. *Concrete: Microstructure, Properties, and Materials*. McGraw-Hill Education.
- Mindess, S., Young, F., Darwin, D., 2002. *Concrete*, 2nd Edition. Prentice Hall.
- MoDOT, 2022. LRFD Bridge Design Guidelines.
- Nadelman, E., Krauss, P., Nelson, T., 2017. Investigation of Bridge Decks (No. WJE No. 2016.3598). Montana Department of Transportation.
- NBI, 2022. National Bridge Inventory ASCII Files.
- NEDOT, 2016. Bridge Office Policies and Procedures.
- Nelson, S.L., 2014. Deterioration rates of Minnesota concrete bridge decks. Minnesota Department of Transportation, Research Services & Library.
- Nowak, A.S., Collins, K.R., 2012. *Reliability of structures*. [electronic resource], Second edition. ed. CRC Press/Taylor & Francis Group.
- NYDOT, 2021. Bridge Manual.
- PADOT, 2019. Design Manual Part 4 - Structures.
- Premo, A., 2022. 2022 Bridge Report. American Road & Transportation Builders Association.
- Qiao, P., McLean, D.I., Zhuang, J., 2010. Mitigation Strategies for Early-Age Shrinkage Cracking in Bridge Decks (No. WA-RD 747.1). Washington State Department of Transportation, Washington.
- Rettner, D.L., 2014. Analysis of Bridge Deck Cracking Data: A Review of Mechanisms, Analysis of MnDOT Bridge Construction Data, and Recommendations for Treatment and Prevention (No. MN/RC 2014-09). Minnesota Department of Transportation.
- Russell, H.G., 2017. Control of Concrete Cracking in Bridges, 500. Transportation Research Board, Washington, D.C.
- Russell, H.G., 2004. Concrete Bridge Deck Performance, 333. Transportation Research Board, Washington, D.C.
- Schindler, A.K., 2004. Effect of Temperature on Hydration of Cementitious Materials. *Mater. J.* 101, 72–81. <https://doi.org/10.14359/12990>

Schindler, A.K., McCullough, B.F., 2002. Importance of Concrete Temperature Control During Concrete Pavement Construction in Hot Weather Conditions. Transp. Res. Rec. 1813, 3–10. <https://doi.org/10.3141/1813-01>

SIMULIA, 2019. SIMULIA User Assistance 2019 - Concrete damaged plasticity [WWW Document]. URL https://help.3ds.com/2019/english/DSSIMULIA_Established/SIMACAEMATRefMap/si-mamat-c-concretedamaged.htm?ContextScope=all&id=49100a4d9dea42749952275e5553720f#Pg0 (accessed 11.10.20).

TRB, 2006. Control of Cracking in Concrete: State of the Art. Transportation Research Board, Washington, D.C. <https://doi.org/10.17226/23231>

TXDOT, 2022. Bridge Design Guide.

UDOT, 2017. Structures Design and Detailing Manual.

USAFacts, 2022. US Transportation & Infrastructure Stats | 2022 State of the Union [WWW Document]. USAFacts. URL <https://usafacts.org/state-of-the-union/transportation-infrastructure/> (accessed 10.26.22).

WJE Associates, 2011. Structural Concrete Bridge Deck Cracking (No. Final). Caltrans.

WVDOT, 2016. Bridge Design Manual.

APPENDIX A INSPECTION REPORTS DATA

Bridge#	Built	Material	Support	Deck Rating	Widened	Year_Wid	Skewness	Length	Span #	Span Length	Deck Widthm	N_Lanes	N_Boxes
02 0036L	1964	R/C	Cont.	7	0	0	50.18	239.00	3	105.2	11.9	2	5
19 0178	2001	P/C	Cont.	7	1	2009	0.00	278.86	2	139.43	22.6	6	9
20 0284L	2007	P/C	Cont.	7	0	0	38.94	562.3	5	127.8	24.6	3	5
27 0115	2006	P/C	Cont.	7	1	2014	5.61	253	2	138	12.6	4	3
28 0183L	1997	P/C	Cont.	7	1	2016	33.00	254	2	134	19	4	5
28C0228	1996	P/C	Simple	7	1	2011	20.00	110	1	110	21.9	3	5
33 0212L	1994	P/C	Cont.	4	1	2010	0.00	243	2	125.6	25.5	3	6
33 0585	1993	P/C	Cont.	7	1	2004	0.00	308	2	156	26.7	6	5
37 0366L	1991	P/C	Cont.	7	1	2007	99.00	228	3	85	19.8	4	7
37 0368L	1990	P/C	Simple	7	1	2007	99.00	124.26	1	124.26	19.8	4	5
37 0414F	1991	P/C	Cont.	7	0	0	99.00	2230.7	13	1223.8	11.7	3	8
37 0420L	1990	P/C	Cont.	7	1	2007	24.00	138	3	62	19.8	4	6
37 0421L	1990	P/C	Cont.	7	1	2007	43.00	186	3	77	21.5	5	7
37 0421R	1990	P/C	Cont.	7	0	0	43.00	182.4	3	77	16.2	3	7
37 0434L	1990	P/C	Simple	7	1	2007	0.00	84.5	1	84.5	19.8	4	6
37 0467L	1991	P/C	Cont.	7	0	0	10.00	1625.6	10	230.97	20.3	4	7
37 0547L	1994	P/C	Cont.	7	1	2004	9.00	175.2	2	87.6	18.4	3	9
37 0547R	1994	P/C	Cont.	7	1	2004	9.00	175.6	2	88.3	22.5	4	7
53 2790L	1994	P/C	Cont.	7	0	0	45.00	758	3	290	25.7	5	5
53 2790R	1994	P/C	Cont.	7	0	0	45.00	758	3	290	25.7	5	5
53 2795F	1994	P/C	Cont.	7	0	0	0.00	1584	10	198.24	16.8	3	3
53 2795G	1994	P/C	Cont.	7	0	0	0.00	1040	7	175	16.8	3	3
54 1114R	1996	P/C	Cont.	7	0	0	2.00	211	2	117.2	24	5	8
54C0617	1991	P/C	Cont.	7	0	0	37.00	144	2	73	37.5	6	13
55 0655	1992	P/C	Simple	5	1	2011	20.00	94.58	1	94.58	79.9	15	26
55 0670	1990	P/C	Cont.	7	1	2001	41.00	825.9	7	156	23.2	6	7
55 0678	1995	P/C	Cont.	7	1	2007	0.00	746.2	5	150.5	52.5	11	20
55 0700L	1995	P/C	Cont.	7	1	2005	0.00	475	8	185	25.5	3	3
55 0701L	1995	P/C	Simple	7	0	0	0.00	163	1	163	25.6	2	2
55 0701R	1995	P/C	Simple	7	0	0	0.00	163	1	163	29.3	4	3
55 0709L	1993	P/C	Simple	5	1	1998	0.00	156.8	1	156.8	17.1	3	3
55 0709R	1993	P/C	Simple	5	1	1997	0.00	156.8	1	156.8	17.1	3	3

55 0759R	1996	P/C	Cont.	5	1	2011	0.00	304.4	2	162.2	23.5	4	4
55 0862R	1996	P/C	Simple	7	1	2011	0.00	99	1	99	25.5	4	7
55C0557	1991	R/C	Cont.	7	0	0	0.00	126	2	63	34	8	16
55C0628	1997	P/C	Cont.	7	0	0	0.00	771.5	5	174	26.8	6	8
55C0629	1997	R/C	Cont.	5	1	2008	0.00	234.8	3	95.2	26.6	4	7
55C0637	2000	P/C	Cont.	7	1	2005	0.00	780	4	219.75	33.5	7	5
56 0362	1992	P/C	Cont.	7	1	2017	0	310	2	166	29.3	7	8
04 0311L	2011	P/C	Simple	7	0	0	0	755	4	225	11.9	3	3
08 0163	2007	P/C	Cont.	5	0	0	0	390	4	111.55	12	2	4
08 0164	2002	P/C	Simple	7	0	0	0	459.2	4	131.2	12	2	4
12 0196	1998	P/C	Cont.	7	0	0	0	165.6	2	82.8	12	2	5
12 0198	2008	P/C	Cont.	7	0	0	0	599.3	6	170.6	11.7	2	2
14 0014	2003	R/C	Cont.	5	0	0	0	383.8	5	82	15.6	3	7
14 0058	1991	P/C	Simple	4	0	0	35	72	1	72	17.8	4	3
15 0086	2009	P/C	Cont.	5	0	0	30	246	3	98.4	12.8	2	5
17 0030	1991	P/C	Simple	5	0	0	99	175.5	1	175.5	17.7	5	3
23 0020	1993	P/C	Cont.	5	0	0	42	191.1	2	111.8	12.2	2	5
23 0205L	1992	P/C	Cont.	5	0	0	34	226.1	3	126.1	11.9	2	5
23 0205R	1992	P/C	Cont.	5	0	0	34	225.9	3	125.9	11.9	2	5
28 0104	1998	P/C	Cont.	7	0	0	0	552	3	276	48.7	11	6
28 0161	1994	P/C	Cont.	5	1	1994	7	191	2	95.5	67.1	10	21
28 0322K	1997	R/C	Cont.	7	0	0	0	181	3	81	8.5	1	3
29 0306L	1992	P/C	Simple	7	0	0	0	157.5	1	157.5	16.6	3	8
29 0306R	1992	P/C	Simple	7	0	0	0	157.5	1	157.5	16.6	3	8
33 0580S	1991	R/C	Cont.	5	0	0	99	262	3	89	7.3	1	3
33 0581S	1991	R/C	Cont.	7	0	0	99	186	3	67	8.5	1	3
33 0582S	1991	R/C	Cont.	7	0	0	99	242	3	84	7.4	1	3
33 0616L	1998	P/C	Cont.	6	0	0	0	3732	26	170	20.7	3	6
33 0616R	1998	P/C	Cont.	6	0	0	0	3621	25	175	20.1	3	6
37 0037S	2005	P/C	Cont.	7	0	0	0	171.2	2	85.6	14.4	3	7
37 0431L	1991	R/C	Cont.	7	0	0	50	180	3	80	11.7	2	5
37 0431R	1991	R/C	Cont.	7	0	0	50	180	3	80	11.7	2	5
37 0470L	1994	P/C	Cont.	7	0	0	3	437	6	87	17.1	3	7
37 0470R	1994	P/C	Cont.	7	0	0	3	434	6	87	17.1	3	7
37 0470S	1994	P/C	Cont.	7	0	0	5	548.8	8	87	8.5	2	3
37 0553	1997	P/C	Cont.	7	0	0	26	355.6	3	170	34.1	4	12
37 0636	2001	P/C	Cont.	7	0	0	30	544	4	157.5	44.7	9	4
37 0660R	2008	P/C	Cont.	5	0	0	99	480.5	3	194.25	10.4	1	3
39 0015L	1997	P/C	Cont.	6	0	0	15	377.5	2	212.6	17.1	2	5
39 0015R	1999	P/C	Cont.	6	0	0	0	373	2	208	11.8	2	3
39 0028R	1997	P/C	Cont.	5	0	0	0	300	3	113.8	11.9	2	2
39 0224R	1997	P/C	Simple	6	0	0	7	94.7	1	94.7	11.9	2	4
39 0225L	1997	P/C	Simple	5	0	0	3	144	1	144	12	2	3
41 0001	1995	R/C	Cont.	7	0	0	16	112	2	56	29.1	4	5
49 0060R	1991	P/C	Cont.	5	0	0	0	651	5	160	11.3	2	4
49 0165R	1992	P/C	Cont.	5	0	0	0	174	3	98	11.9	2	4
51 0162K	1997	R/C	Cont.	7	0	0	20	162	3	63	7.3	1	4
51 0162L	1997	R/C	Cont.	7	0	0	23	150	3	60	17.1	3	5
55 0730L	1996	P/C	Cont.	7	0	0	41	672	4	190	17	3	5
55 0730R	1996	P/C	Cont.	7	0	0	41	685	4	188	20.8	4	5
55 0850R	1995	P/C	Cont.	7	0	0	20	269.2	2	134.6	12.2	2	3
57 1019L	1999	P/C	Simple	7	0	0	48	177	1	177	11.9	2	4
57 1019R	1999	P/C	Cont.	5	0	0	48	177	1	177	11.9	2	4
04 0311R	2012	R/C	Cont.	7	0	0	0	750	4	225	11.9	3	8
28 0389L	2008	P/C	Cont.	5	0	0	30	485	3	170.6	19.7	3	6
28 0389R	2008	P/C	Cont.	5	0	0	27	482.5	3	173.5	16.8	3	4
39 0225R	1997	P/C	Cont.	7	0	0	3	144	1	144	12	2	3
49 0060L	1991	P/C	Cont.	7	0	0	0	678	5	160	11.3	2	4
49 0165L	1992	P/C	Cont.	5	0	0	1	174	3	98	11.9	2	4
55 0850L	2014	P/C	Cont.	5	0	0	20	270	2	137.2	11.2	2	5
57 1017L	1999	P/C	Cont.	5	0	0	10	745	6	141	11.9	2	3
57 1017R	1999	P/C	Cont.	5	0	0	10	745	6	141	11.9	2	3

APPENDIX B FHWA WIM DATA

B.1ADTT

ID	WIM	Name	ADT	ADTT	%	Lanes
1	11100	.5 MI. N/O RTE 211 HUM10165.6	22,823	2,333	10.2	4
2	17720	S/O PARKWAY LAK29R44.46	12,561	727	5.8	4
3	19330	UKIAH, MEN101R21.59	16,449	3,191	19.4	4
4	21500	STANDISH ROAD LAS39551.87	5,065	894	17.7	2
5	23090	.8 MI. N/O MOUNTAIN GATE RD SH	22,268	7,631	34.3	4
6	23100	.2 MILE N/O LASSEN AVENUE SIS5	20,166	6,228	30.9	4
7	23110	1.7 -MI. S/O BALL MOUNTAIN RD-	3,439	1,234	35.9	2
8	23130	SUNSET HILLS DRIVE-COTTONWOOD	66,400	16,503	24.9	4
9	23140	BOWMAN RD TEH541.525	18,153	4,747	26.1	4
10	32000	LORENSEN RD PLA49R8.973	40,091	2,531	6.3	4
11	32010	CHICO, COHASSET HIGHWAY BUT99R	70,834	6,437	9.1	4
12	32020	COUNTY RD 48, N/O JCT RTE 162,	28,805	8,323	28.9	4
13	32990	ANTELOPE RD, SAC8016.69	92,049	5,225	5.7	10
14	33000	ANTELOPE RD, SAC8016.69	83,114	4,025	4.8	10
15	34090	E/O RTE 80 YOL50.6	91,120	6,362	7.0	8
16	34580	BOWMAN PLA80R23.43	45,590	6,788	14.9	6
17	35010	N/O ARNO RD SAC996.9	85,561	10,530	12.3	4
18	35440	S/O ELVERTA RD SAC9935.37	52,456	5,268	10.0	4
19	37620	UNION HILLS BRIDGE OH NEV8020.	32,604	6,665	20.4	4
20	49000	N/O ALCOSTA BL CC680R0.02	152,078	9,381	6.2	8
21	49010	1.5 MILES E/O RTE 505 SOL8030.	70,713	5,597	7.9	8
22	49020	APPIAN WAY CC807.6	151,569	12,091	8.0	8
23	49030	MIDWAY RD SOL505R3.058	31,586	4,187	13.3	4
24	49040	1 MILE S/O CANADA BLVD SM280R5	57,259	1,952	3.4	8
25	49050	S/O MILLBRARE AVE SM10117.5	253,073	10,591	4.2	10
26	49060	.2 MILE E/O NAPASOLANO LINE NA	43,402	4,157	9.6	4
27	49070	PACHECO CREEK BRIDGE SCL152R26	41,929	6,110	14.6	4
28	49090	.2 MILE N/O INDUSTRIAL BLVD AL	198,711	10,803	5.4	8
29	49100	FOSTER CITY SM92R13.83	110,290	6,943	6.3	6
30	49110	GILROY SCL101R10.27	114,687	7,797	6.8	6
31	49140	S/O SHERIDAN RD ALA680R8.312	49,127	2,785	5.7	8
32	55440	MC MILLAN CANYON RD SLO4141.15	18,635	3,721	20.0	2
33	55490	POSITAS, SB10116.2	69,081	3,635	5.3	6
34	55550	TEMPLETON, SLO10149.5	69,266	7,745	11.2	4
35	57410	N/O TEAGUE AVE MON10147.964	28,652	3,825	13.3	4
36	62010	STOCKDALE KER0547.546	42,347	10,707	25.3	4
37	62020	BAKERSFIELD KER9920.555	51,873	5,005	9.6	6
38	69730	AVENUE 184 TUL6523.333	24,524	2,224	9.1	4
39	74210	N/O DEL AMO BLVD LA71011.5	193,774	29,110	15.0	10
40	79020	.5 MI. N/O SHERMAN WAY SB LA40	115,458	4,339	3.8	10
41	79040	ARTESIA, LA0917.5	182,281	16,090	8.8	10
42	79050	GLENDORA, LA210R41.594	255,004	20,423	8.0	10
43	79060	N/O RTE 126 LA5R56.1	120,862	19,714	16.3	10
44	79080	CAMARILLO, PLEASANT VALLEY VEN	67,119	3,141	4.7	6
45	79090	THOUSAND OAKS, WENDY DRIVE, VE	58,962	3,392	5.8	6
46	86040	CALICO SBD15R81.83	46,693	8,139	17.4	4
47	86050	FONTANA SBD155.97	90,002	7,591	8.4	8

48	86060	DEVORE SBD21514.1	71,688	8,757	12.2	4
49	86070	HINKLEY SBD58R20.63	13,763	5,387	39.1	4
50	86090	RAINBOW TRUCK FACILITY RIV15R1	76,041	5,026	6.6	8
51	86100	S/O MESA DR RIV10R145.118	11,108	4,199	37.8	4
52	86220	N/O MAIN ST RIV1521.6	88,525	8,351	9.4	8
53	87570	SOLANO/YOLO COUNTY LINE YOL-80	97,718	4,648	4.8	4
54	87780	AIRPORT BLVD R16.744	34,688	6,523	18.8	4
55	88240	COLTON, SBD1012.4	206,735	24,176	11.7	8
56	88550	3.6 MILES W/O HECTOR RD SBD402	14,426	7,439	51.6	4
57	88690	N/O SCHAEFER AVE SBD835.42	27,030	3,924	14.5	4
58	88730	0.5 MI. E/O DILLON ROAD RIV10R5	29,433	10,577	35.9	4
59	88770	ARCHIBALD AVE SBD60R7.873	113,621	14,298	12.6	10
60	88810	N/O PINE AVE OC SBD71R6.52	86,678	6,127	7.1	6
61	98460	Weigh in Motion @ 4.3 MI INY3959	7,777	2,080	26.7	4
62	100220	W/O SANTA FE RD MER15223.0	23,605	3,631	15.4	4
63	100240	4.1 MI. N/O RTE 12 SJ543.7	61,316	14,419	23.5	4
64	100820	N/O JCT RTE 33 SJ57.4	26,715	9,105	34.1	4
65	101210	E/O MACARTHUR DR SJ205R9.6	118,803	12,850	10.8	6
66	102840	1.6 MI. S/O RTE 33 MER520.2	32,825	10,923	33.3	4
67	102850	3 MI. S/O RTE 33 MER523.6	41,894	11,830	28.2	4
68	103490	KEYS STA998.693	120,200	15,161	12.6	6
69	104200	N/O KISTLER RANCH UC TUO120R5	12,689	1,360	10.7	4
70	104210	W/O RTE 132 SJ5806.4	42,821	7,275	17.0	4
71	116210	CAMERON DR SD8R51.98	15,423	1,701	11.0	4
72	116240	DUNAWAY RD IMP8R23.48	15,126	2,032	13.4	4
73	116380	JCT RTE 111 IMP8R40.944	33,244	3,090	9.3	4
74	116610	LEUCADIA, SD005R42.712	111,798	8,937	8.0	8
75	116770	.1 MI. N/O RANCHO SANTA FE SD7	116,158	5,112	4.4	6
76	116820	CLAREMONT MESA, SD015R9.995	157,364	8,935	5.7	8
77	116830	GOVERNOR, SD80524.440	99,679	5,139	5.2	10
78	116840	NAPLE STREET UNDERCROSSIN SD80	95,145	4,502	4.7	10
79	116850	S/O KEARNEY VILLA RD SD163R10	156,983	5,746	3.7	8
80	116890	SIEMPRE VIVA ROAD SD-905-11.59	2,414	2,286	94.7	4
81	126580	BREA, LAMBERT ROAD ORA5720.884	82,528	3,341	4.0	10
82	126590	WESTMINSTER, WESTMINSTER ORA40	266,129	10,832	4.1	10
83	128080	E/O IMPERIAL HWY RT 90 ORA91R1	180,166	14,548	8.1	10
84	129000	.2 MI N/O JEFFERY RD ORA525.0	284,675	13,123	4.6	12

B.2 WIM records

Number of WIM records per year for selected FHWA sites in California

ID	WIM	2014	2015	2016	2017	2018	2019
1	11100	2,973,143	7,171,253	6,064,011	8,066,773	7,869,870	4,130,461
2	17720	0	0	3,469,039	4,309,131	3,976,324	3,177,957
3	19330	2,122,084	5,401,467	5,950,168	6,451,397	5,673,107	312,510
4	21500	640,679	1,085,262	962,278	729,520	1,678,971	131,744
5	23090	2,198,016	6,444,251	4,489,670	7,515,173	7,139,282	5,344,492
6	23100	856,373	6,149,346	4,163,462	6,547,664	2,564,778	625,135
7	23110	208,990	755,441	796,711	832,687	992,340	722,385
8	23130	2,495,352	5,487,143	6,330,453	7,289,758	440,250	663,998
9	23140	4,296,458	5,857,593	6,065,145	6,920,218	5,545,726	2,632,068
10	32000	505,218	10,377,923	12,572,105	14,499,190	13,108,871	0
11	32010	4,978,403	19,292,590	18,131,948	15,505,521	15,603,680	16,221,231
12	32020	2,949,538	8,063,283	8,753,249	10,489,127	3,250,370	7,661,971
13	32990	19,948,466	29,941,708	20,587,730	33,167,384	26,688,734	12,150,161
14	33000	21,342,142	23,654,038	17,969,514	13,090,987	25,572,958	9,474,990
15	34090	1,840,903	9,650,823	10,031,218	18,709,031	28,372,160	18,549,413
16	34580	4,189,812	12,537,915	8,855,142	5,022,246	4,558,503	7,021,025
17	35010	9,521,298	8,411,030	10,967,996	26,036,646	12,812,693	16,855,723
18	35440	0	0	15,830,293	17,275,283	1,486,979	5,245,423
19	37620	0	0	9,878,714	9,344,307	10,659,242	8,281,782
20	49000	10,919,808	36,356,273	51,809,929	54,600,873	48,364,709	27,558,816
21	49010	6,274,630	27,457,481	19,600,290	29,860,182	41,517,135	18,809,582
22	49020	8,879,331	43,454,869	47,428,101	54,462,360	45,636,351	17,784,366
23	49030	3,257,653	9,135,898	9,925,524	11,366,785	3,254,440	6,822,713
24	49040	10,910,521	16,399,474	14,864,283	20,443,584	16,937,902	5,951,915
25	49050	13,171,539	41,994,411	68,526,517	91,687,956	83,030,768	59,516,308
26	49060	3,585,422	11,715,276	10,239,766	14,646,716	14,296,104	11,067,857
27	49070	2,968,706	7,560,209	8,250,216	10,513,202	9,167,961	8,804,942
28	49090	35,463,082	41,029,605	20,341,161	43,421,485	63,121,956	14,710,327
29	49100	0	0	18,860,132	17,590,117	32,044,008	13,676,334
30	49110	12,494,331	34,753,910	34,323,808	28,823,102	34,592,404	28,557,296
31	49140	4,533,759	6,780,959	4,640,367	5,039,778	6,730,256	0
32	55440	0	0	5,045,386	5,970,003	5,417,708	4,920,199
33	55490	0	0	51,530,026	56,870,424	63,592,828	2,694,021
34	55550	8,716,080	20,727,620	14,238,172	8,783,540	12,328,564	4,987,068
35	57410	2,915,690	8,668,439	7,858,419	9,849,515	9,393,058	7,621,594
36	62010	4,060,523	13,076,709	10,676,285	12,074,018	13,581,159	10,714,775
37	62020	4,490,706	12,675,967	8,333,009	9,261,308	10,668,691	8,662,860
38	69730	2,913,537	7,198,164	7,430,078	8,064,536	2,613,159	4,733,691
39	74210	36,010,993	34,096,295	29,439,014	33,916,757	43,311,292	39,524,805
40	79020	12,144,301	19,871,075	19,237,362	8,649,504	13,269,112	11,892,451
41	79040	15,270,404	22,711,485	36,528,405	68,000,282	41,094,406	25,015,989
42	79050	13,932,541	19,130,260	33,821,902	61,624,755	40,532,292	0
43	79060	13,847,419	19,161,043	18,422,349	36,836,994	25,527,979	0
44	79080	13,071,049	20,151,342	20,829,335	24,154,219	19,698,487	12,215,970
45	79090	13,272,764	19,237,404	18,836,975	21,672,500	16,912,988	14,917,288
46	86040	4,826,567	11,585,432	13,752,045	10,422,082	5,937,438	6,536,516
47	86050	20,341,450	21,019,566	18,482,259	33,203,684	2,549,315	0
48	86060	6,999,990	16,557,756	20,480,729	24,258,887	22,482,270	10,538,324
49	86070	526,784	3,030,684	3,310,746	1,478,836	1,108,100	908,430
50	86090	17,509,551	21,615,402	14,357,477	27,095,657	21,811,267	9,352,920
51	86100	1,810,549	0	0	0	0	0
52	86220	11,967,957	13,983,131	13,956,558	14,720,289	18,062,385	2,810,360
53	87570	4,227,016	24,471,143	30,788,771	25,546,973	3,600,951	12,703,495

54	87780	1,408,330	6,533,102	9,405,173	11,593,033	10,961,445	0
55	88240	10,476,698	8,033,115	6,734,699	62,676,517	65,251,196	52,345,864
56	88550	0	0	4,038,993	4,333,606	4,512,061	1,875,882
57	88690	3,628,859	7,920,079	8,354,665	4,888,774	5,229,818	7,134,974
58	88730	1,057,545	5,253,178	6,474,850	8,254,052	3,251,650	3,385,044
59	88770	15,703,099	22,029,718	26,118,678	27,570,363	0	0
60	88810	5,415,517	4,389,259	19,309,478	20,217,543	25,907,136	19,502,612
61	98460	344,907	1,479,049	1,766,825	2,656,587	2,421,523	2,030,410
62	100220	1,286,136	5,594,974	6,539,350	7,728,039	5,121,780	4,744,573
63	100240	2,475,253	1,196,796	4,668,866	6,636,460	4,589,720	7,602,951
64	100820	3,168,727	2,684,426	4,764,471	8,476,879	7,489,459	5,076,514
65	101210	16,850,565	30,775,498	28,958,939	24,004,578	14,868,734	5,108,609
66	102840	4,697,138	7,089,519	5,780,108	11,783,916	2,508,832	3,741,956
67	102850	2,342,258	5,005,334	7,893,363	10,389,937	7,564,980	4,911,890
68	103490	0	0	29,090,263	40,755,163	27,247,962	30,410,777
70	104210	4,600,258	5,875,662	8,533,142	7,482,943	163,344	4,025,370
71	116210	2,070,314	4,596,018	3,504,951	2,791,748	1,665,833	0
72	116240	1,609,864	4,589,506	4,476,183	3,162,572	1,343,258	3,267,498
69	104200	841,346	3,826,903	4,055,658	4,521,182	3,732,913	1,928,377
73	116380	842,455	10,271,562	8,327,699	6,515,873	0	0
74	116610	31,241,213	62,552,003	42,233,193	62,485,187	68,431,043	9,390,843
75	116770	7,326,984	26,157,332	21,916,281	6,253,838	30,721,258	16,726,854
76	116820	10,803,628	22,619,259	31,425,918	45,487,134	50,826,702	35,746,369
77	116830	2,815,134	0	9,369,269	32,915,107	19,899,023	13,655,956
78	116840	4,505,754	0	1,274,251	43,152,121	18,234,692	3,900,944
79	116850	10,114,689	29,497,915	29,411,865	37,453,256	34,771,947	30,788,773
80	116890	202,147	545,578	392,887	49,717	635,164	0
81	126580	9,598,588	32,989,768	22,389,826	38,444,584	51,518,704	2,640,965
82	126590	21,770,987	31,070,233	43,430,145	92,187,273	54,291,429	0
83	128080	24,524,315	27,201,724	24,438,218	38,495,437	53,834,861	35,781,730
84	129000	51,698,108	68,314,606	67,543,724	86,271,062	70,122,696	70,811,017
Total		655,802,344	1,203,980,464	1,370,656,173	1,856,347,427	1,617,301,444	899,750,433

B.3 Wim Quality Control

Test description	001 Lodi	002 Redding	003 Antelope EB	004 Antelope WB	005 Indio	027 Tracy	030-Mt Shasta	037 Elsinore SB	038-Isinore NB
Correct timestamp	100.0	100.0	100.0	100.0	100.0	100.0	100.0	100.0	100.0
Correct class number	100.0	100.0	100.0	100.0	100.0	100.0	100.0	100.0	100.0
Correct speed	97.6	97.4	97.6	97.3	96.0	95.1	96.2	96.9	96.4
Measurement violation is zero	99.8	99.9	99.9	99.9	99.9	98.8	100.0	99.8	99.1
GVW is over zero	100.0	100.0	100.0	100.0	100.0	100.0	100.0	100.0	100.0
Number of axles and number of axle weights is over zero	100.0	100.0	100.0	100.0	100.0	100.0	100.0	100.0	100.0
Number of axles spacings is over zero	100.0	100.0	100.0	100.0	100.0	99.9	100.0	100.0	100.0
Number of axles is over zero	100.0	100.0	100.0	100.0	100.0	100.0	100.0	100.0	100.0
GVW+/-20% of Axle Weights	100.0	100.0	100.0	100.0	100.0	100.0	100.0	100.0	100.0
1 st axle weight is equal a sum of left and right wheel weight with of tolerance 20%	100.0	100.0	100.0	100.0	99.9	100.0	100.0	100.0	100.0
2 nd axle weight is equal a sum of left and right wheel weight with of tolerance 20%	100.0	100.0	100.0	100.0	100.0	100.0	100.0	100.0	100.0
3 rd axle weight is equal a sum of left and right wheel weight with of tolerance 20%	100.0	100.0	100.0	100.0	100.0	100.0	100.0	100.0	100.0
4 th axle weight is equal a sum of left and right wheel weight with of tolerance 20%	100.0	100.0	100.0	100.0	100.0	100.0	100.0	100.0	100.0
5 th axle weight is equal a sum of left and right wheel weight with of tolerance 20%	100.0	100.0	100.0	100.0	100.0	100.0	100.0	100.0	100.0
6 th axle weight is equal a sum of left and right wheel weight with of tolerance 20%	100.0	100.0	100.0	100.0	100.0	100.0	100.0	100.0	100.0
7 th axle weight is equal a sum of left and right wheel weight with of tolerance 20%	100.0	100.0	100.0	100.0	100.0	100.0	100.0	100.0	100.0
8 th axle weight is equal a sum of left and right wheel weight with of tolerance 20%	100.0	100.0	100.0	100.0	100.0	100.0	100.0	100.0	100.0
9 th axle weight is equal a sum of left and right wheel weight with of tolerance 20%	100.0	100.0	100.0	100.0	100.0	100.0	100.0	100.0	100.0
1 st axle, left and right wheel weight differ less than 40%	91.8	93.2	98.3	99.7	95.2	97.0	92.5	98.8	96.1
2 nd axle, left and right wheel weight differ less than 40%	91.4	94.0	97.2	99.4	95.8	96.8	96.1	95.4	93.1

Test description	001 Lodi	002 Redding	003 Antelope EB	004 Antelope WB	005 Indio	027 Tracy	030-Mt Shasta	037 Elsinore SB	038-Isinore NB
3 rd axle, left and right wheel weight differ less than 40%	94.4	95.1	98.0	99.3	95.8	97.0	94.2	95.7	91.5
4 th axle, left and right wheel weight differ less than 40%	93.2	95.7	98.3	99.1	94.3	96.7	97.1	96.0	93.3
5 th axle, left and right wheel weight differ less than 40%	94.1	96.1	98.7	99.1	94.1	96.9	97.7	97.0	94.6
6 th axle, left and right wheel weight differ less than 40%	99.8	99.8	99.9	100.0	99.7	99.8	99.8	99.9	99.8
7 th axle, left and right wheel weight differ less than 40%	100.0	100.0	100.0	100.0	100.0	99.9	99.9	100.0	100.0
8 th axle, left and right wheel weight differ less than 20%	100.0	100.0	100.0	100.0	100.0	100.0	100.0	100.0	100.0
9 th axle, left and right wheel weight differ less than 20%	100.0	100.0	100.0	100.0	100.0	100.0	100.0	100.0	100.0
Axle 1-2 spacing in range 4 - 70 ft	99.8	99.9	99.8	100.0	99.9	99.4	99.9	99.9	99.9
Axle 2-3 spacing in range 4 - 70 ft	99.8	99.8	99.8	99.8	99.5	99.5	99.9	99.9	99.8
Axle 3-4 spacing in range 4 - 70 ft	96.8	94.9	97.2	96.3	96.8	96.8	96.8	96.8	97.1
Axle 4-5 spacing in range 4 - 70 ft	99.5	99.5	99.7	99.7	99.3	99.4	99.5	99.5	99.4
Axle 5-6 spacing in range 4 - 70 ft	99.9	99.9	99.9	100.0	99.9	99.6	99.8	99.9	99.8
Axle 6-7 spacing in range 4 - 70 ft	99.9	99.9	100.0	100.0	99.9	99.8	99.9	100.0	99.9
Axle 7-8 spacing in range 4 - 70 ft	100.0	100.0	100.0	100.0	99.9	99.9	99.9	100.0	100.0
Axle 8-9 spacing in range 4 - 70 ft	100.0	100.0	100.0	100.0	100.0	99.9	99.9	100.0	100.0
Sum of axle spacings > 6 ft	100.0	100.0	100.0	100.0	100.0	100.0	100.0	100.0	100.0
1st axle weight over 1 and below 40 kips	100.0	99.9	99.9	100.0	100.0	99.9	100.0	100.0	100.0
2nd axle weight over 1 and below 60 kips	100.0	100.0	100.0	99.6	98.4	99.9	99.5	100.0	99.8
3rd axle weight over 1 and below 60 kips	99.9	99.8	99.8	99.7	99.6	99.8	99.8	99.9	99.6
4th axle weight over 1 and below 60 kips	99.9	99.9	99.9	99.8	99.7	99.9	99.7	99.9	99.7
5th axle weight over 1 and below 60 kips	99.9	100.0	100.0	99.8	99.2	99.9	99.6	100.0	99.8
6th axle weight over 1 and below 60 kips	100.0	100.0	100.0	99.9	99.5	99.9	99.7	100.0	99.7
7th axle weight over 1 and below 60 kips	100.0	100.0	100.0	99.9	99.7	99.9	99.9	100.0	99.9
8th axle weight over 1 and below 60 kips	100.0	100.0	100.0	99.9	99.5	100.0	99.8	100.0	100.0
9th axle weight over 1 and below 60 kips	100.0	100.0	100.0	100.0	99.7	100.0	99.8	100.0	100.0

Test description	001 Lodi	002 Redding	003 Antelope EB	004 Antelope WB	005 Indio	027 Tracy	030-Mt Shasta	037 Elsinore SB	038-Isinore NB
1-2 wheels tandem weight below 80 kips	99.8	99.9	99.8	100.0	99.9	99.4	99.9	99.9	100.0
2-3 wheels tandem weight below 80 kips	99.8	99.8	99.8	99.8	99.5	99.5	99.9	99.9	99.8
3-4 wheels tandem weight below 80 kips	96.8	94.9	97.2	96.3	96.8	96.8	96.8	96.7	97.1
4-5 wheels tandem weight below 80 kips	99.5	99.5	99.7	99.7	99.3	99.4	99.5	99.5	99.4
5-6 wheels tandem weight below 80 kips	99.9	99.9	99.9	100.0	99.9	99.6	99.8	99.9	99.8
6-7 wheels tandem weight below 80 kips	99.9	99.9	100.0	100.0	99.9	99.8	99.9	100.0	99.9
7-8 wheels tandem weight below 80 kips	100.0	100.0	100.0	100.0	99.9	99.9	99.9	100.0	100.0
8-9 wheels tandem weight below 80 kips	100.0	100.0	100.0	100.0	100.0	99.9	99.9	100.0	100.0
1-2-3 wheels tridem weight below 120 kips	99.9	99.9	99.9	100.0	100.0	99.9	100.0	100.0	100.0
2-3-4 wheels tridem weight below 120 kips	99.9	99.9	99.9	100.0	99.9	99.7	100.0	100.0	99.9
3-4-5 wheels tridem weight below 120 kips	99.7	99.6	99.8	99.8	99.6	99.6	99.7	99.5	99.5
4-5-6 wheels tridem weight below 120 kips	99.9	99.9	100.0	100.0	99.9	99.8	99.9	99.9	99.9
5-6-7 wheels tridem weight below 120 kips	100.0	100.0	100.0	100.0	100.0	99.9	100.0	100.0	100.0
6-7-8 wheels tridem weight below 120 kips	100.0	100.0	100.0	100.0	100.0	99.9	100.0	100.0	100.0
7-8-9 wheels tridem weight below 120 kips	100.0	100.0	100.0	100.0	100.0	99.9	99.9	100.0	100.0
Not the same axle weight from 1st axle	100.0	100.0	100.0	100.0	100.0	100.0	99.9	100.0	100.0
Not the same axle weight from 2nd axle	100.0	100.0	100.0	100.0	100.0	100.0	99.9	100.0	100.0
Not the same axle weight from 3rd axle	100.0	100.0	100.0	100.0	100.0	100.0	100.0	100.0	100.0
Not the same axle weight from 4th axle	100.0	100.0	100.0	100.0	100.0	100.0	100.0	100.0	100.0
Not the same axle weight from 5th axle	100.0	100.0	100.0	100.0	100.0	100.0	100.0	100.0	100.0
Not the same axle weight from 6th axle	100.0	100.0	100.0	100.0	100.0	100.0	100.0	100.0	100.0
Correct timestamp	100.0	100.0	100.0	100.0	100.0	100.0	100.0	100.0	100.0
Correct class number	100.0	100.0	100.0	100.0	100.0	100.0	100.0	100.0	100.0
Correct speed	97.3	97.2	94.4	95.7	97.5	97.0	96.1	98.3	96.5
Measurement violation is zero	99.9	99.9	99.4	99.7	99.9	99.8	99.9	99.8	99.7
GVW is over zero	100.0	100.0	100.0	100.0	100.0	100.0	100.0	100.0	100.0

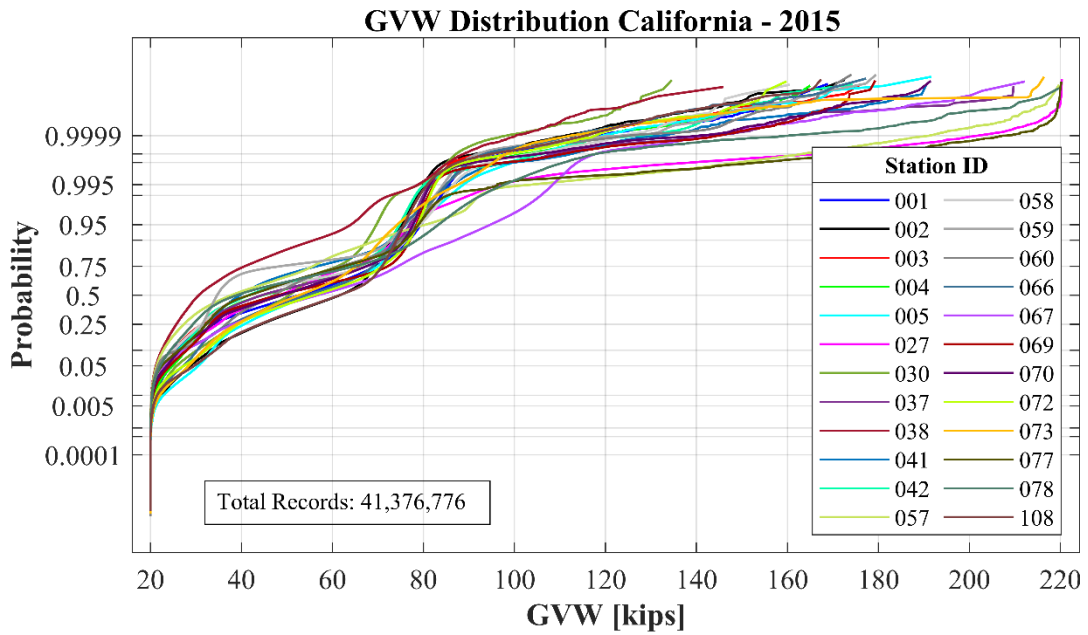
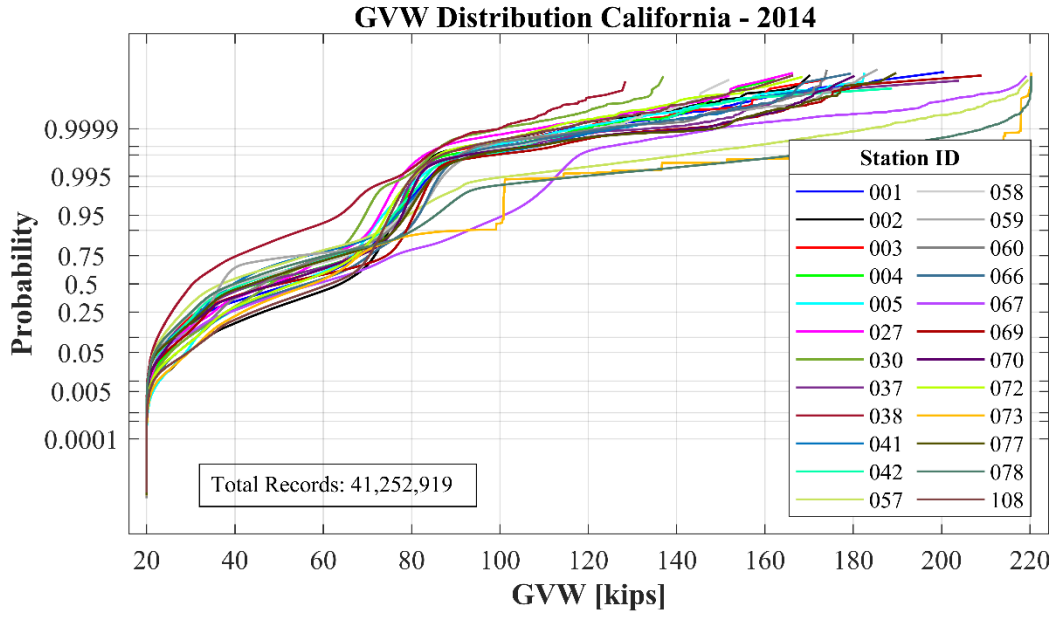
Test description	001 Lodi	002 Redding	003 Antelope EB	004 Antelope WB	005 Indio	027 Tracy	030-Mt Shasta	037 Elsinore SB	038-Isinore NB
Number of axles and number of axle weights is over zero	100.0	100.0	100.0	100.0	100.0	100.0	100.0	100.0	100.0
Number of axles spacings is over zero	100.0	100.0	100.0	100.0	100.0	100.0	100.0	100.0	100.0
Number of axles is over zero	100.0	100.0	100.0	100.0	100.0	100.0	100.0	100.0	100.0
GVW+/-20% of Axle Weights	100.0	100.0	100.0	100.0	100.0	100.0	100.0	100.0	100.0
1 st axle weight is equal a sum of left and right wheel weight with of tolerance 20%	100.0	100.0	100.0	100.0	100.0	100.0	100.0	100.0	100.0
2 nd axle weight is equal a sum of left and right wheel weight with of tolerance 20%	100.0	100.0	100.0	100.0	100.0	100.0	100.0	100.0	100.0
3 rd axle weight is equal a sum of left and right wheel weight with of tolerance 20%	100.0	100.0	100.0	100.0	100.0	100.0	100.0	100.0	100.0
4 th axle weight is equal a sum of left and right wheel weight with of tolerance 20%	100.0	100.0	100.0	100.0	100.0	100.0	100.0	100.0	100.0
5 th axle weight is equal a sum of left and right wheel weight with of tolerance 20%	100.0	100.0	100.0	100.0	100.0	100.0	100.0	100.0	100.0
6 th axle weight is equal a sum of left and right wheel weight with of tolerance 20%	100.0	100.0	100.0	100.0	100.0	100.0	100.0	100.0	100.0
7 th axle weight is equal a sum of left and right wheel weight with of tolerance 20%	100.0	100.0	100.0	100.0	100.0	100.0	100.0	100.0	100.0
8 th axle weight is equal a sum of left and right wheel weight with of tolerance 20%	100.0	100.0	100.0	100.0	100.0	100.0	100.0	100.0	100.0
9 th axle weight is equal a sum of left and right wheel weight with of tolerance 20%	100.0	100.0	100.0	100.0	100.0	100.0	100.0	100.0	100.0
1 st axle, left and right wheel weight differ less than 20%	97.2	98.8	89.8	98.1	97.0	98.3	96.6	98.8	95.1
2 nd axle, left and right wheel weight differ less than 20%	94.8	98.2	90.4	97.5	94.2	97.3	91.0	97.9	93.6
3 rd axle, left and right wheel weight differ less than 20%	95.5	98.6	96.4	98.4	95.6	98.2	95.3	97.9	97.2
4 th axle, left and right wheel weight differ less than 20%	97.4	98.4	96.5	98.1	94.9	98.0	93.2	97.2	96.7
5 th axle, left and right wheel weight differ less than 20%	97.6	98.7	97.1	98.2	95.7	97.7	95.5	96.9	97.0
6 th axle, left and right wheel weight differ less than 20%	99.9	100.0	99.9	99.9	99.9	99.9	99.6	99.9	99.8
7 th axle, left and right wheel weight differ less than 20%	100.0	100.0	99.9	100.0	100.0	100.0	99.9	100.0	100.0
8 th axle, left and right wheel weight differ less than 20%	100.0	100.0	99.9	100.0	100.0	100.0	100.0	100.0	100.0

Test description	001 Lodi	002 Redding	003 Antelope EB	004 Antelope WB	005 Indio	027 Tracy	030-Mt Shasta	037 Elsinore SB	038-Isinore NB
9 th axle, left and right wheel weight differ less than 20%	100.0	100.0	100.0	100.0	100.0	100.0	100.0	100.0	100.0
Axle 1-2 spacing in range 4 - 70 ft	99.9	100.0	99.3	99.8	99.9	99.9	99.8	100.0	99.9
Axle 2-3 spacing in range 4 - 70 ft	99.8	99.9	99.0	99.8	99.9	99.7	99.7	99.9	99.9
Axle 3-4 spacing in range 4 - 70 ft	95.9	95.9	98.5	99.0	99.4	99.3	96.5	96.9	97.4
Axle 4-5 spacing in range 4 - 70 ft	99.5	99.5	99.4	99.8	99.8	99.7	99.3	99.4	99.7
Axle 5-6 spacing in range 4 - 70 ft	99.9	100.0	99.7	99.9	100.0	99.8	99.6	100.0	100.0
Axle 6-7 spacing in range 4 - 70 ft	100.0	100.0	99.8	100.0	100.0	99.9	99.9	100.0	100.0
Axle 7-8 spacing in range 4 - 70 ft	100.0	100.0	99.9	100.0	100.0	99.9	100.0	100.0	100.0
Axle 8-9 spacing in range 4 - 70 ft	100.0	100.0	99.9	100.0	100.0	100.0	100.0	100.0	100.0
Sum of axle spacings > 6 ft	100.0	100.0	100.0	100.0	100.0	100.0	100.0	100.0	100.0
1st axle weight over 1 and below 40 kips	100.0	100.0	99.2	100.0	100.0	100.0	100.0	100.0	99.8
2nd axle weight over 1 and below 60 kips	100.0	100.0	99.7	100.0	100.0	100.0	100.0	100.0	99.9
3rd axle weight over 1 and below 60 kips	100.0	99.8	99.6	99.8	99.9	100.0	100.0	99.9	99.8
4th axle weight over 1 and below 60 kips	100.0	99.9	99.8	99.9	100.0	100.0	100.0	99.9	99.9
5th axle weight over 1 and below 60 kips	100.0	100.0	99.9	100.0	100.0	100.0	100.0	100.0	100.0
6th axle weight over 1 and below 60 kips	100.0	100.0	99.9	100.0	100.0	100.0	100.0	100.0	100.0
7th axle weight over 1 and below 60 kips	100.0	100.0	99.9	100.0	100.0	100.0	100.0	100.0	100.0
8th axle weight over 1 and below 60 kips	100.0	100.0	100.0	100.0	100.0	100.0	100.0	100.0	100.0
9th axle weight over 1 and below 60 kips	100.0	100.0	100.0	100.0	100.0	100.0	100.0	100.0	100.0
1-2 wheels tandem weight below 80 kips	99.9	100.0	99.3	99.8	99.9	99.9	99.8	100.0	99.9
2-3 wheels tandem weight below 80 kips	99.8	99.9	98.9	99.8	99.9	99.7	99.7	99.9	99.8
3-4 wheels tandem weight below 80 kips	95.9	95.9	98.5	99.0	99.4	99.3	96.5	96.9	97.4
4-5 wheels tandem weight below 80 kips	99.5	99.5	99.4	99.8	99.8	99.7	99.3	99.4	99.7
5-6 wheels tandem weight below 80 kips	99.9	100.0	99.7	99.9	100.0	99.8	99.6	100.0	100.0
6-7 wheels tandem weight below 80 kips	100.0	100.0	99.8	100.0	100.0	99.9	99.9	100.0	100.0

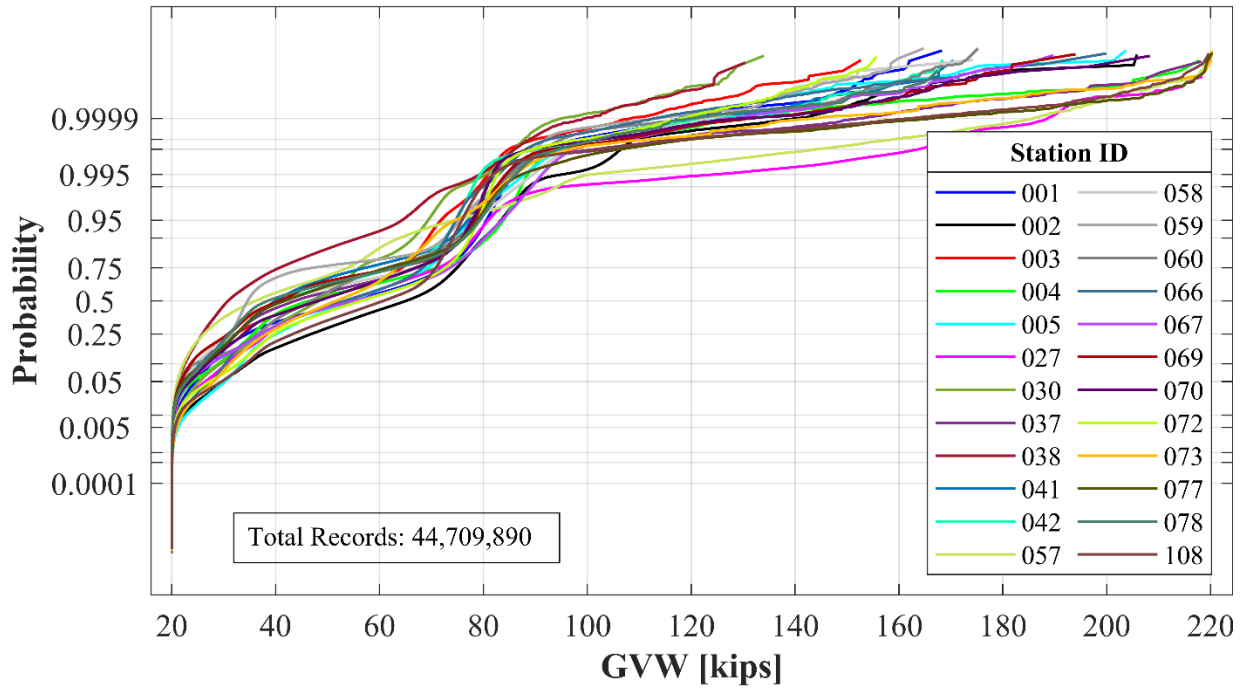
Test description	001 Lodi	002 Redding	003 Antelope EB	004 Antelope WB	005 Indio	027 Tracy	030-Mt Shasta	037 Elsinore SB	038-Isinore NB
7-8 wheels tandem weight below 80 kips	100.0	100.0	99.9	100.0	100.0	99.9	100.0	100.0	100.0
8-9 wheels tandem weight below 80 kips	100.0	100.0	99.9	100.0	100.0	100.0	100.0	100.0	100.0
1-2-3 wheels tridem weight below 120 kips	100.0	100.0	99.7	100.0	100.0	99.9	100.0	100.0	100.0
2-3-4 wheels tridem weight below 120 kips	100.0	100.0	99.6	100.0	100.0	99.8	99.8	100.0	100.0
3-4-5 wheels tridem weight below 120 kips	99.6	99.5	99.6	99.9	99.9	99.8	99.5	99.5	99.8
4-5-6 wheels tridem weight below 120 kips	99.9	100.0	99.7	100.0	100.0	99.9	99.6	100.0	100.0
5-6-7 wheels tridem weight below 120 kips	100.0	100.0	99.8	100.0	100.0	99.9	99.9	100.0	100.0
6-7-8 wheels tridem weight below 120 kips	100.0	100.0	99.9	100.0	100.0	99.9	100.0	100.0	100.0
7-8-9 wheels tridem weight below 120 kips	100.0	100.0	99.9	100.0	100.0	100.0	100.0	100.0	100.0
Not the same axle weight from 1st axle	100.0	100.0	100.0	100.0	100.0	100.0	100.0	100.0	100.0
Not the same axle weight from 2nd axle	100.0	100.0	100.0	99.9	100.0	100.0	100.0	100.0	100.0
Not the same axle weight from 3rd axle	100.0	100.0	100.0	100.0	100.0	100.0	100.0	100.0	100.0
Not the same axle weight from 4th axle	100.0	100.0	100.0	100.0	100.0	100.0	100.0	100.0	100.0
Not the same axle weight from 5th axle	100.0	100.0	100.0	100.0	100.0	100.0	100.0	100.0	100.0
Not the same axle weight from 6th axle	100.0	100.0	100.0	100.0	100.0	100.0	100.0	100.0	100.0

APPENDIX C WIM DATA PLOTS

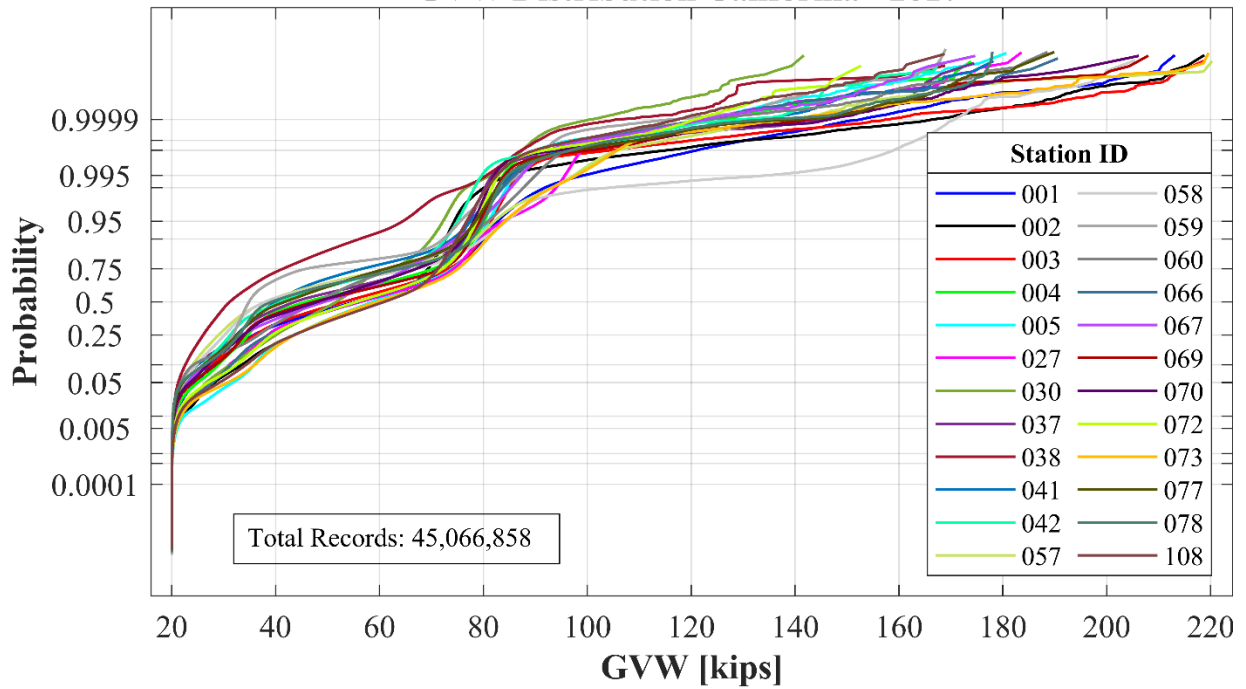
C.1 Gross Vehicle Weight Per Year



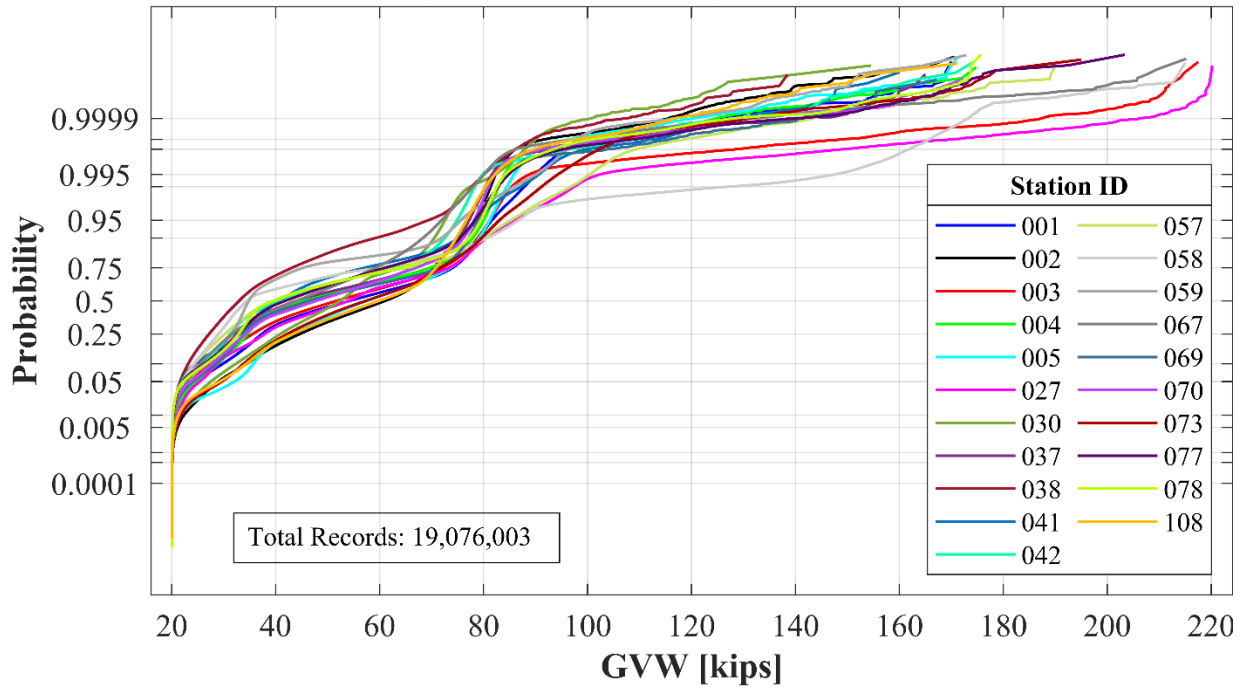
GVW Distribution California - 2016



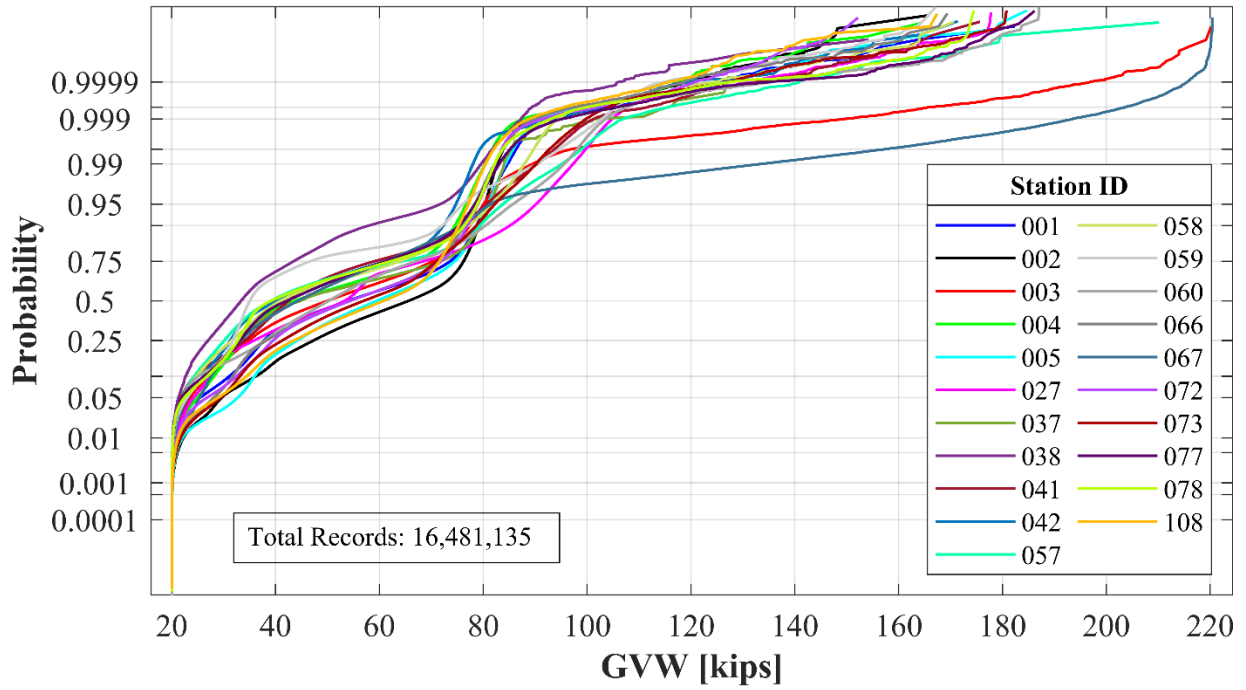
GVW Distribution California - 2017



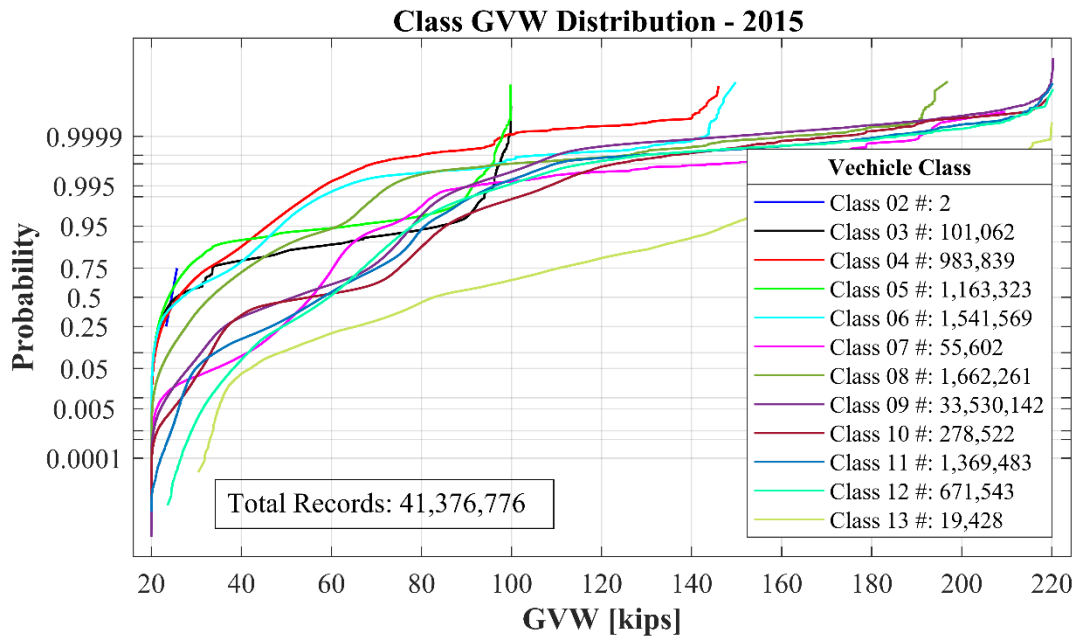
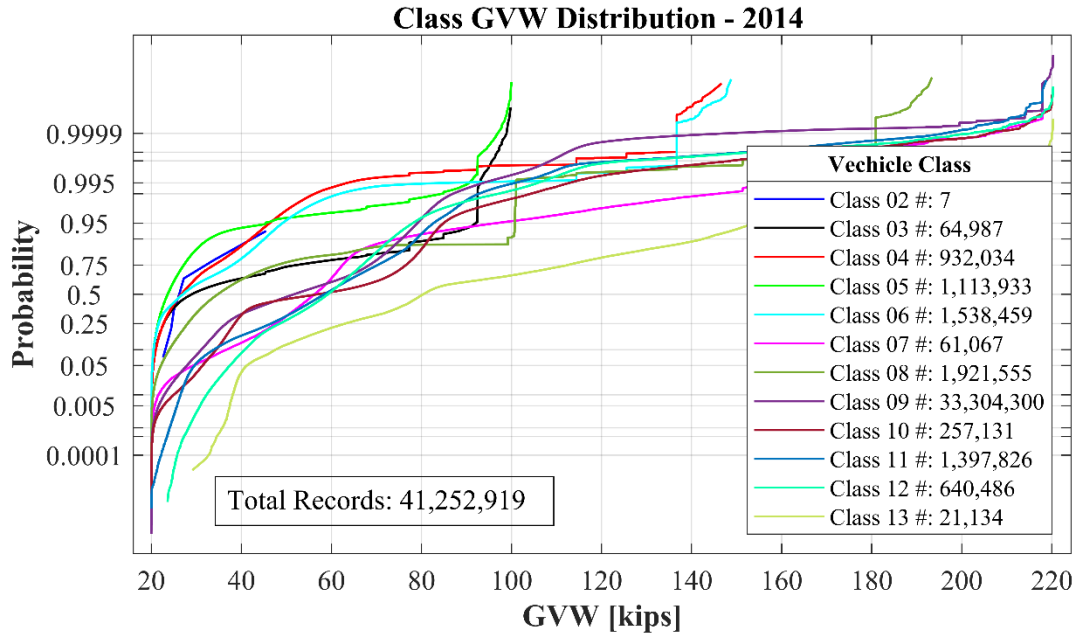
GVW Distribution California - 2018



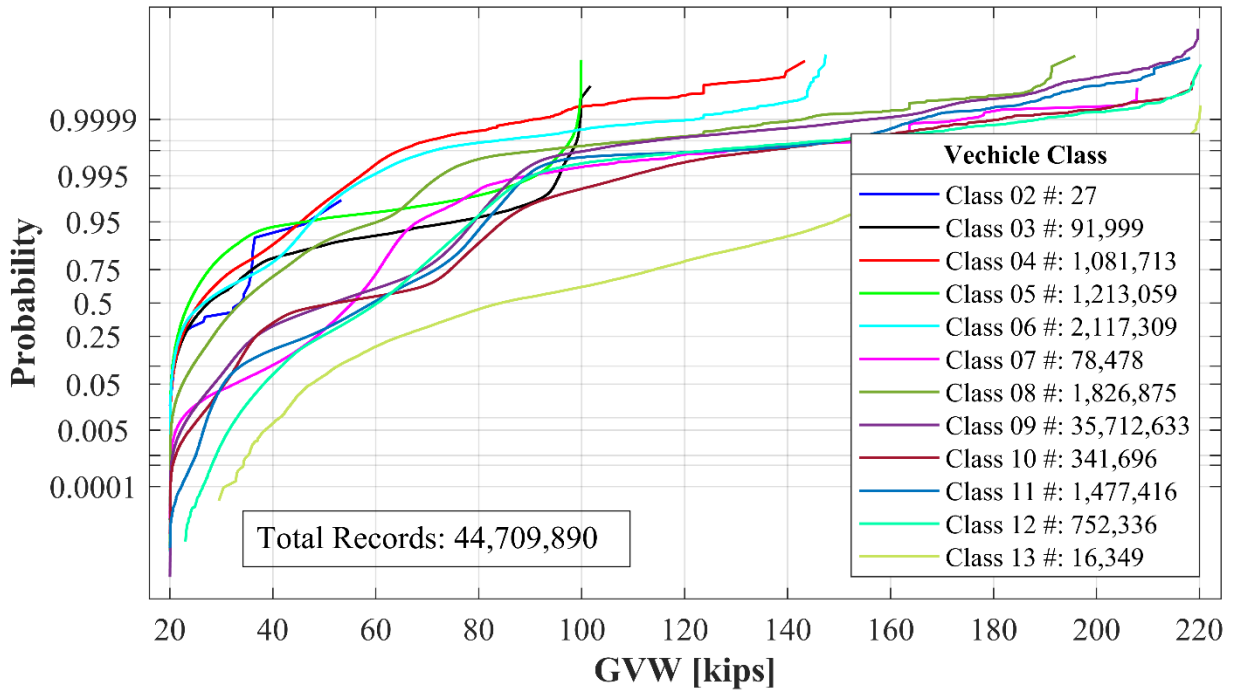
GVW Distribution California - 2019



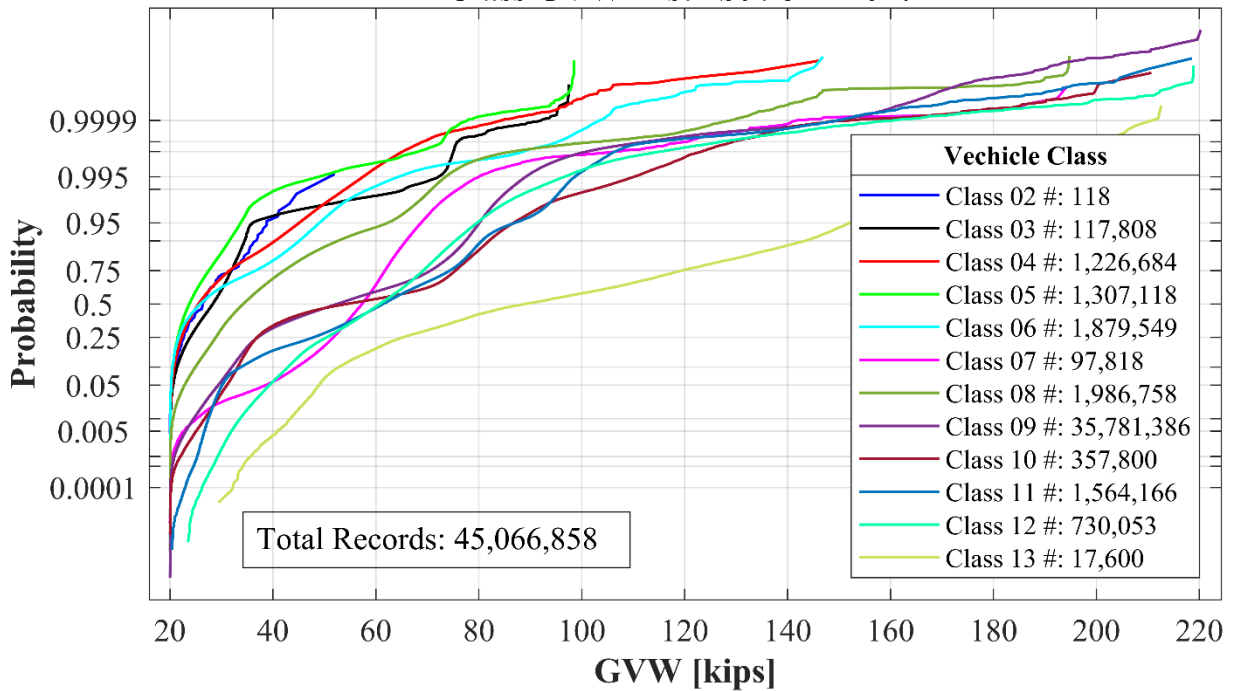
C.2 Gross Vehicle Weight By Class



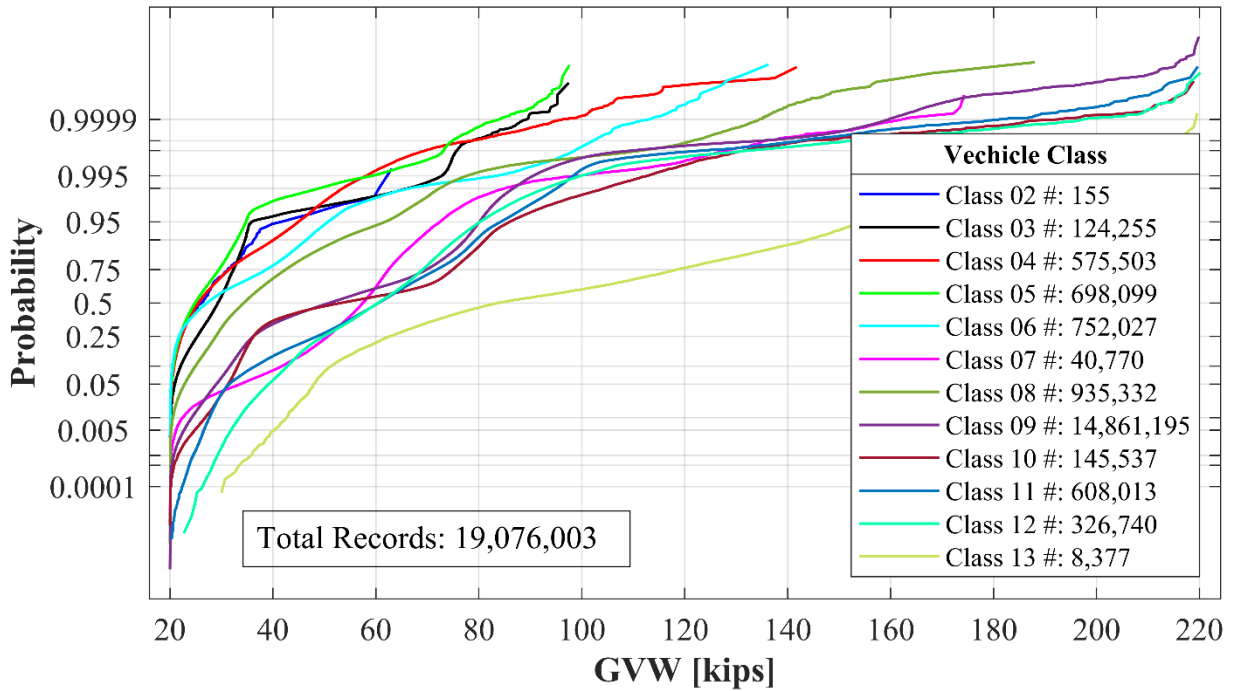
Class GVW Distribution - 2016



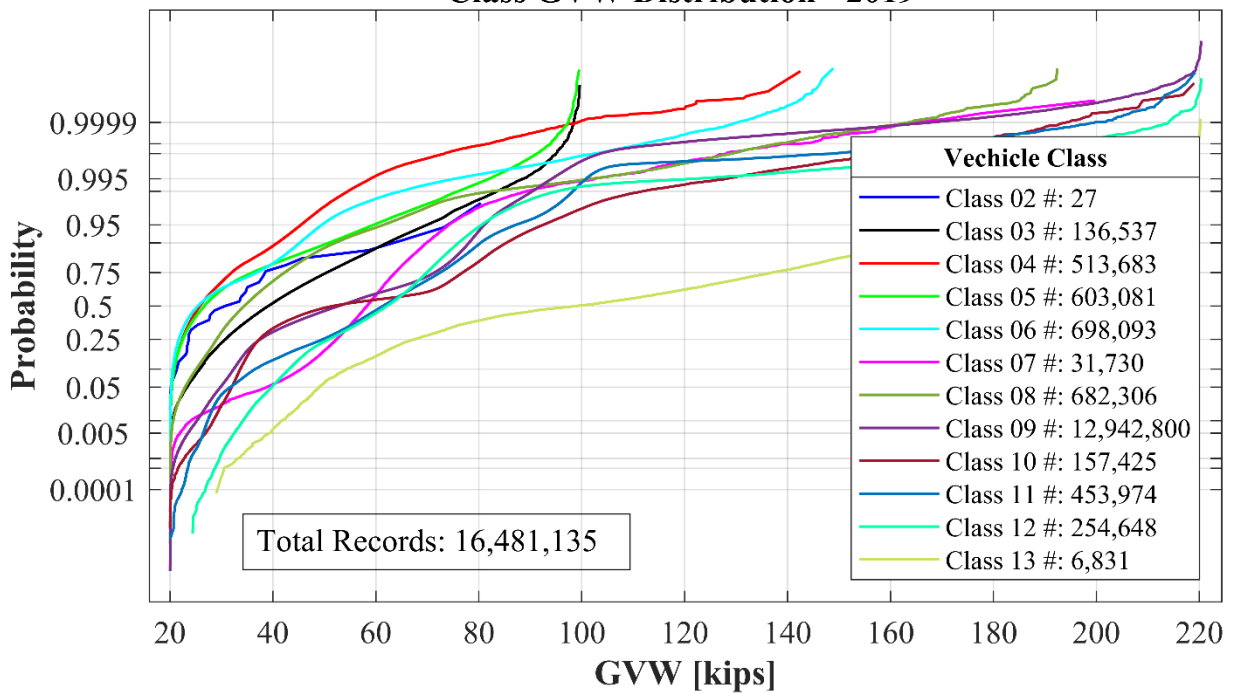
Class GVW Distribution - 2017



Class GVW Distribution - 2018

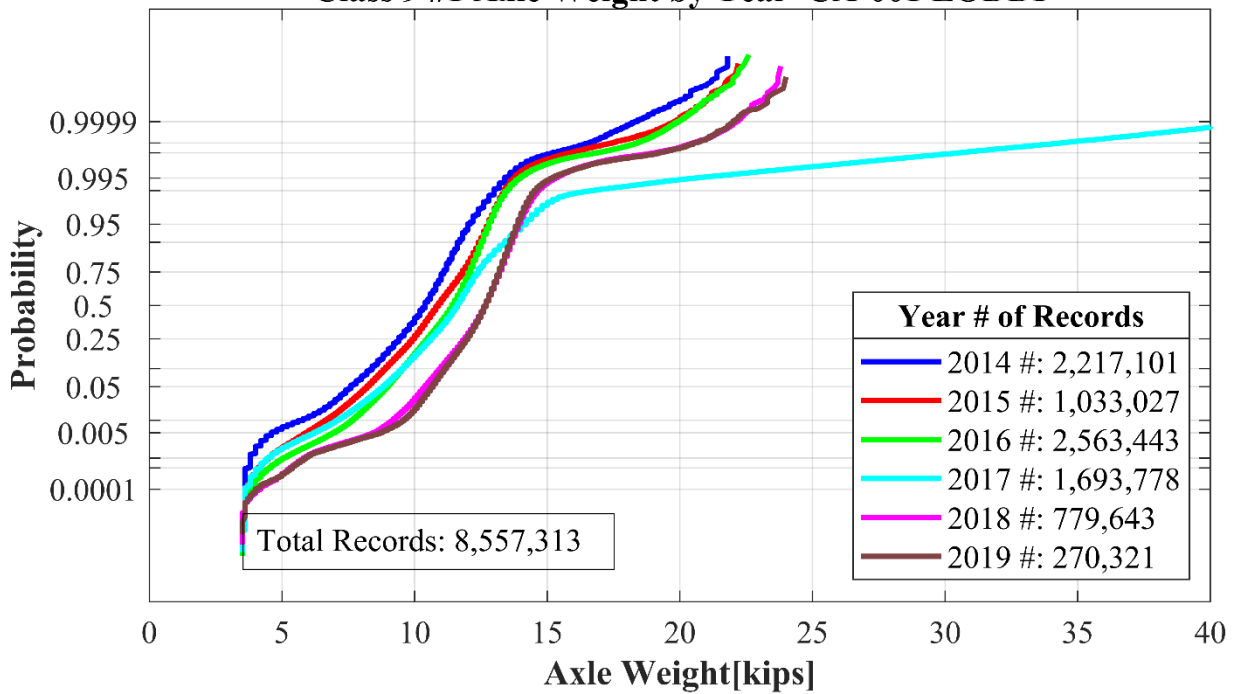


Class GVW Distribution - 2019

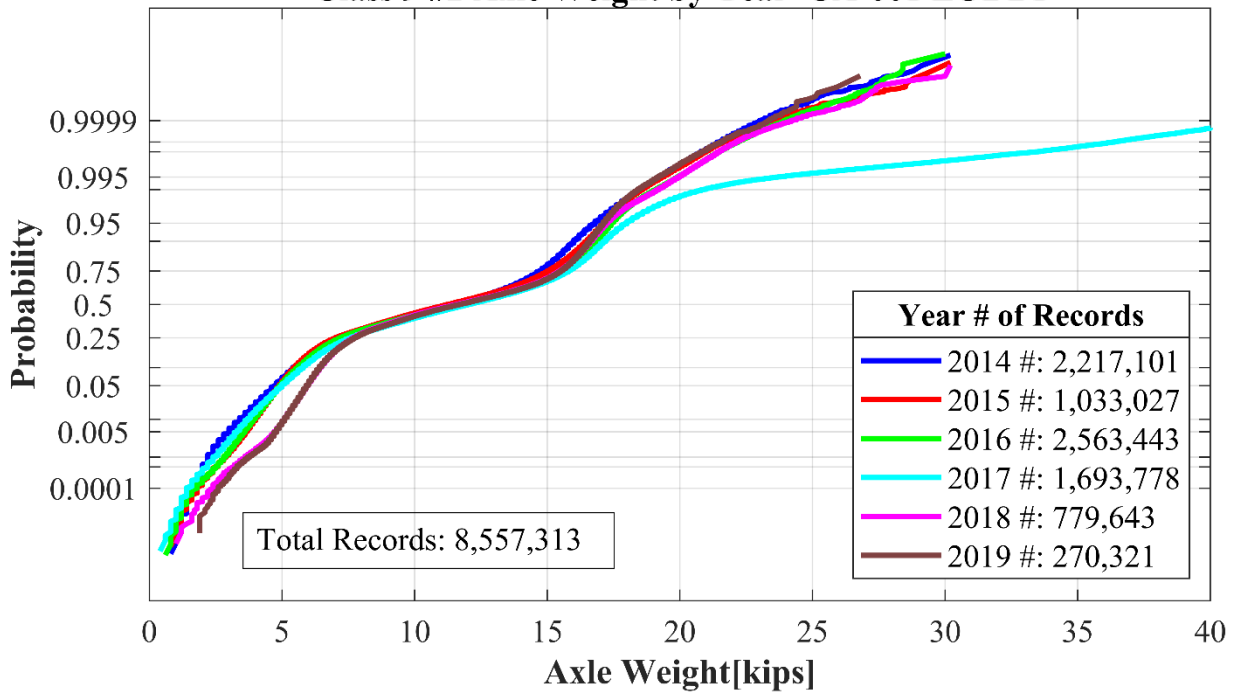


C.3 Axle Loads

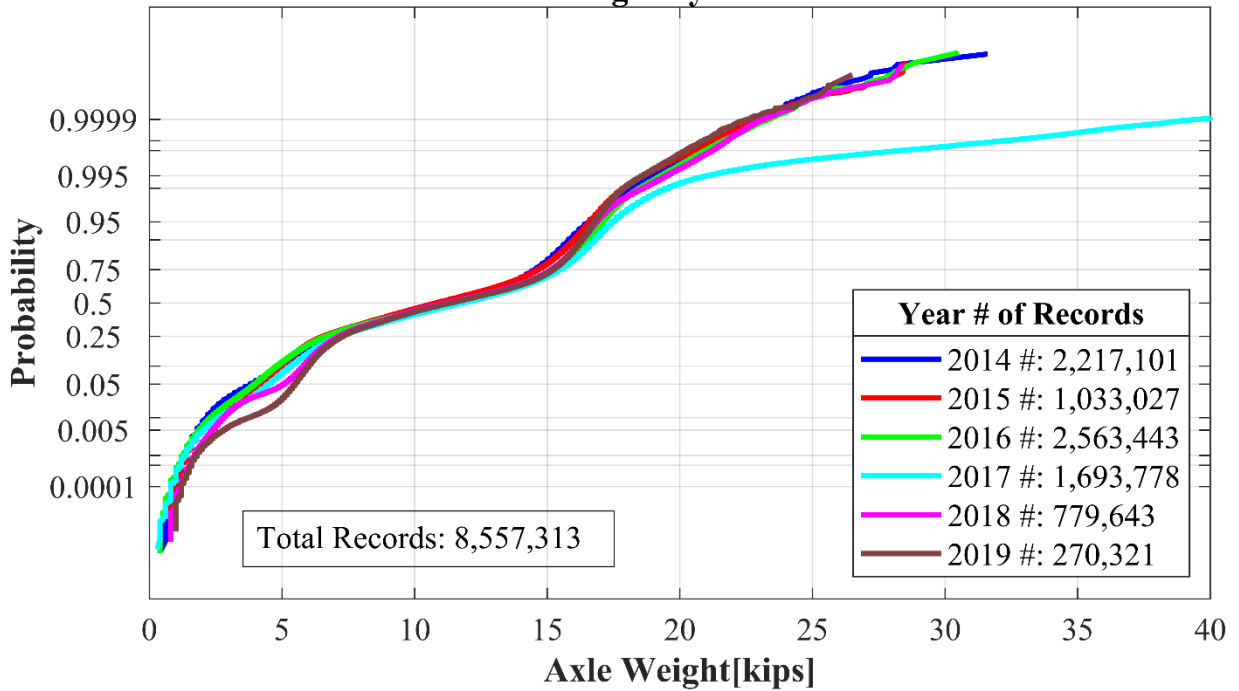
Class 9 #1 Axle Weight by Year CA-001 LODDI



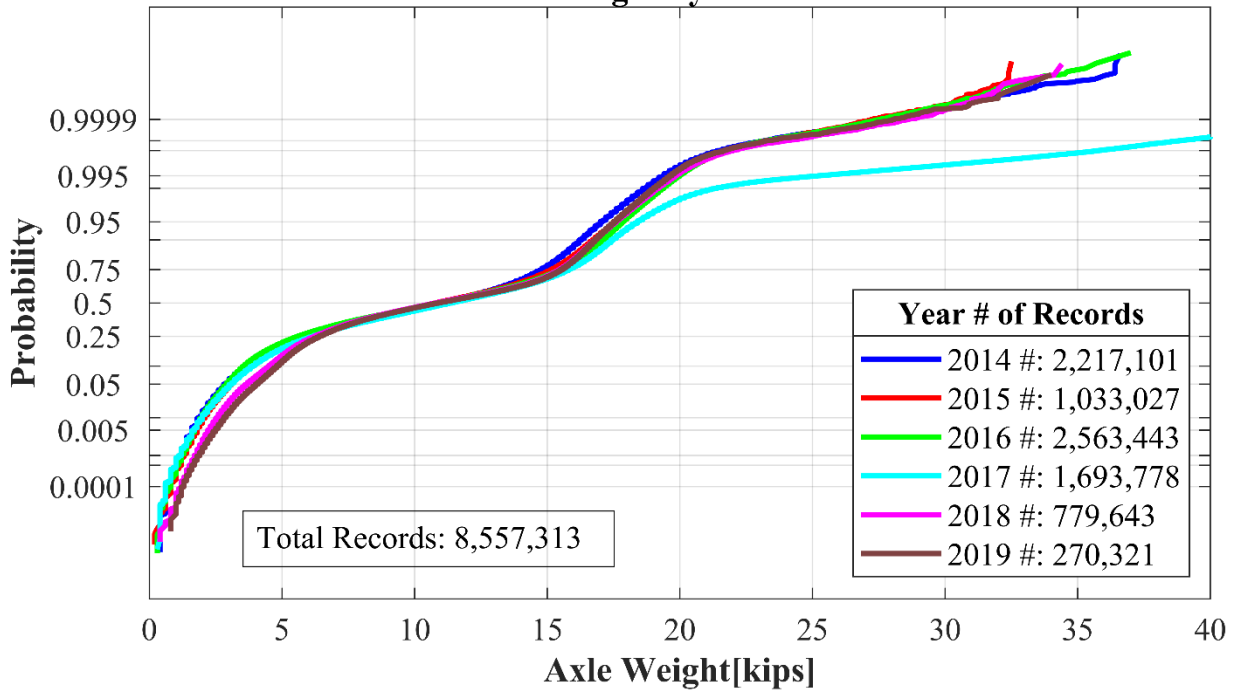
Class 9 #2 Axle Weight by Year CA-001 LODDI



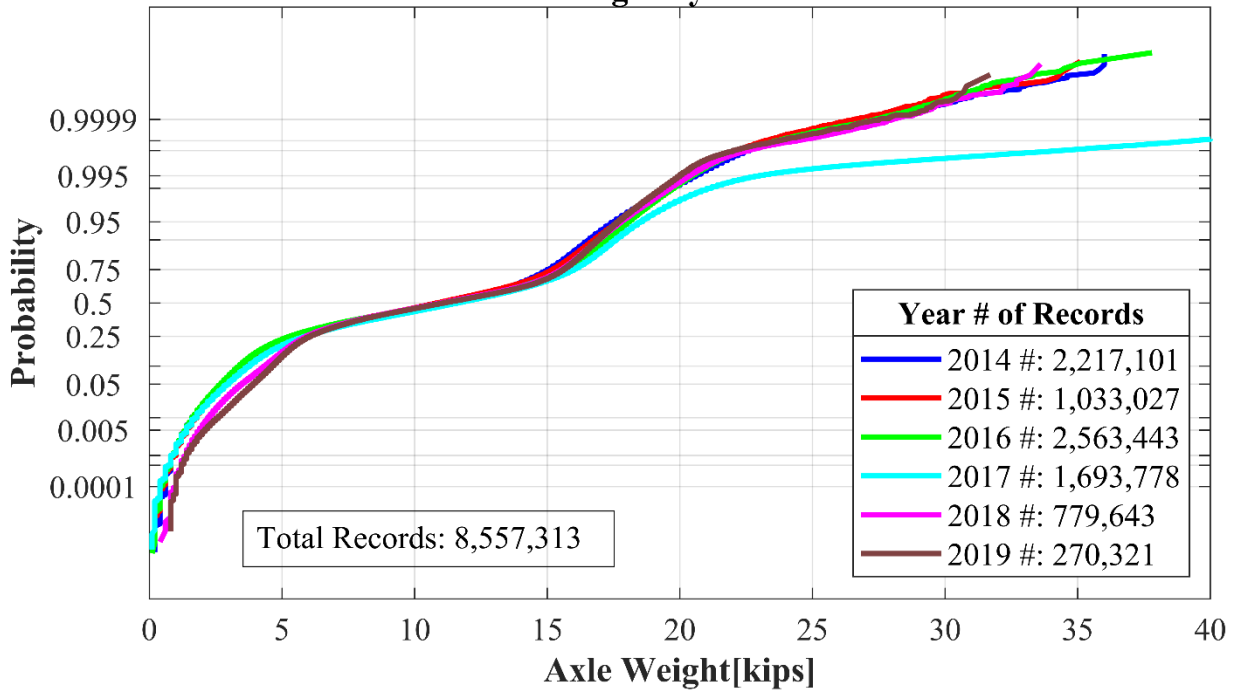
Class 9 #3 Axle Weight by Year CA-001 LODDI



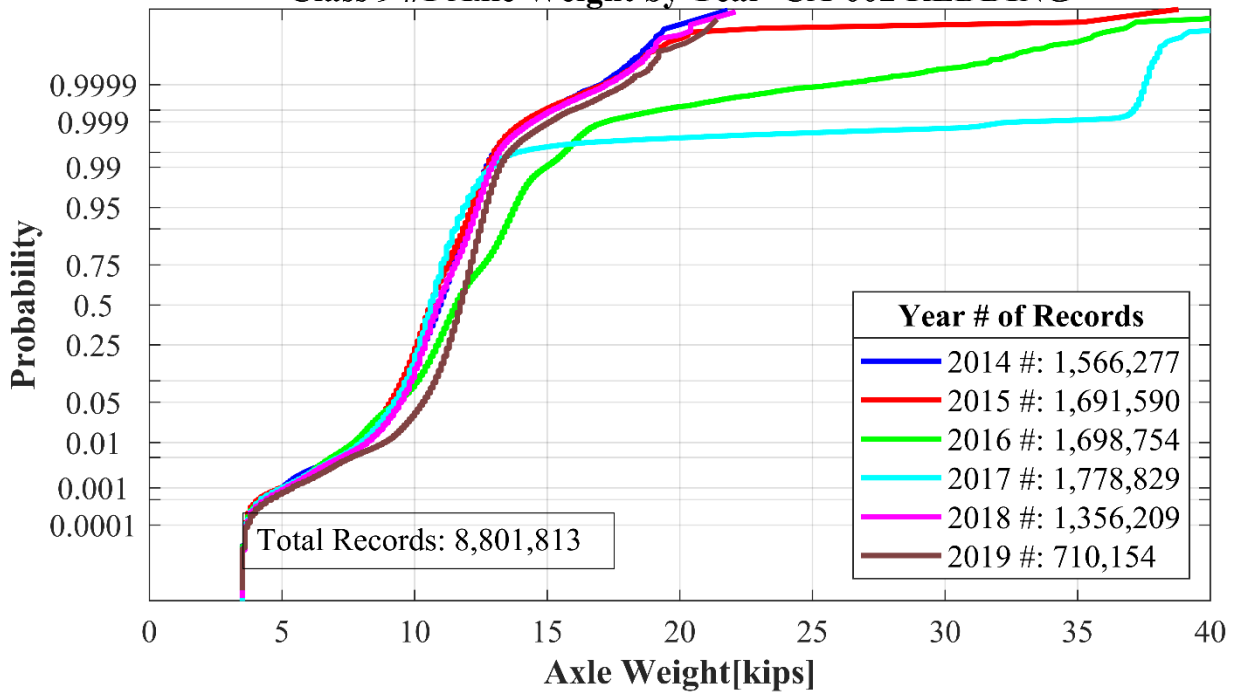
Class 9 #4 Axle Weight by Year CA-001 LODDI



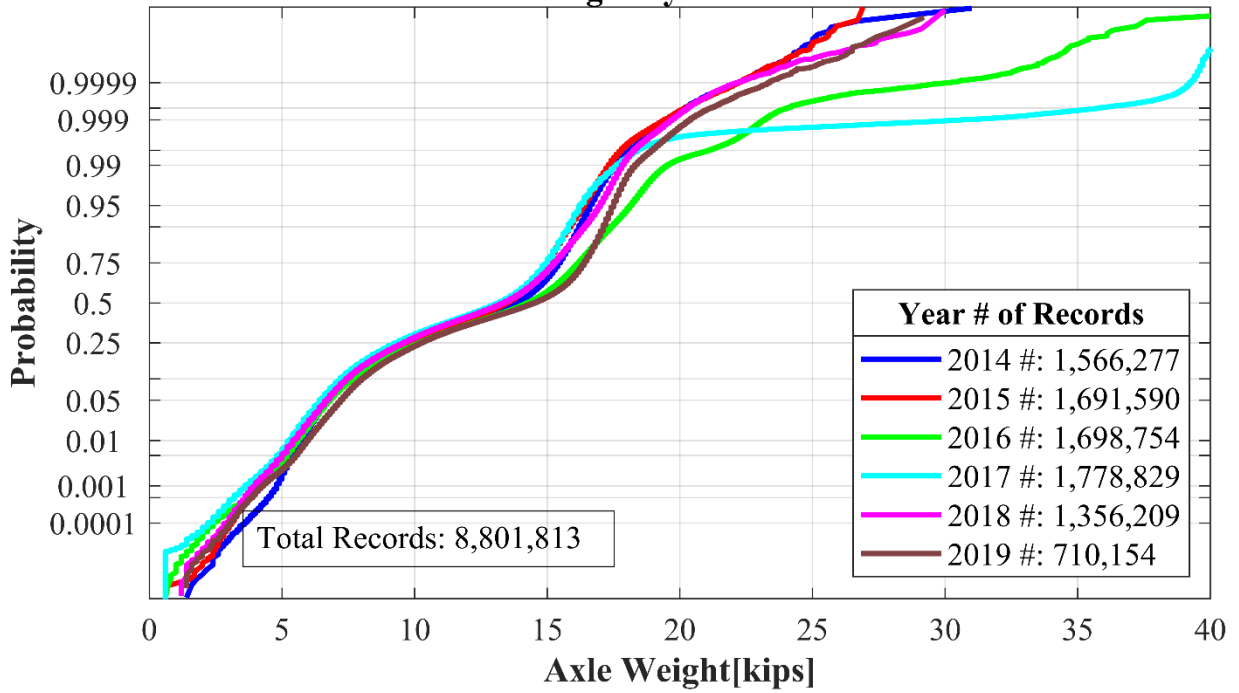
Class 9 #5 Axle Weight by Year CA-001 LODDI



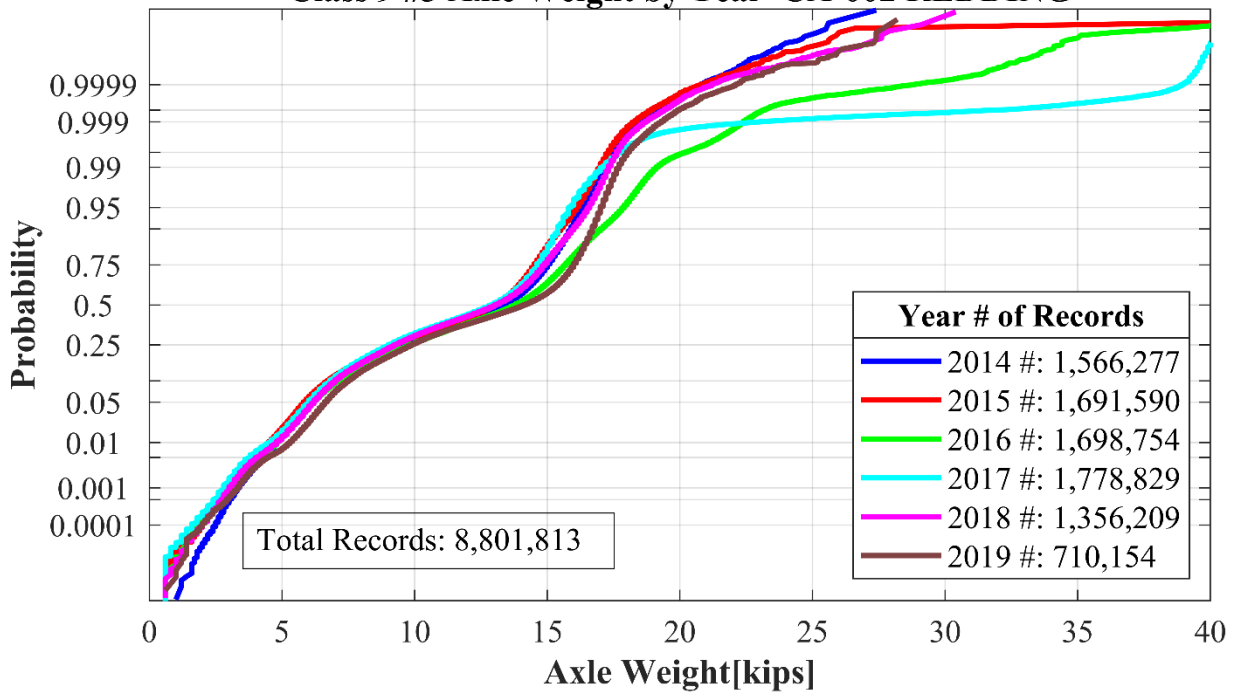
Class 9 #1 Axle Weight by Year CA-002 REDDING



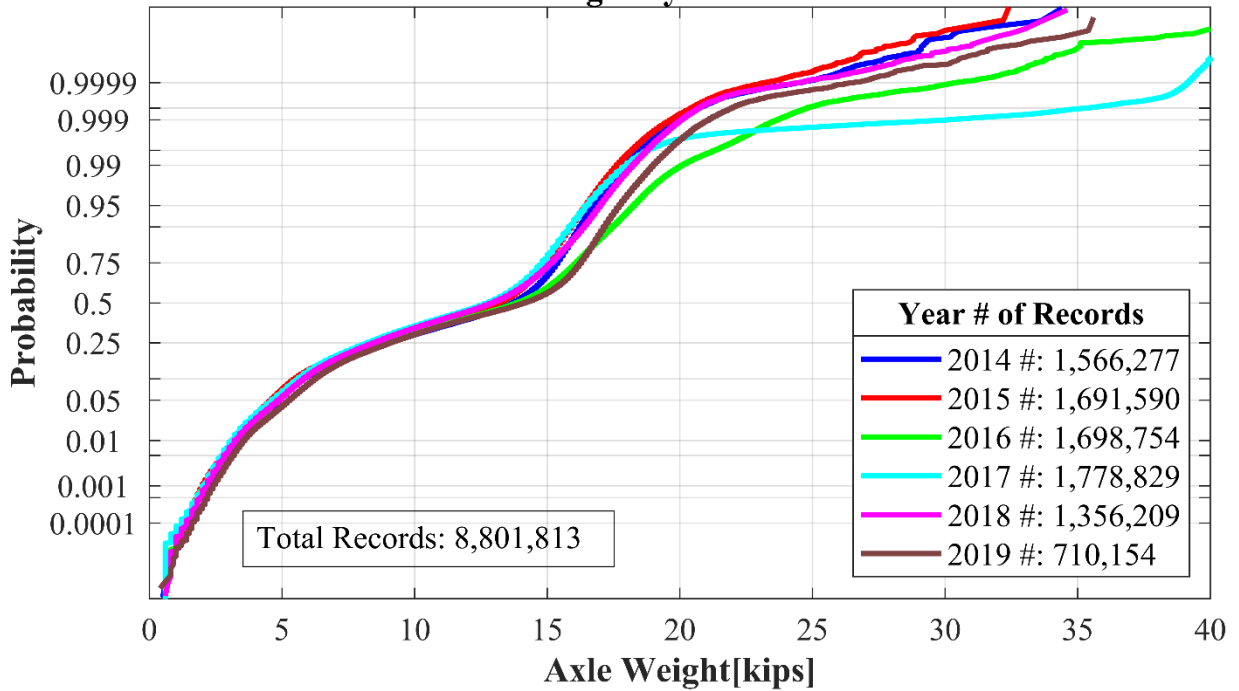
Class 9 #2 Axle Weight by Year CA-002 REDDING



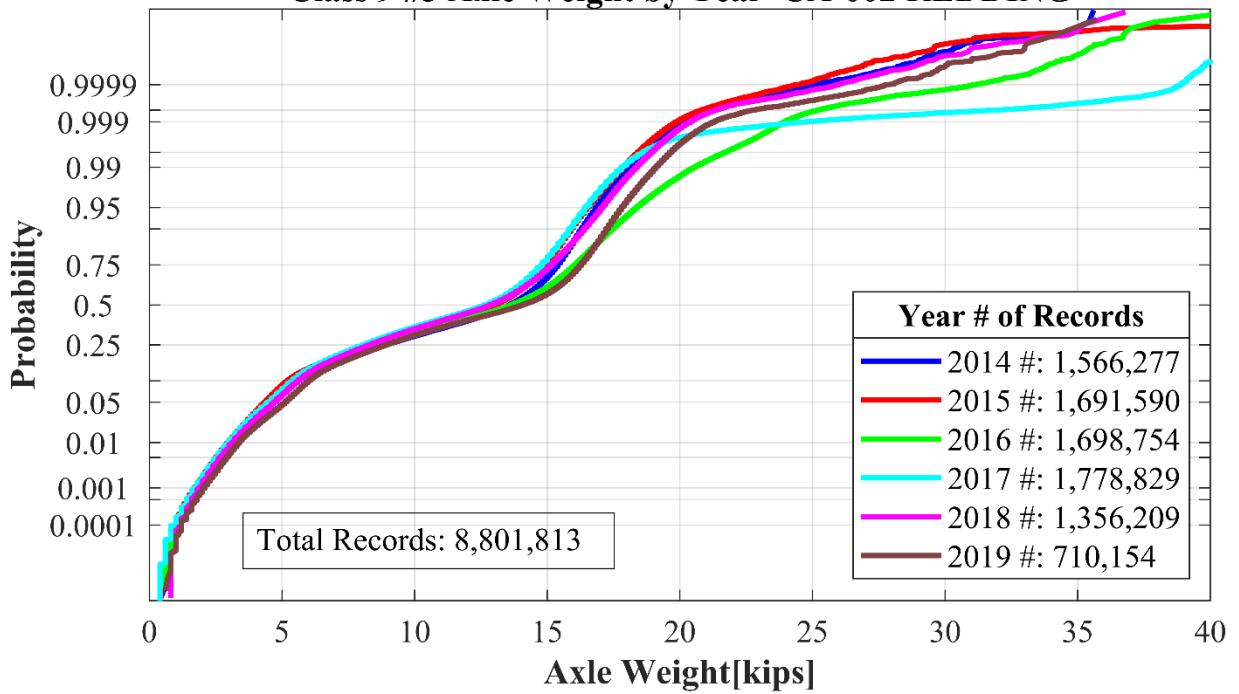
Class 9 #3 Axle Weight by Year CA-002 REDDING



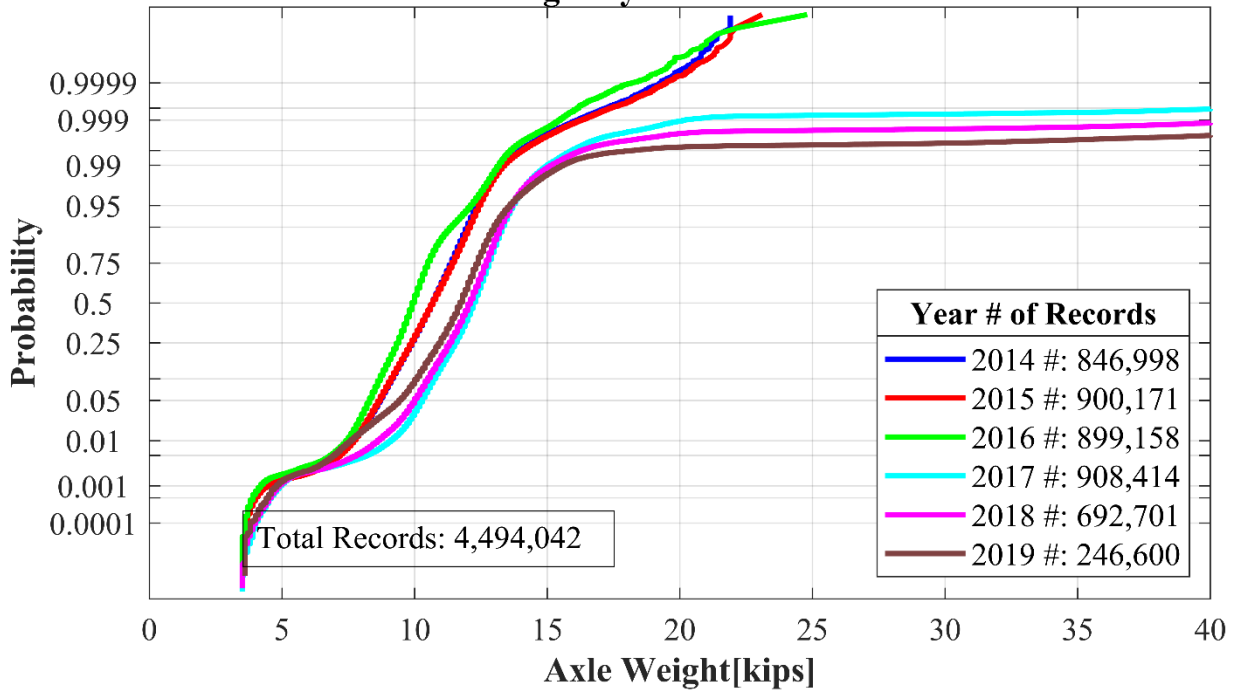
Class 9 #4 Axle Weight by Year CA-002 REDDING



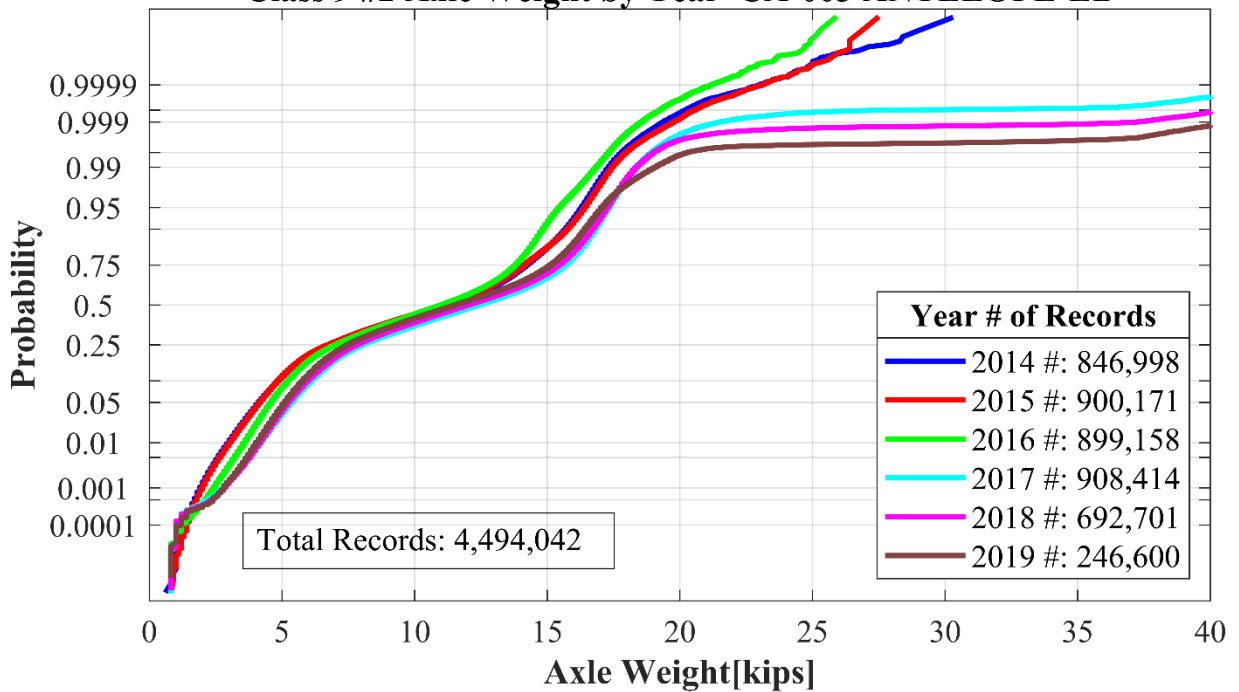
Class 9 #5 Axle Weight by Year CA-002 REDDING



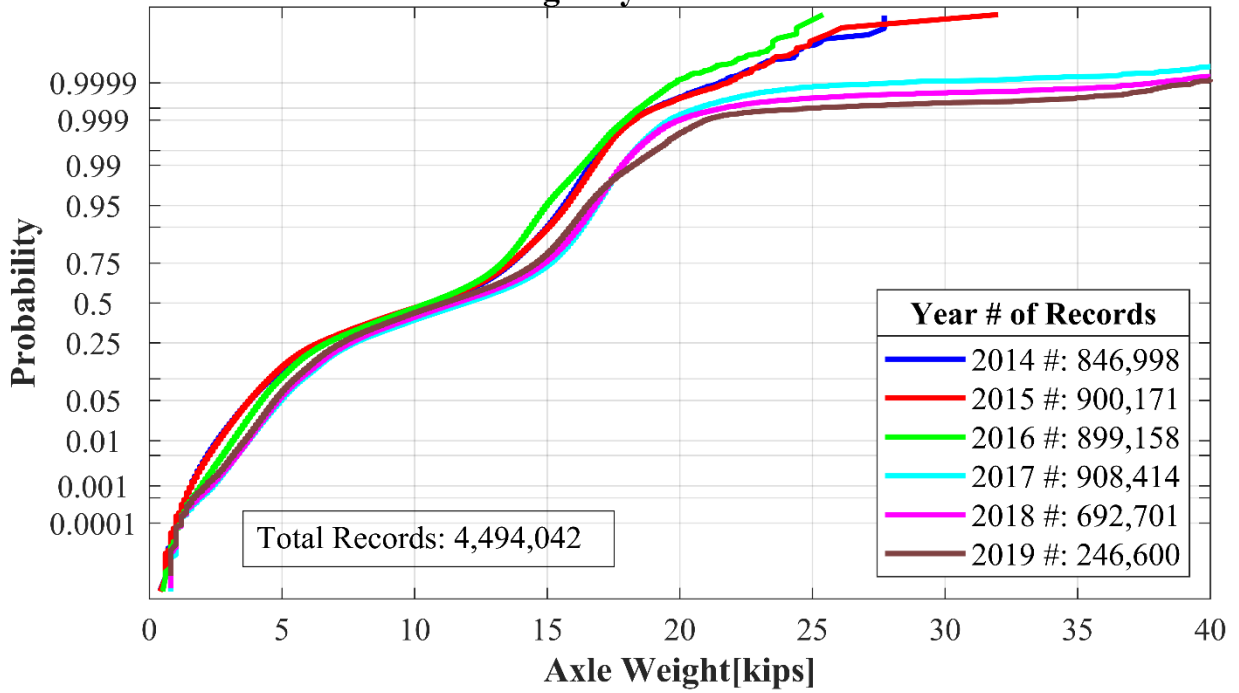
Class 9 #1 Axle Weight by Year CA-003 ANTELOPE-EB



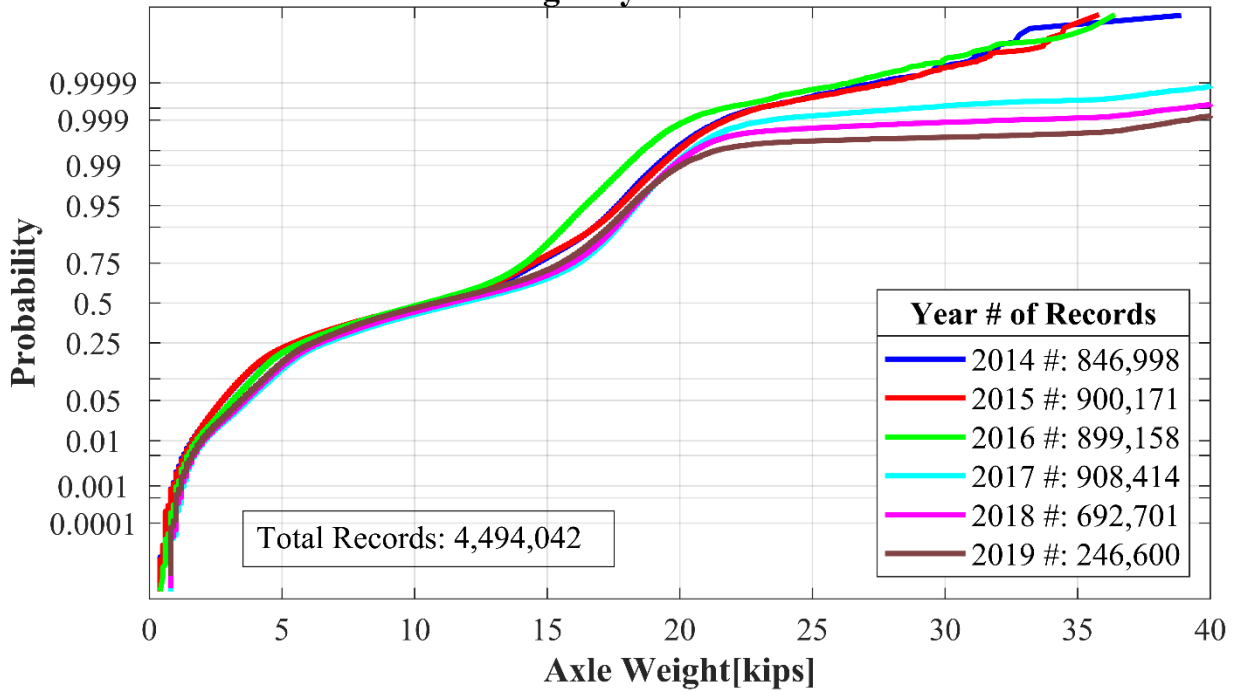
Class 9 #2 Axle Weight by Year CA-003 ANTELOPE-EB



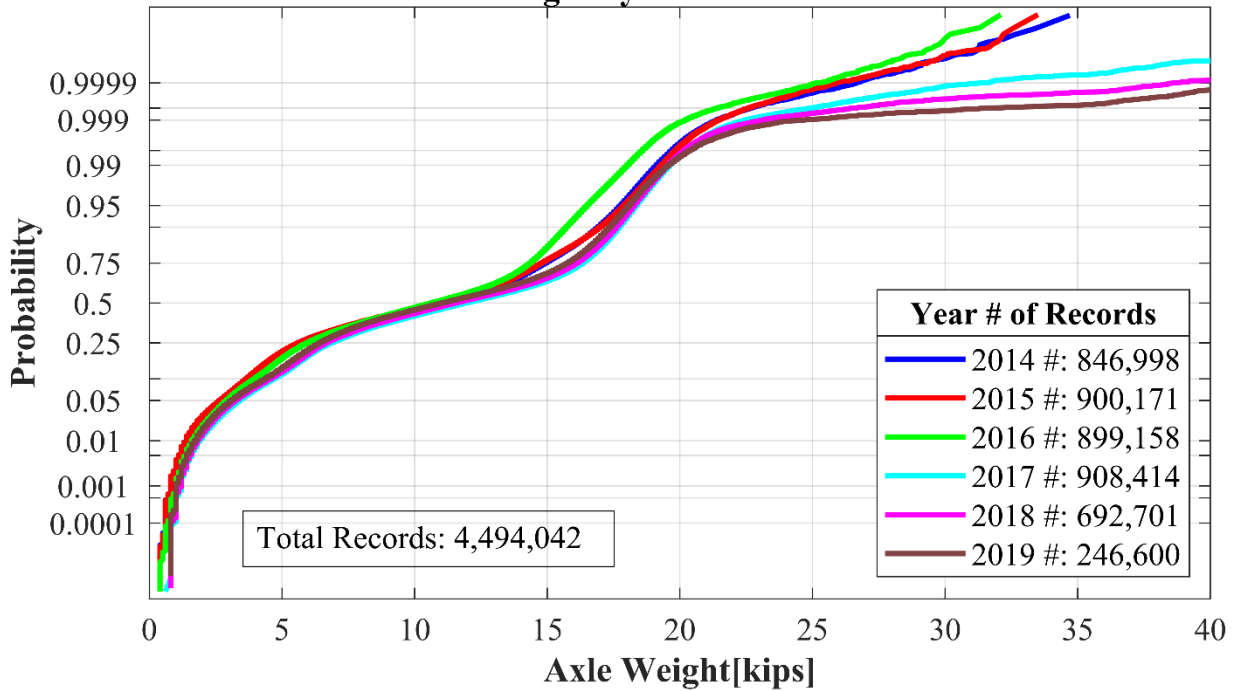
Class 9 #3 Axle Weight by Year CA-003 ANTELOPE-EB



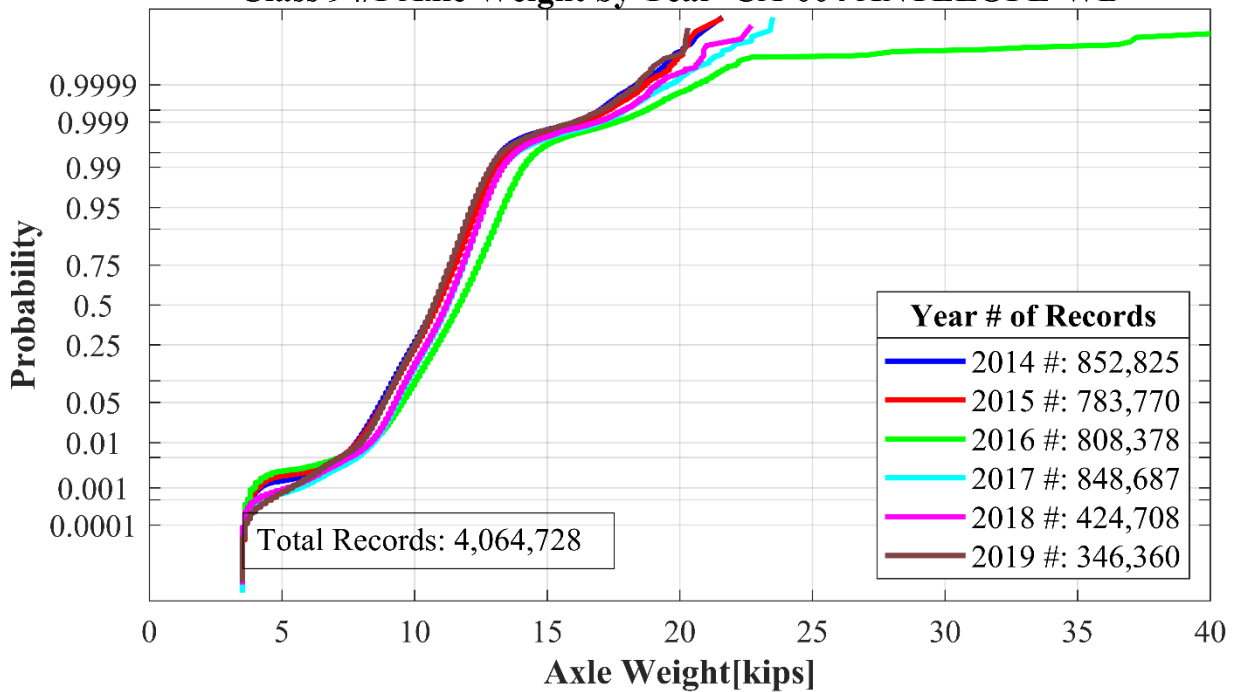
Class 9 #4 Axle Weight by Year CA-003 ANTELOPE-EB



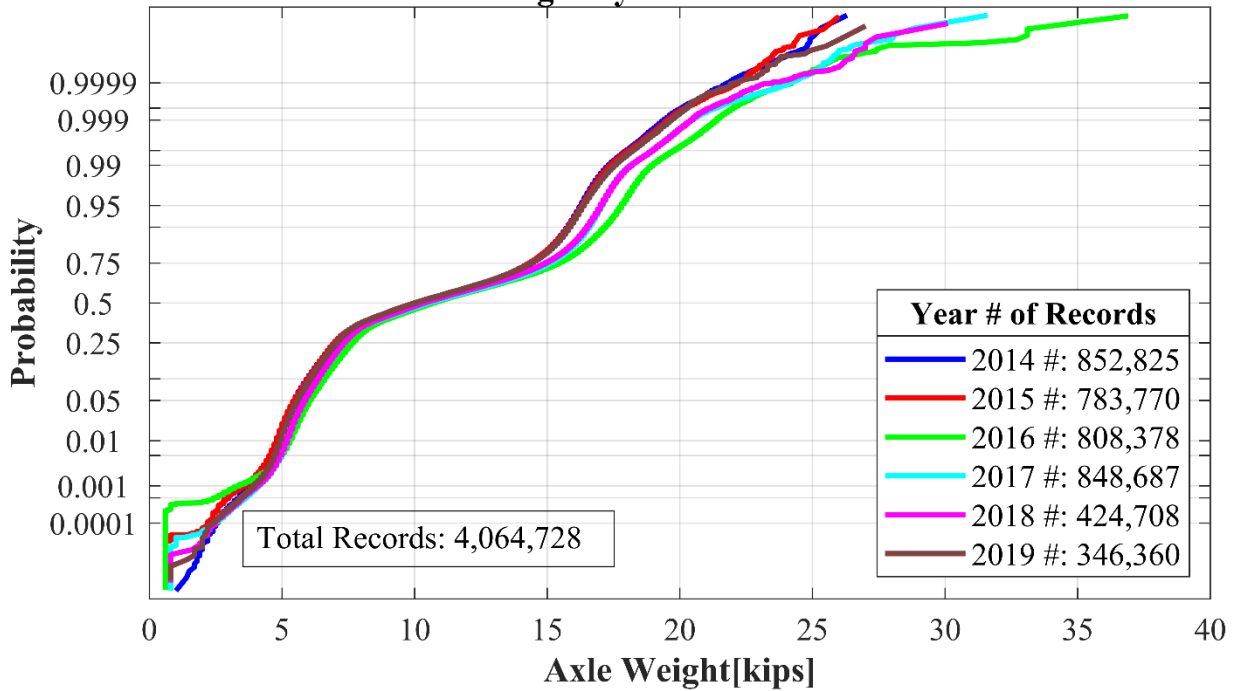
Class 9 #5 Axle Weight by Year CA-003 ANTELOPE-EB



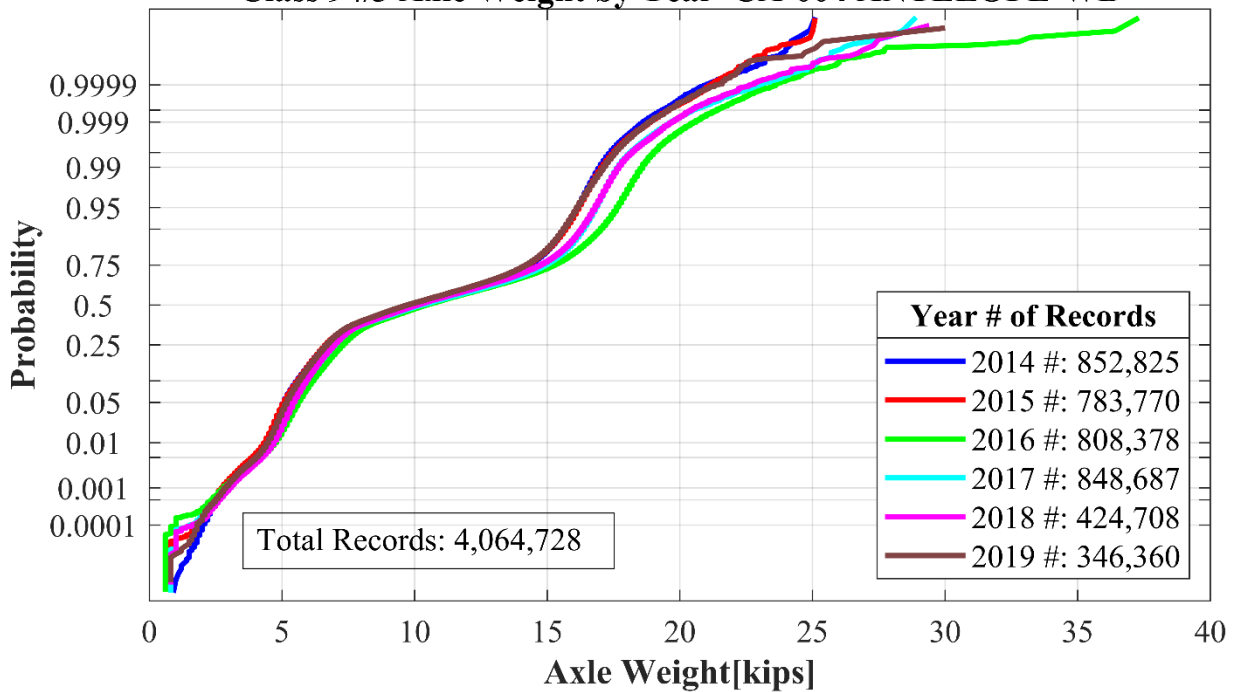
Class 9 #1 Axle Weight by Year CA-004 ANTELOPE-WB



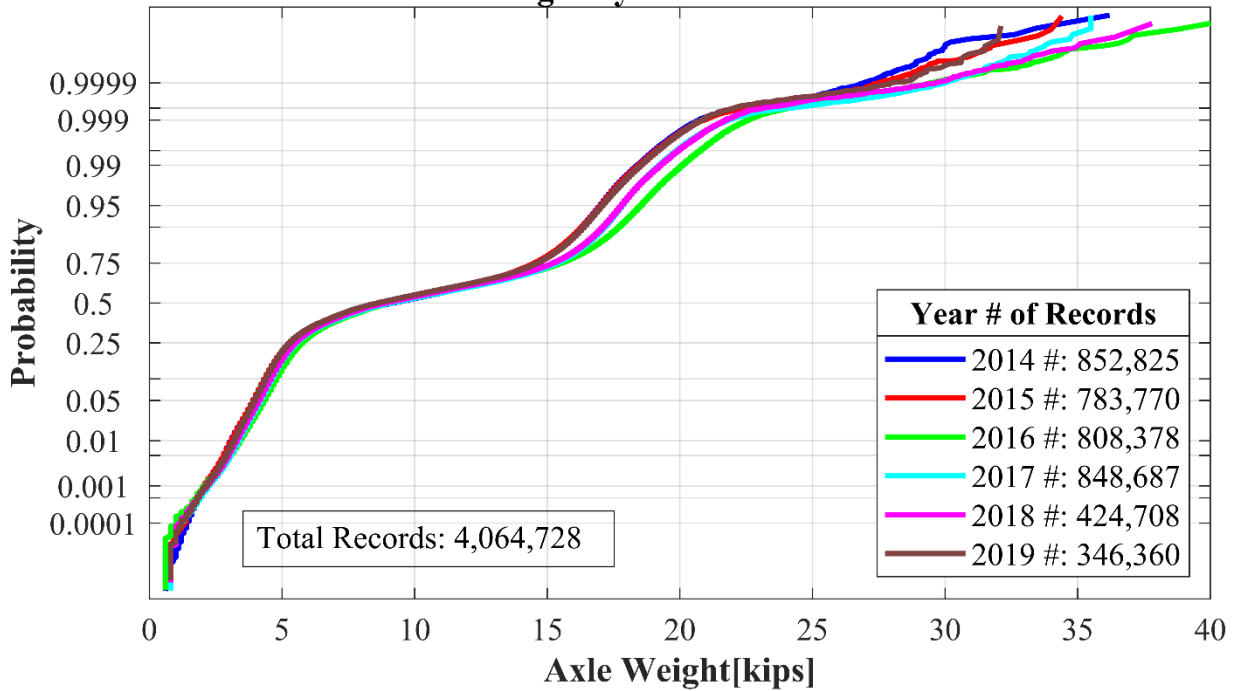
Class 9 #2 Axle Weight by Year CA-004 ANTELOPE-WB



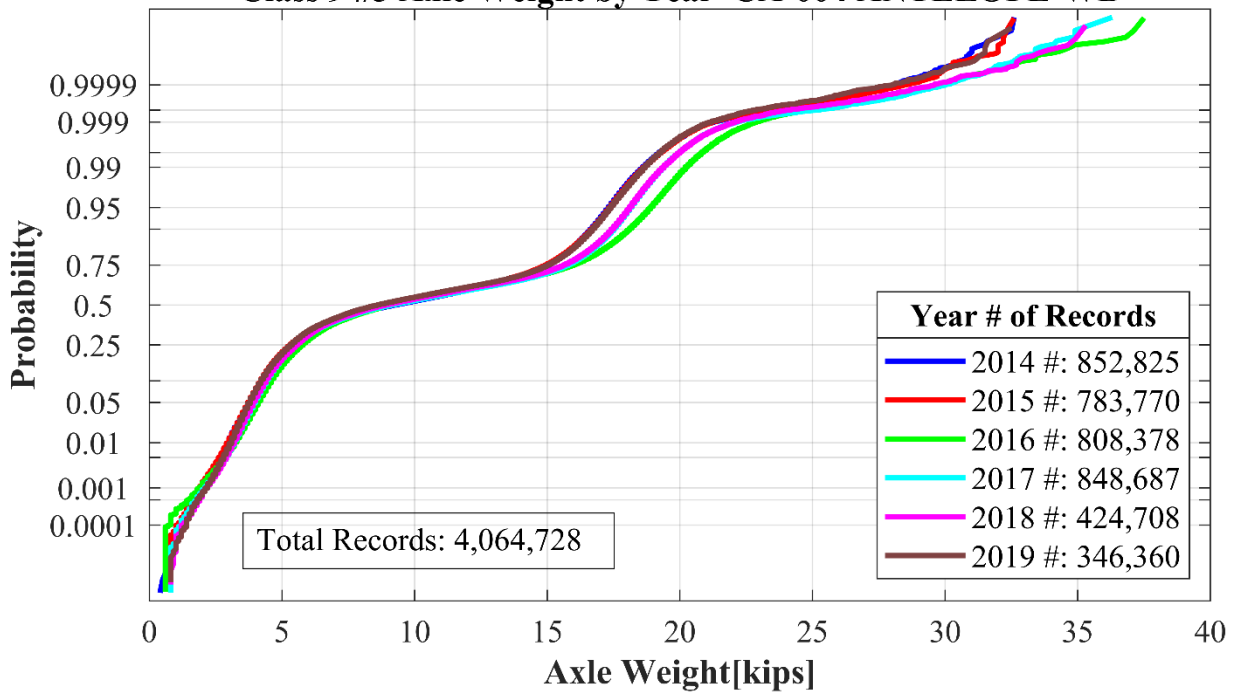
Class 9 #3 Axle Weight by Year CA-004 ANTELOPE-WB



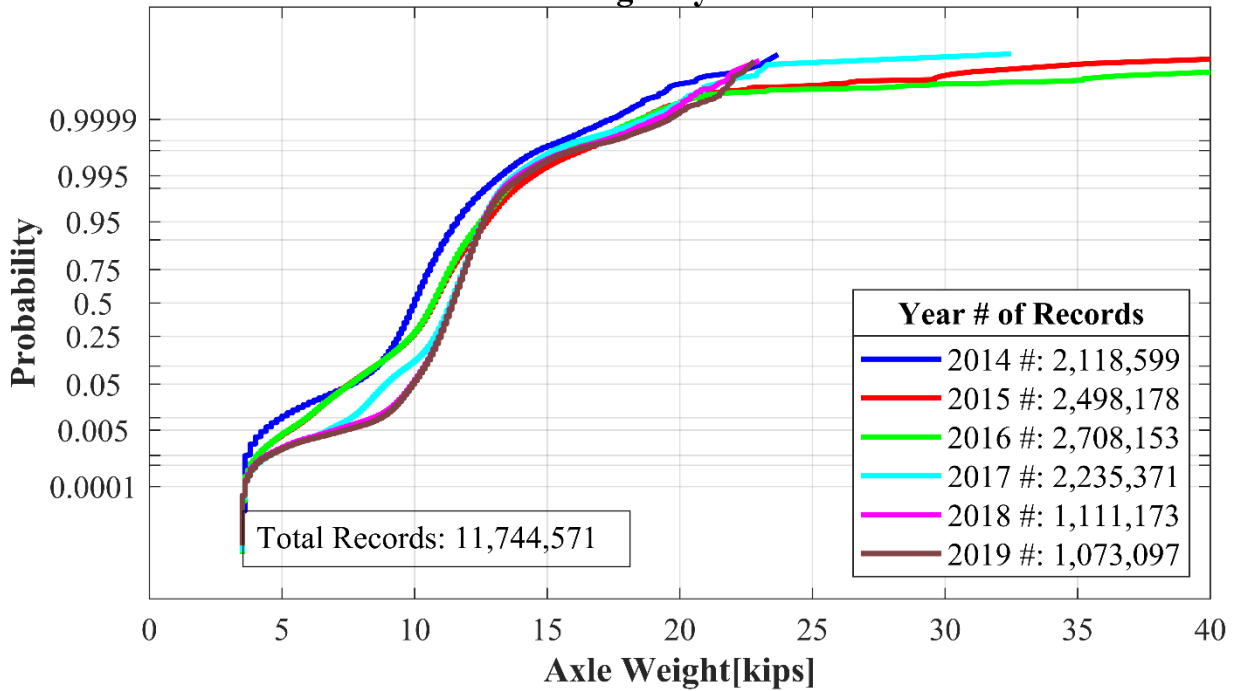
Class 9 #4 Axle Weight by Year CA-004 ANTELOPE-WB



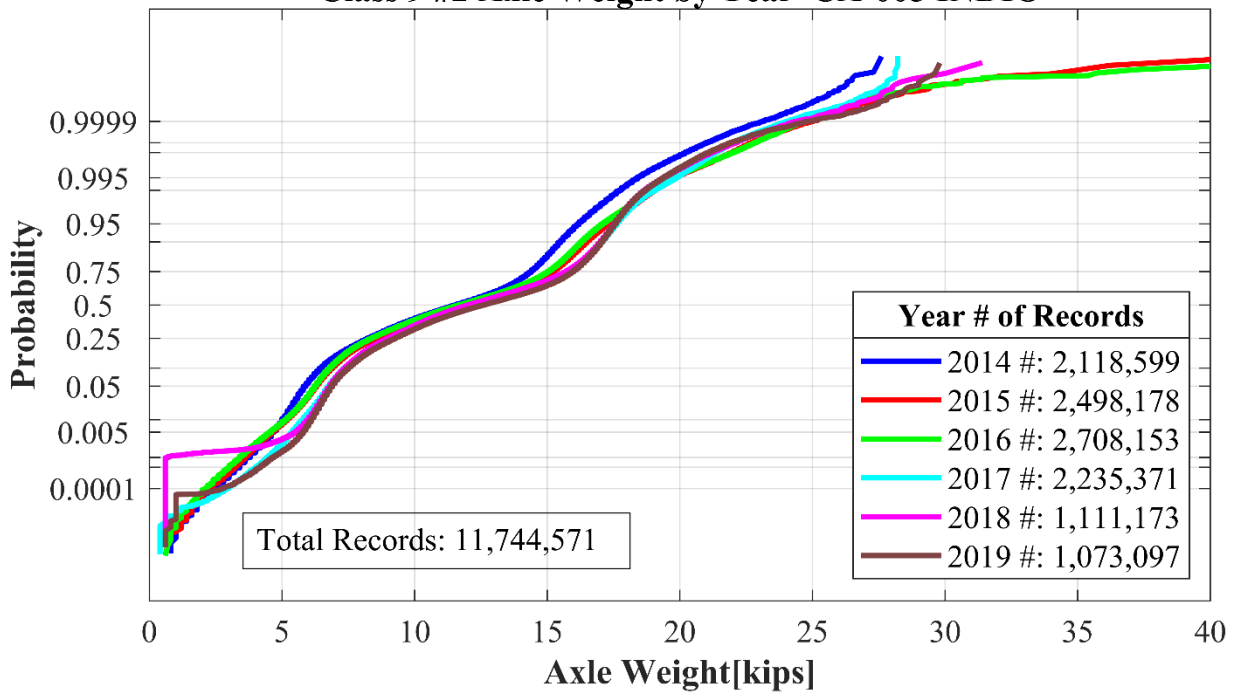
Class 9 #5 Axle Weight by Year CA-004 ANTELOPE-WB



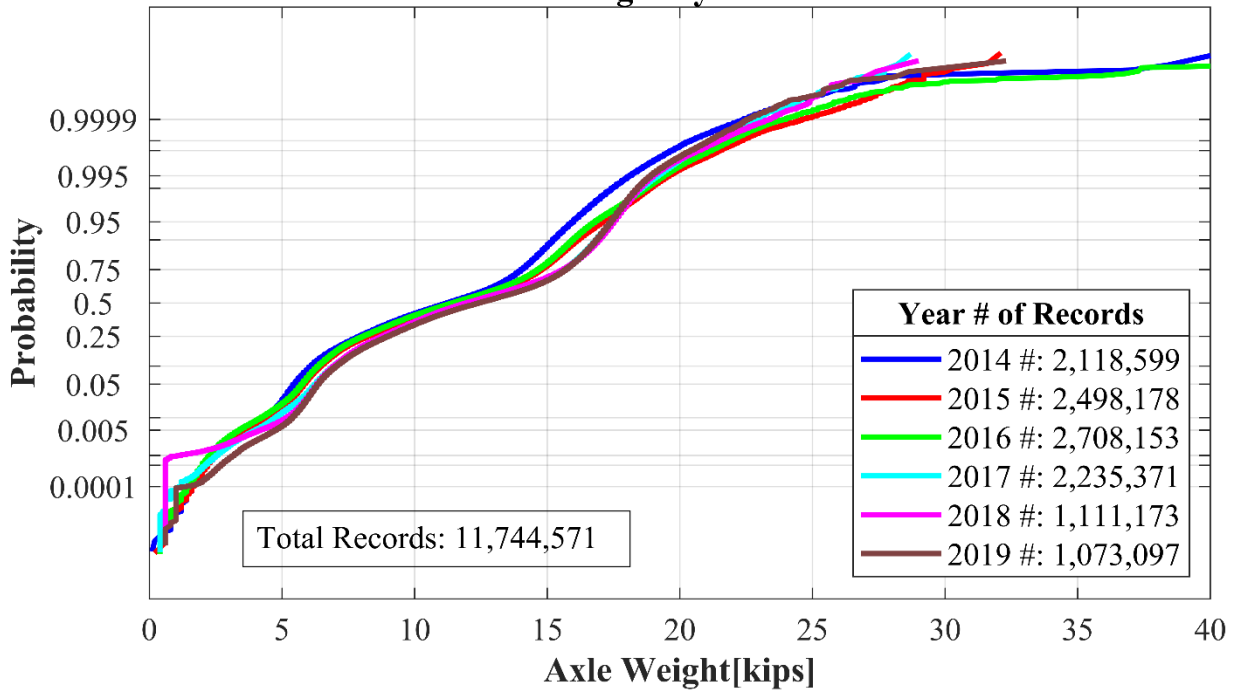
Class 9 #1 Axle Weight by Year CA-005 INDIO



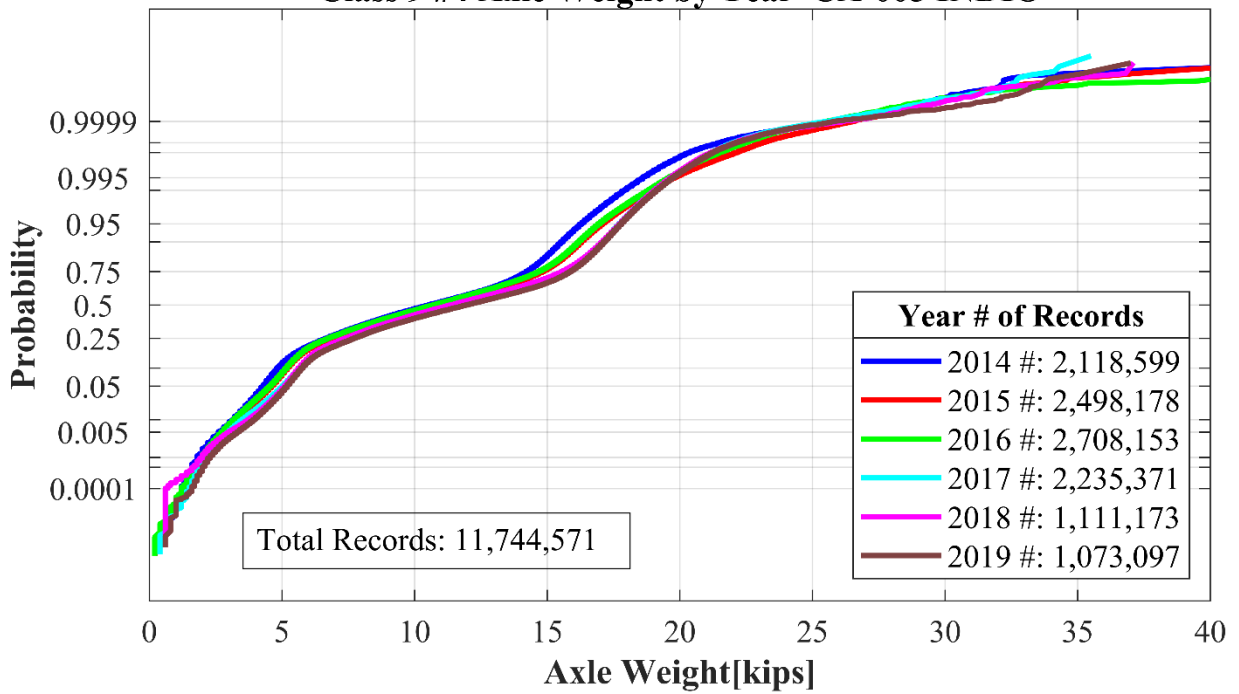
Class 9 #2 Axle Weight by Year CA-005 INDIO



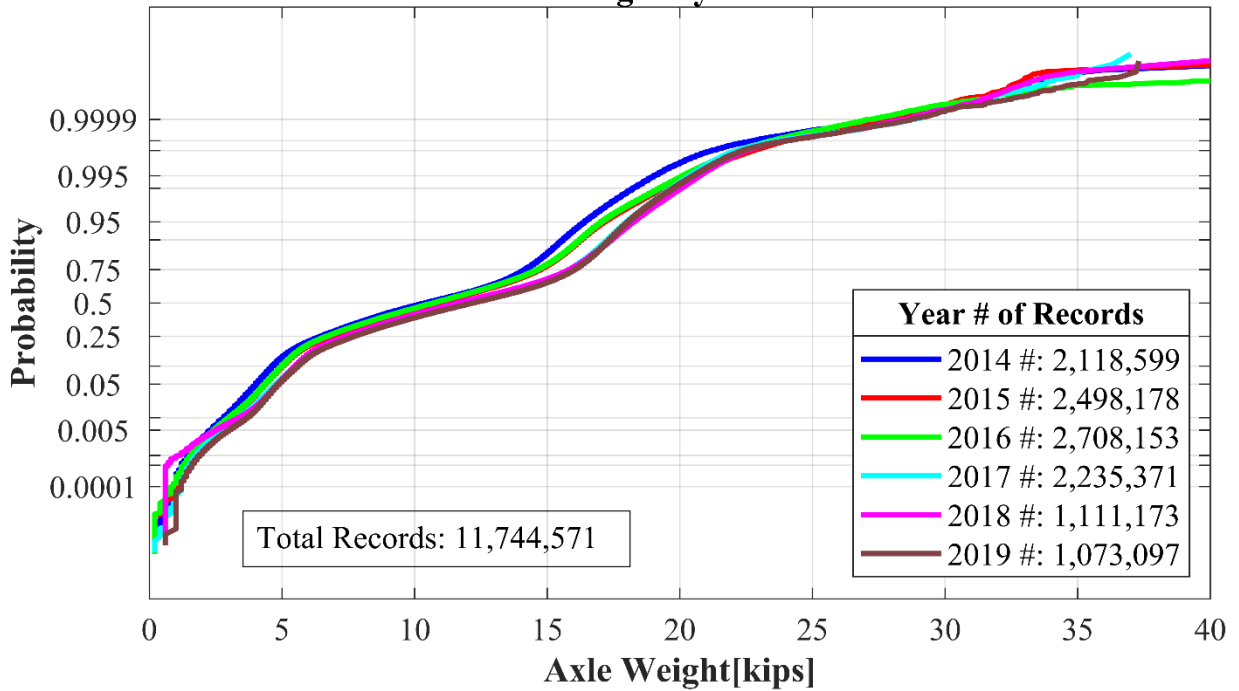
Class 9 #3 Axle Weight by Year CA-005 INDIO



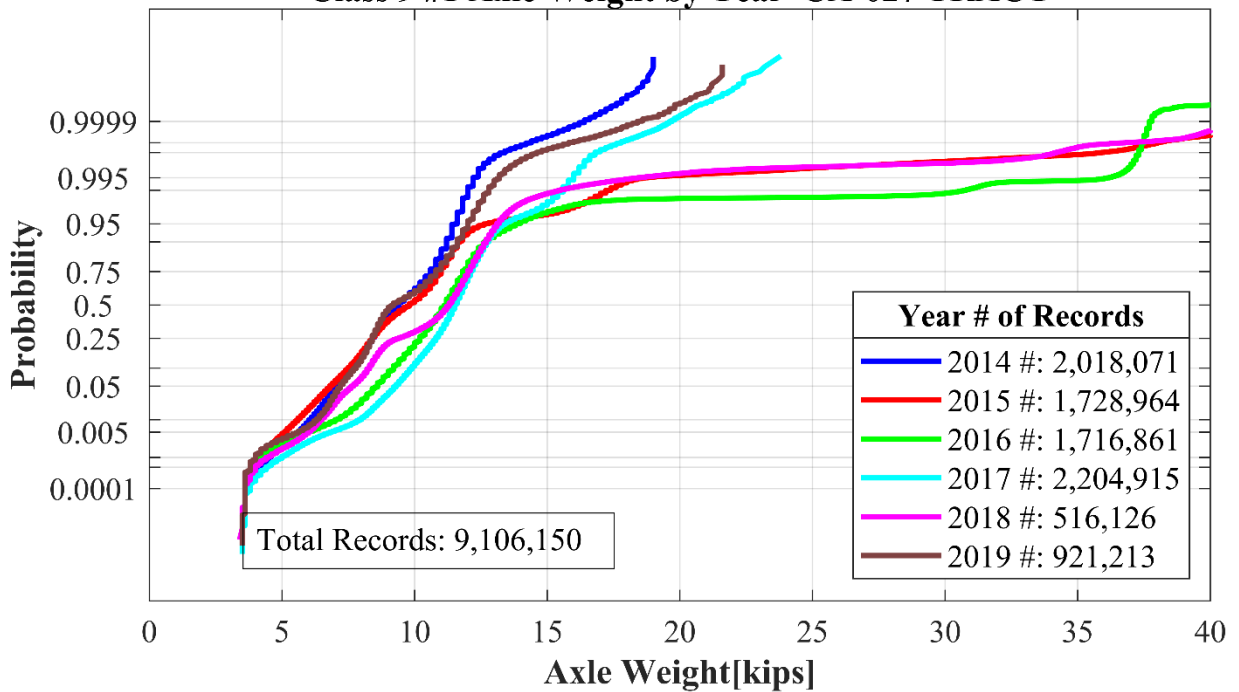
Class 9 #4 Axle Weight by Year CA-005 INDIO



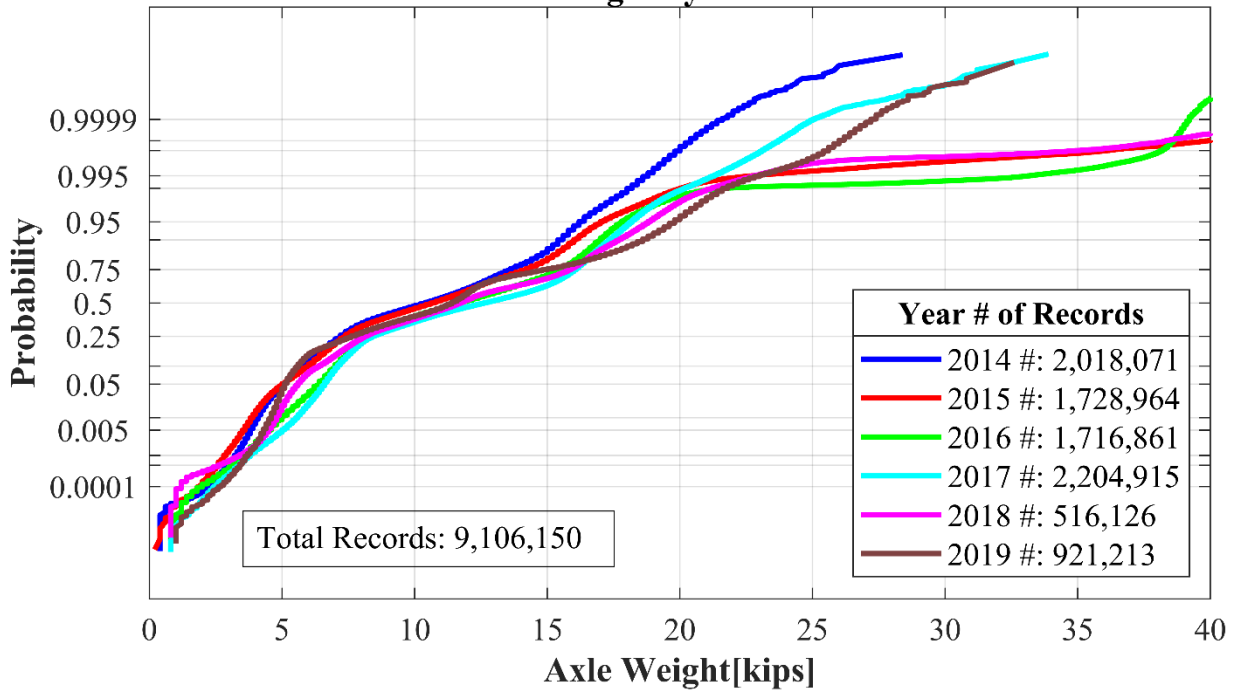
Class 9 #5 Axle Weight by Year CA-005 INDIO



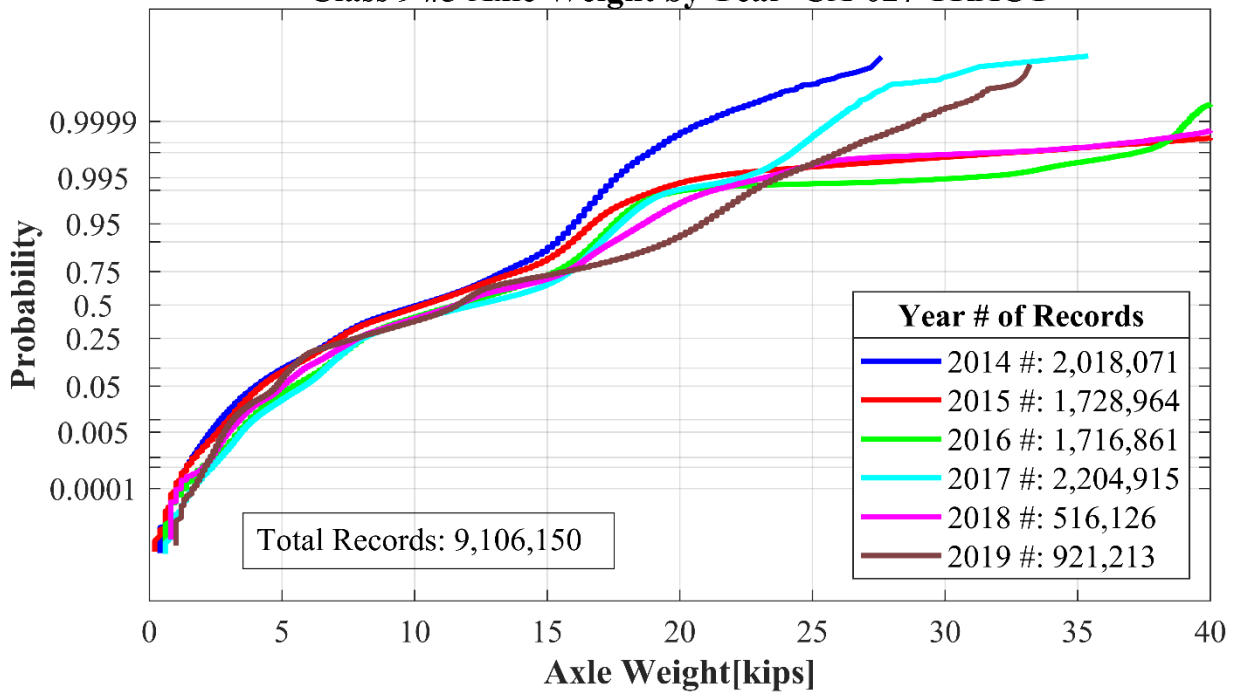
Class 9 #1 Axle Weight by Year CA-027 TRACY



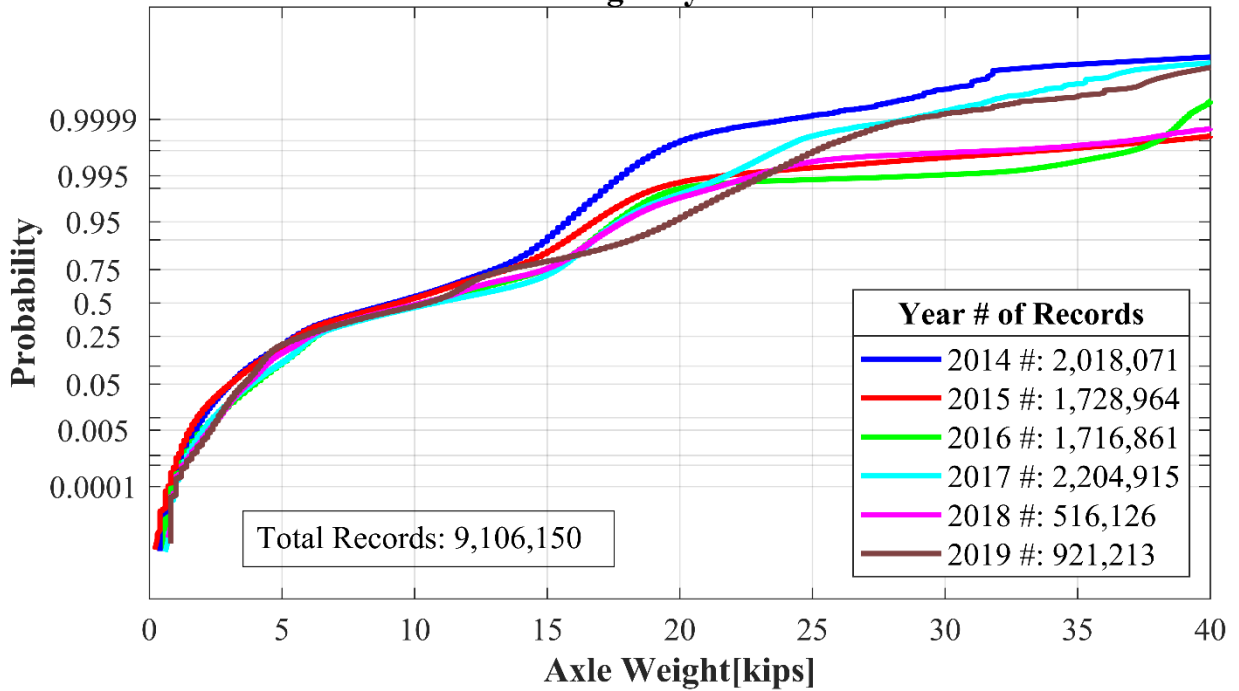
Class 9 #2 Axle Weight by Year CA-027 TRACY



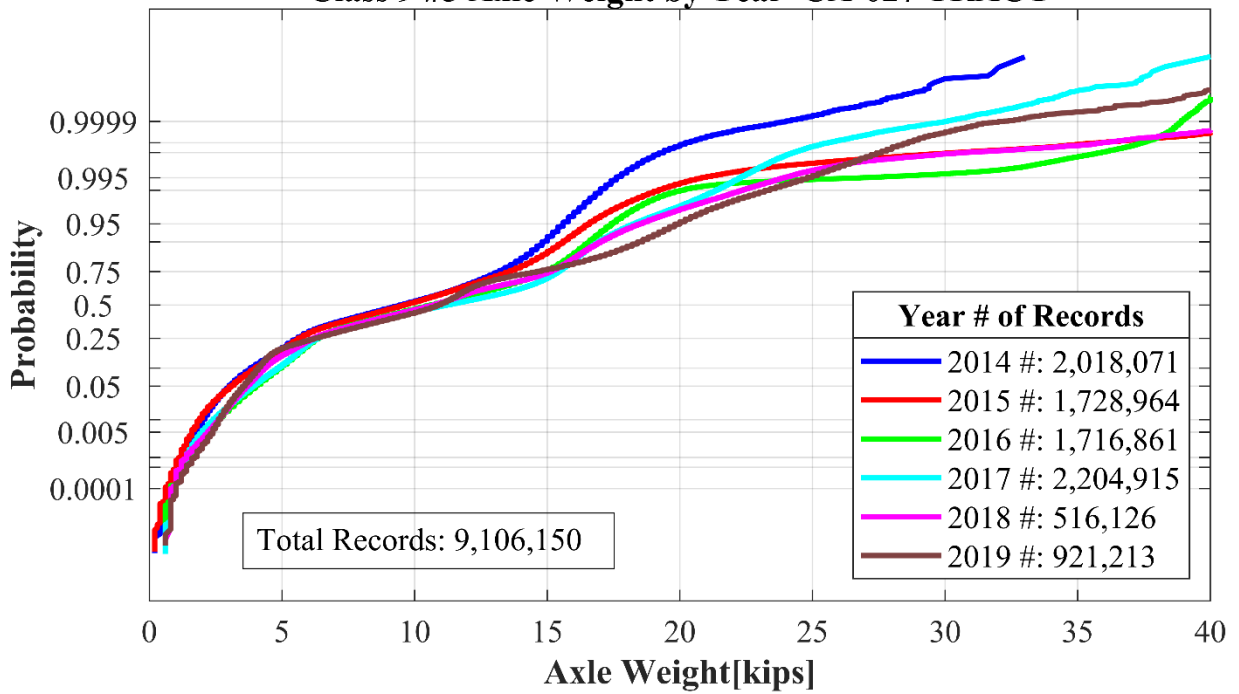
Class 9 #3 Axle Weight by Year CA-027 TRACY



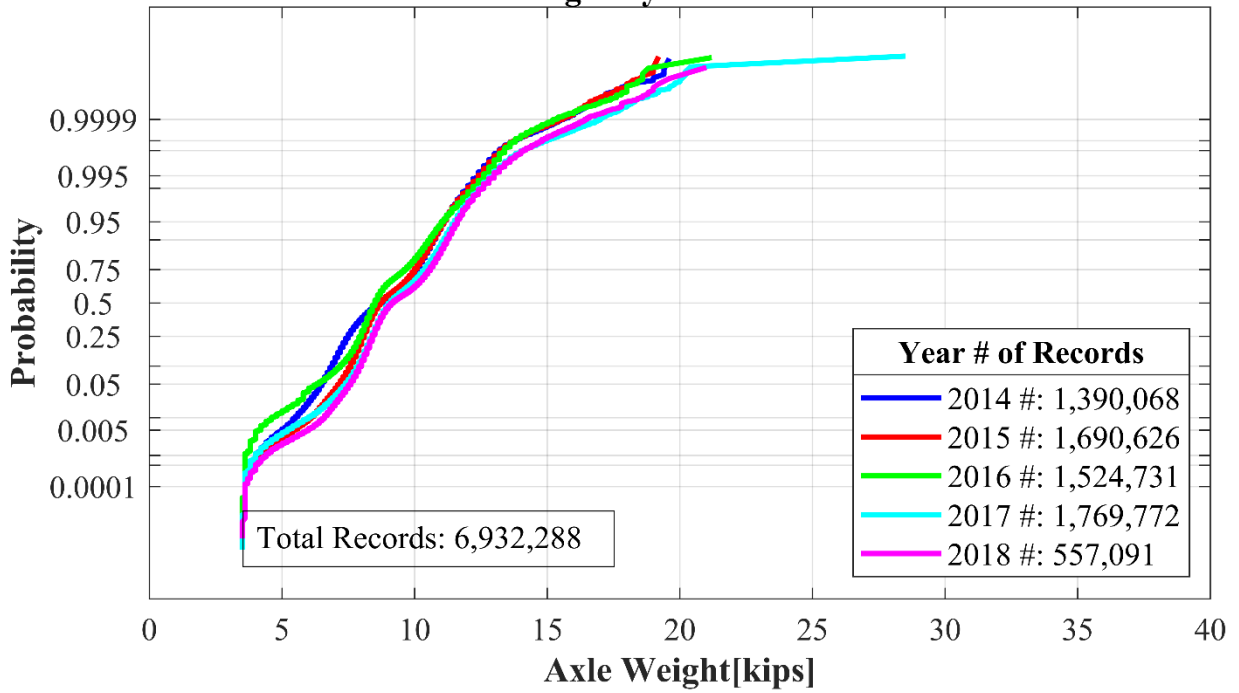
Class 9 #4 Axle Weight by Year CA-027 TRACY



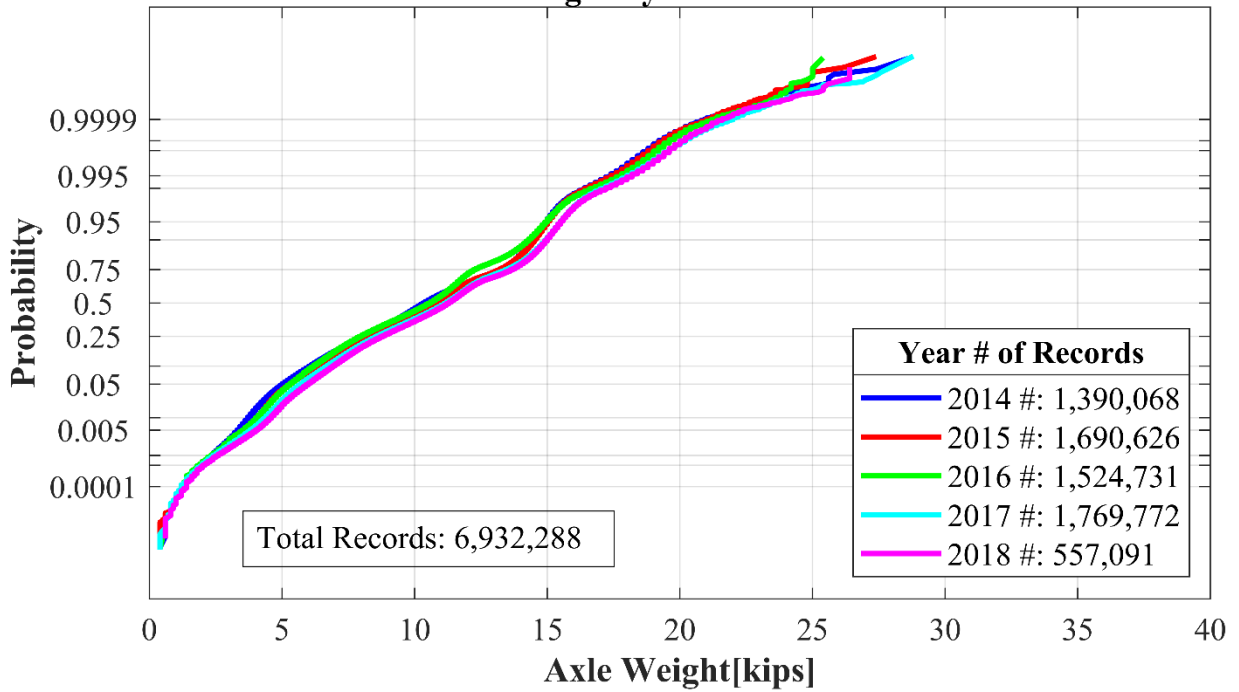
Class 9 #5 Axle Weight by Year CA-027 TRACY



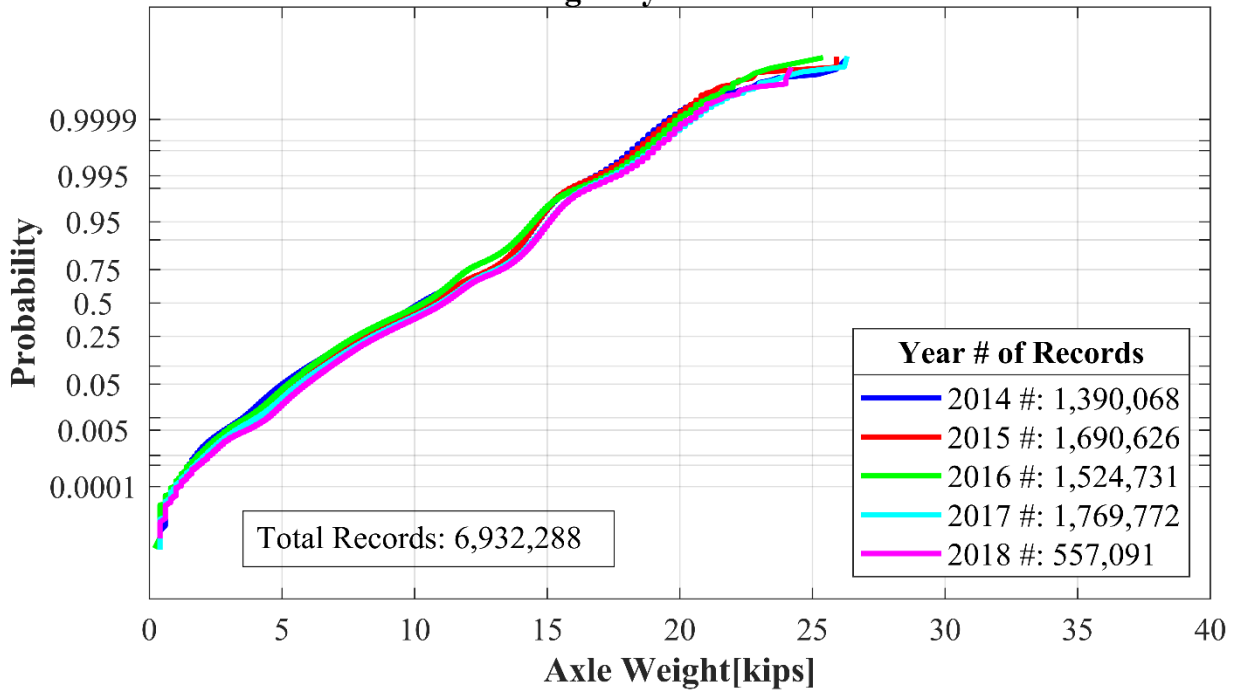
Class 9 #1 Axle Weight by Year CA-030 MT-SHASTA



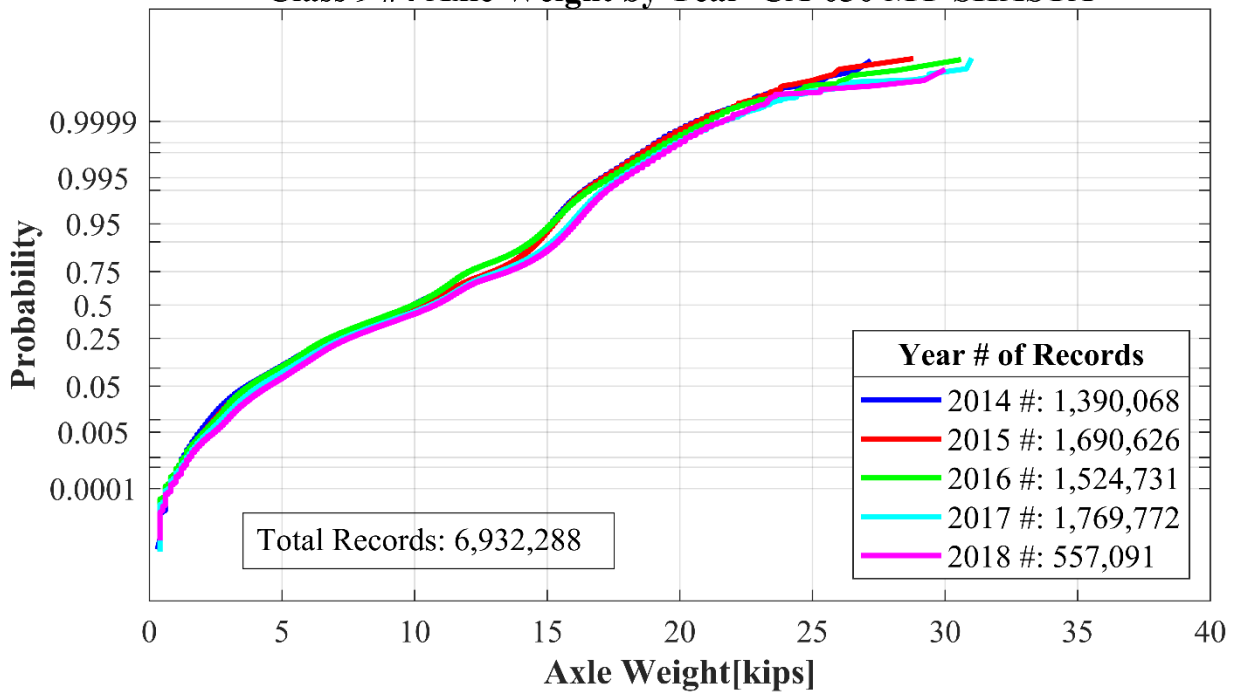
Class 9 #2 Axle Weight by Year CA-030 MT-SHASTA



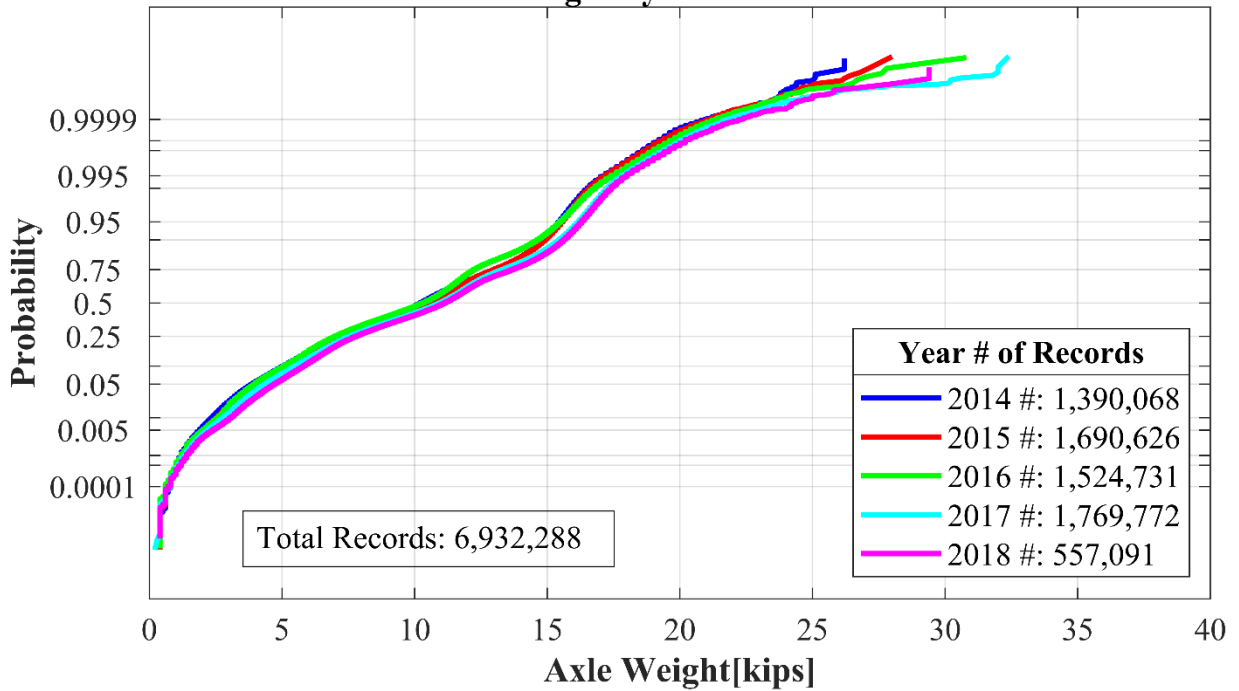
Class 9 #3 Axle Weight by Year CA-030 MT-SHASTA



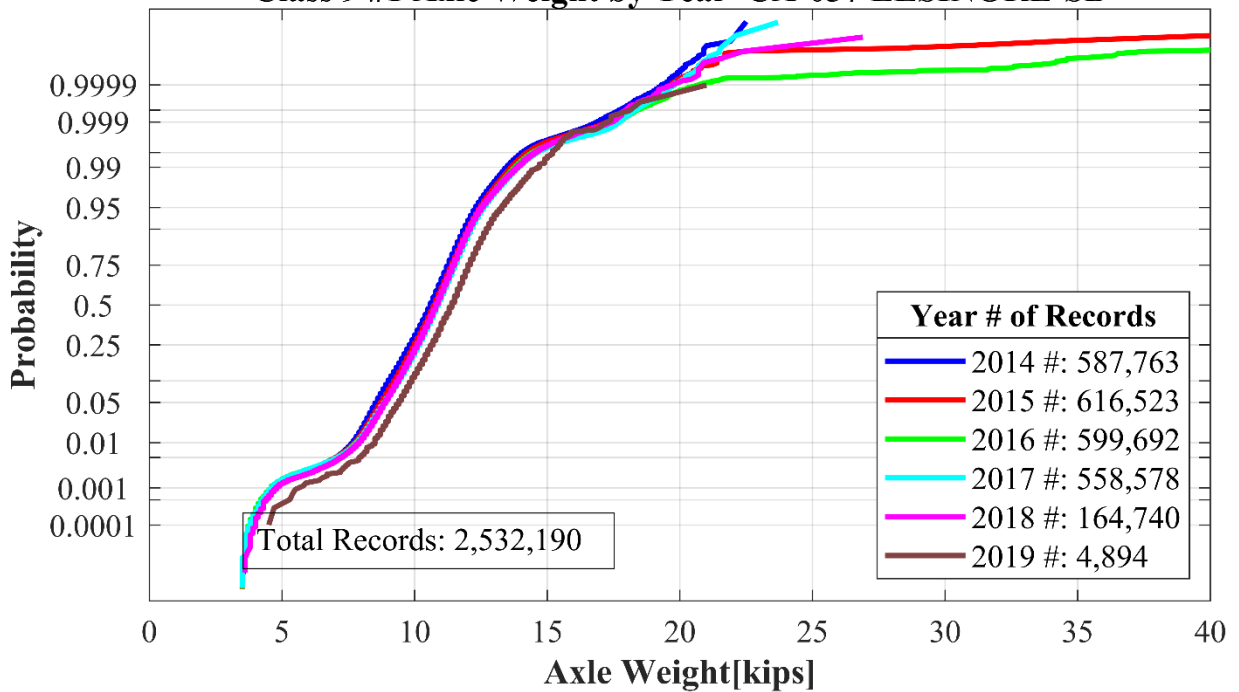
Class 9 #4 Axle Weight by Year CA-030 MT-SHASTA



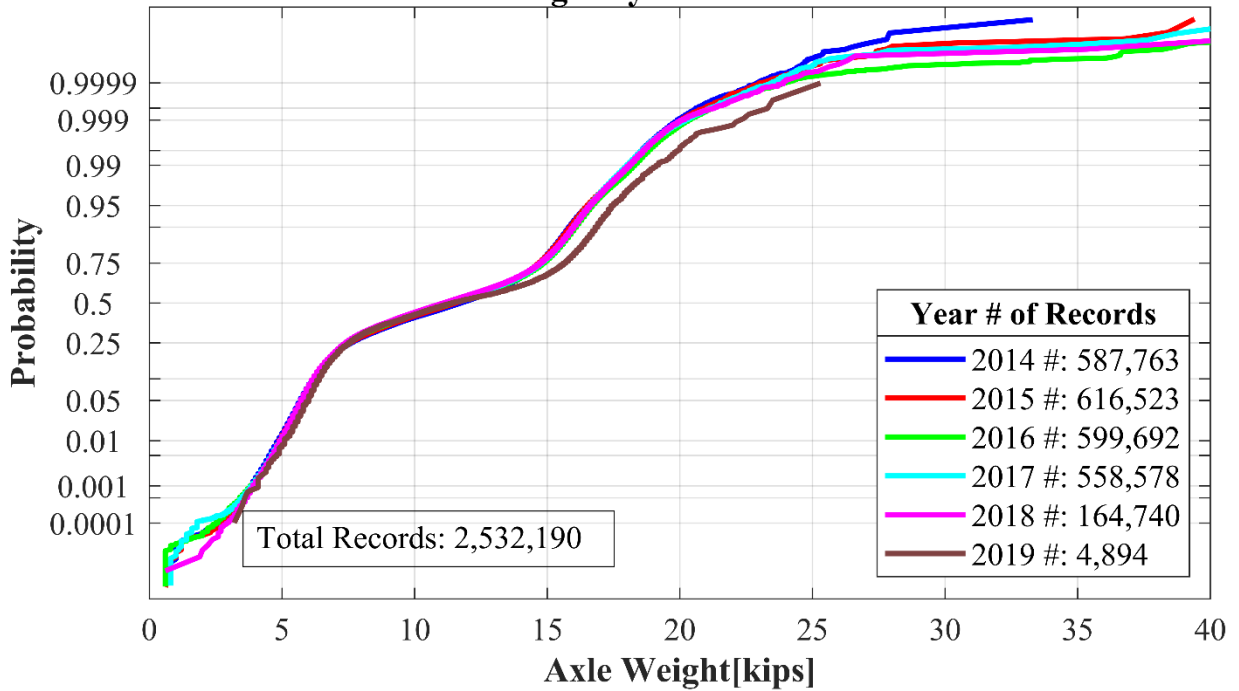
Class 9 #5 Axle Weight by Year CA-030 MT-SHASTA



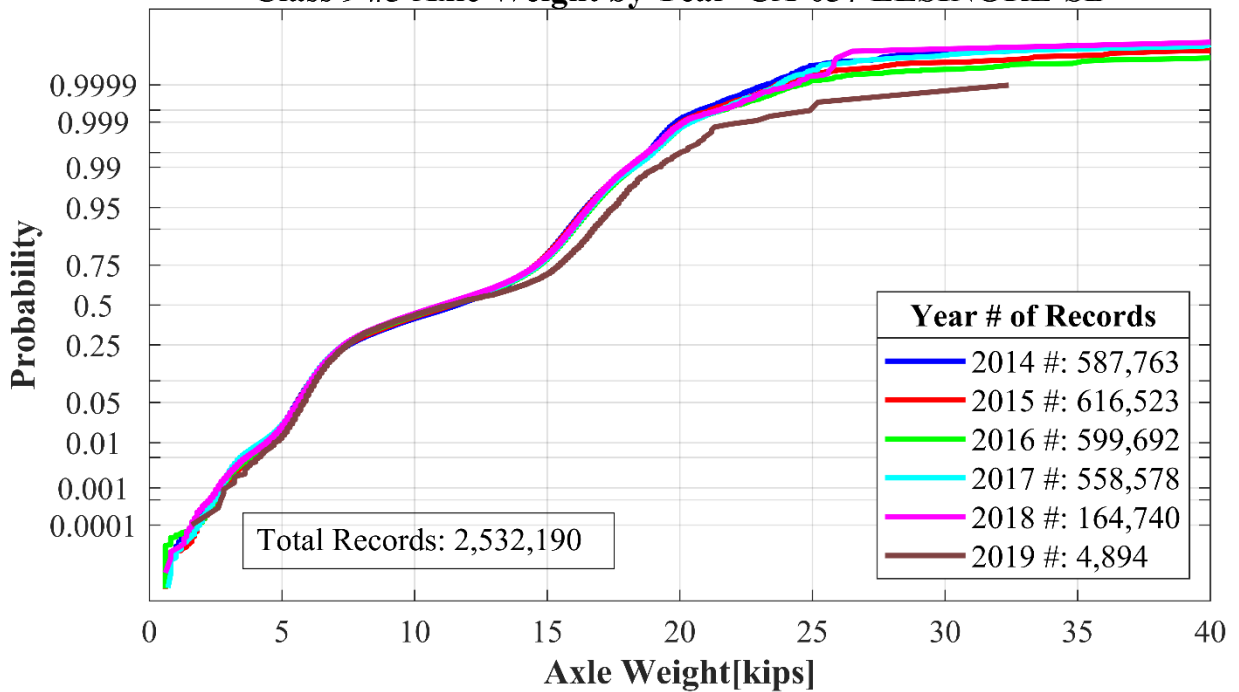
Class 9 #1 Axle Weight by Year CA-037 ELSINORE-SB



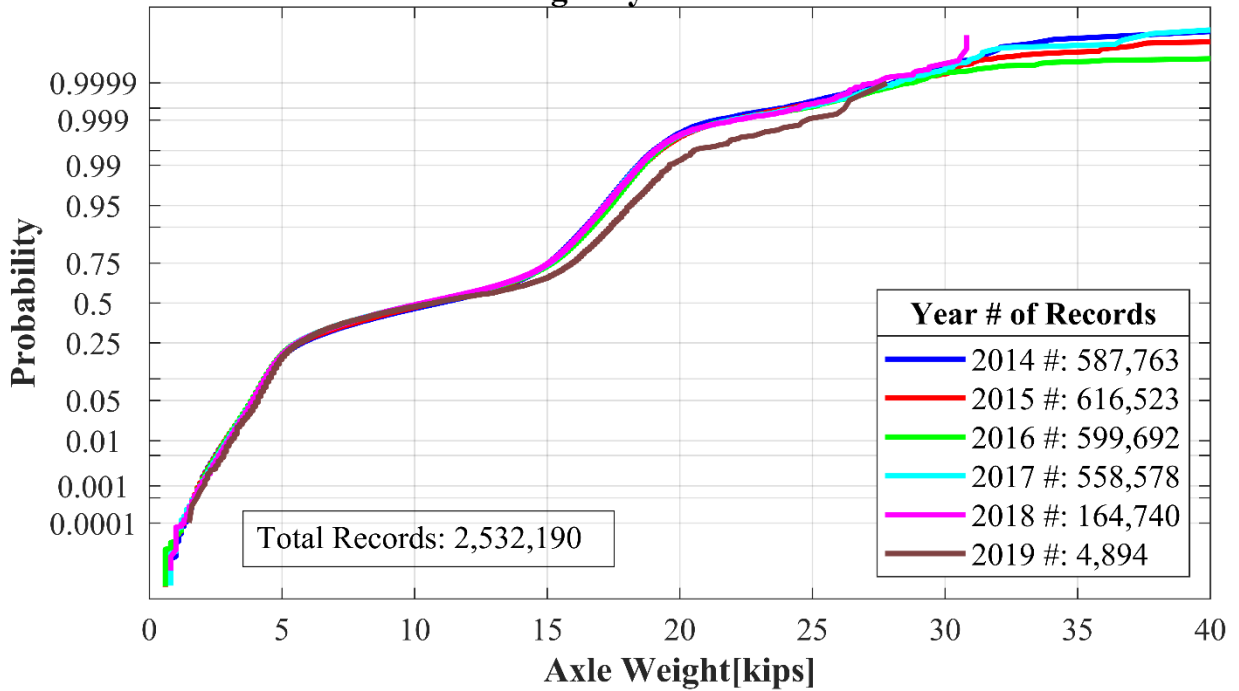
Class 9 #2 Axle Weight by Year CA-037 ELSINORE-SB



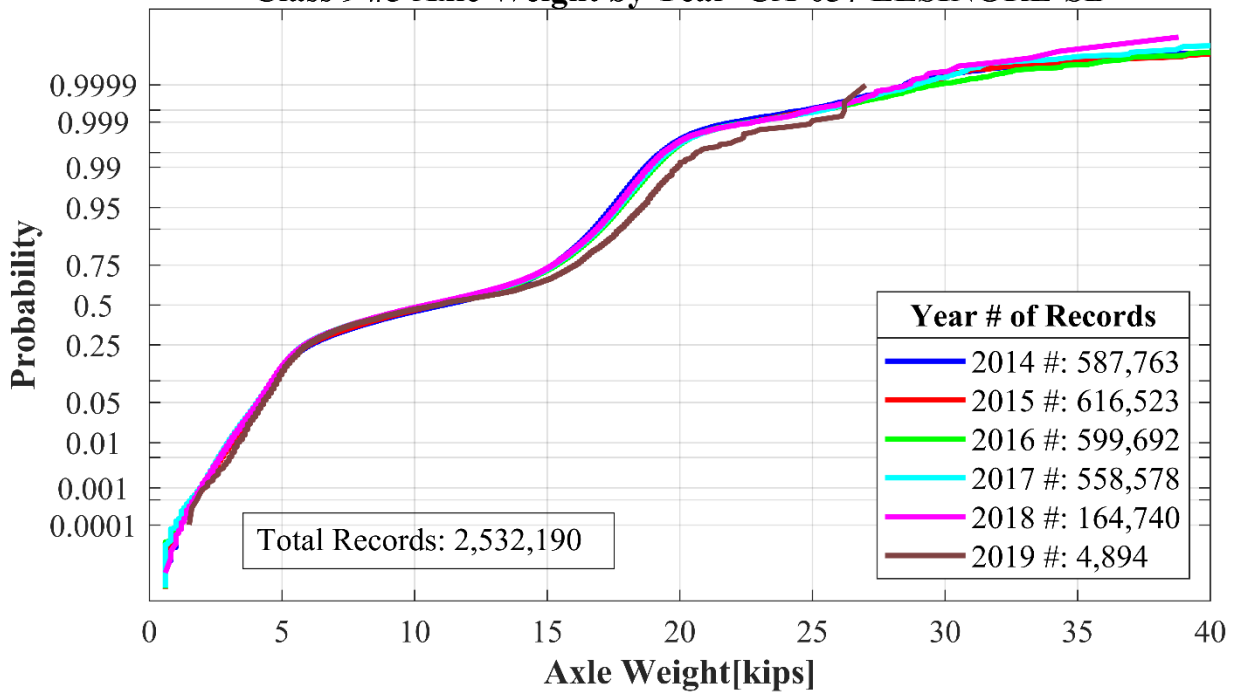
Class 9 #3 Axle Weight by Year CA-037 ELSINORE-SB



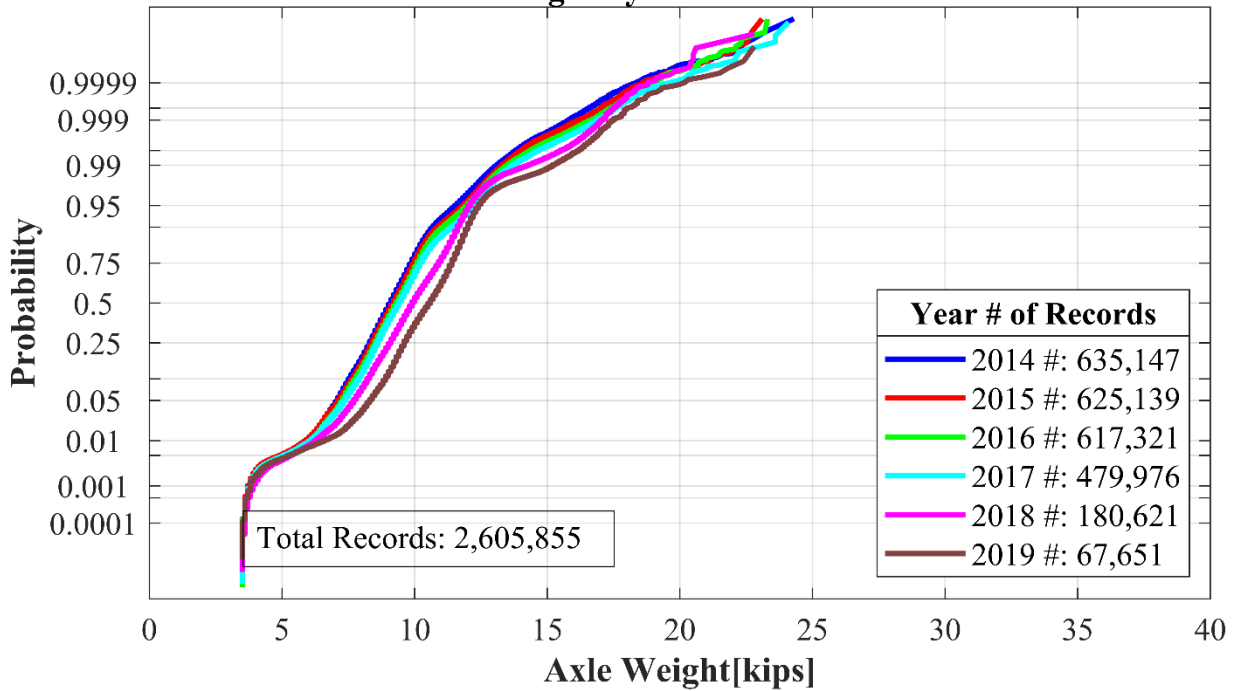
Class 9 #4 Axle Weight by Year CA-037 ELSINORE-SB



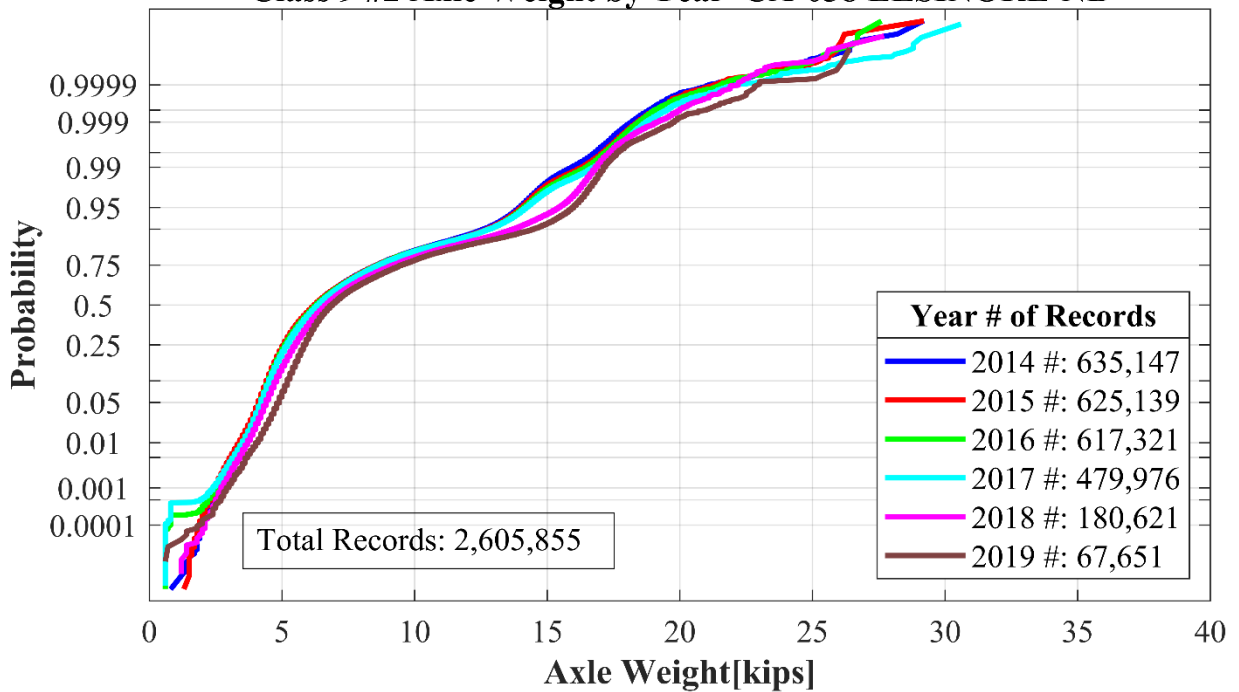
Class 9 #5 Axle Weight by Year CA-037 ELSINORE-SB



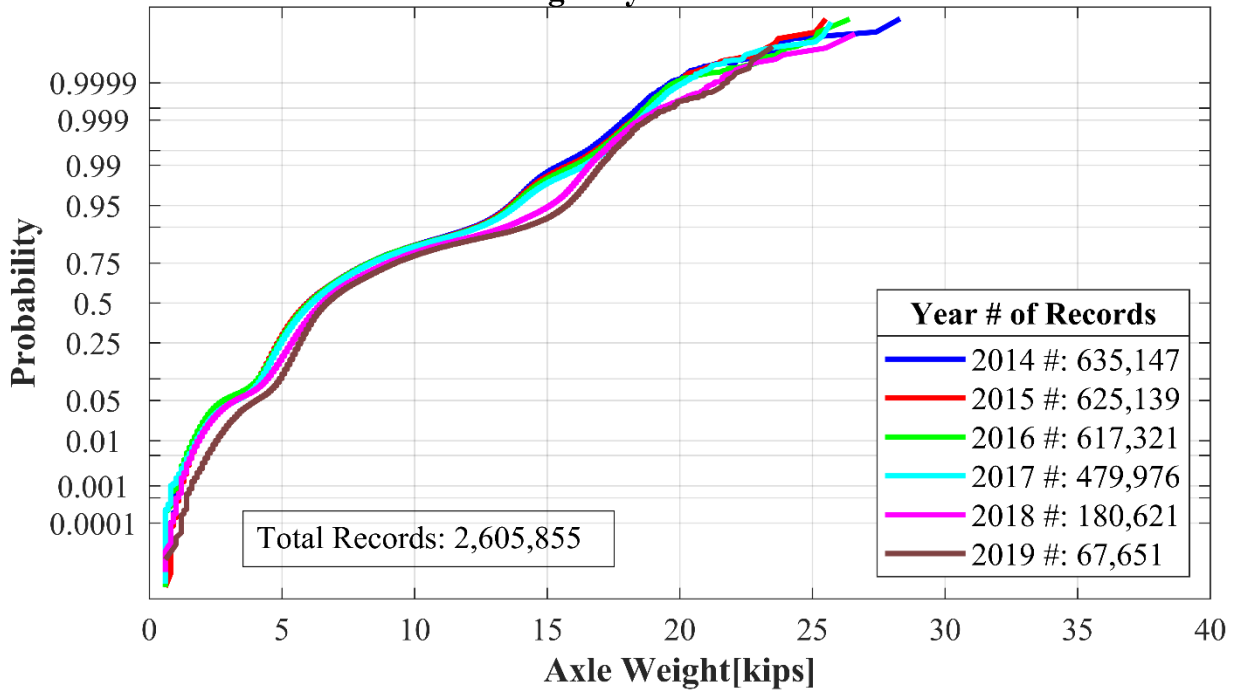
Class 9 #1 Axle Weight by Year CA-038 ELSINORE-NB



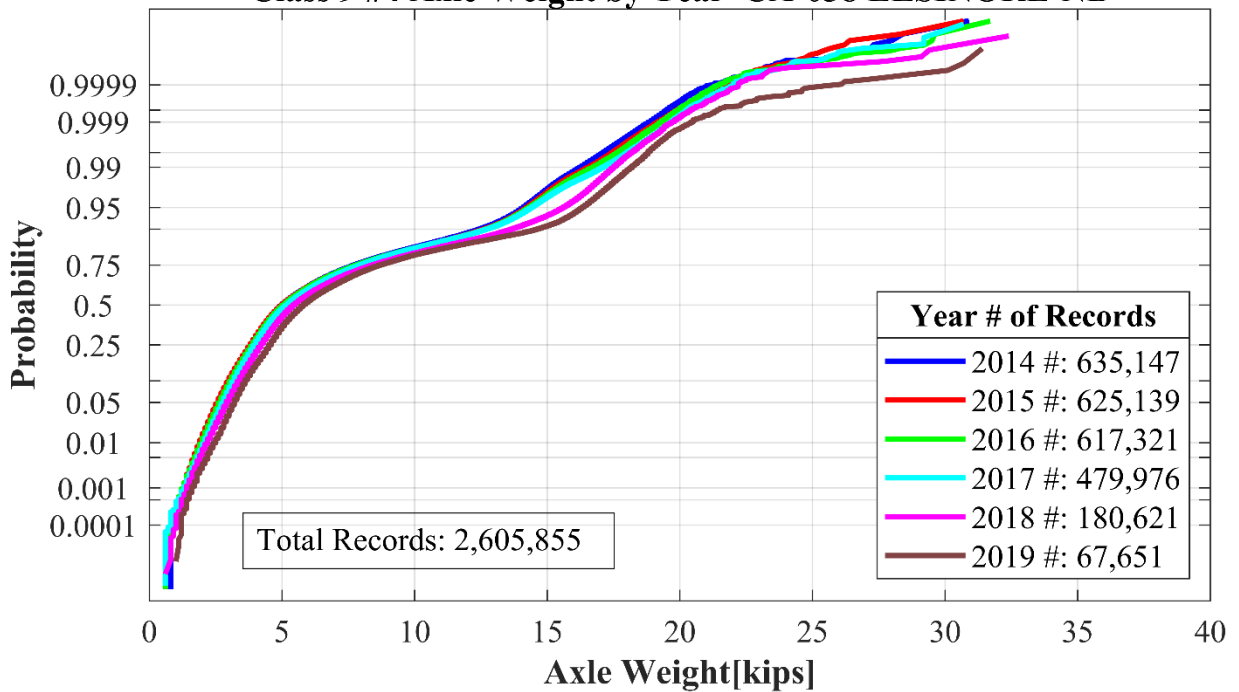
Class 9 #2 Axle Weight by Year CA-038 ELSINORE-NB



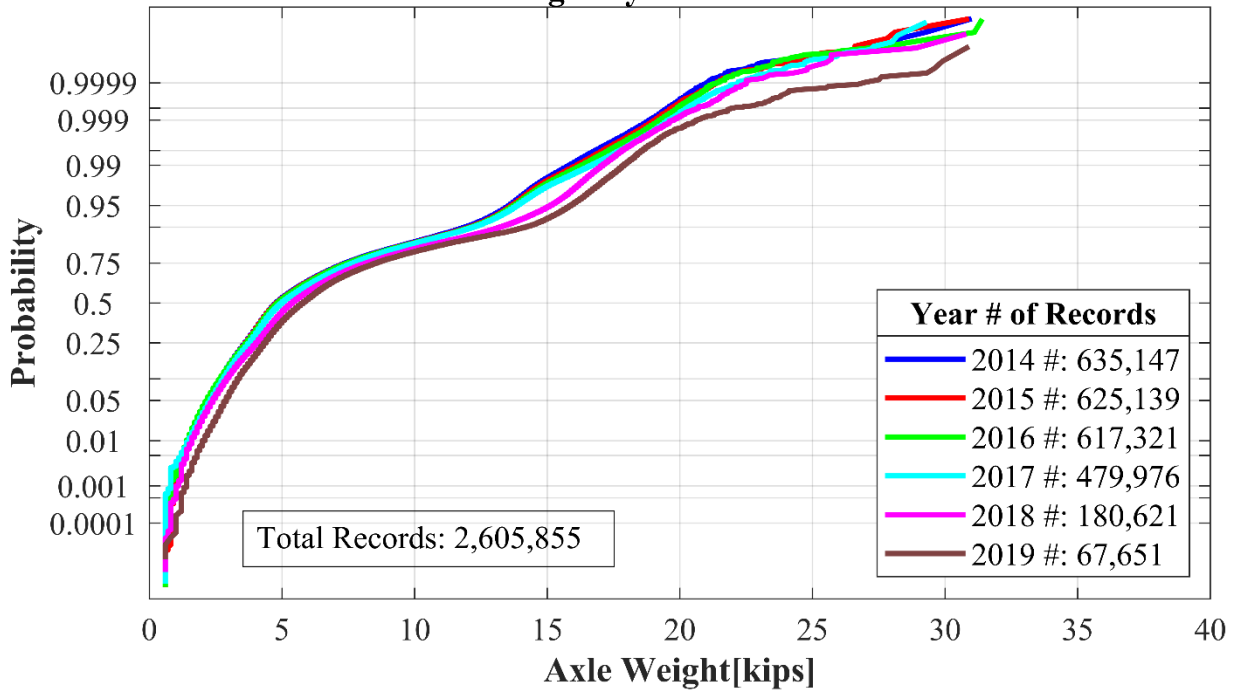
Class 9 #3 Axle Weight by Year CA-038 ELSINORE-NB



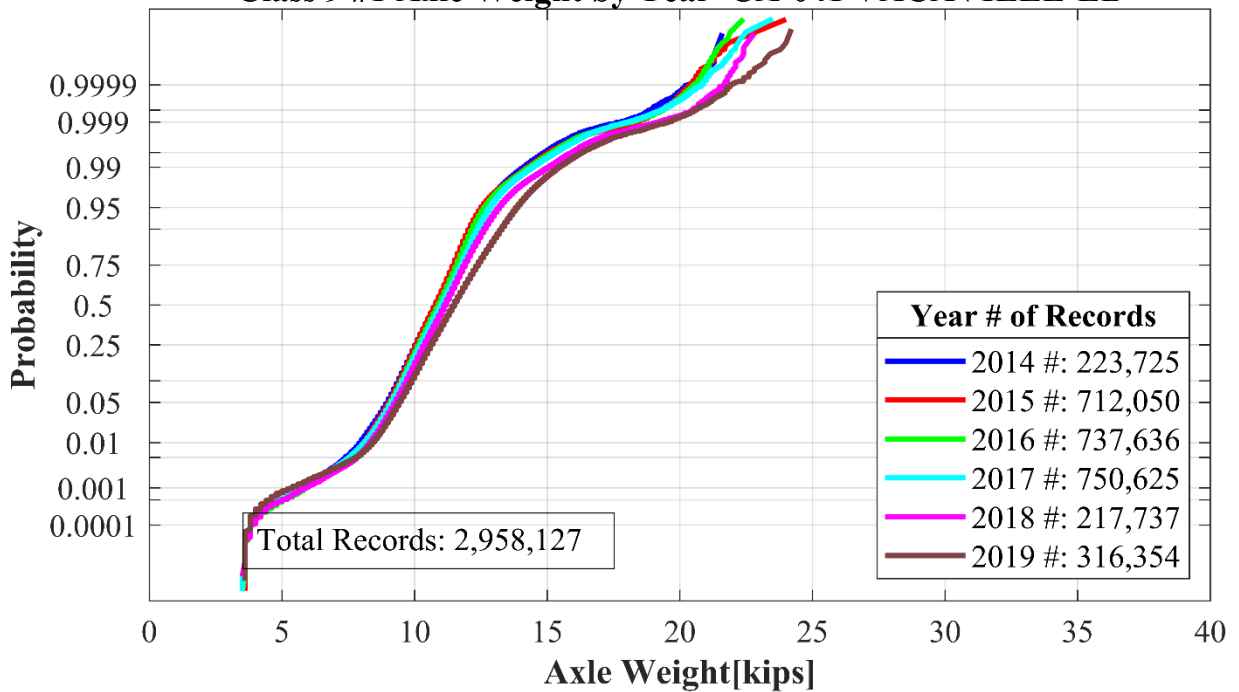
Class 9 #4 Axle Weight by Year CA-038 ELSINORE-NB



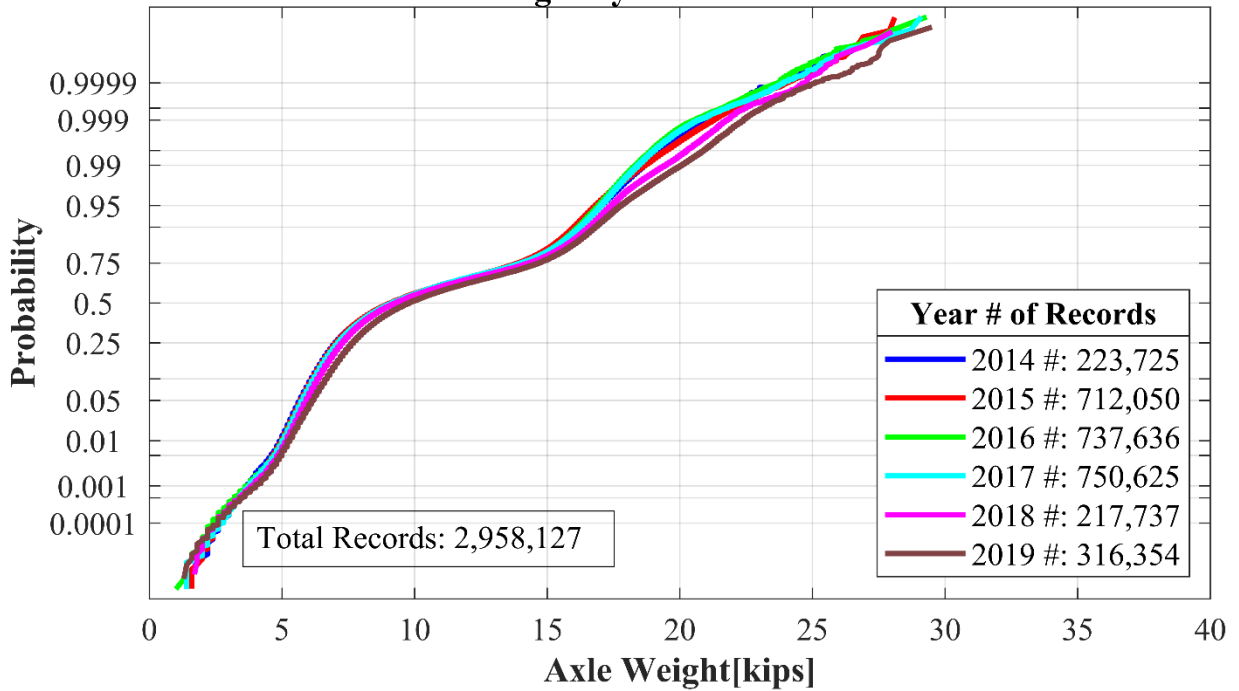
Class 9 #5 Axle Weight by Year CA-038 ELSINORE-NB



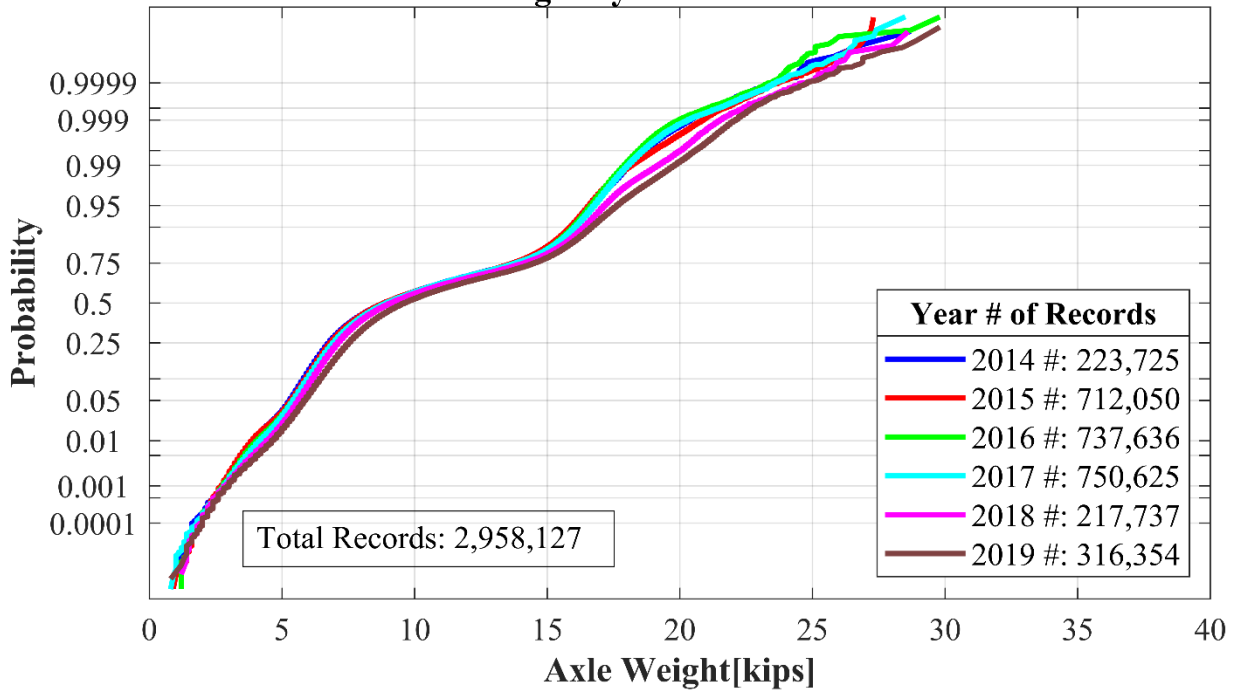
Class 9 #1 Axle Weight by Year CA-041 VACAVILLE-EB



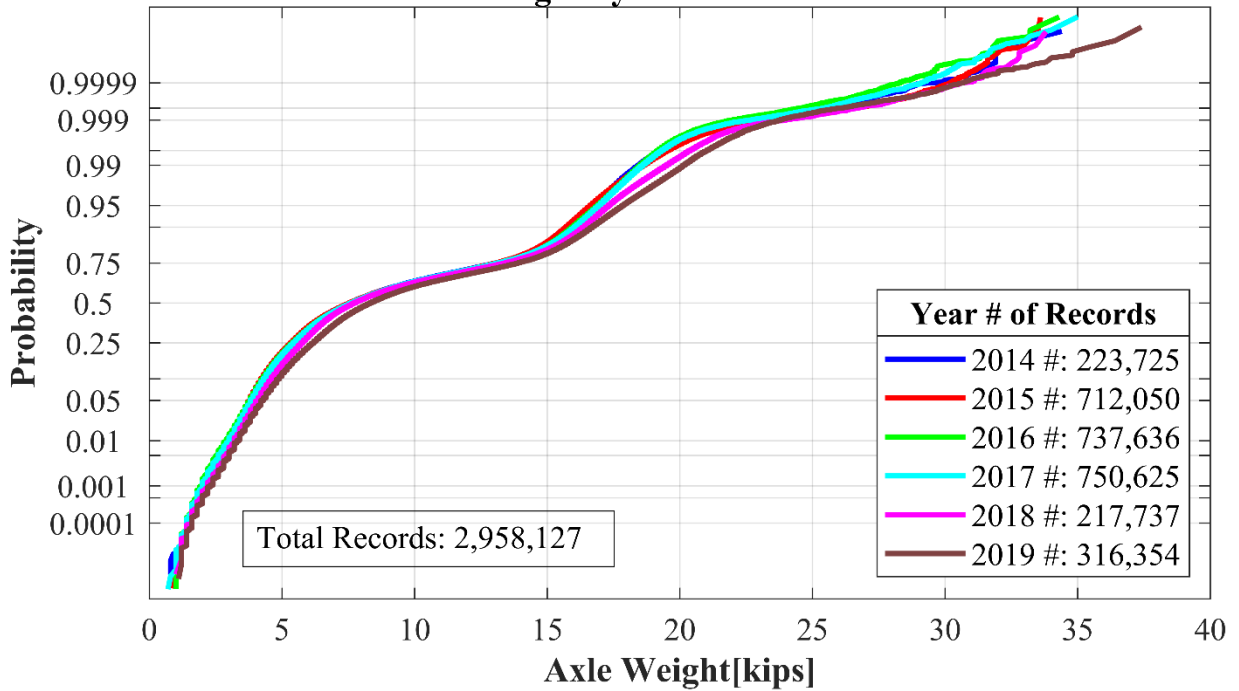
Class 9 #2 Axle Weight by Year CA-041 VACAVILLE-EB



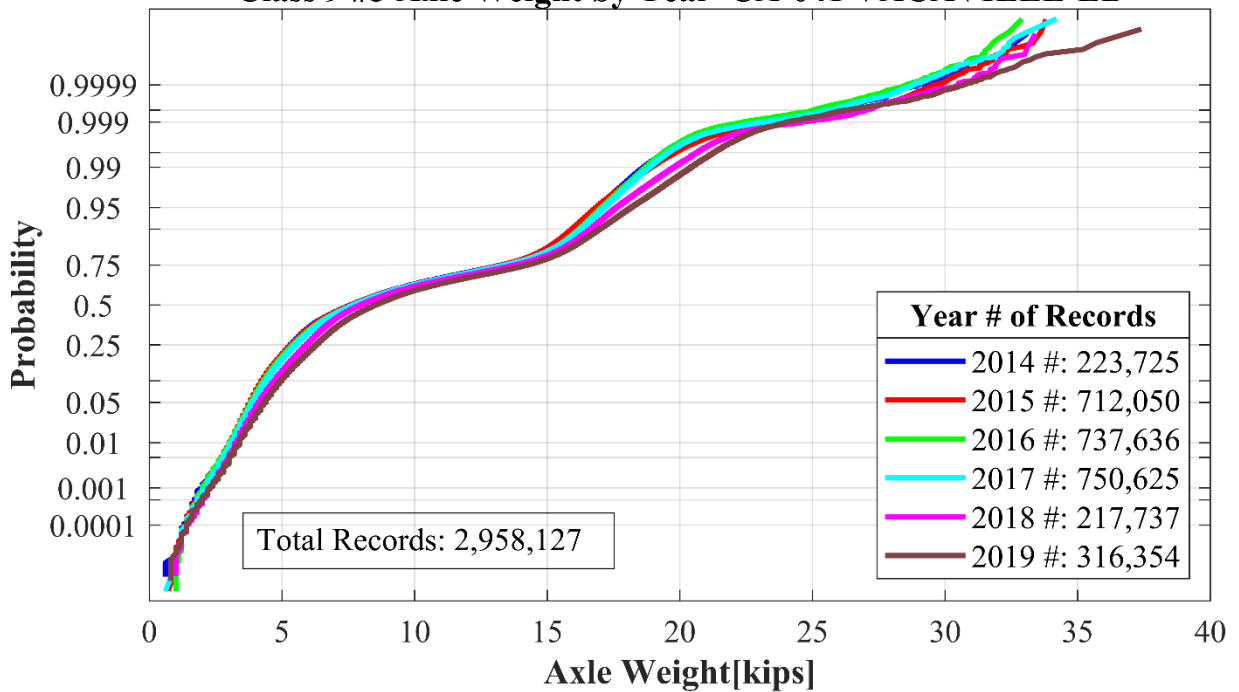
Class 9 #3 Axle Weight by Year CA-041 VACAVILLE-EB



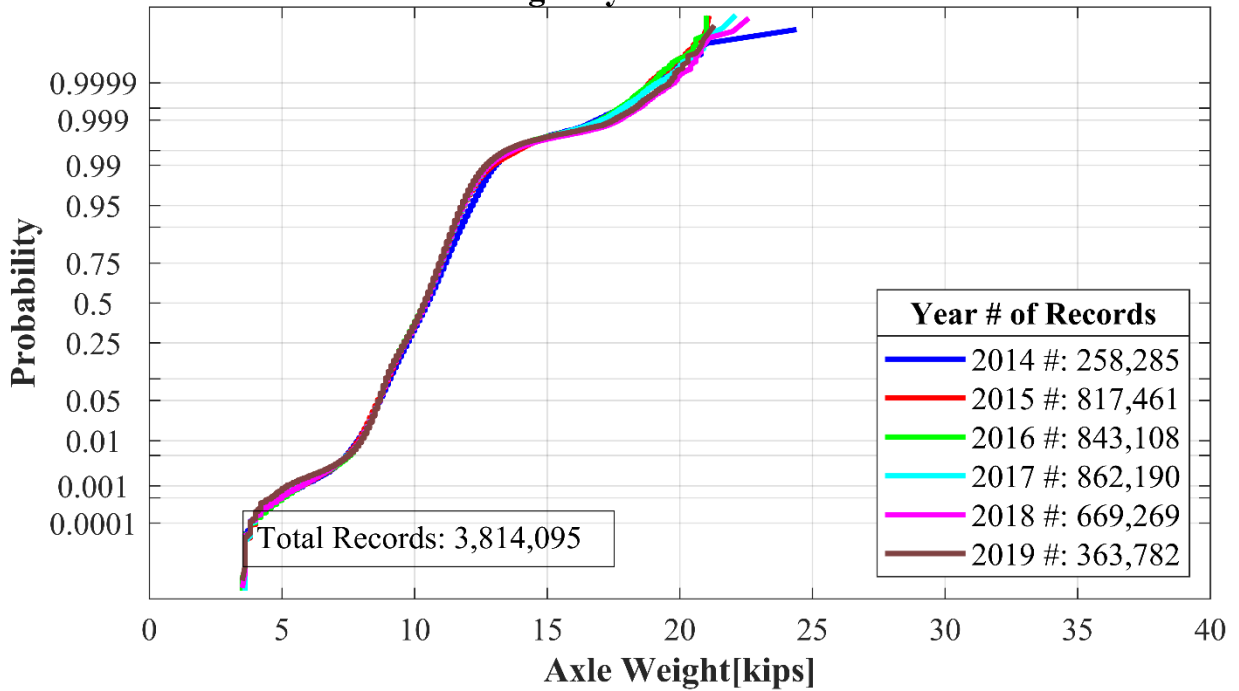
Class 9 #4 Axle Weight by Year CA-041 VACAVILLE-EB



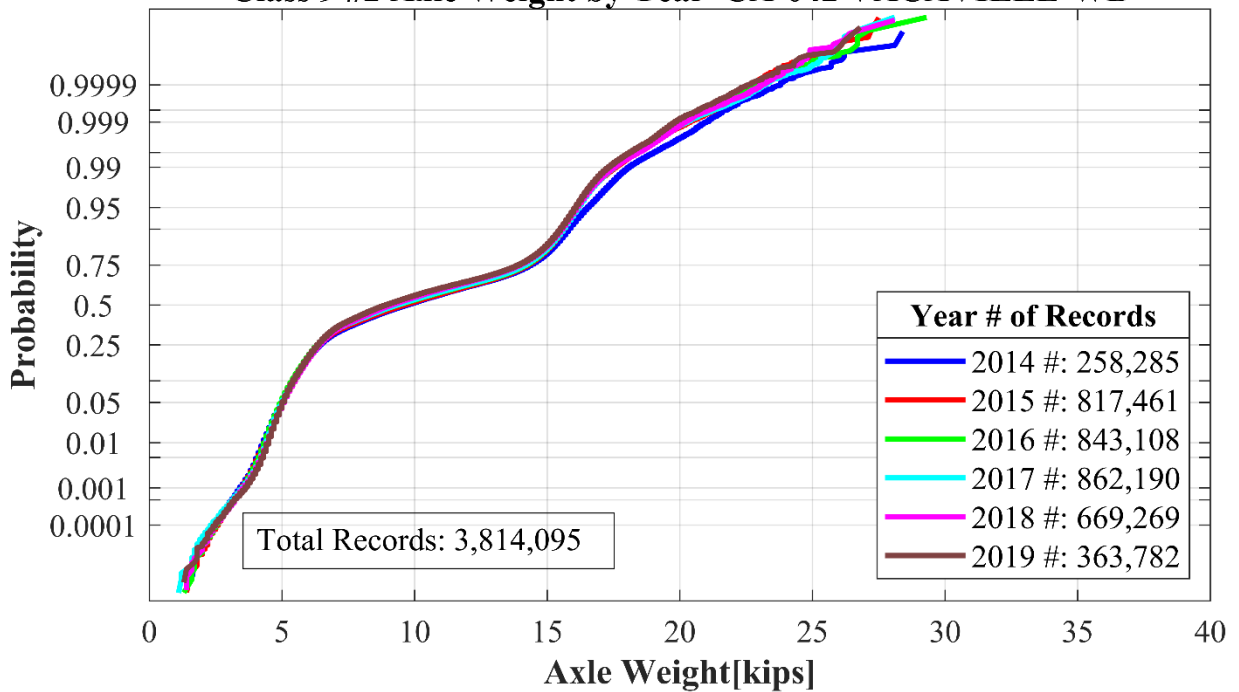
Class 9 #5 Axle Weight by Year CA-041 VACAVILLE-EB



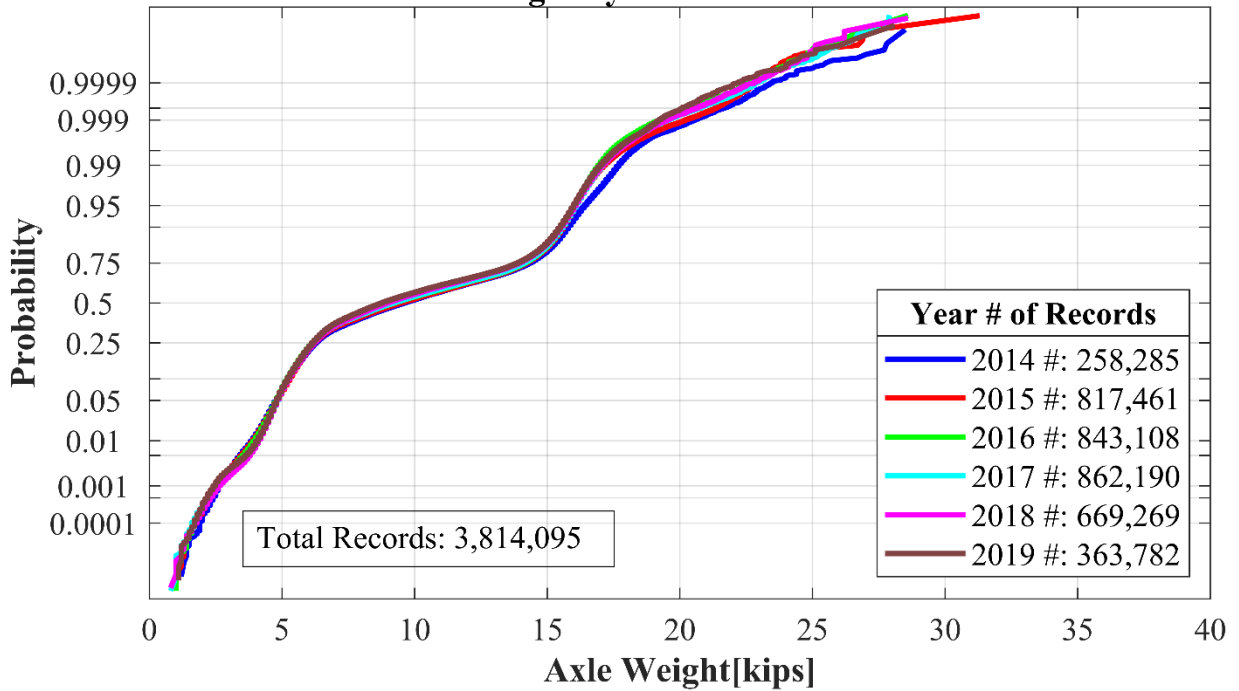
Class 9 #1 Axle Weight by Year CA-042 VACAVILLE-WB



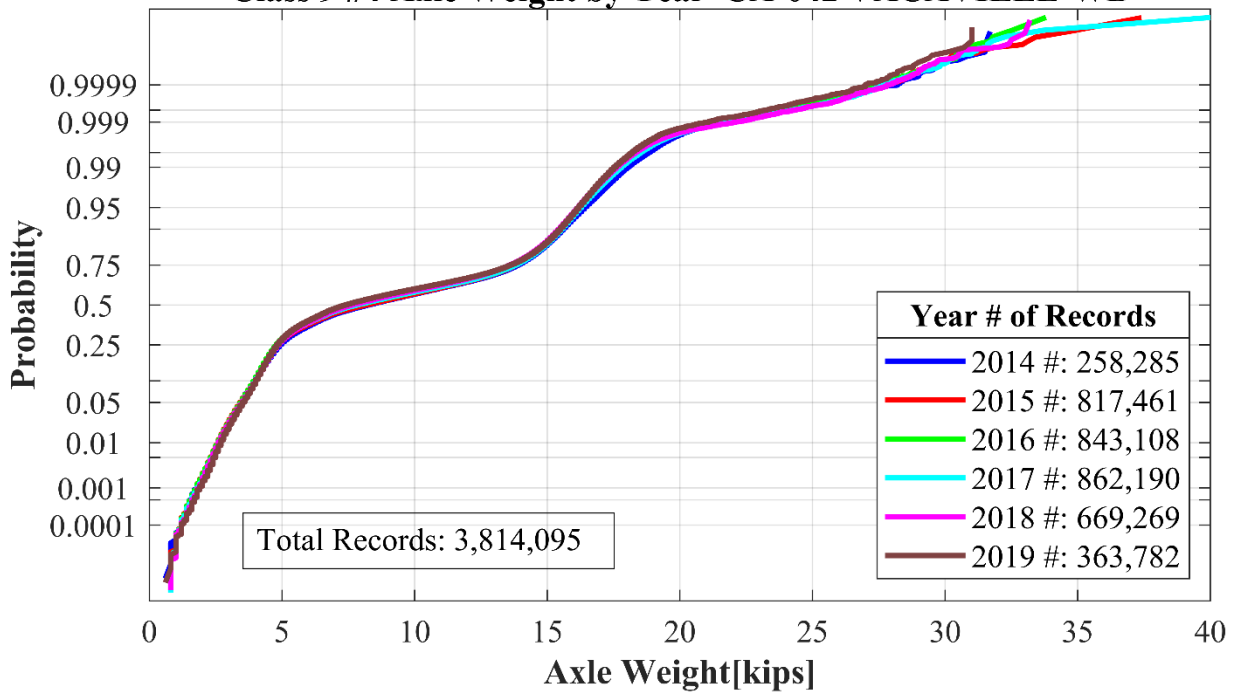
Class 9 #2 Axle Weight by Year CA-042 VACAVILLE-WB



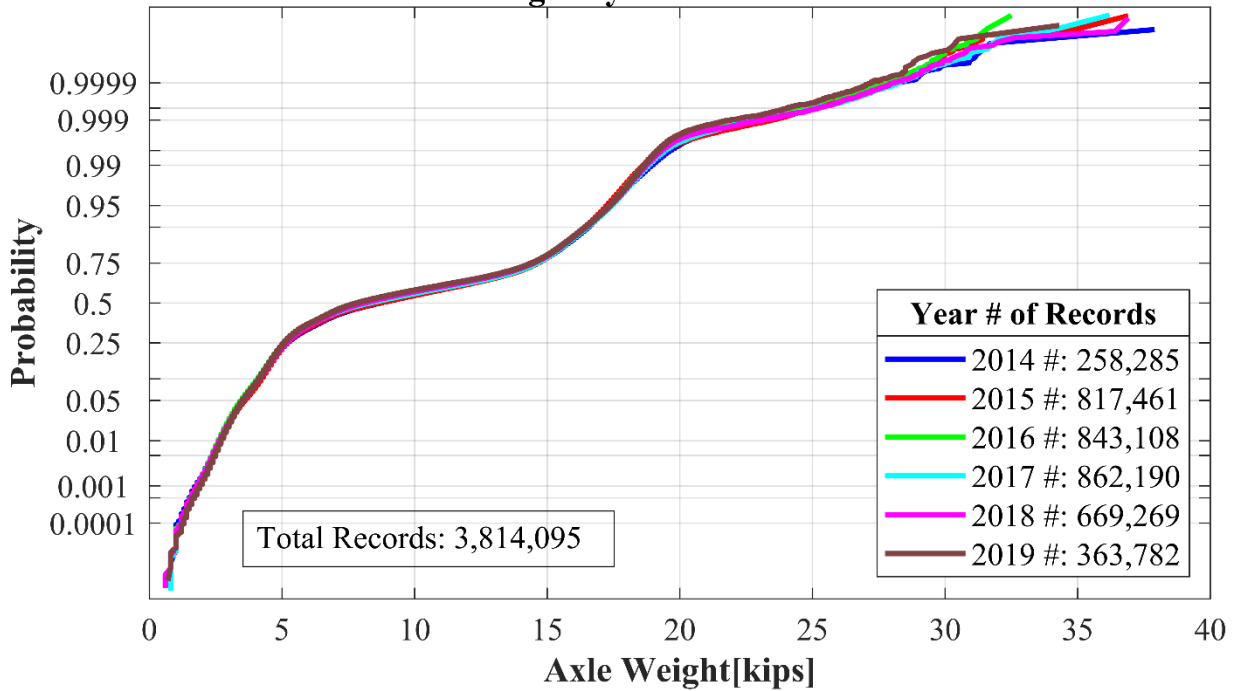
Class 9 #3 Axle Weight by Year CA-042 VACAVILLE-WB



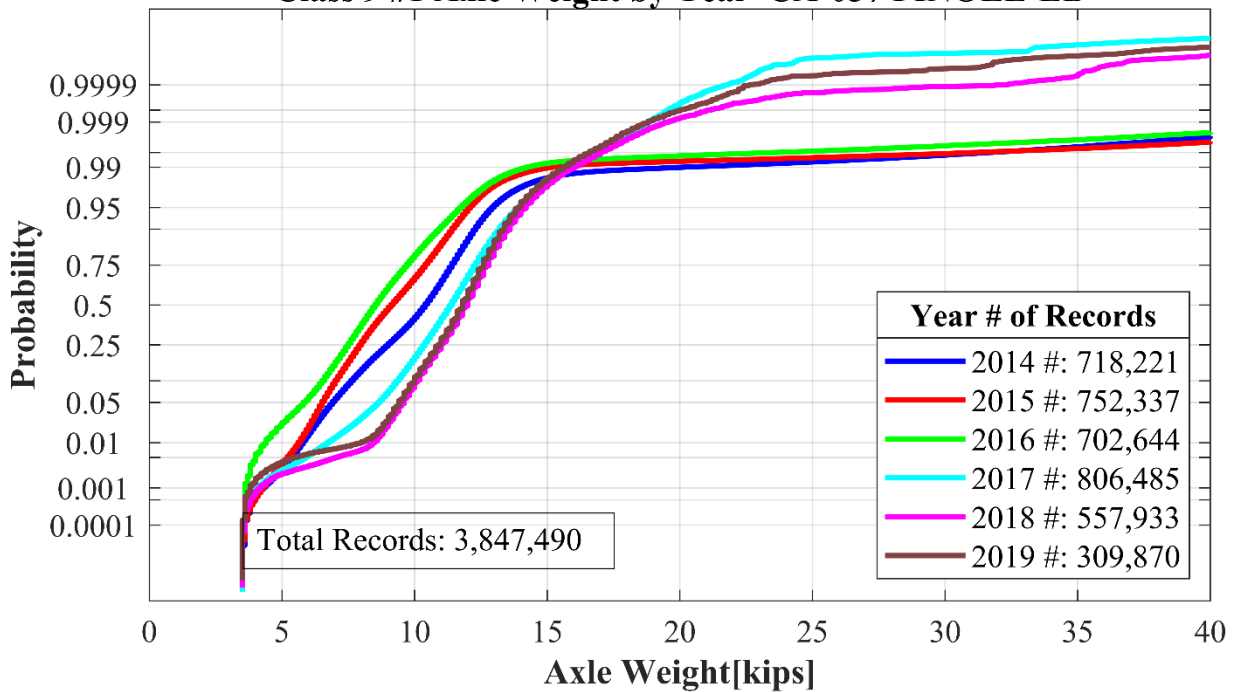
Class 9 #4 Axle Weight by Year CA-042 VACAVILLE-WB



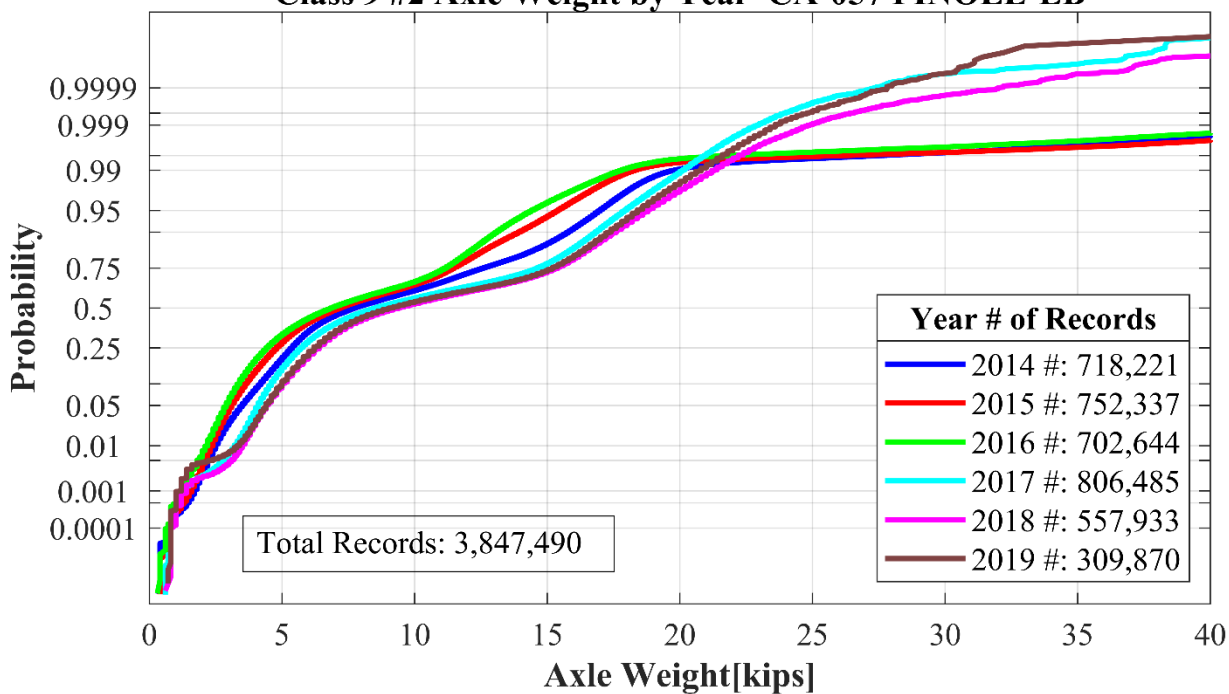
Class 9 #5 Axle Weight by Year CA-042 VACAVILLE-WB



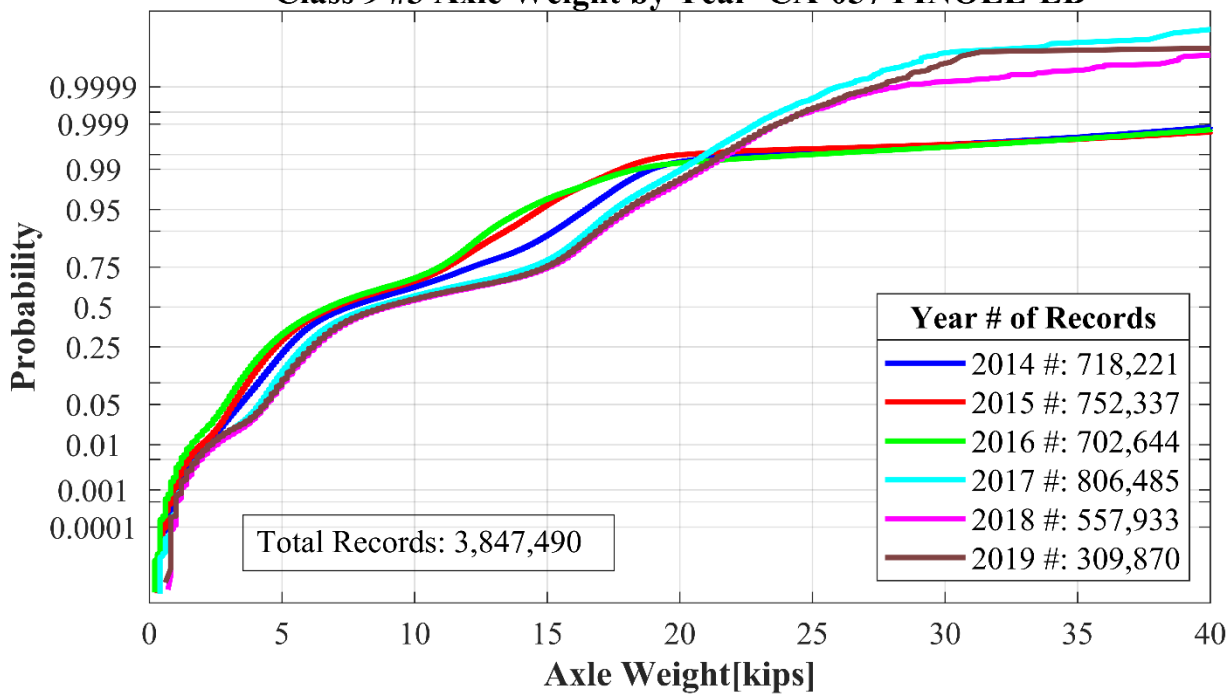
Class 9 #1 Axle Weight by Year CA-057 PINOLE-EB



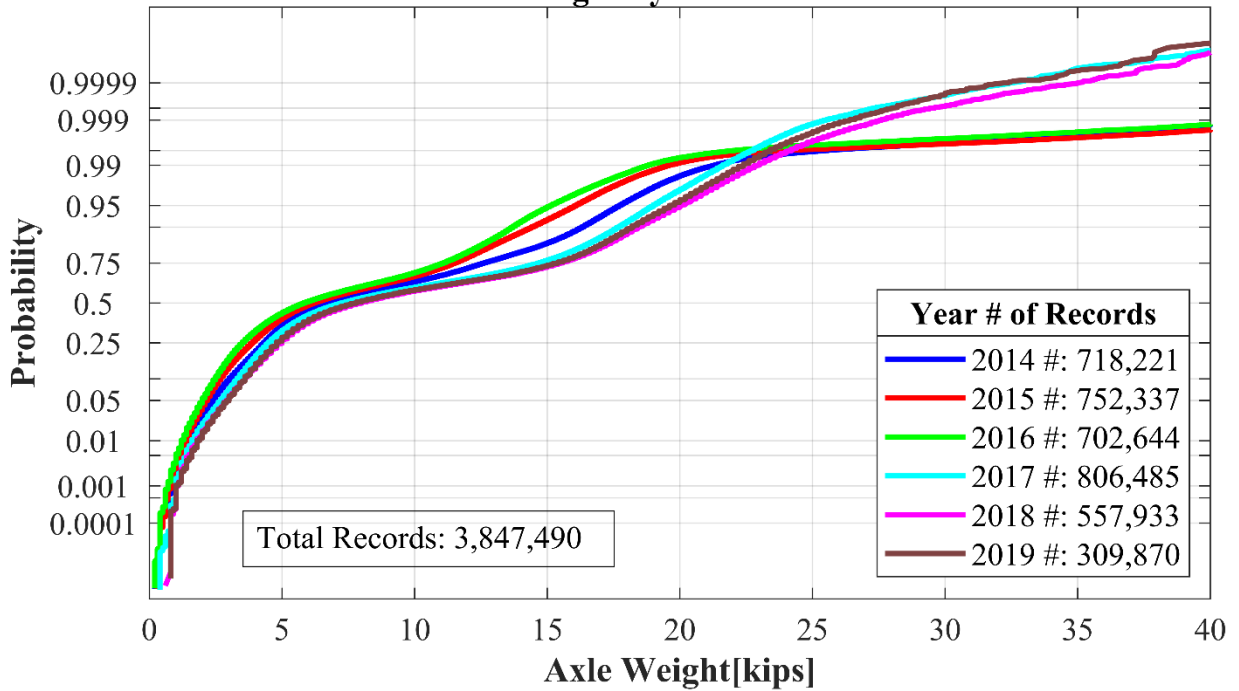
Class 9 #2 Axle Weight by Year CA-057 PINOLE-EB



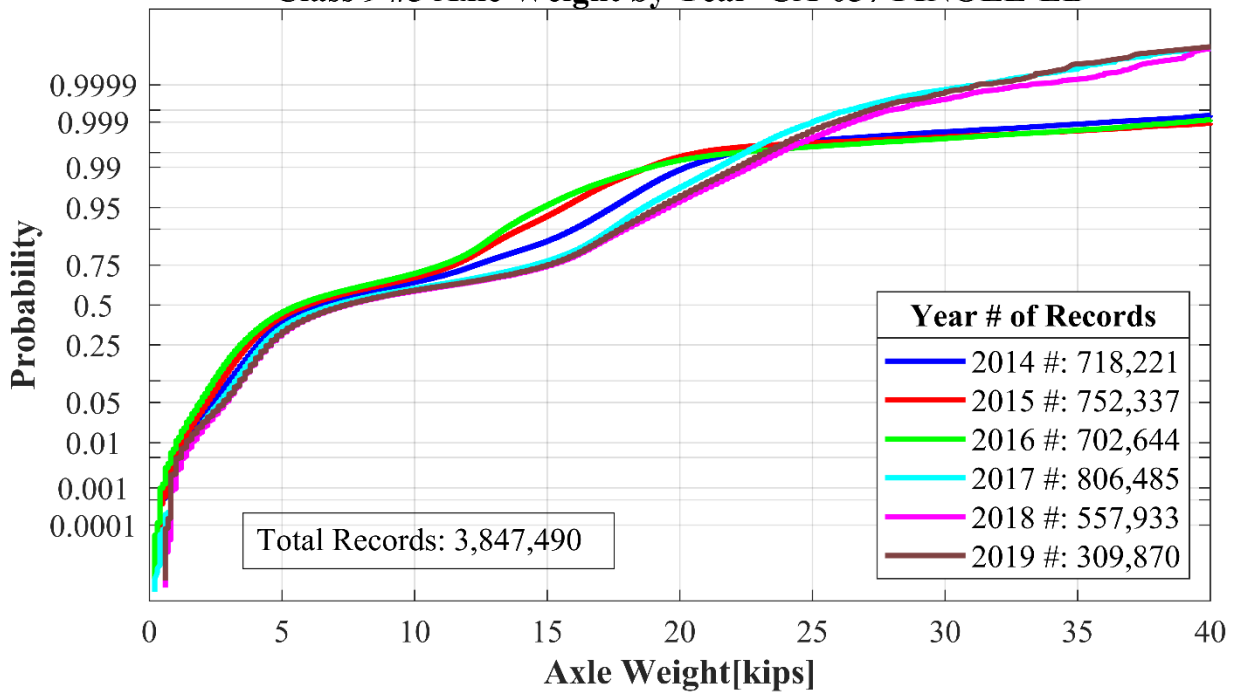
Class 9 #3 Axle Weight by Year CA-057 PINOLE-EB



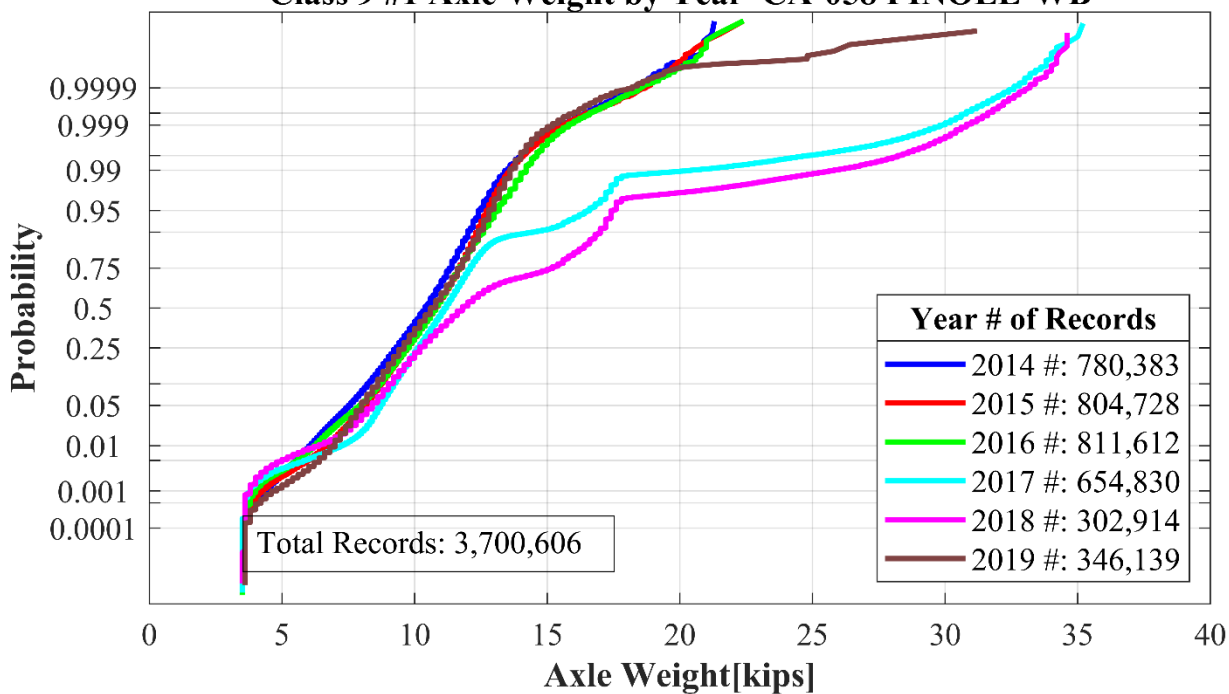
Class 9 #4 Axle Weight by Year CA-057 PINOLE-EB



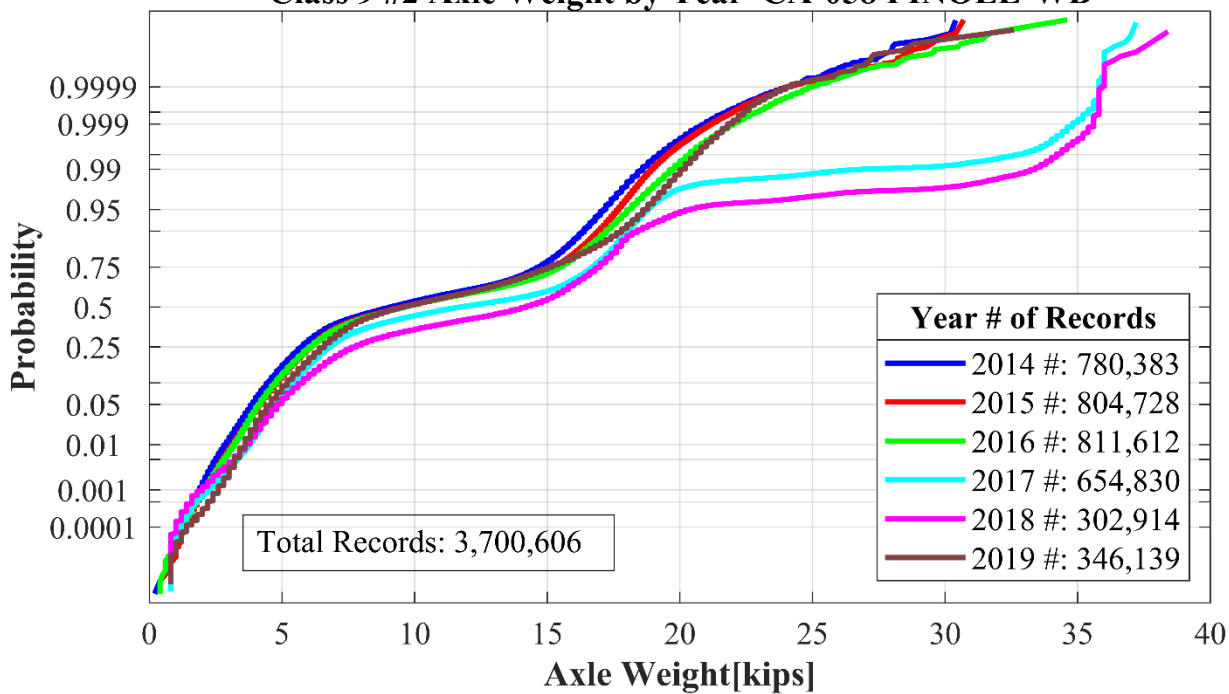
Class 9 #5 Axle Weight by Year CA-057 PINOLE-EB



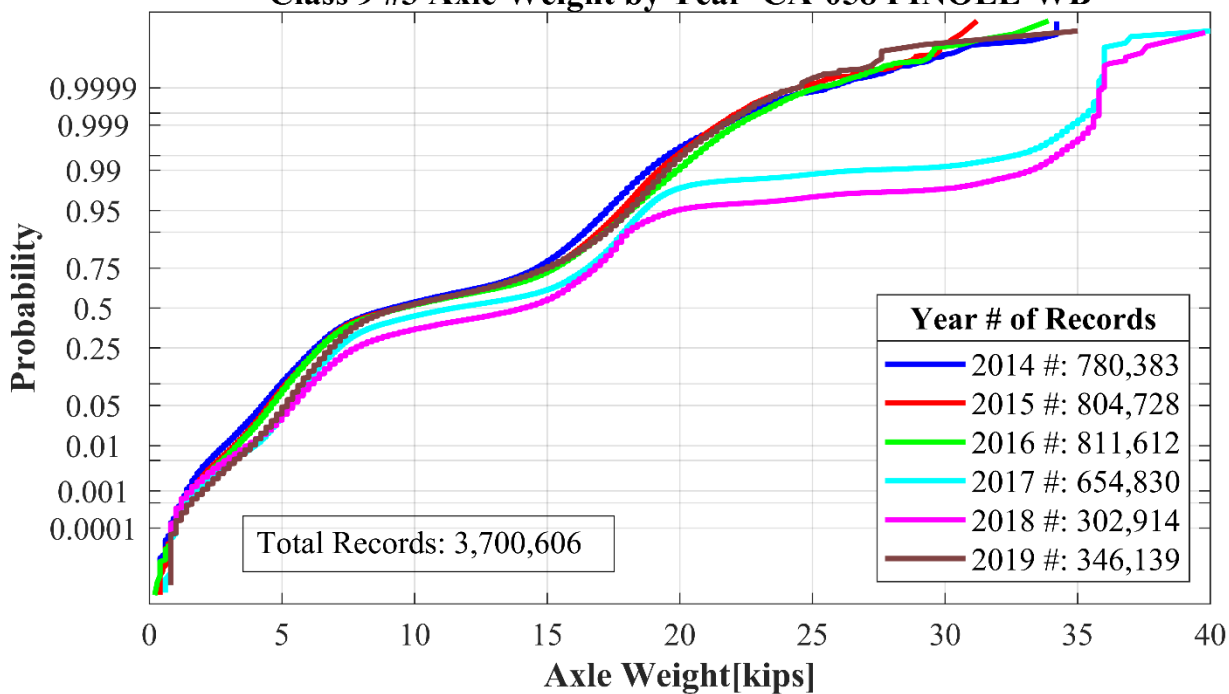
Class 9 #1 Axle Weight by Year CA-058 PINOLE-WB



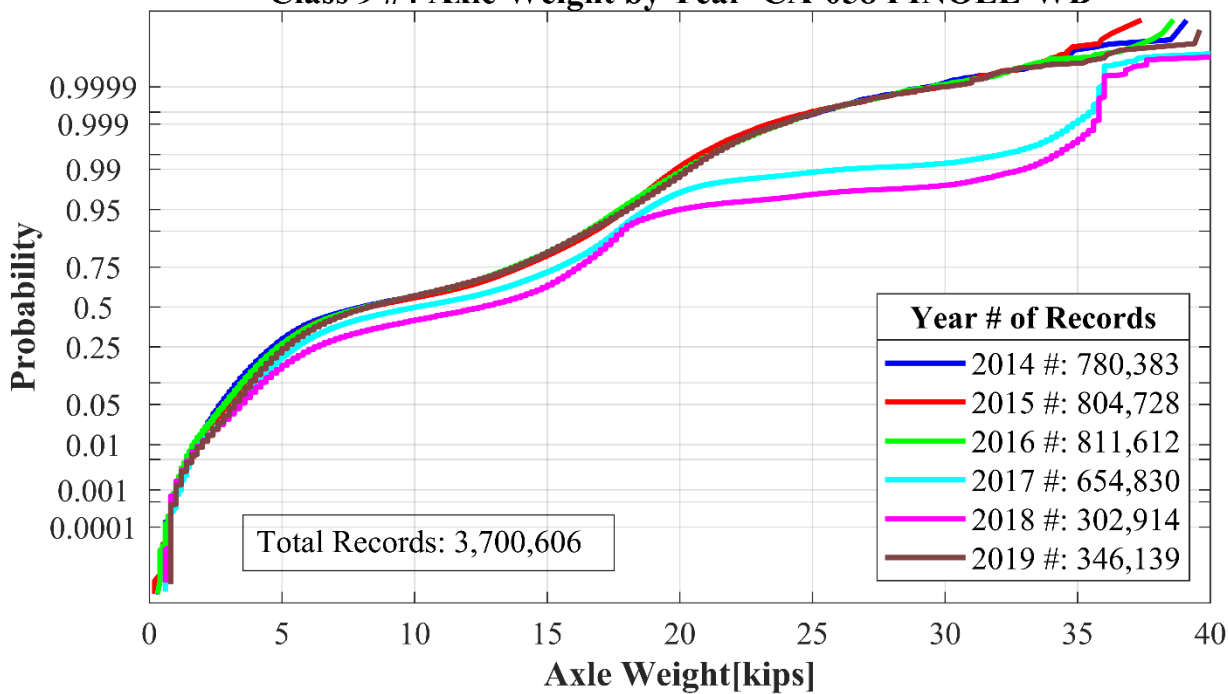
Class 9 #2 Axle Weight by Year CA-058 PINOLE-WB



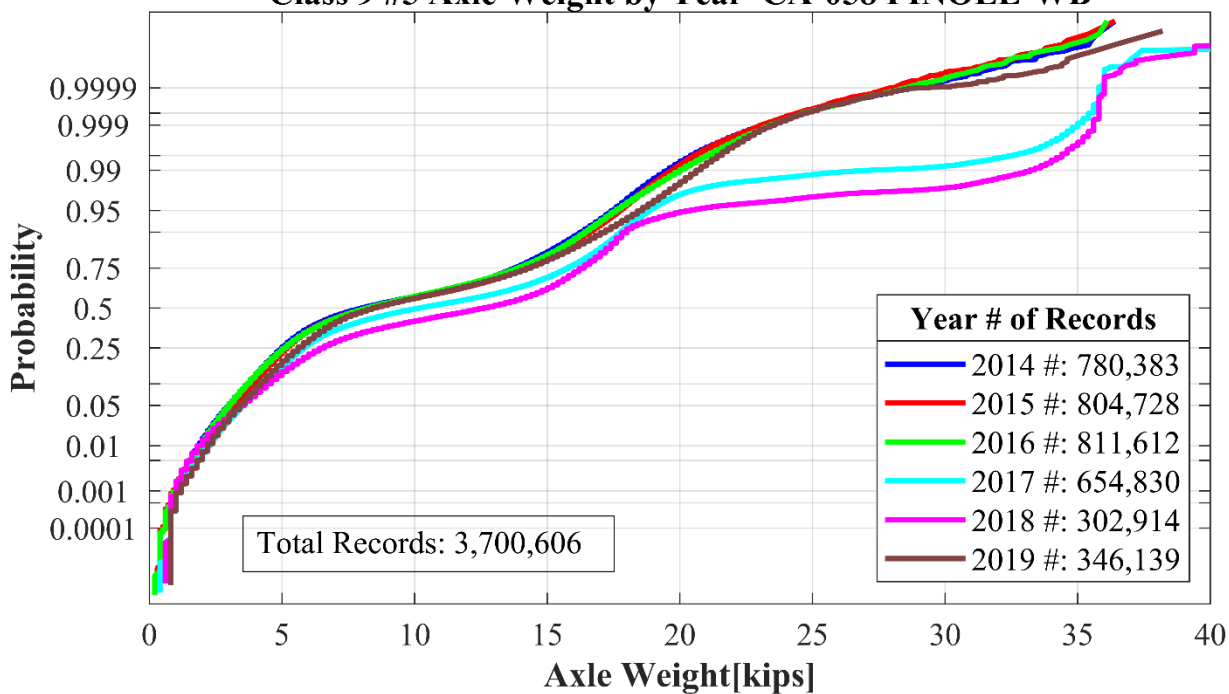
Class 9 #3 Axle Weight by Year CA-058 PINOLE-WB



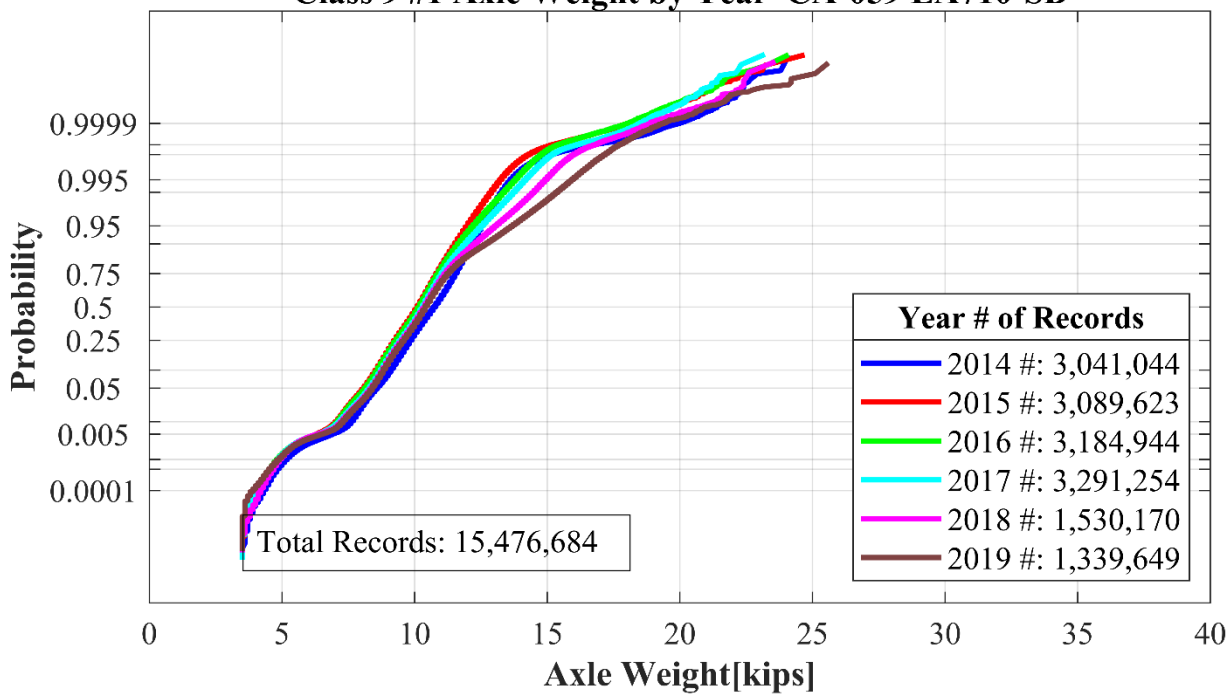
Class 9 #4 Axle Weight by Year CA-058 PINOLE-WB

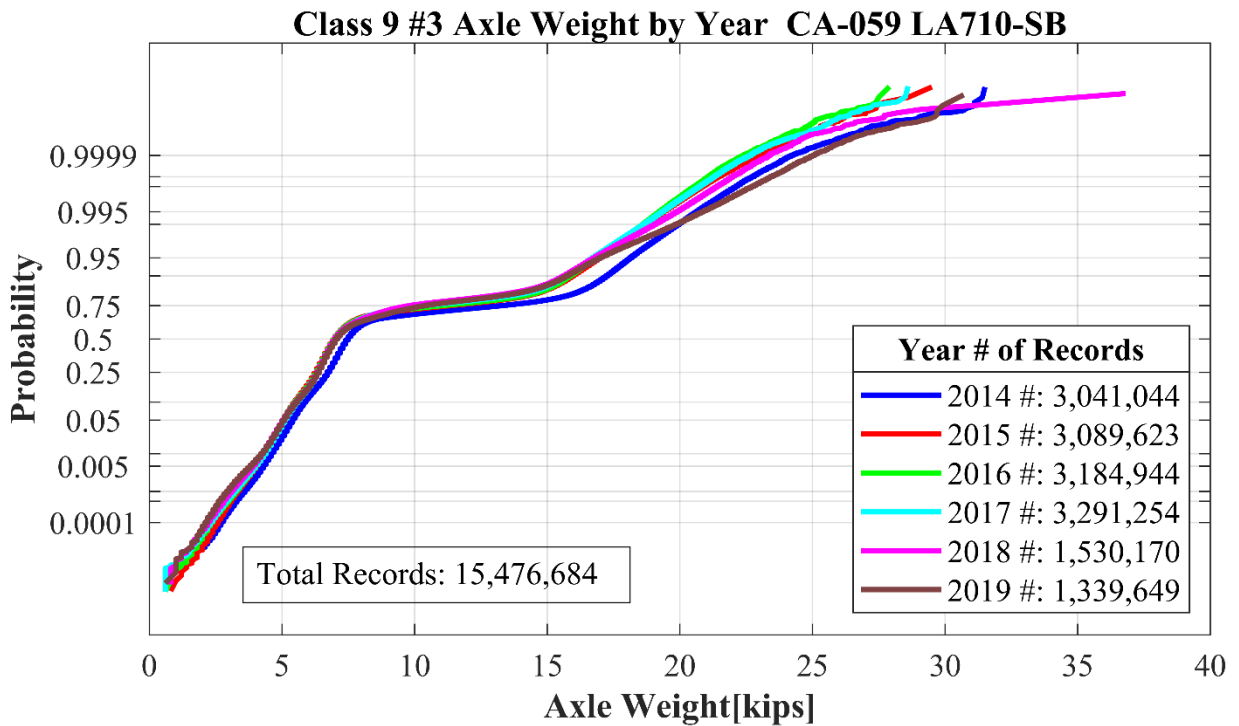
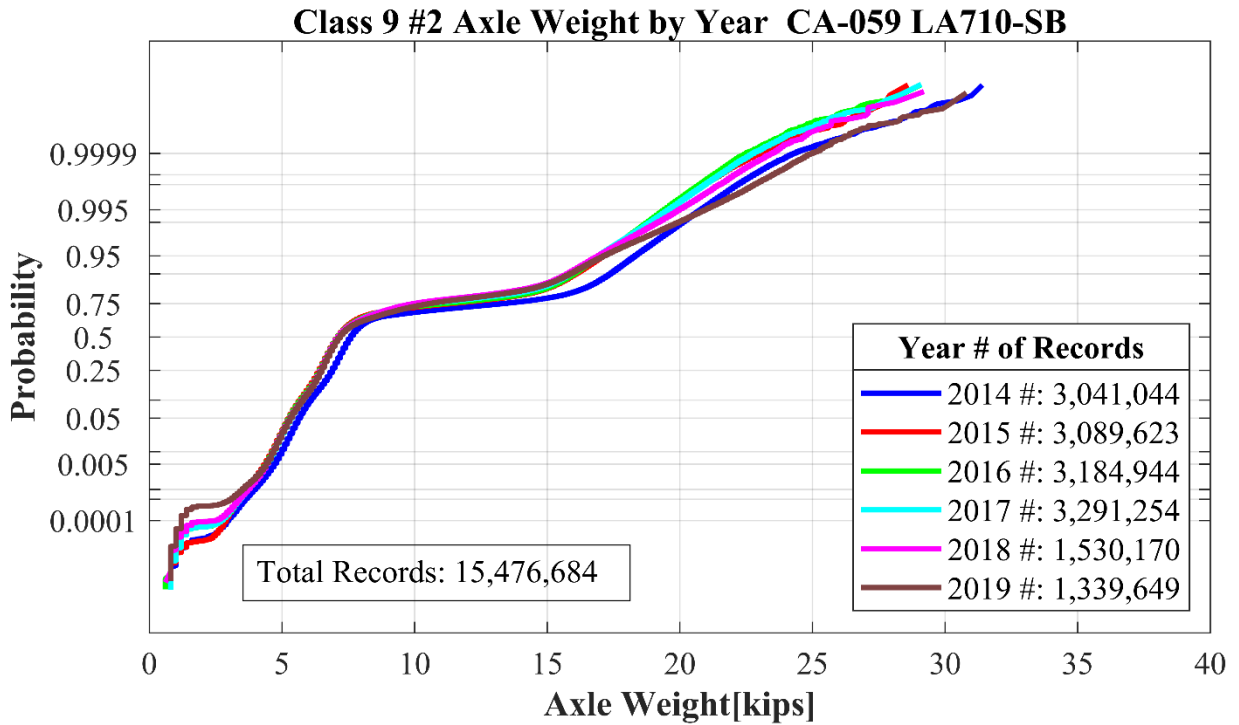


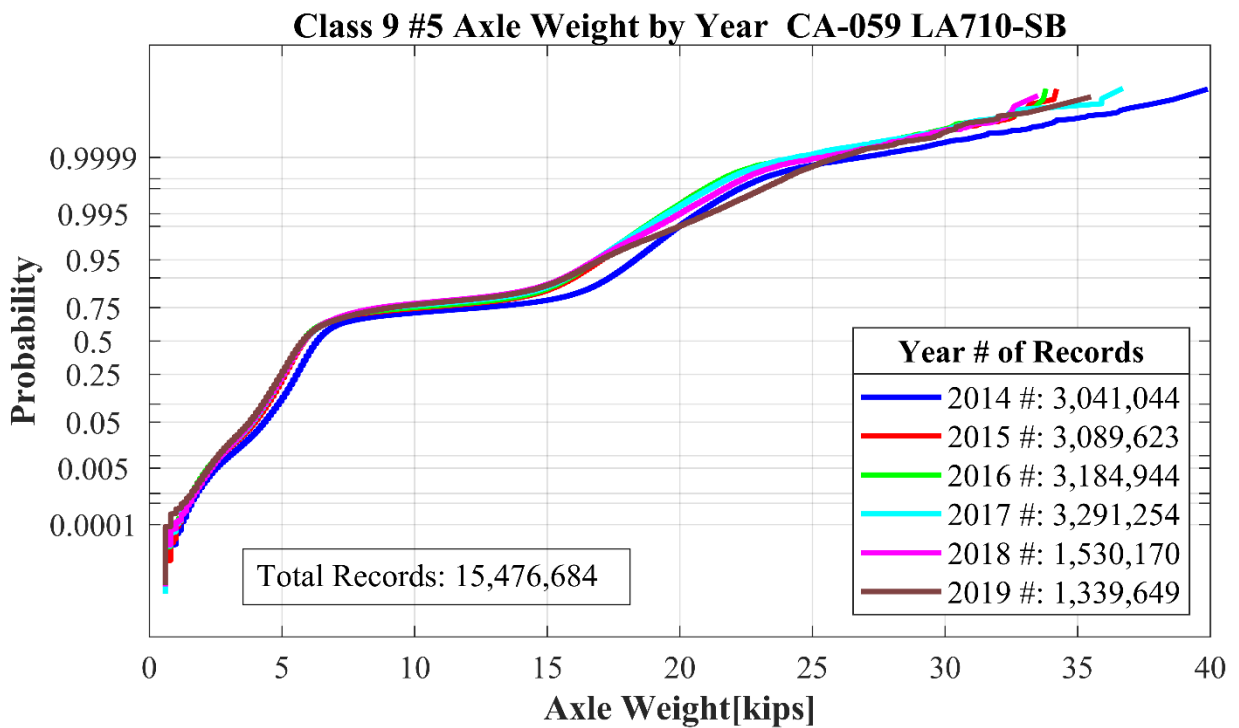
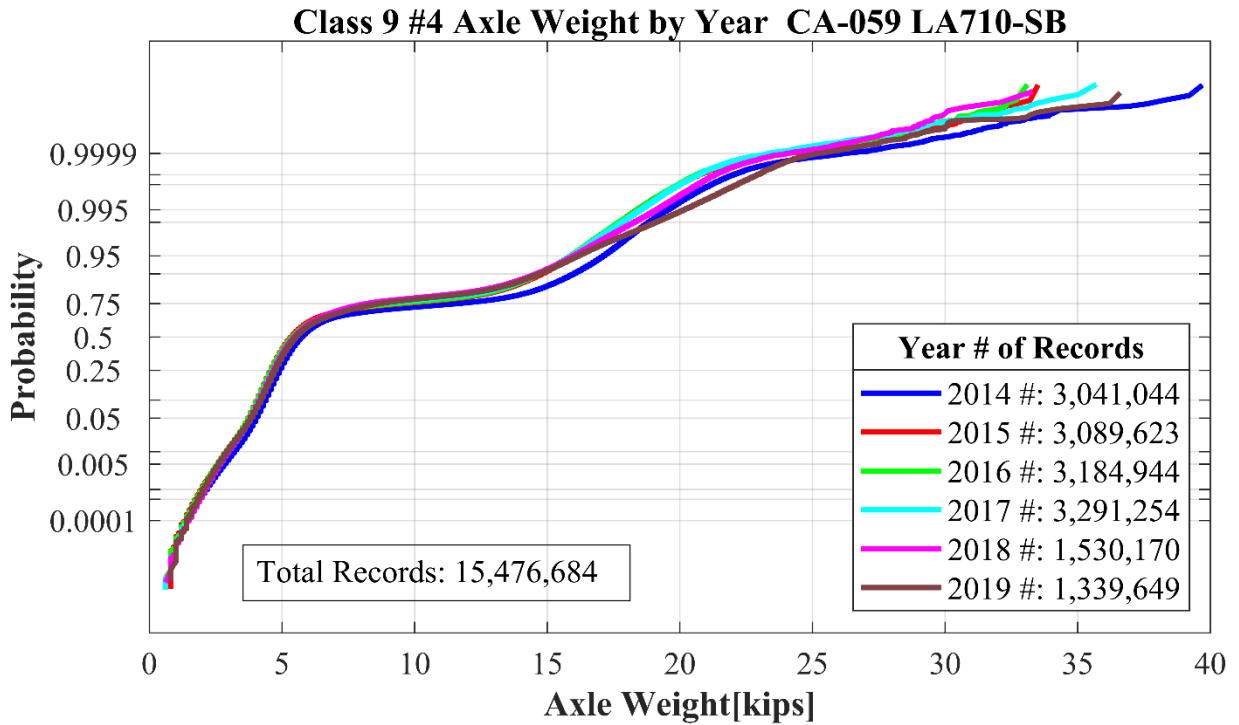
Class 9 #5 Axle Weight by Year CA-058 PINOLE-WB



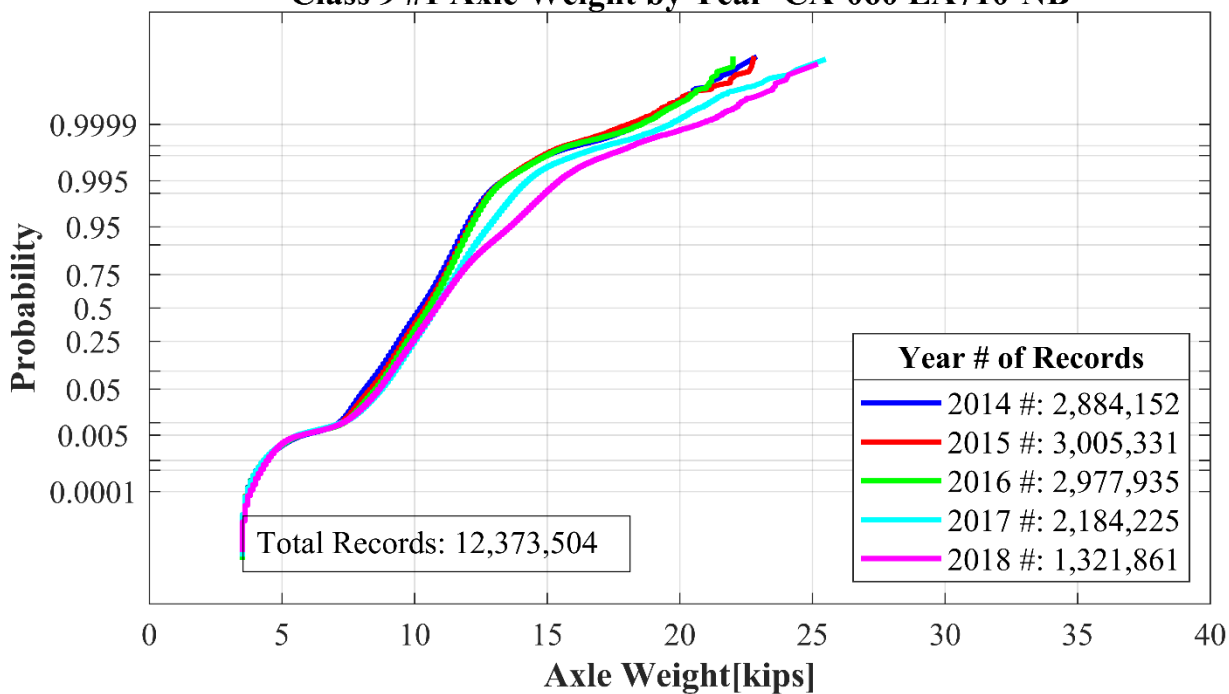
Class 9 #1 Axle Weight by Year CA-059 LA710-SB



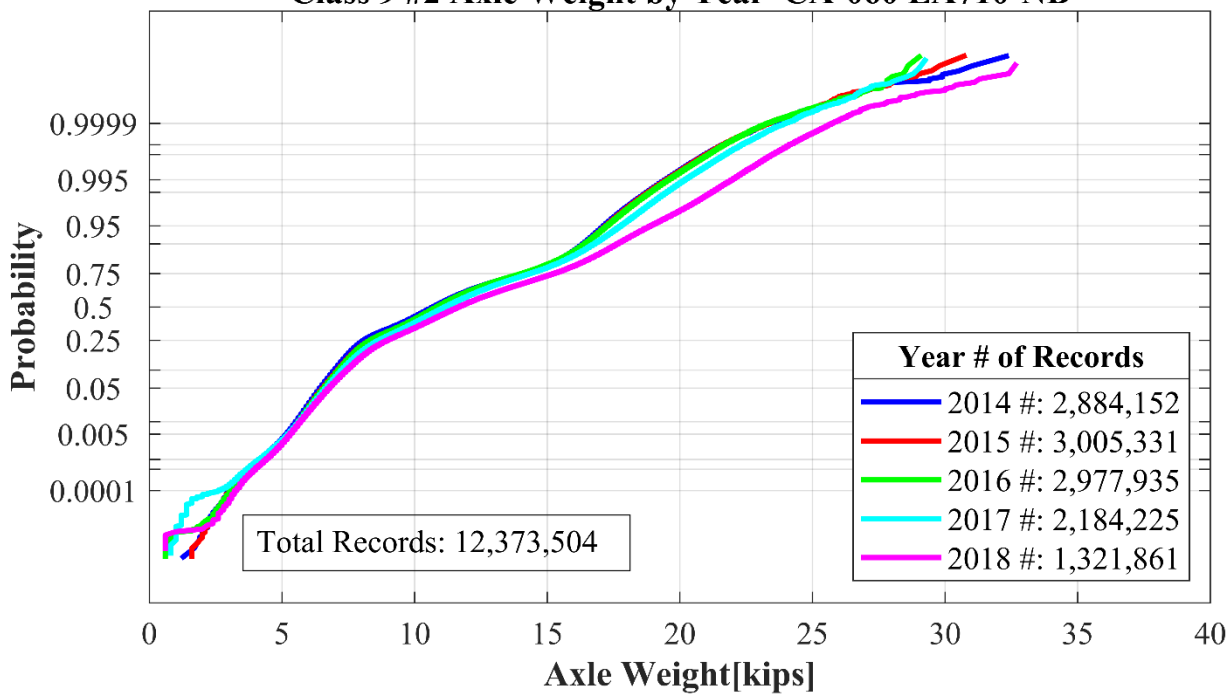




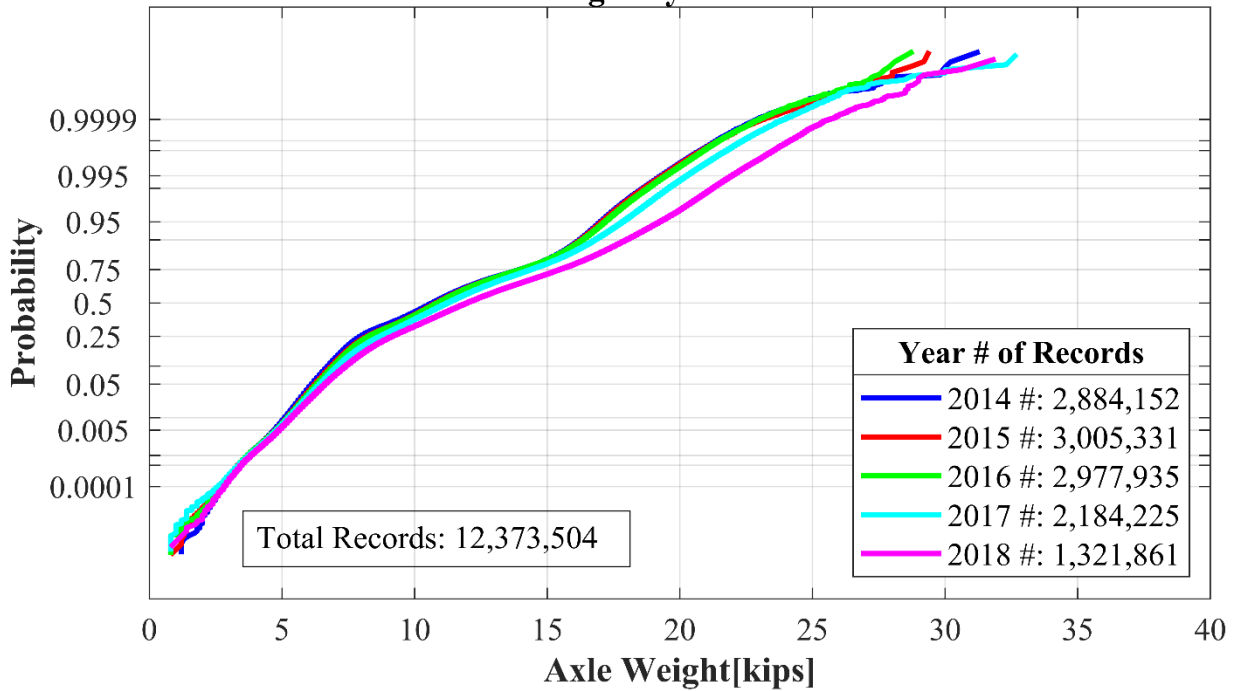
Class 9 #1 Axle Weight by Year CA-060 LA710-NB



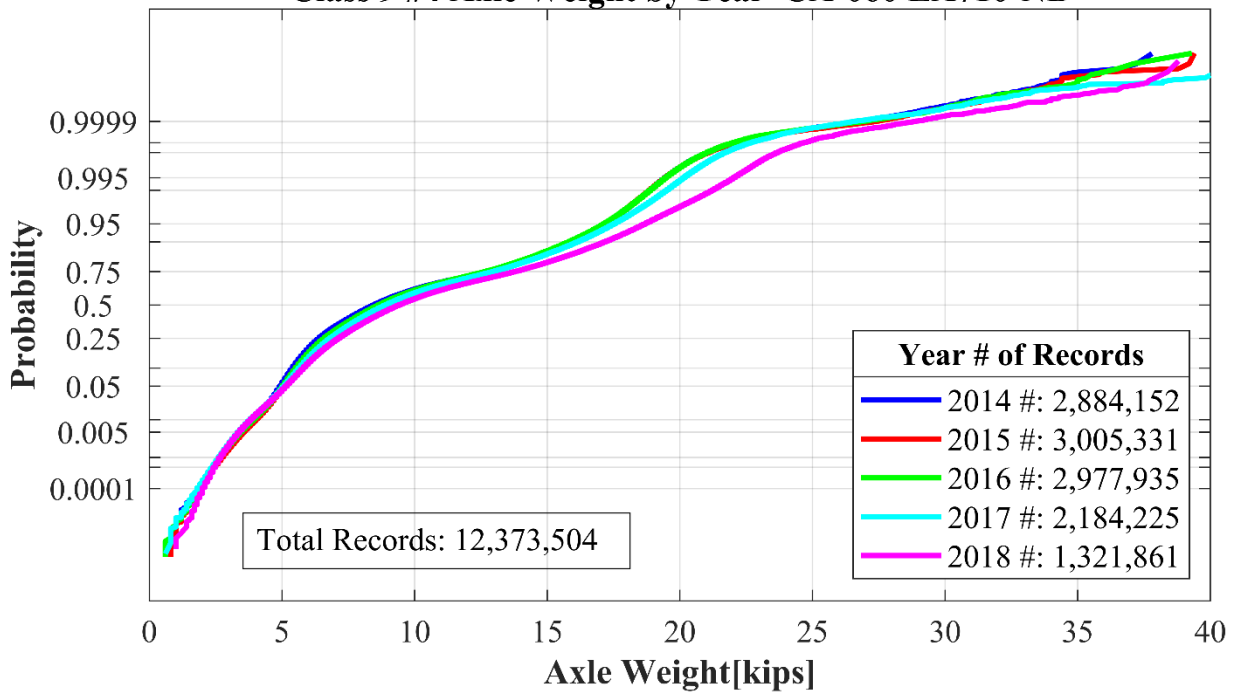
Class 9 #2 Axle Weight by Year CA-060 LA710-NB



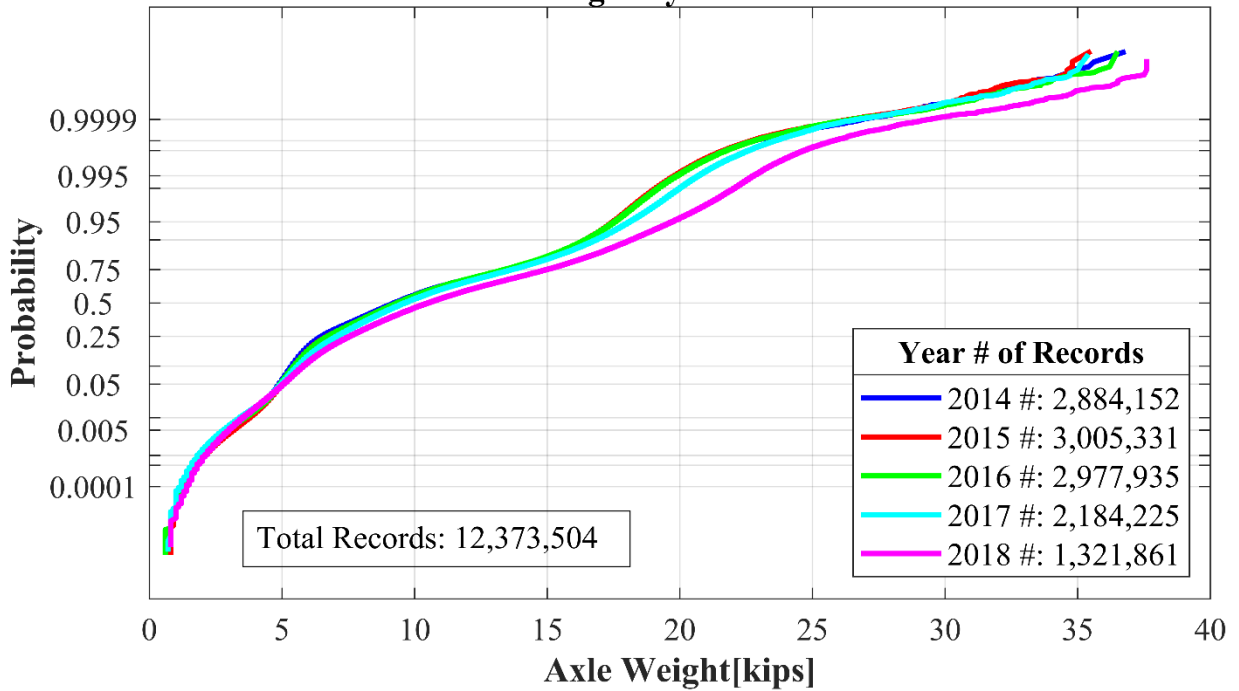
Class 9 #3 Axle Weight by Year CA-060 LA710-NB



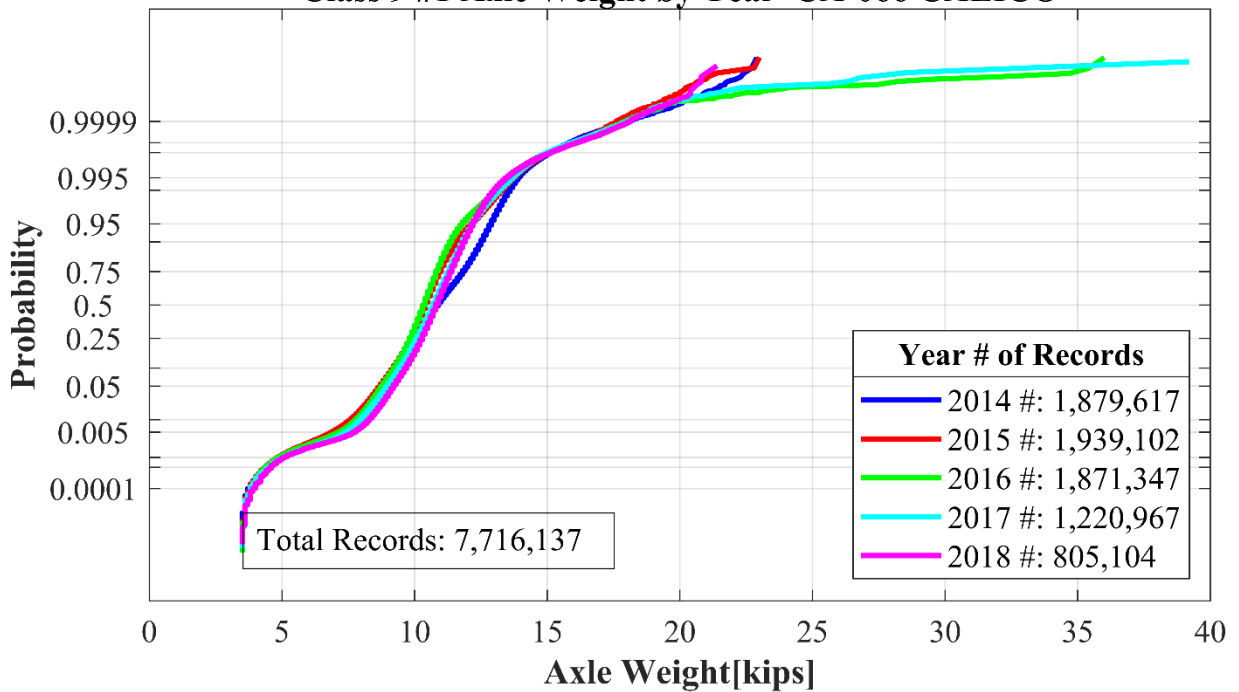
Class 9 #4 Axle Weight by Year CA-060 LA710-NB



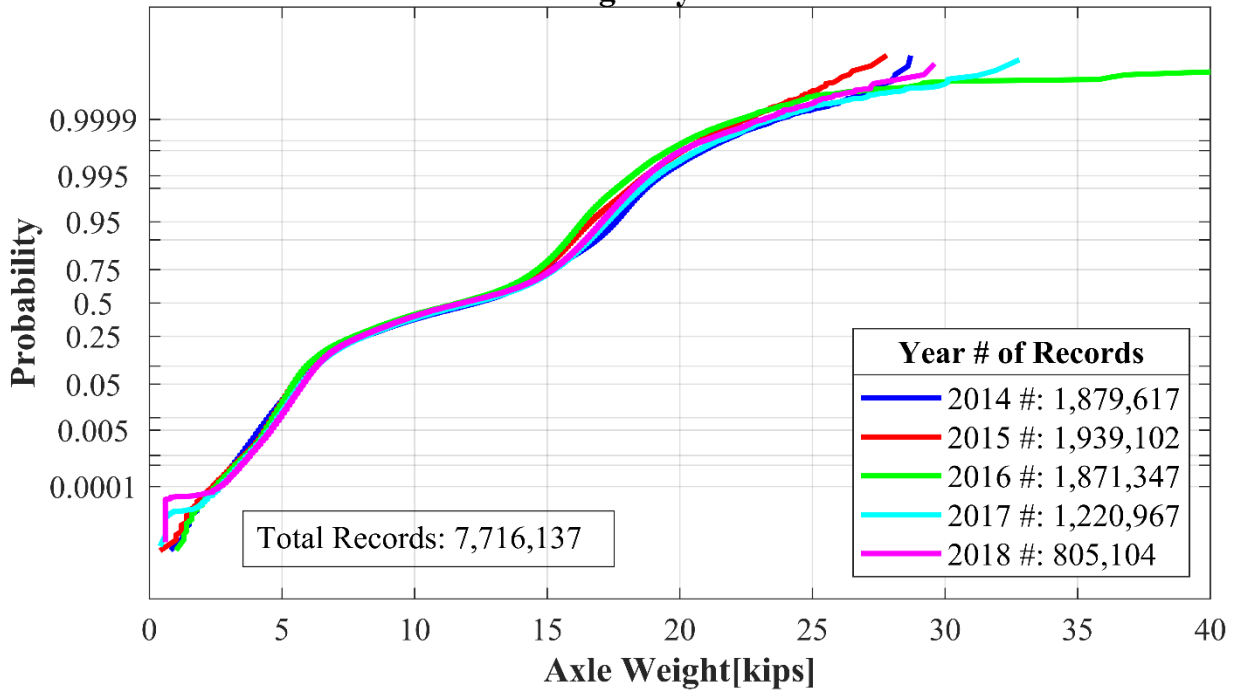
Class 9 #5 Axle Weight by Year CA-060 LA710-NB



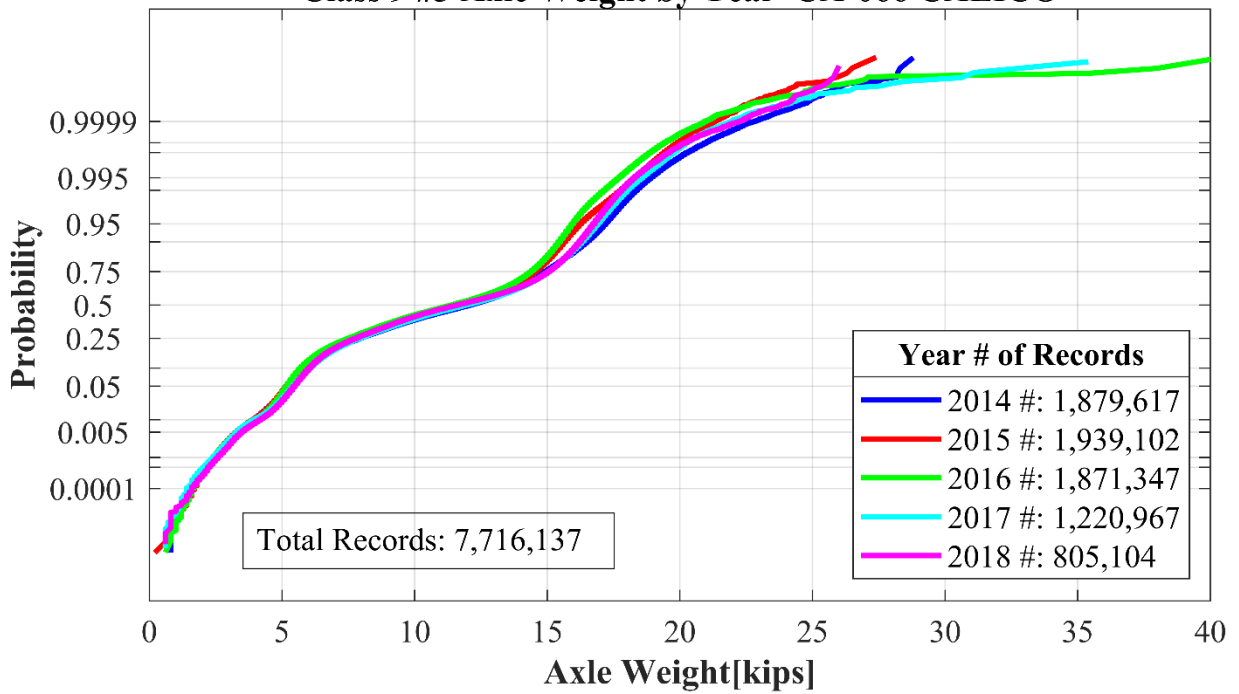
Class 9 #1 Axle Weight by Year CA-066 CALICO



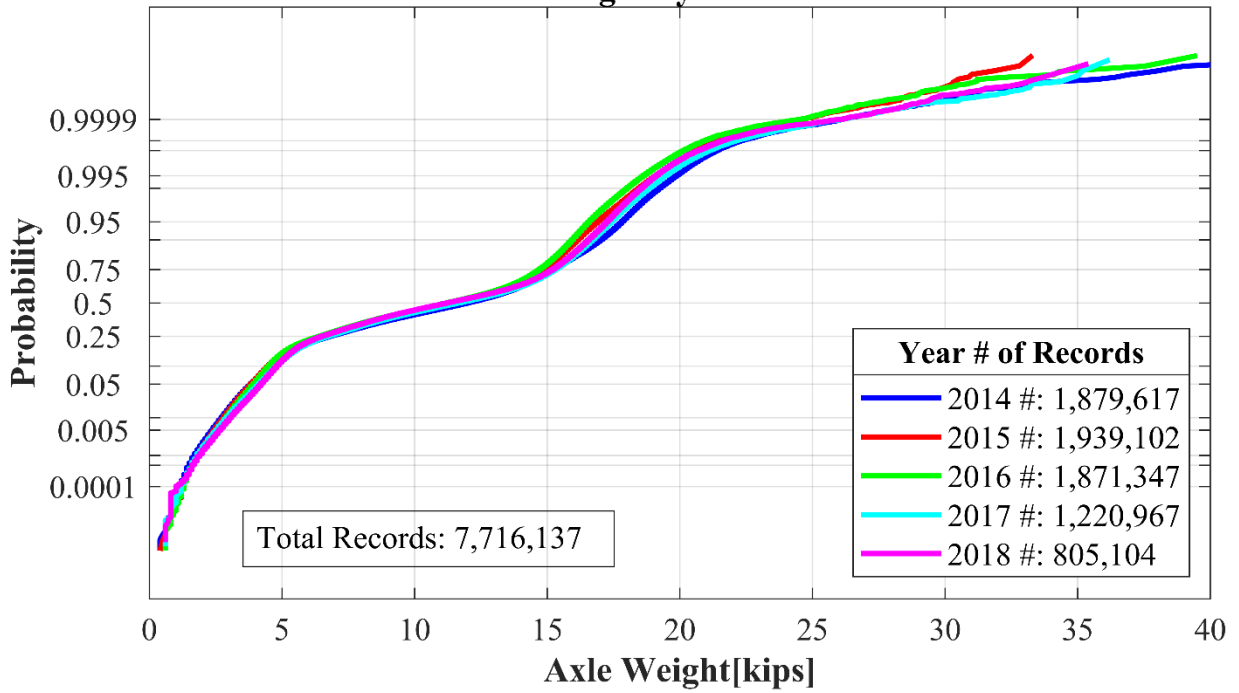
Class 9 #2 Axle Weight by Year CA-066 CALICO



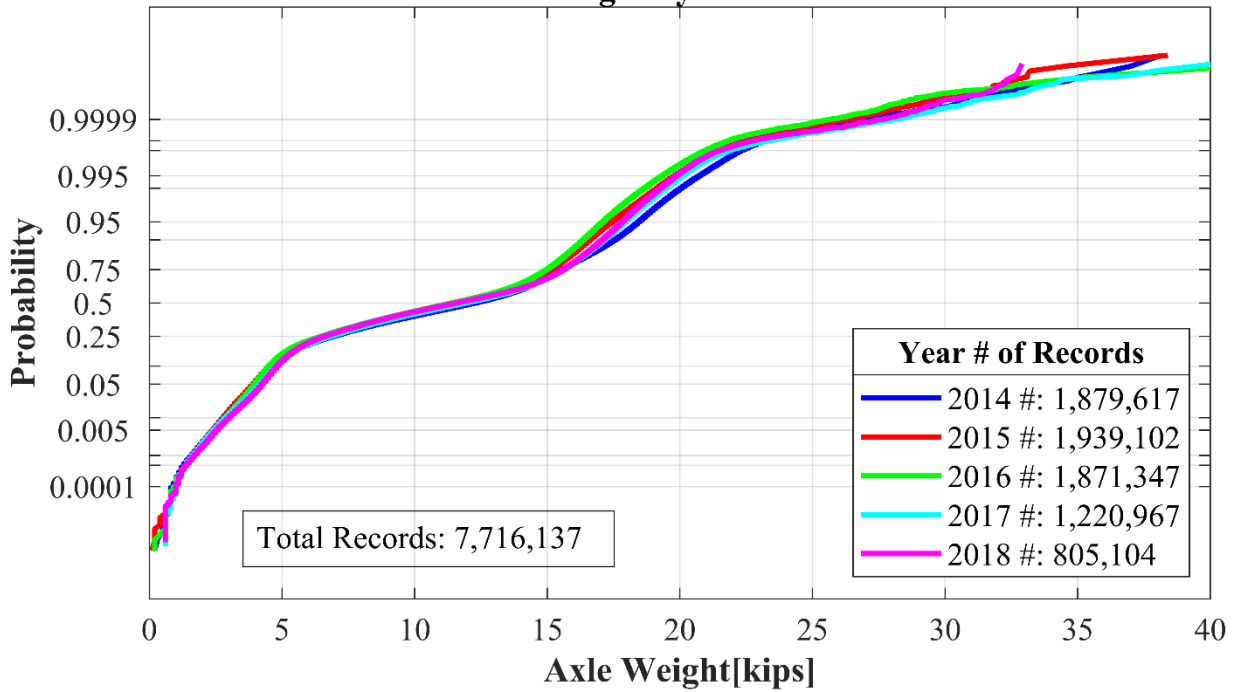
Class 9 #3 Axle Weight by Year CA-066 CALICO

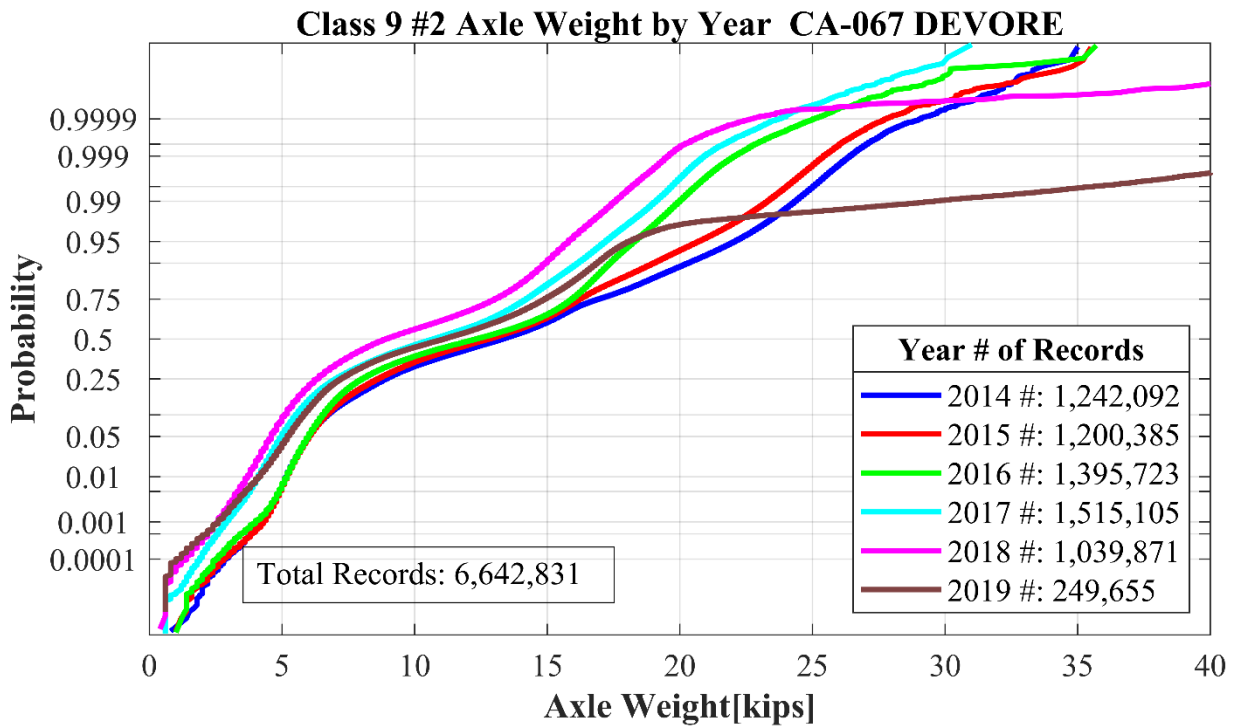
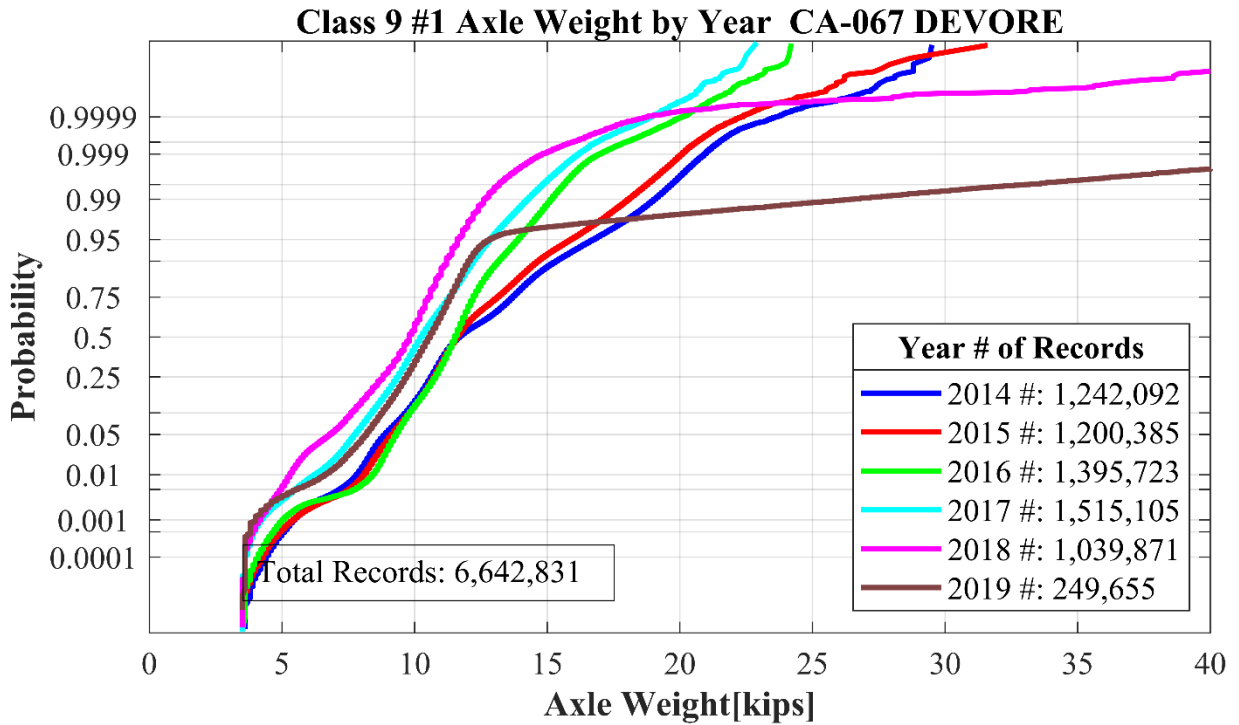


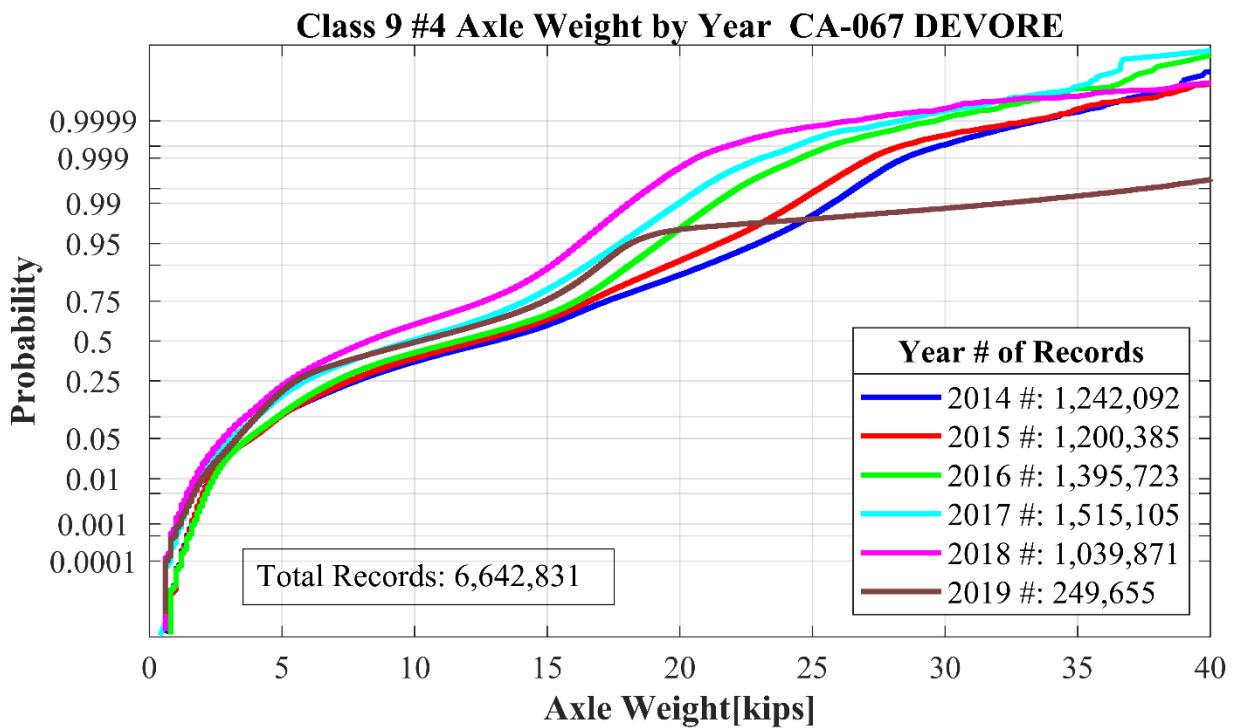
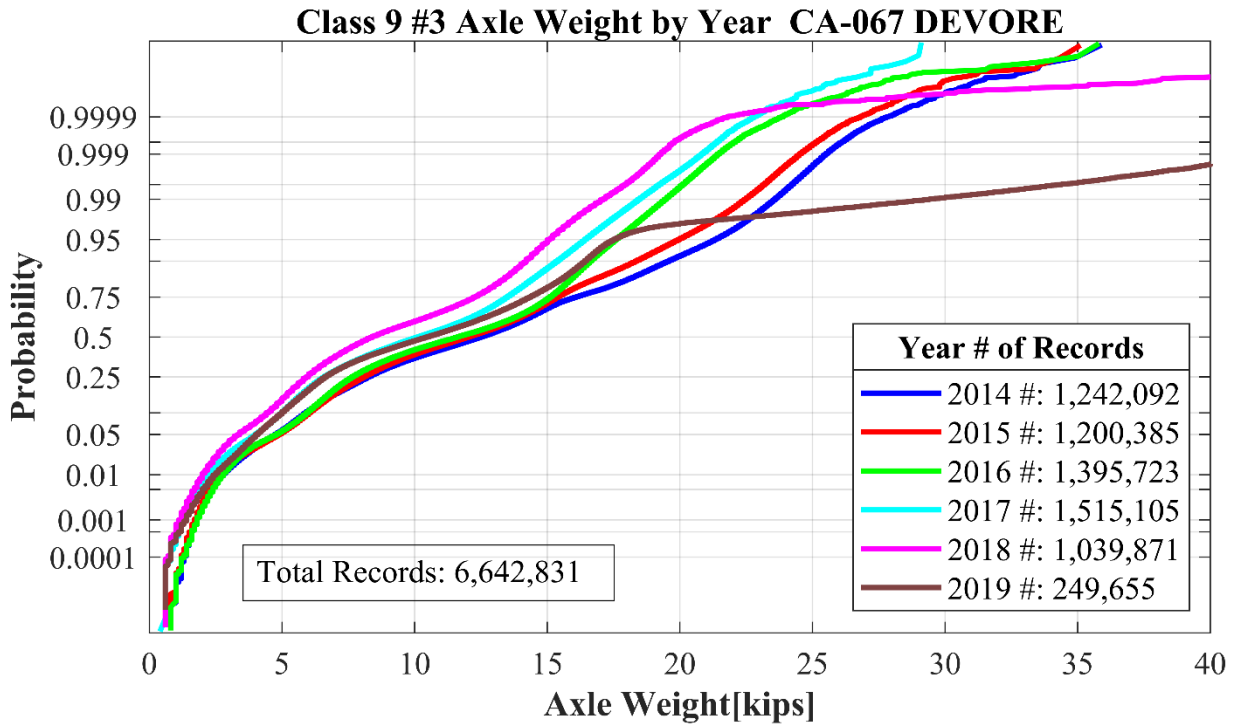
Class 9 #4 Axle Weight by Year CA-066 CALICO

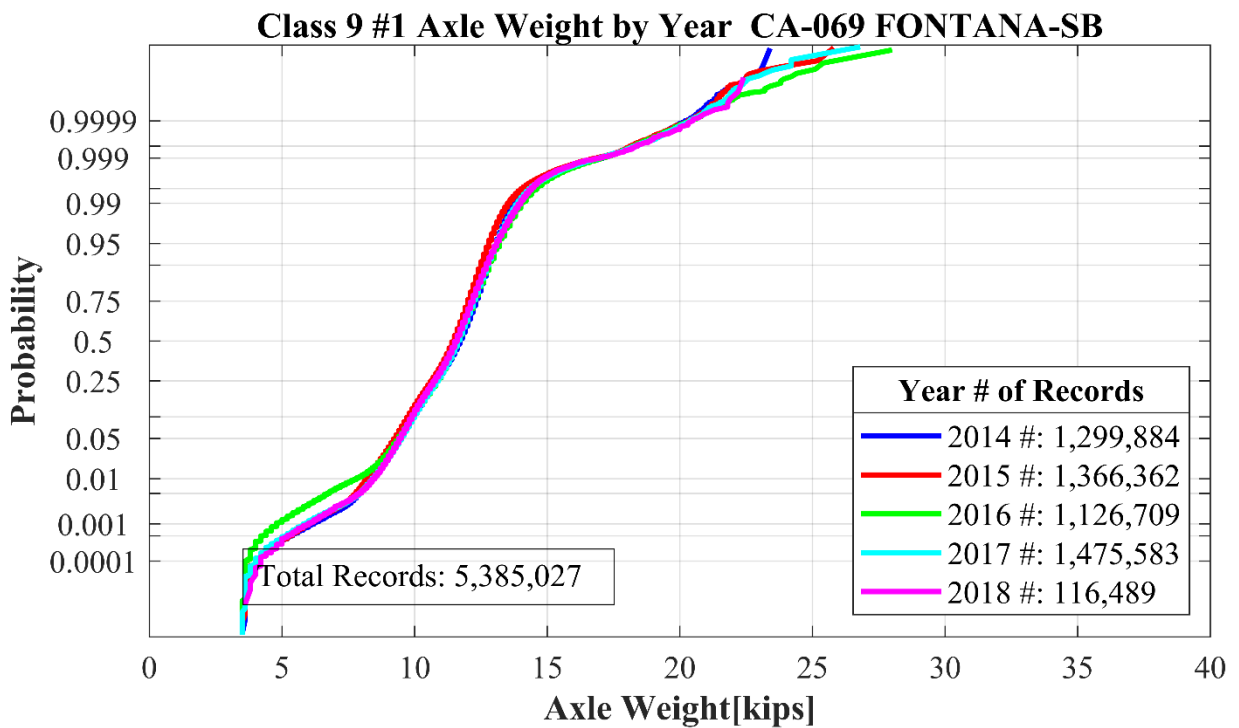
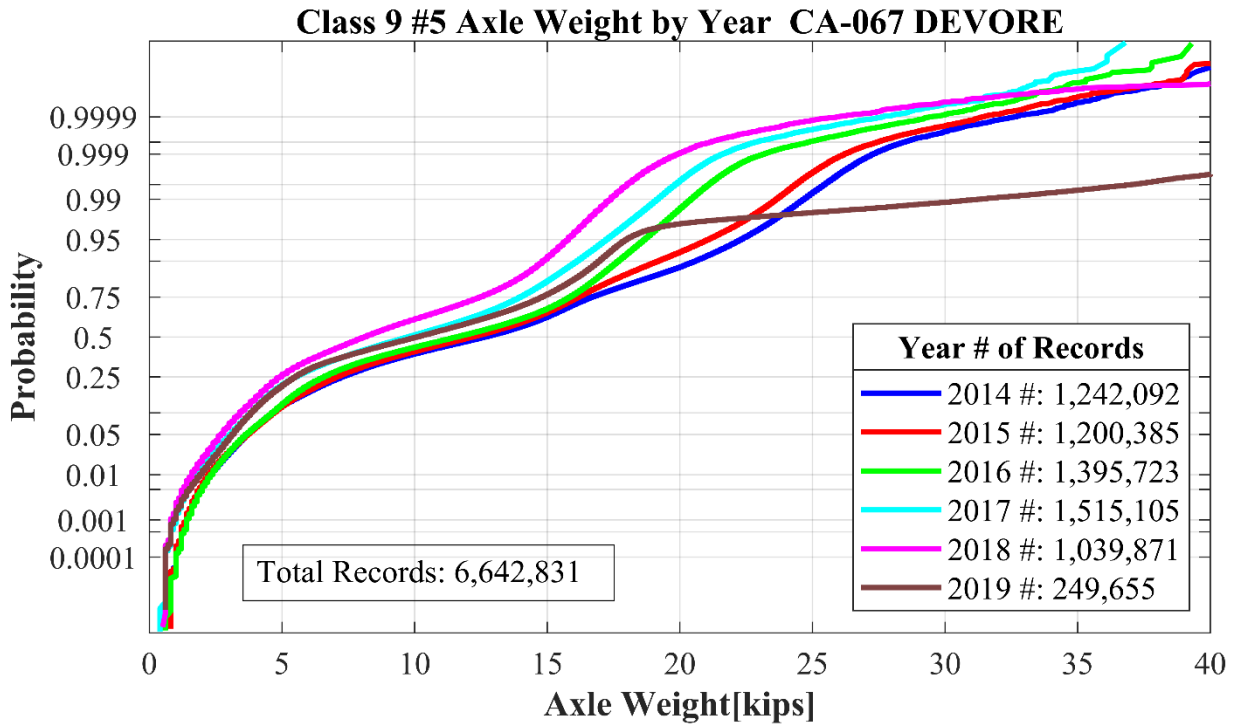


Class 9 #5 Axle Weight by Year CA-066 CALICO

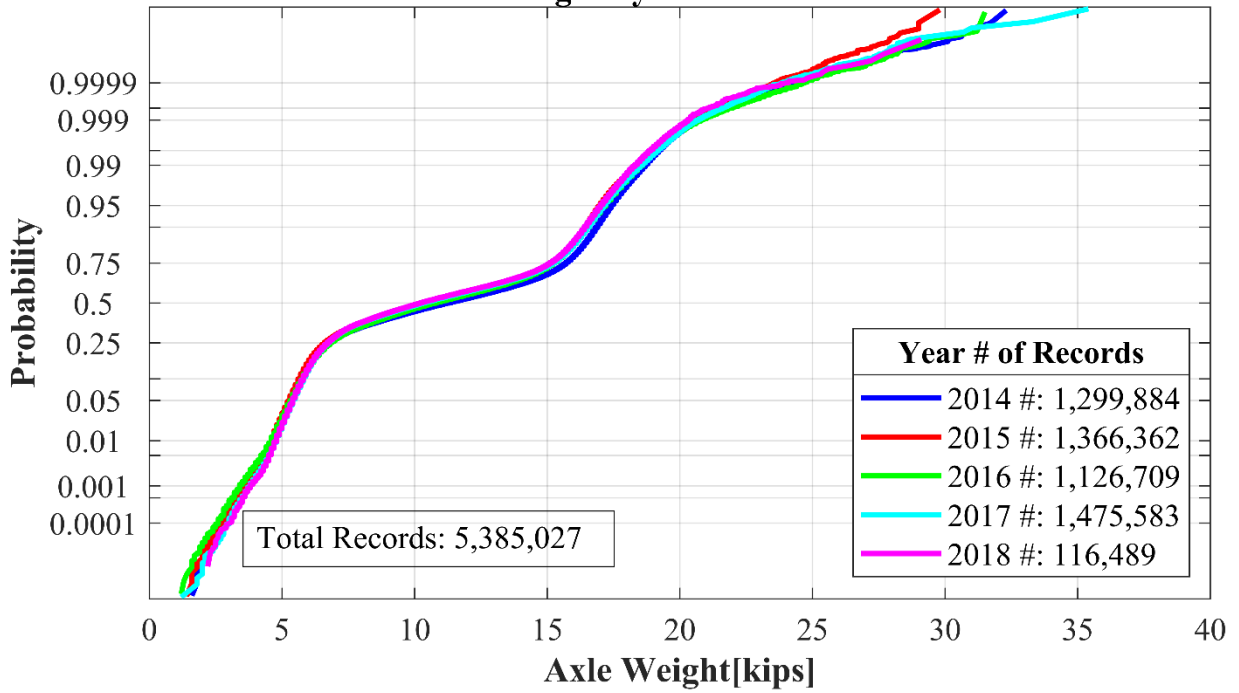




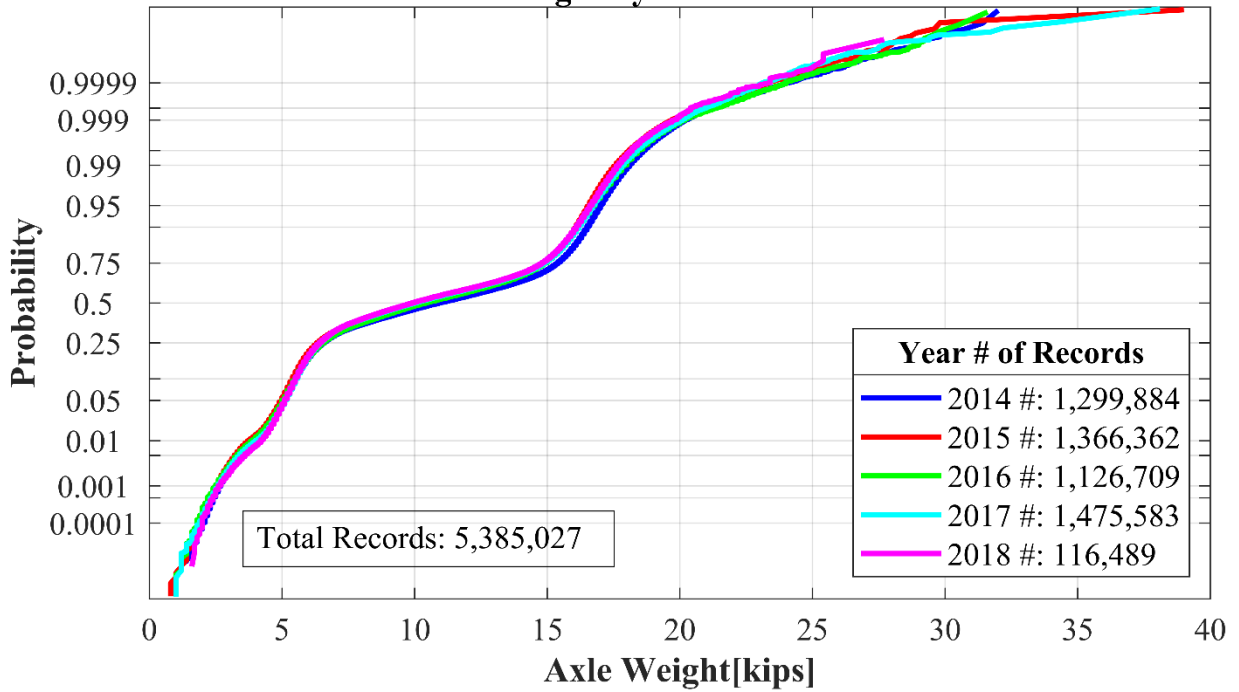




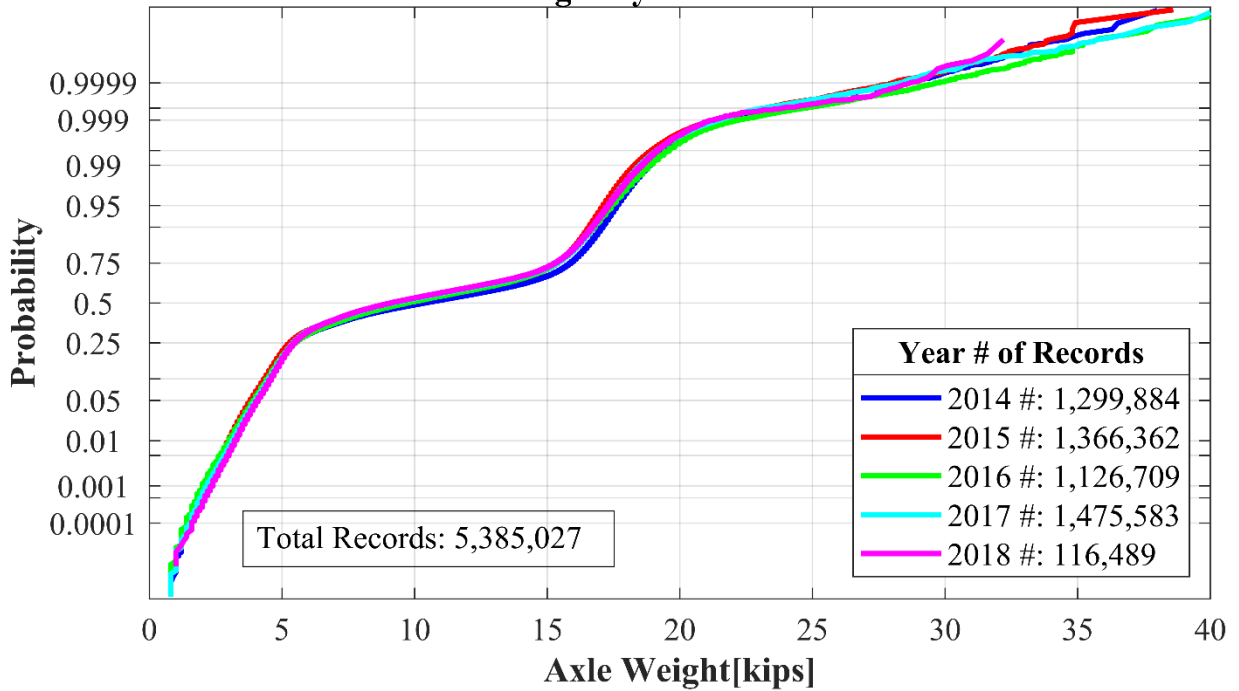
Class 9 #2 Axle Weight by Year CA-069 FONTANA-SB



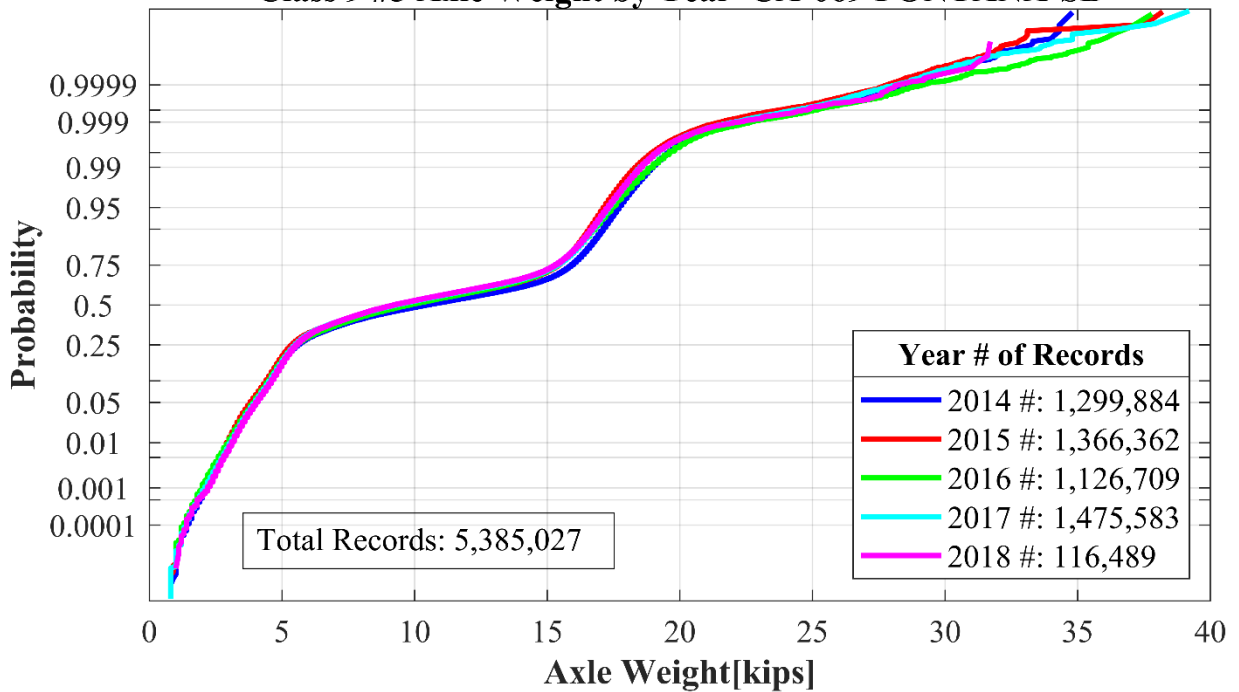
Class 9 #3 Axle Weight by Year CA-069 FONTANA-SB



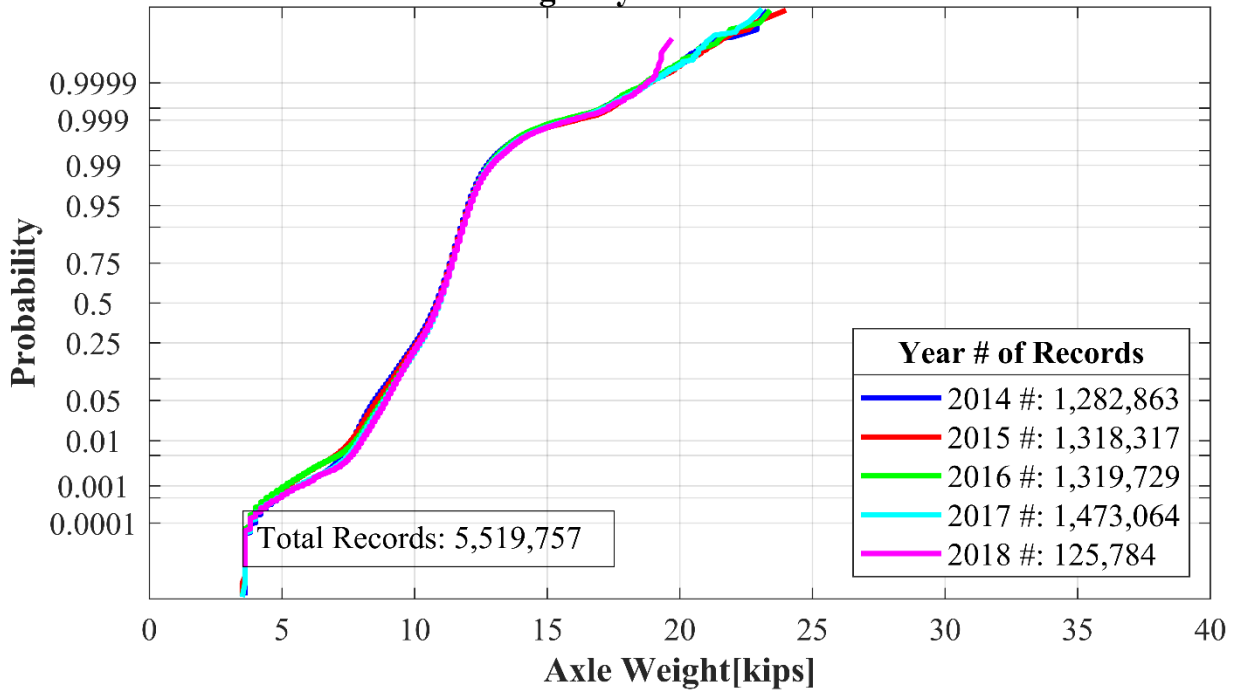
Class 9 #4 Axle Weight by Year CA-069 FONTANA-SB



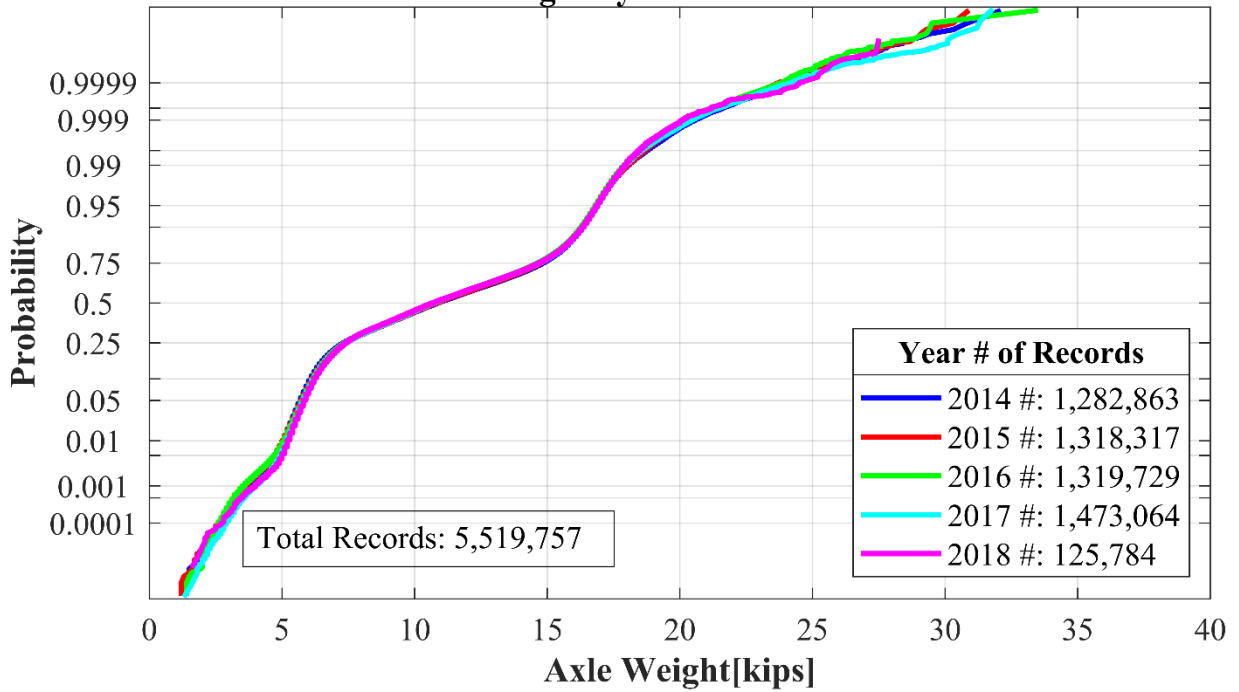
Class 9 #5 Axle Weight by Year CA-069 FONTANA-SB



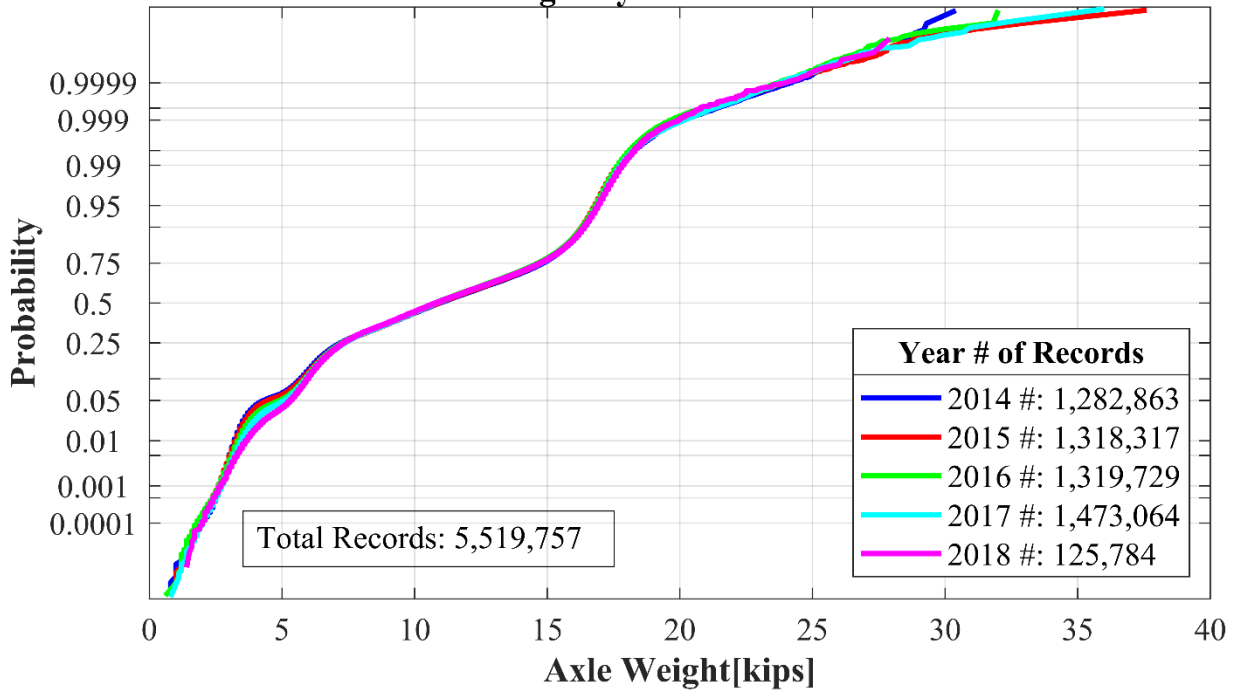
Class 9 #1 Axle Weight by Year CA-070 DFONTANA-NB



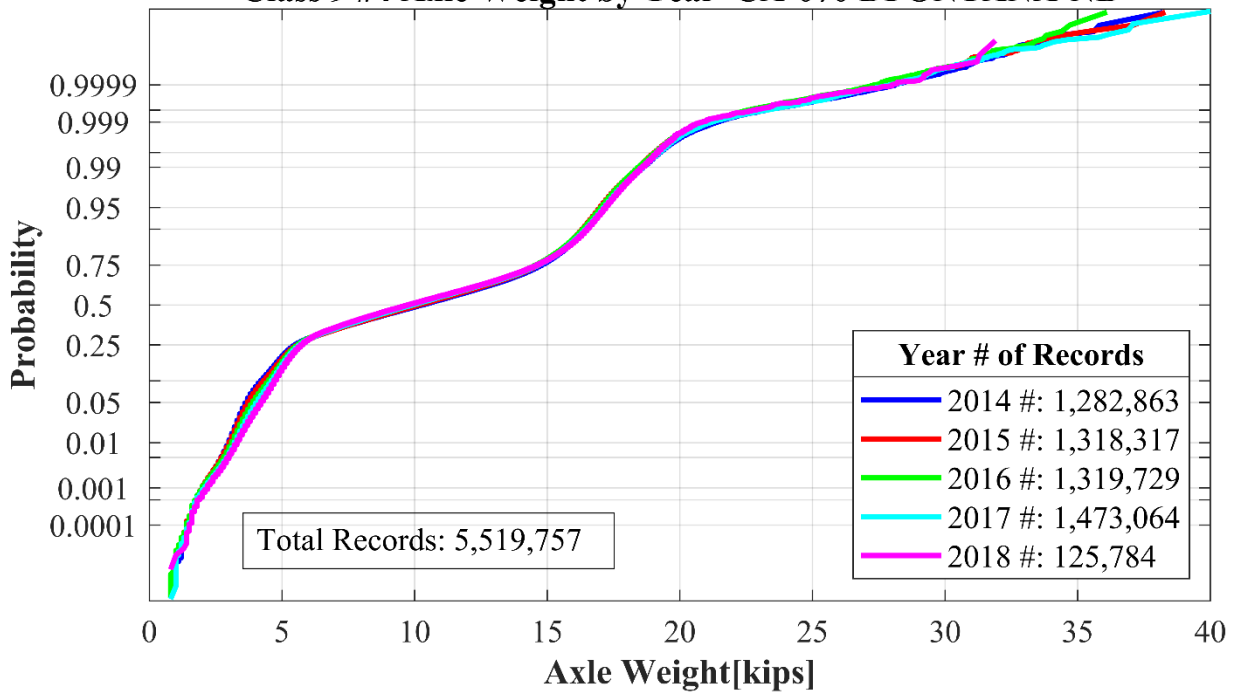
Class 9 #2 Axle Weight by Year CA-070 DFONTANA-NB

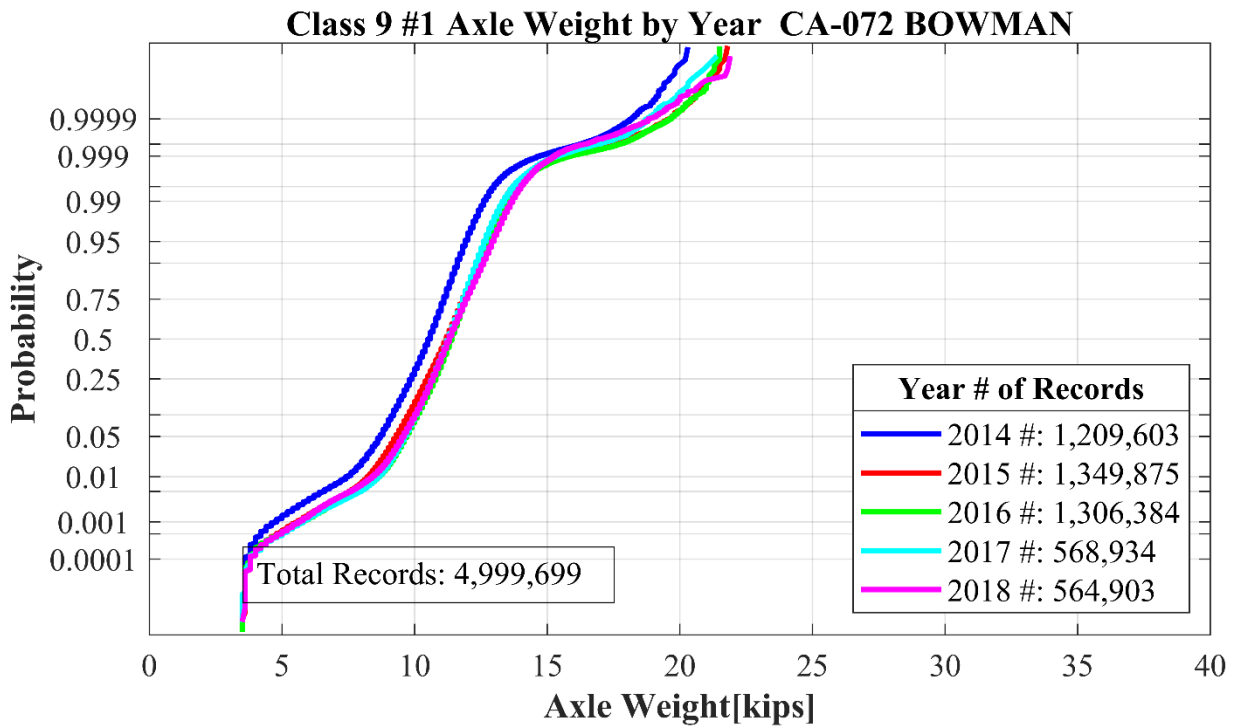
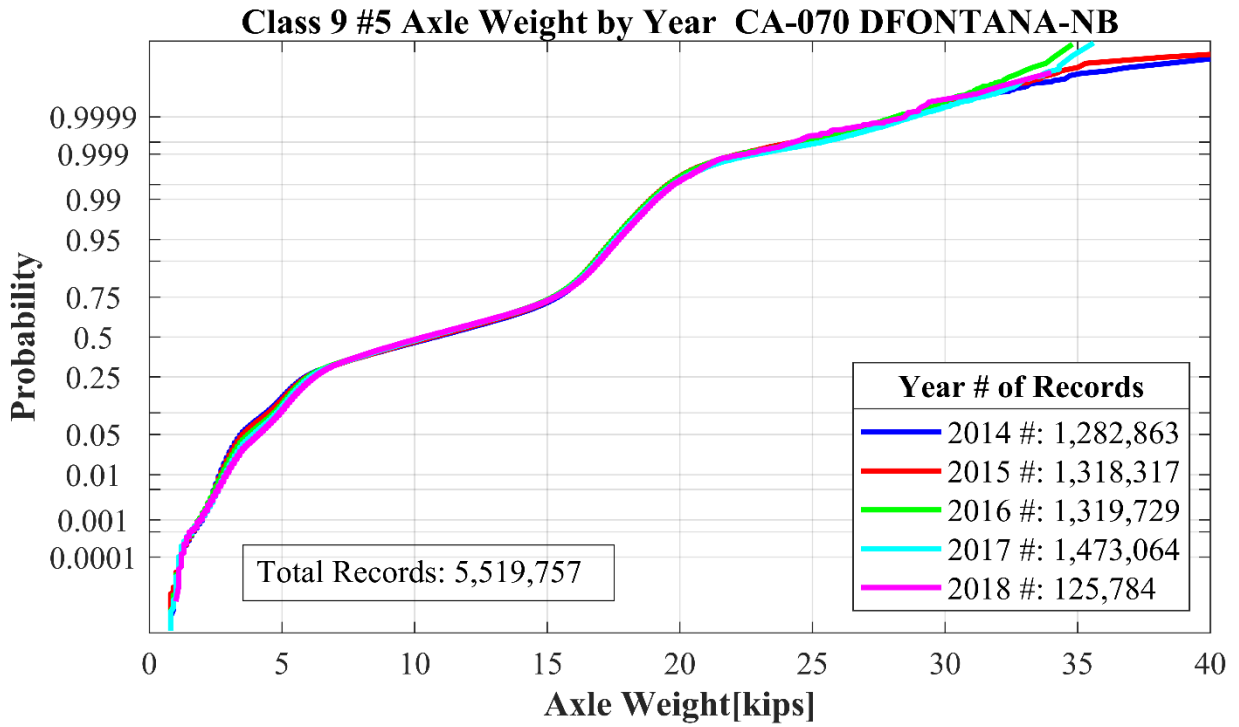


Class 9 #3 Axle Weight by Year CA-070 DFONTANA-NB

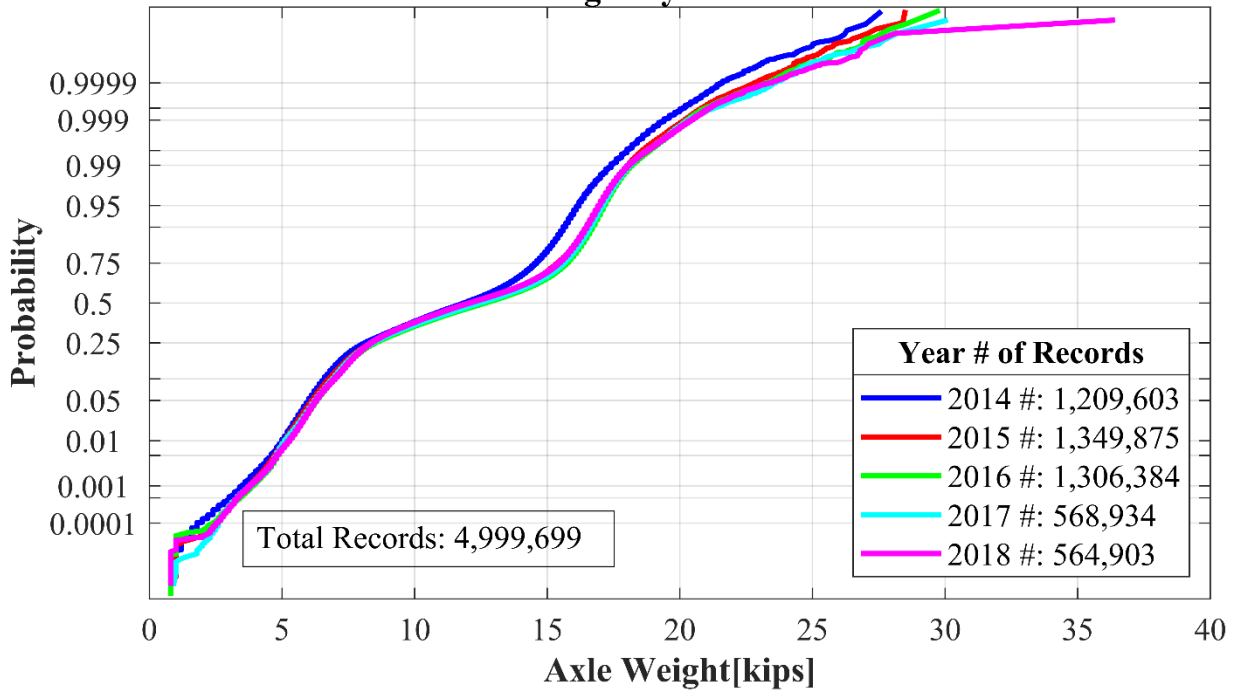


Class 9 #4 Axle Weight by Year CA-070 DFONTANA-NB

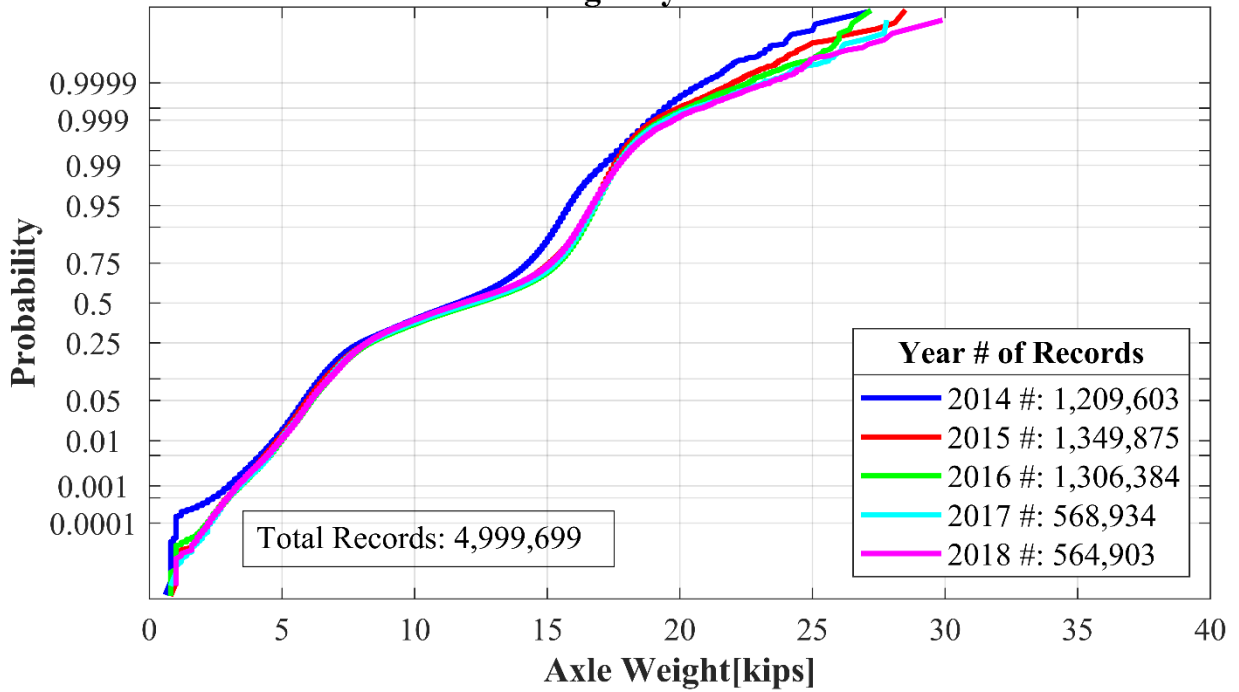




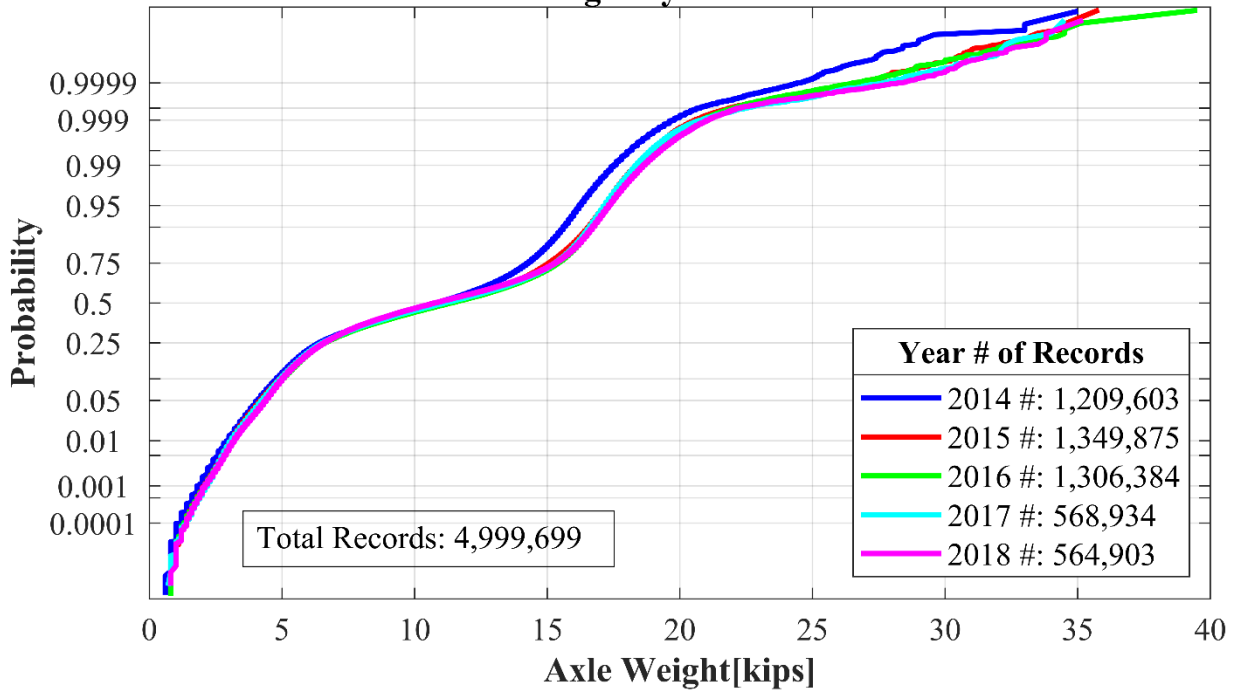
Class 9 #2 Axle Weight by Year CA-072 BOWMAN



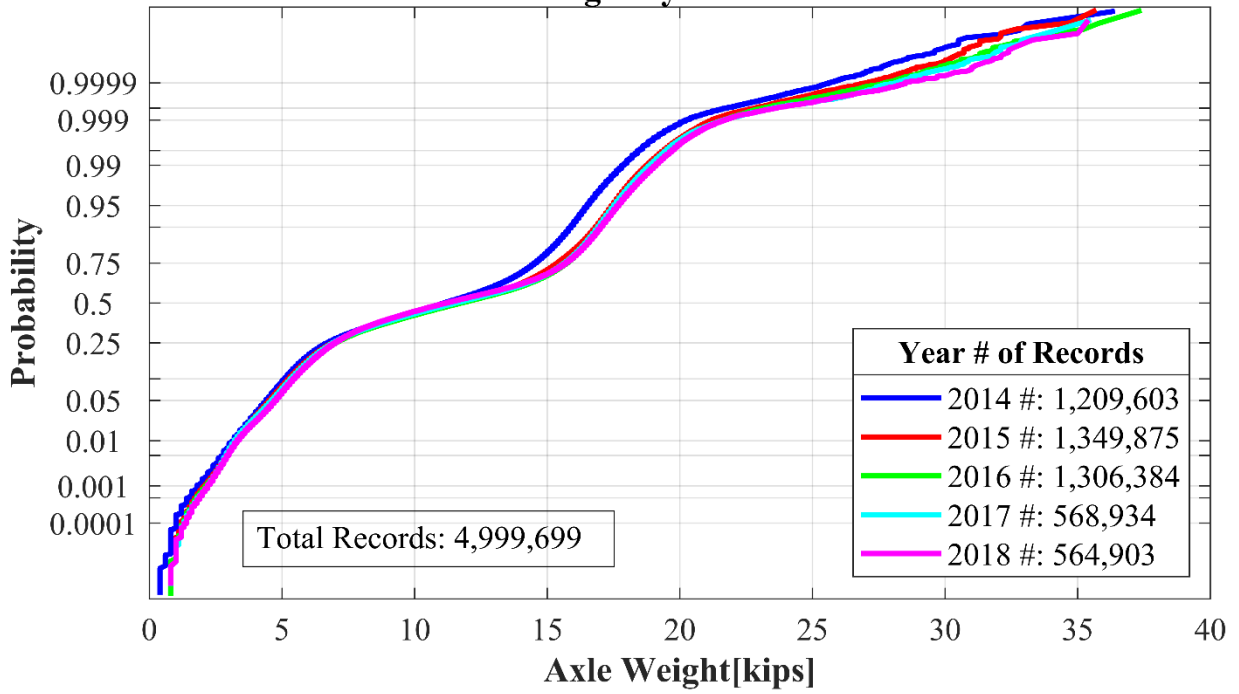
Class 9 #3 Axle Weight by Year CA-072 BOWMAN



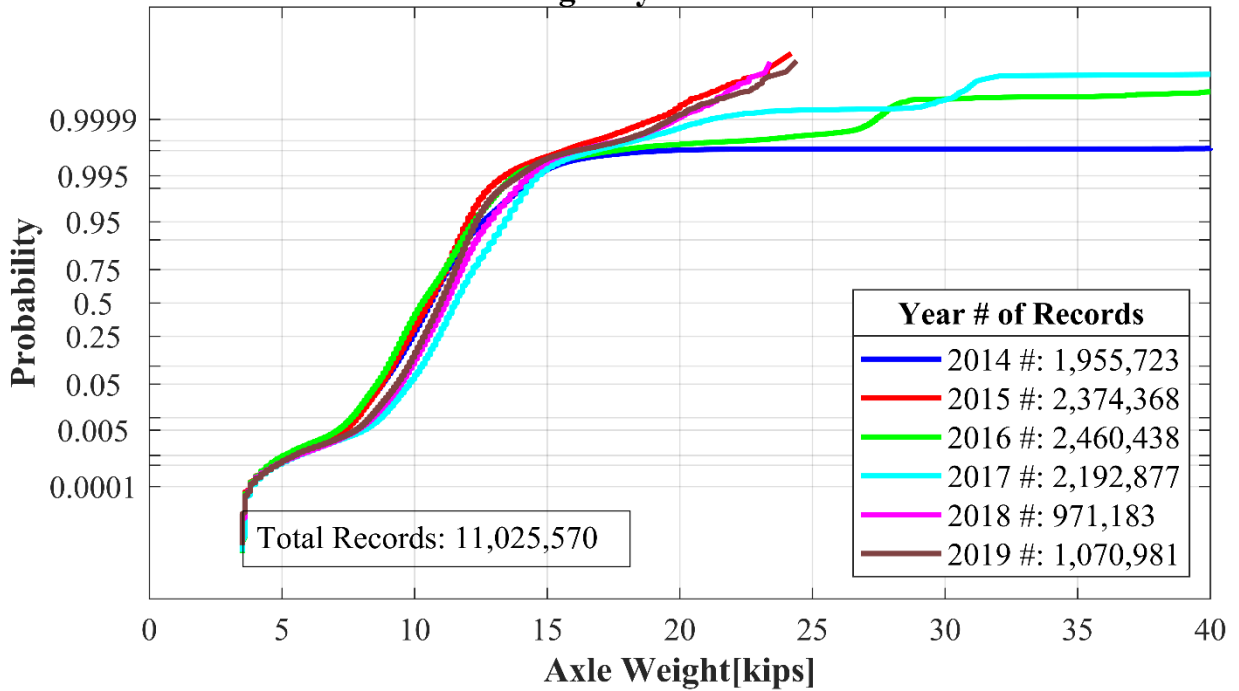
Class 9 #4 Axle Weight by Year CA-072 BOWMAN



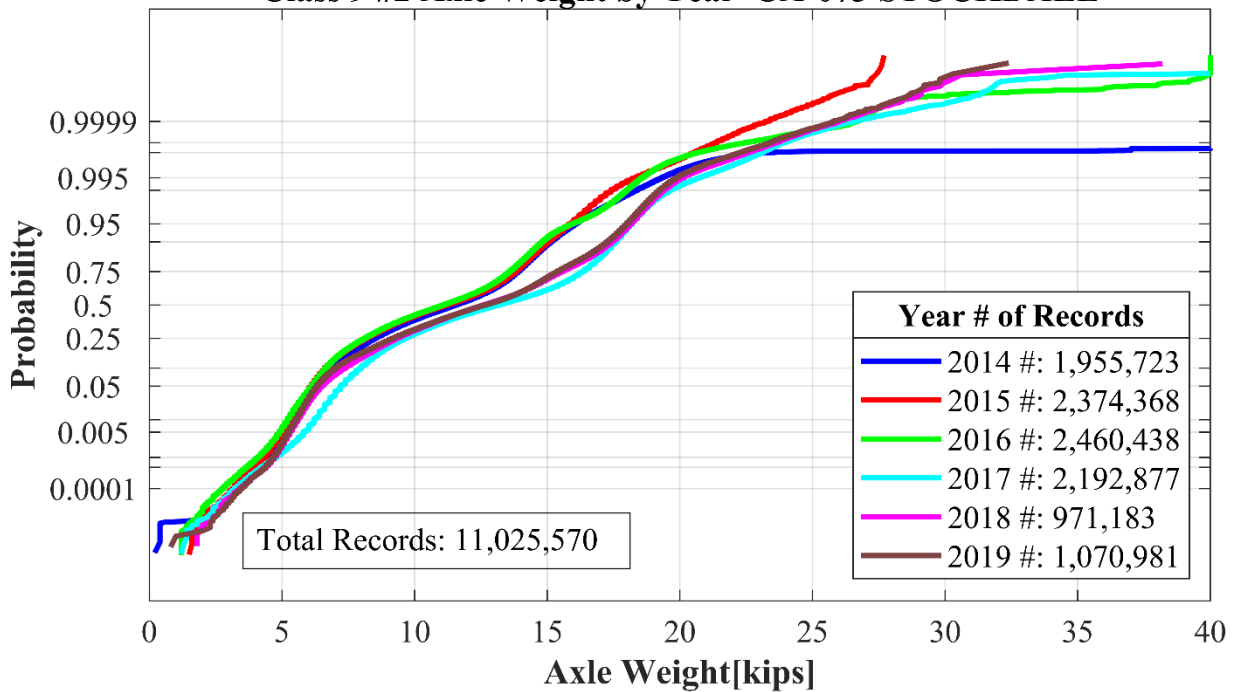
Class 9 #5 Axle Weight by Year CA-072 BOWMAN



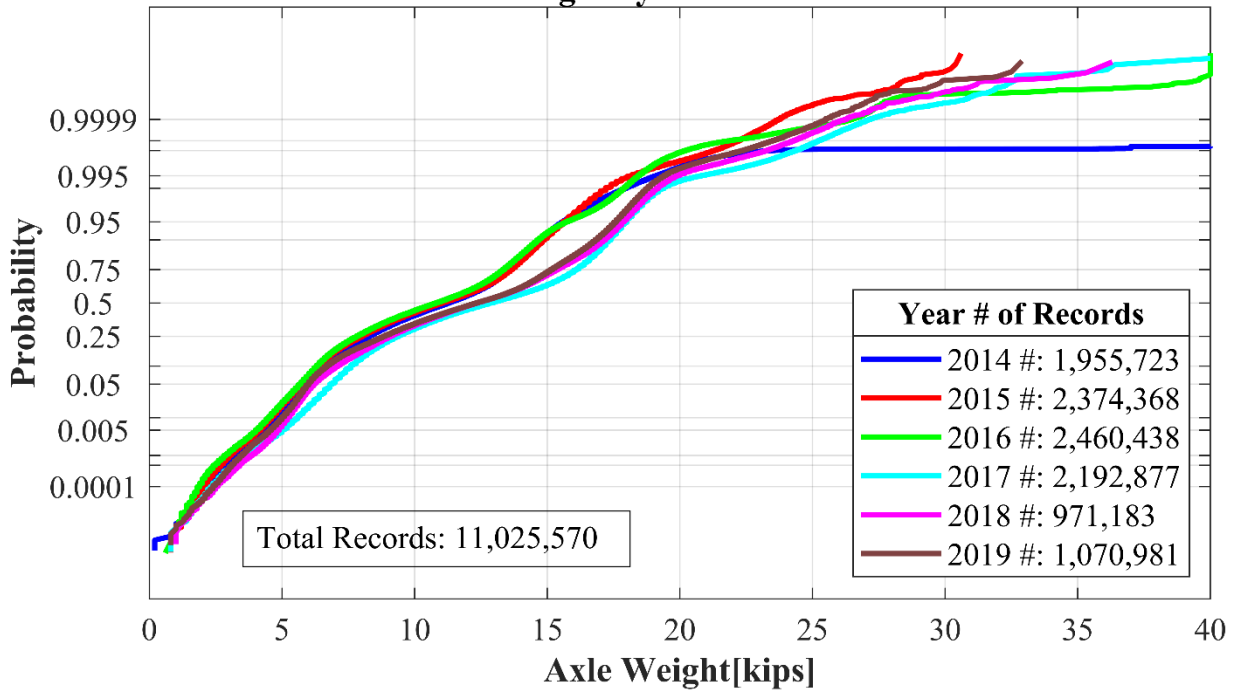
Class 9 #1 Axle Weight by Year CA-073 STOCKDALE



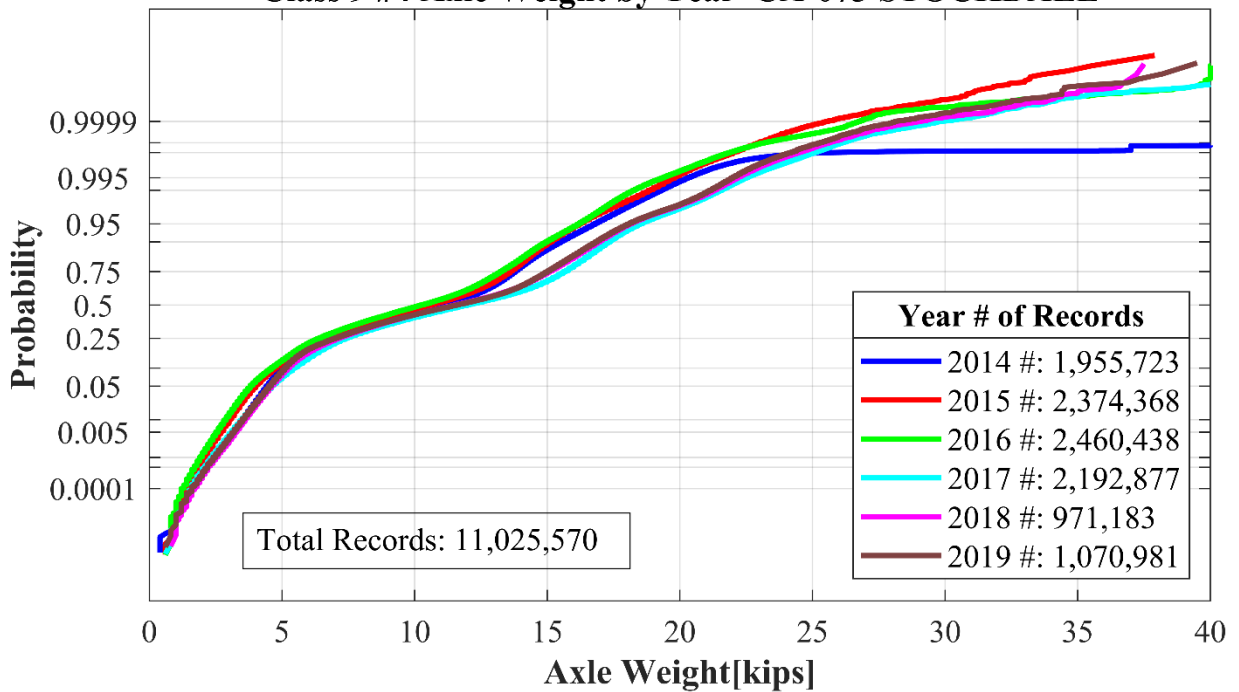
Class 9 #2 Axle Weight by Year CA-073 STOCKDALE



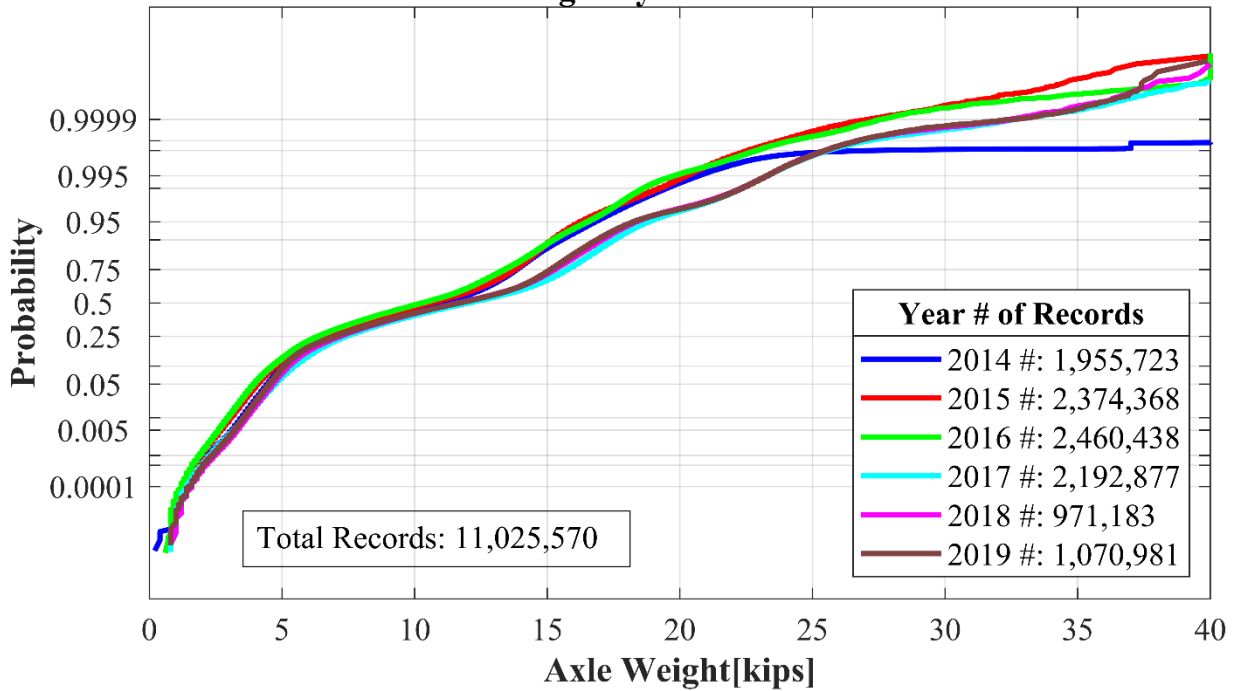
Class 9 #3 Axle Weight by Year CA-073 STOCKDALE



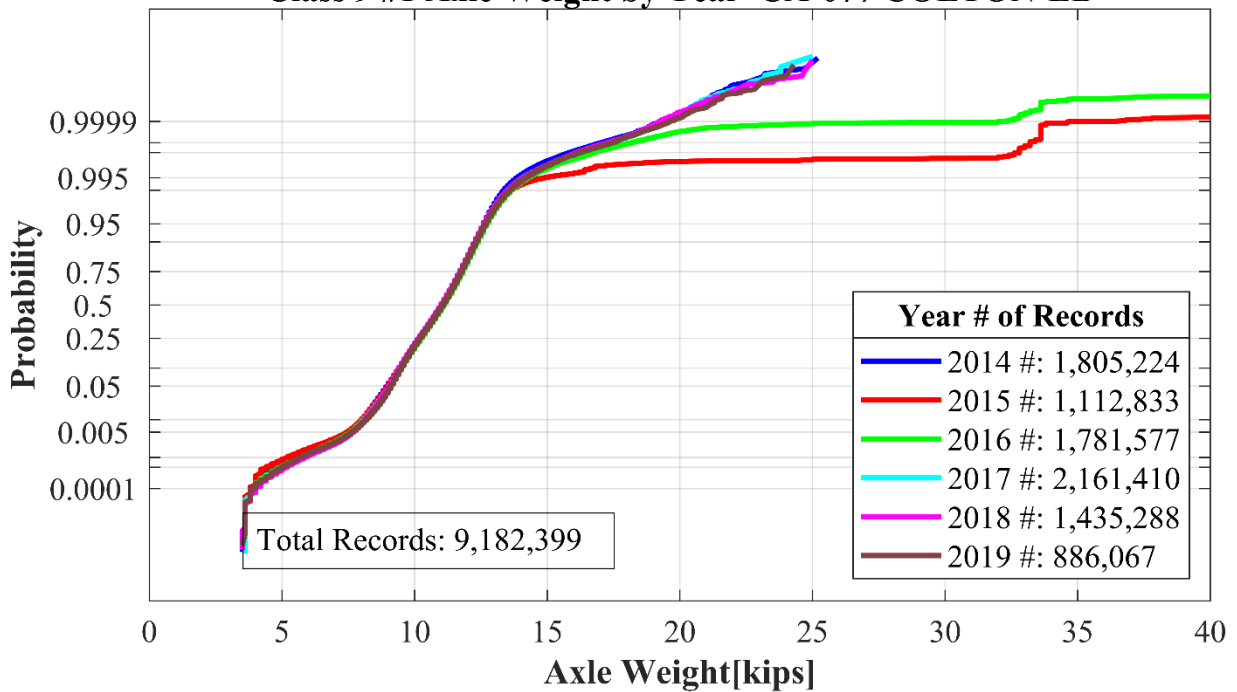
Class 9 #4 Axle Weight by Year CA-073 STOCKDALE



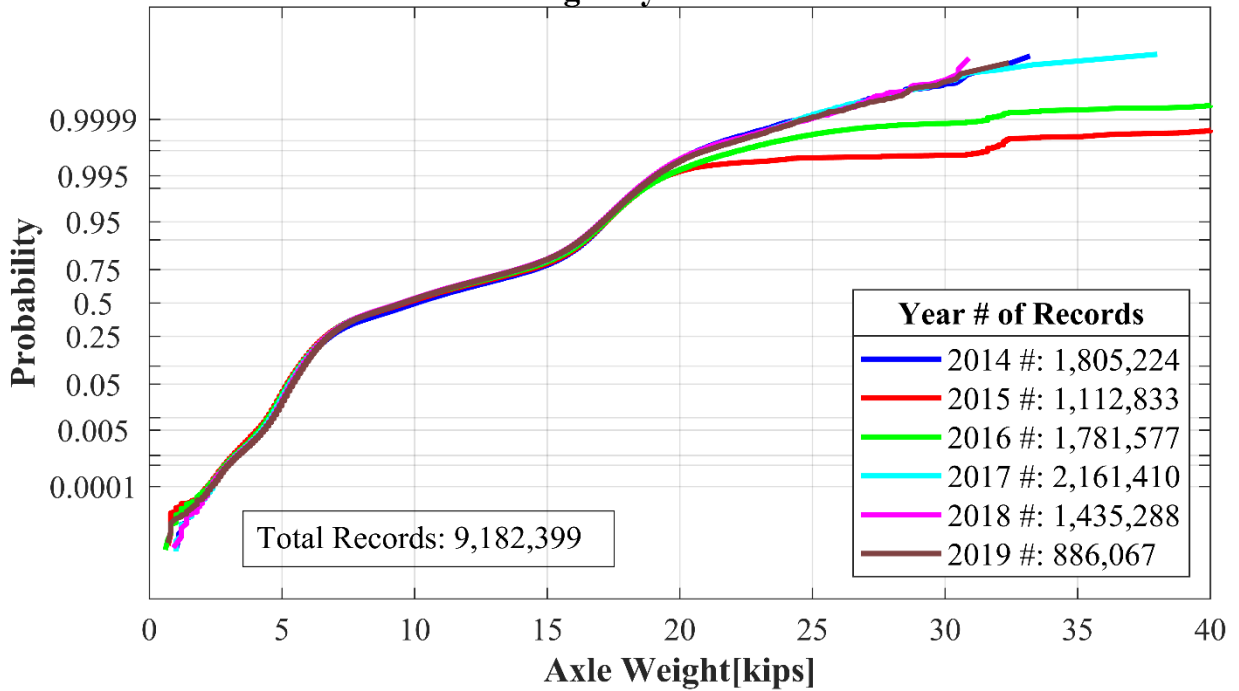
Class 9 #5 Axle Weight by Year CA-073 STOCKDALE



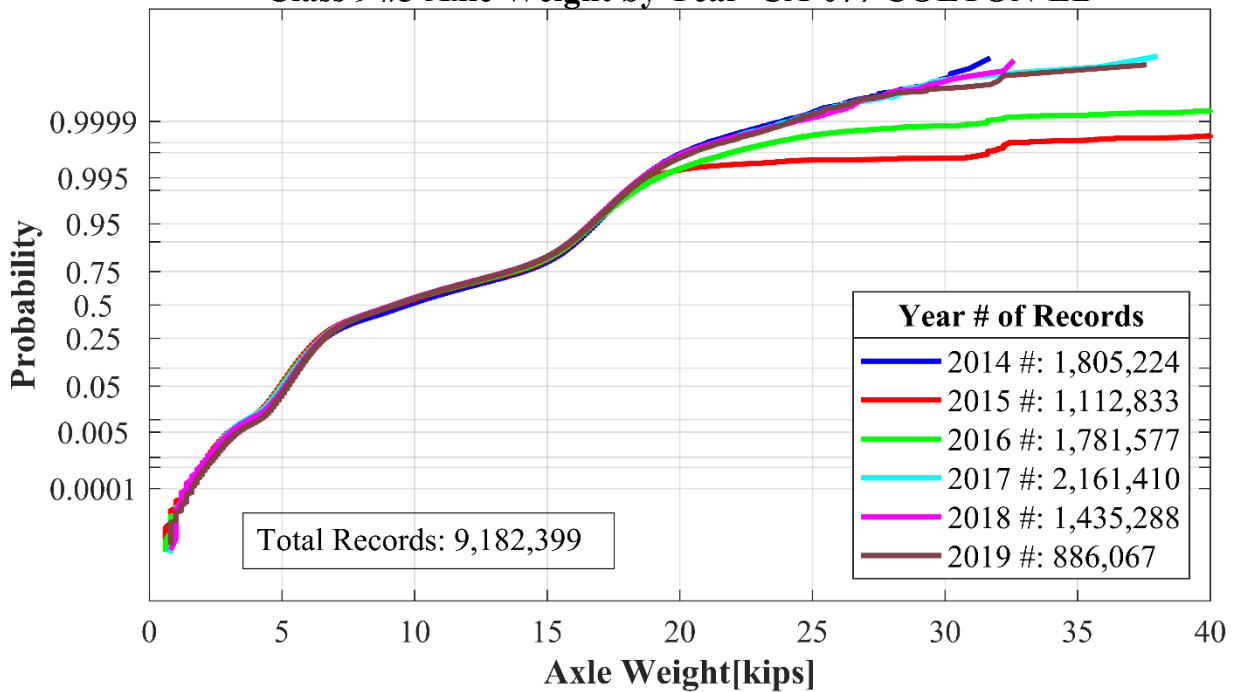
Class 9 #1 Axle Weight by Year CA-077 COLTON-EB



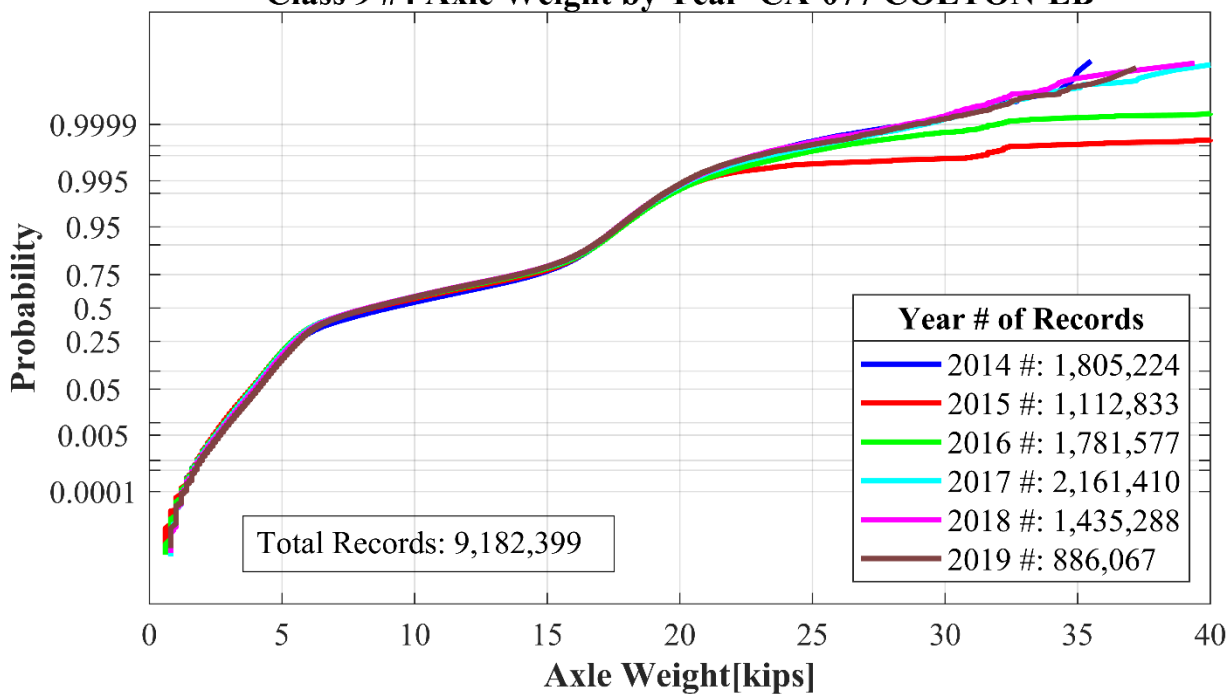
Class 9 #2 Axle Weight by Year CA-077 COLTON-EB



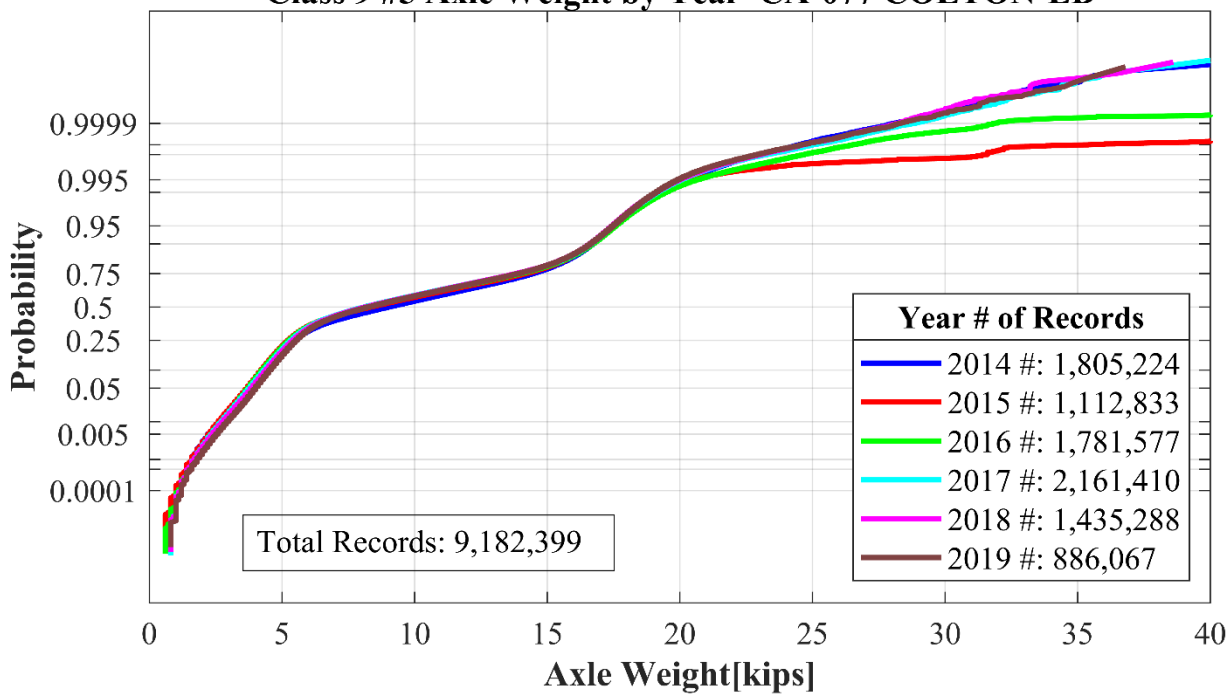
Class 9 #3 Axle Weight by Year CA-077 COLTON-EB



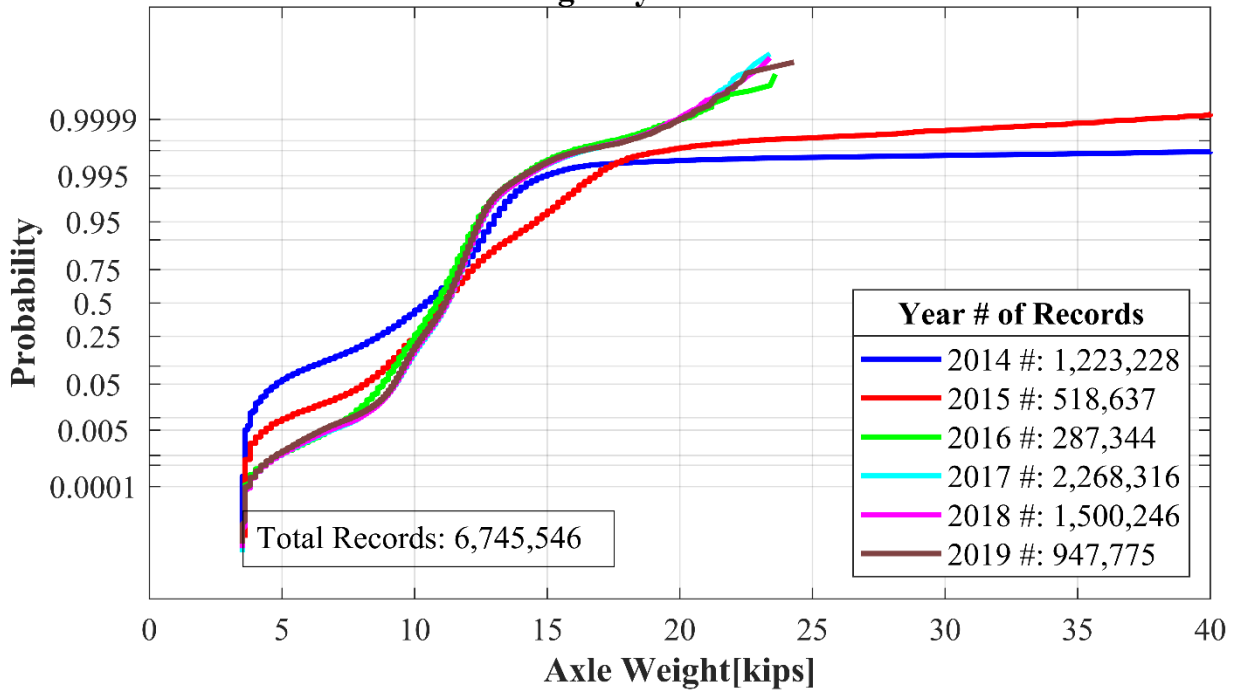
Class 9 #4 Axle Weight by Year CA-077 COLTON-EB



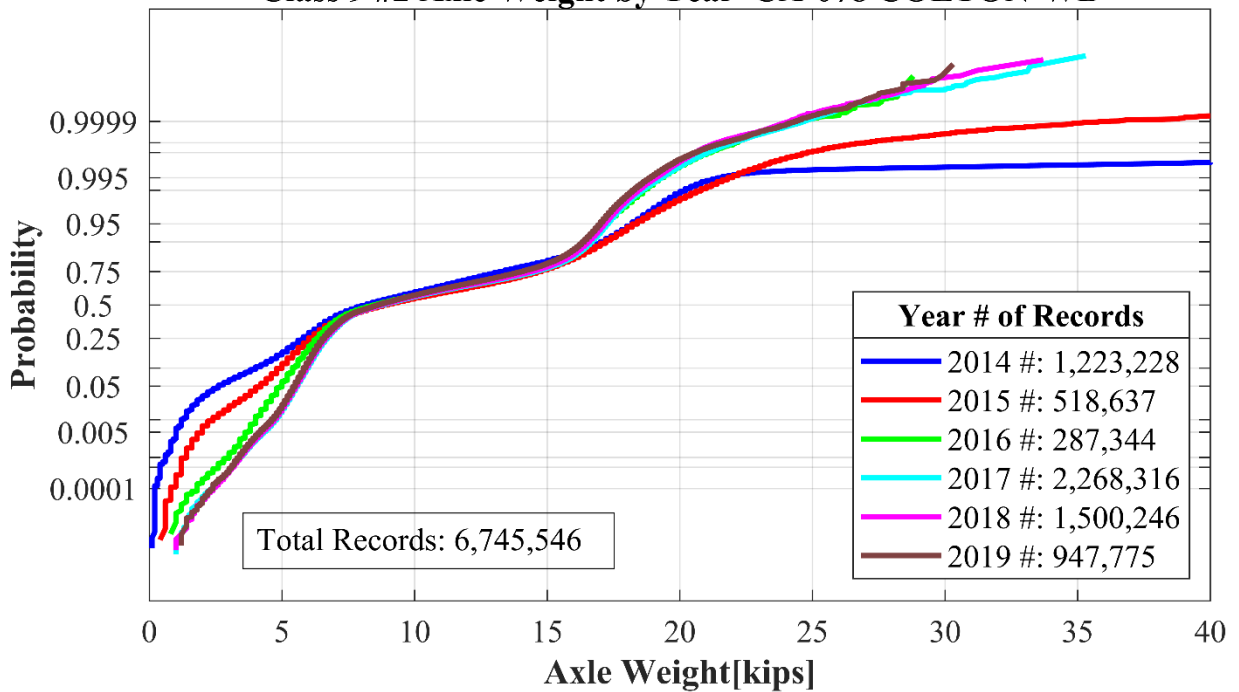
Class 9 #5 Axle Weight by Year CA-077 COLTON-EB



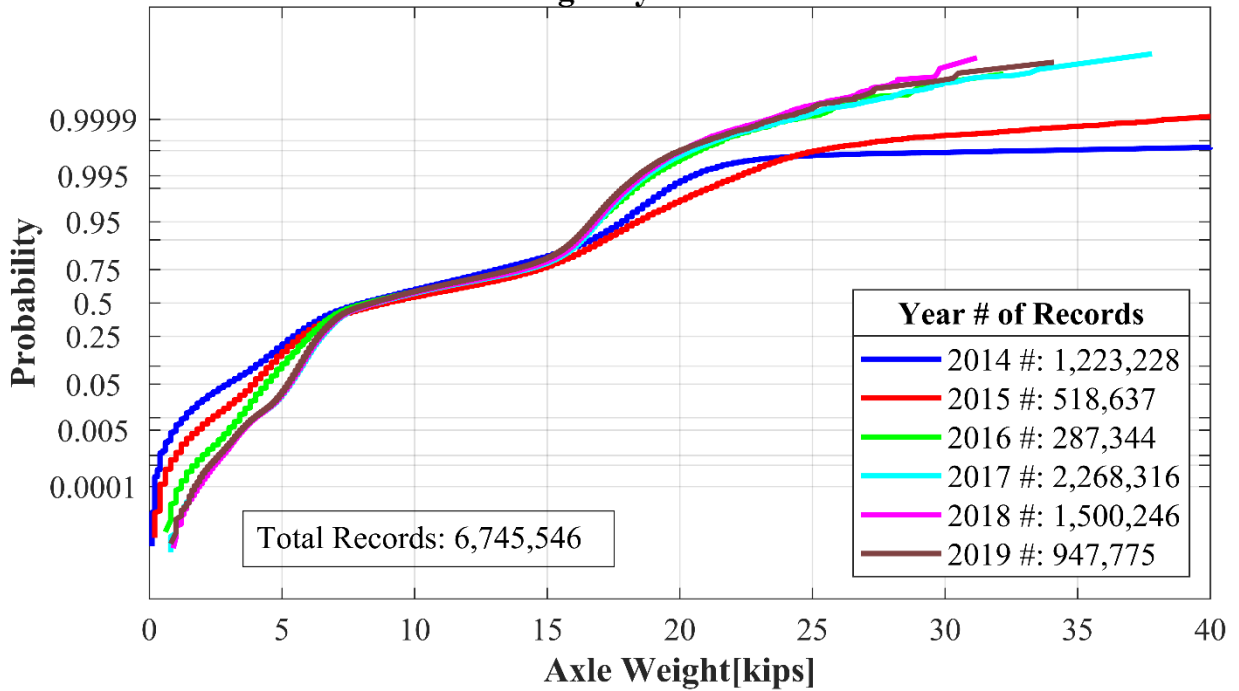
Class 9 #1 Axle Weight by Year CA-078 COLTON-WB



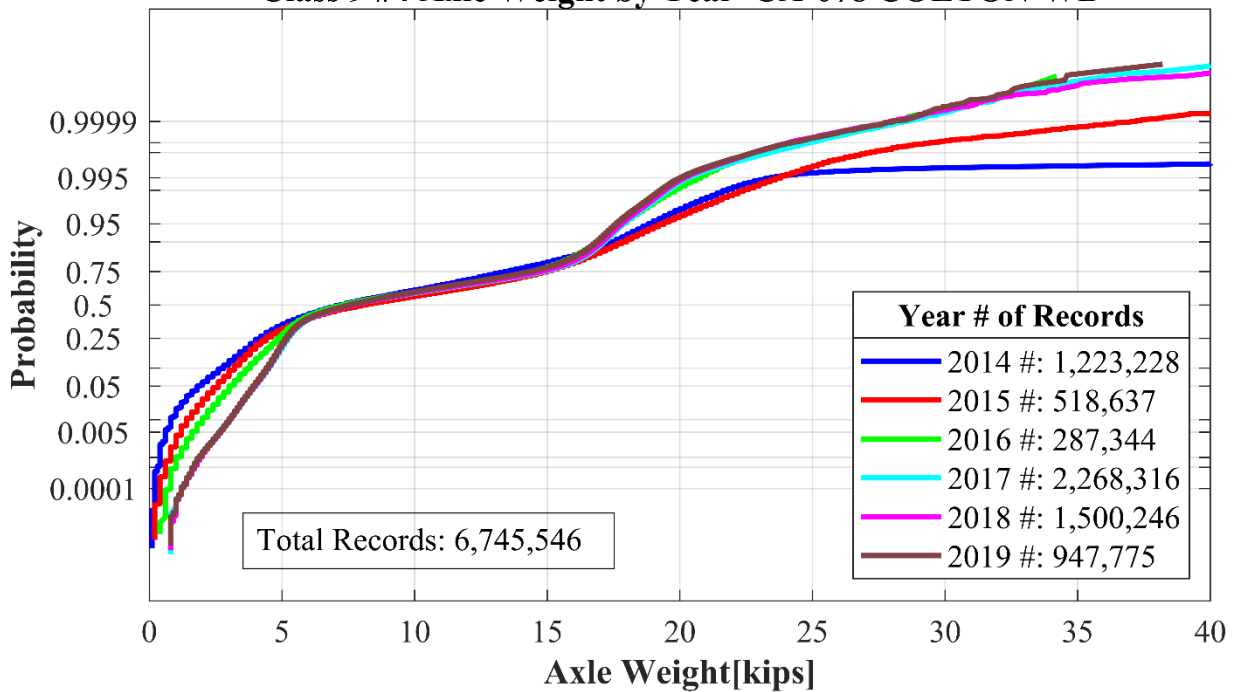
Class 9 #2 Axle Weight by Year CA-078 COLTON-WB



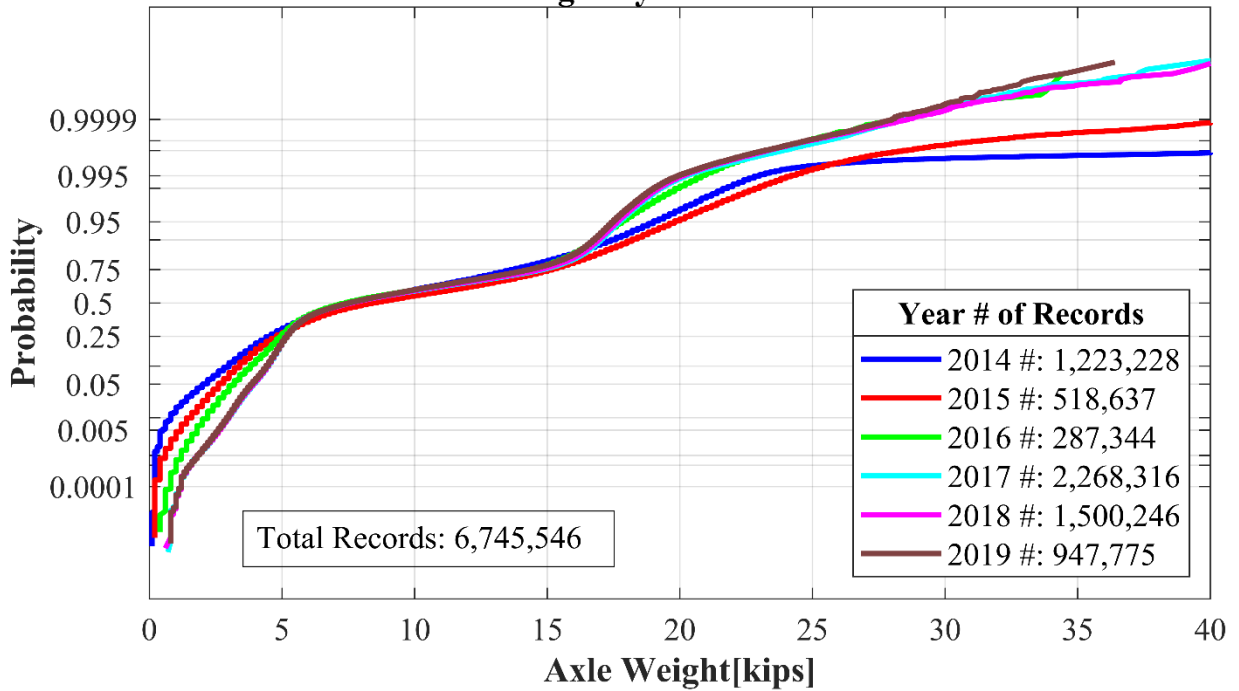
Class 9 #3 Axle Weight by Year CA-078 COLTON-WB



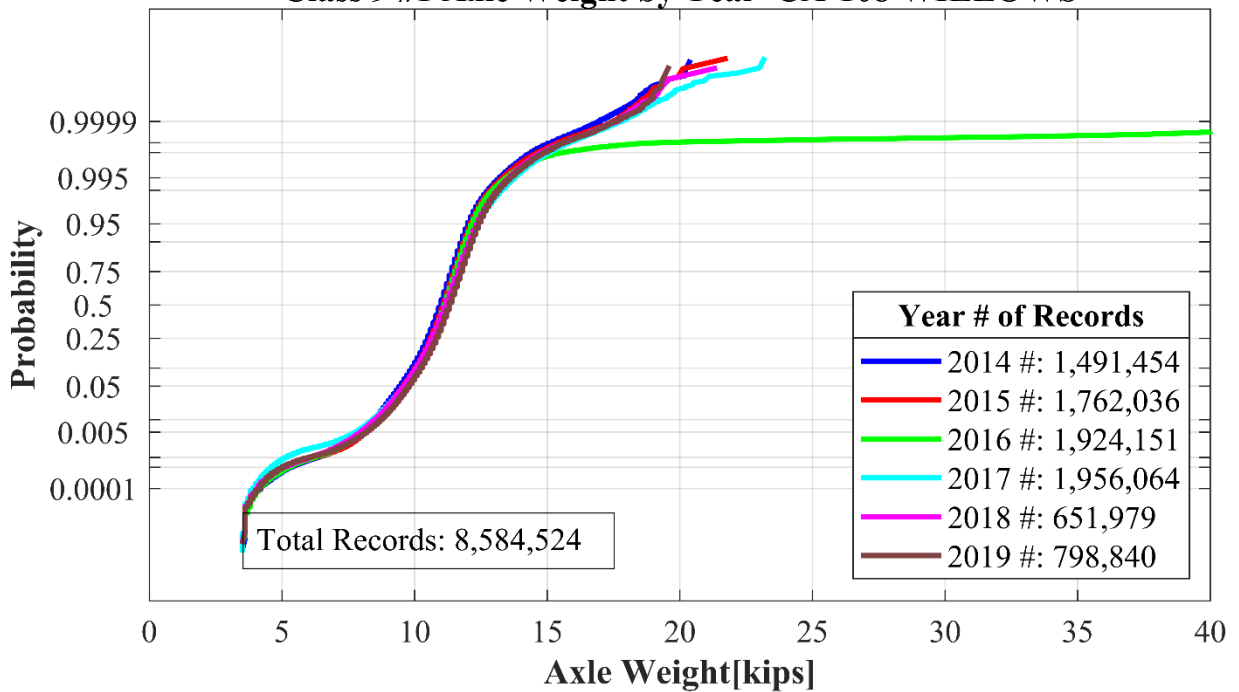
Class 9 #4 Axle Weight by Year CA-078 COLTON-WB



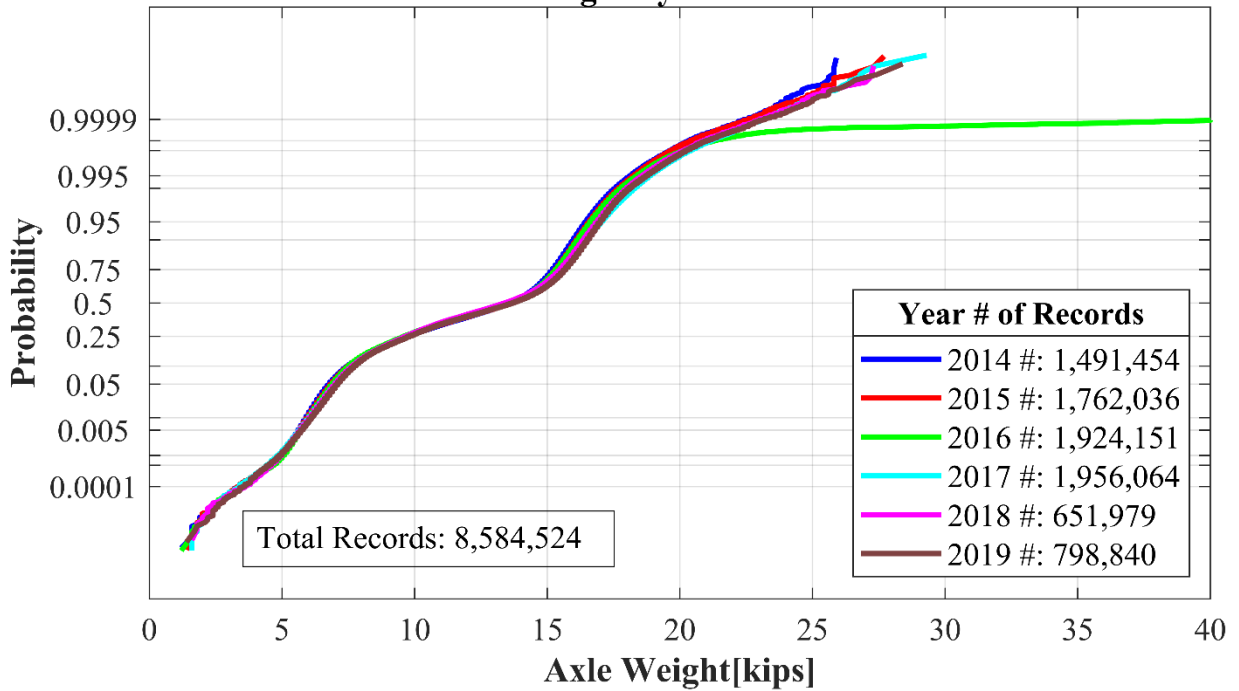
Class 9 #5 Axle Weight by Year CA-078 COLTON-WB



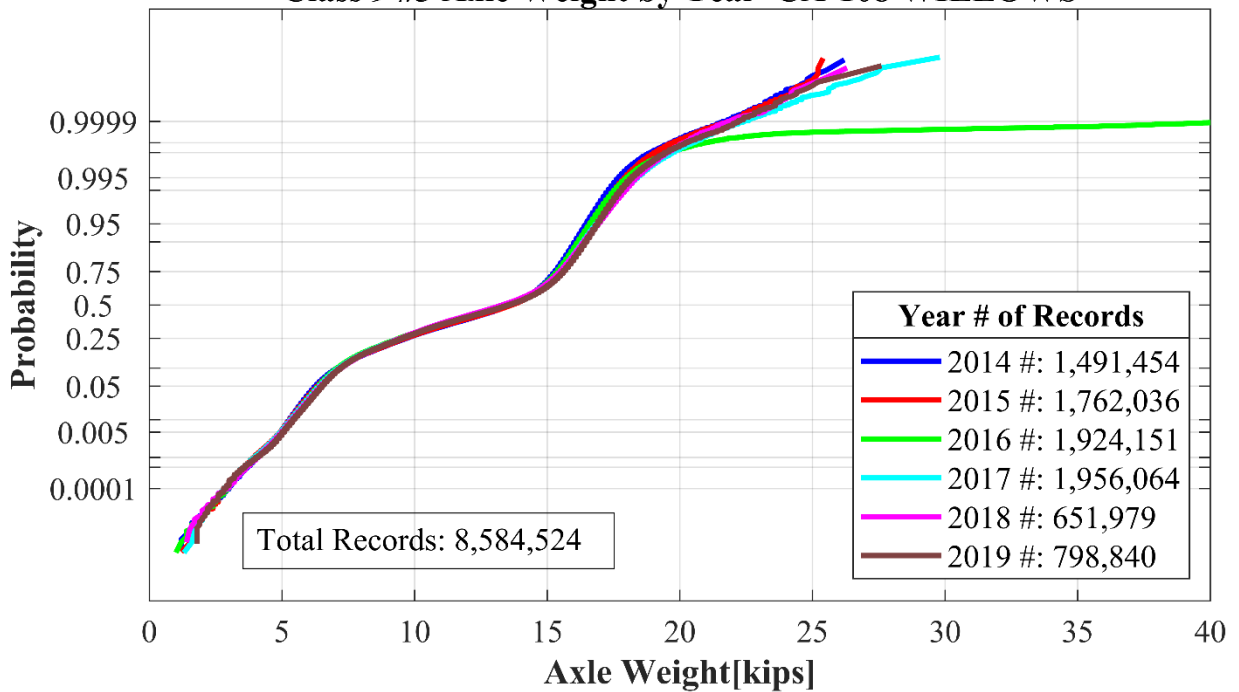
Class 9 #1 Axle Weight by Year CA-108 WILLOWS



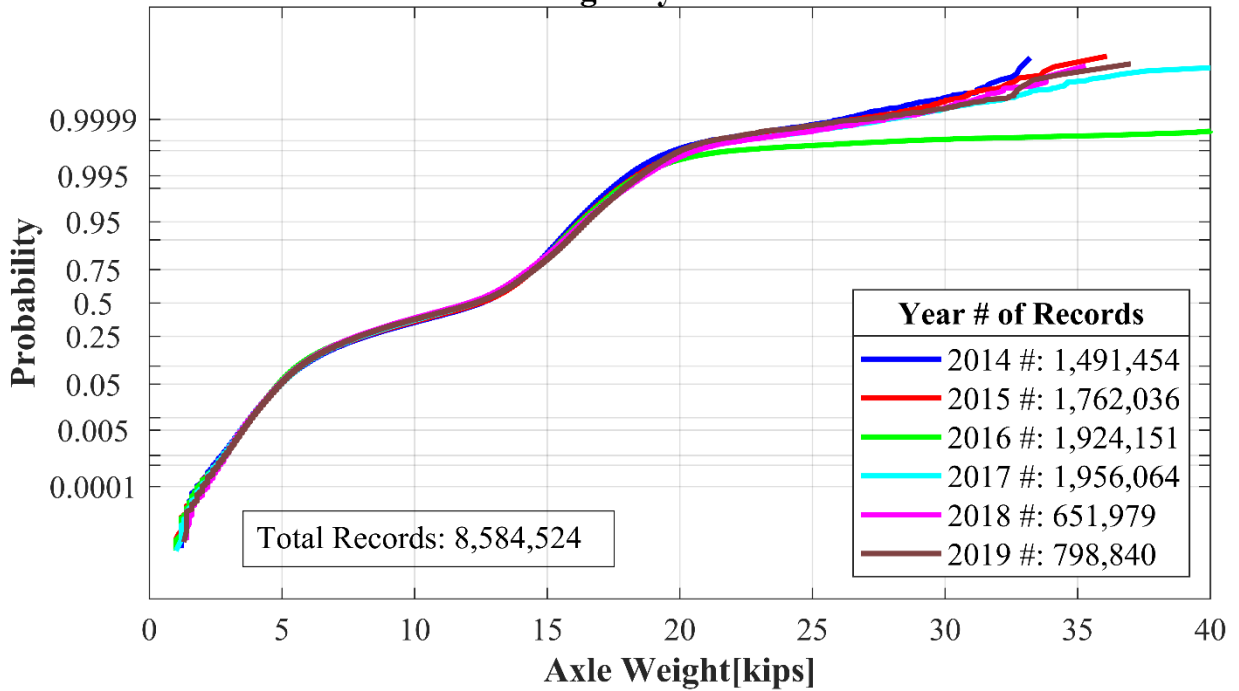
Class 9 #2 Axle Weight by Year CA-108 WILLOWS



Class 9 #3 Axle Weight by Year CA-108 WILLOWS



Class 9 #4 Axle Weight by Year CA-108 WILLOWS



Class 9 #5 Axle Weight by Year CA-108 WILLOWS

